REFERENCE ONLY

UNIVERSITY OF LONDON THESIS

Degree PhD Year 2006 Name of Author SHARLOTT, A.V.

The Role of Oscillatory Population Activity in Cortico-Basal Ganglia Circuits

Andrew David Sharott

Sobell Department of Motor Neuroscience
and Movement Disorders
Institute of Neurology
University College London
Queen Square
London WC1N 3BG

ProQuest LLC
789 East Eisenhower Parkway
P.O. Box 1346
Ann Arbor, MI 48106-1346

Abstract

The basal ganglia (BG) are a group of subcortical brain nuclei that are anatomically situated between the cortex and thalamus. Hitherto, models of basal ganglia function have been based solely on the anatomical connectivity and changes in the rate of neurons mediated by inhibitory and excitatory neurotransmitter interactions and modulated by dopamine. Depletion of striatal dopamine as occurs in Parkinson's Disease (PD) however, leads primarily to changes in the rhythmicity of basal ganglia neurons. The general aim of this thesis is to use frontal electrocorticogram (ECoG) and basal ganglia local field potential (LFP) recordings in the rat to further investigate the putative role for oscillations and synchronisation in these structures in the healthy and dopamine depleted brain. In the awake animal, lesion of the SNc lead to a dramatic increase in the power and synchronisation of β-frequency band oscillations in the cortex and subthalamic nucleus (STN) compared to the sham lesioned animal. These results are highly similar to those in human patients and provide further evidence for a direct pathophysological role for β-frequency band oscillations in PD. In the healthy, anaesthetised animal, LFPs recorded in the STN, globus pallidus (GP) and substantia nigra *pars reticulata* (SNr) were all found to be coherent with the ECoG. A detailed analysis of the interdependence and direction of these activities during two different brain states, prominent slow wave activity (SWA) and global activation, lead to the hypothesis that there were state dependant changes in the dominance of the cortico-subthalamic and cortico-striatal pathways. Multiple LFP recordings in the striatum and GP provided further evidence for this hypothesis, as coherence between the ECoG and GP was found to be dependent on the striatum. Together these results suggest that oscillations and synchronisation may mediate information flow in cortico-basal ganglia networks in both health and disease.

Acknowledgements

I would especially like to thank the following people without whom this work would not have been possible:

Firstly, my supervisor Professor Peter Brown for his constant enthusiasm, support and invaluable assistance.

Secondly Dr Peter Magill for being a great collaborator and unofficial second supervisor.

Professor Paul Bolam for both his valuable input and continued faith in this work.

Dr Wassilios Meissner and Dr Daniel Harnack for both their crucial practical support and being excellent hosts in Berlin.

The Brain Research Trust who funded this PhD.

My parents for their continual support of my education and everything else.

I would also like to thank

Joseph Csicsvari, Liz Norman, Caroline Francis and Ben Micklem for there technical assistance with all experiments performed in Oxford.

Andreas Kupsch for his support of the work performed in Berlin.

Peter Asselman for his help and technical support.

Publications

Publications incorporated in this thesis:

Sharott A, Magill PJ, Bolam JP, Brown P (2005) Directional analysis of coherent oscillatory field potentials in the cerebral cortex and basal ganglia of the rat. J Physiol 562: 951-63.

Sharott A, Magill PJ, Harnack D, Kupsch A, Meissner W, Brown P (2005) Dopamine depletion increases the power and coherence of β-oscillations in the cerebral cortex and subthalamic nucleus of the awake rat. Eur J Neurosci 21: 1413-22.

Magill PJ, Sharott A, Bolam JP, Brown P (2004) Brain state-dependency of coherent oscillatory activity in the cerebral cortex and basal ganglia of the rat. J Neurophysiol 92: 2122-36.

Publications related to this thesis:

Magill PJ, Sharott A, Bolam JP, Brown P (2006) Delayed synchronisation of activity in cortex and subthalamic nucleus following cortical stimulation in the rat. J Physiol. *In Press*

Magill PJ, Pogosyan A, Sharott A, Csicsvari J, Bolam JP, Brown P (2006) Changes in functional connectivity within the rat striato-pallidal axis during global brain activation *in vivo.* J. Neurosci. 26:6318-29.

Magill PJ, Sharott A, Harnack D, Kupsch A, Meissner W, Brown P (2005) Coherent spike-wave oscillations in the cortex and subthalamic nucleus of the freely moving rat. Neuroscience 132: 659-64.

Magill PJ, Sharott A, Bevan MD, Brown P, Bolam JP (2004) Synchronous unit activity and local field potentials evoked in the subthalamic nucleus by cortical stimulation. J Neurophysiol 92: 700-14.

Brown P, Kupsch A, Magill PJ, Sharott A, Harnack D, Meissner W (2003) Oscillatory local field potentials recorded from the subthalamic nucleus of the alert rat. Exp Neurol 177: 581-5.

Additional published work during the PhD program:

Kuhn AA, Sharott A, Trottenberg T, Kupsch A, Brown P (2004) Motor cortex inhibition induced by acoustic stimulation. Exp Brain Res 158: 120-4.

Fisher RJ, Sharott A, Kuhn AA, Brown P (2004) Effects of combined cortical and acoustic stimuli on muscle activity. Exp Brain Res 157: 1-9.

Grosse P, Salih E, Sharott A, Khatami R, Trottenberg T, Schneider G, Kupsch A, Brown P (2004) Functional connectivity in the human motor system across the sleep-wake cycle. J Neurology 251: 34-34 Suppl. 3.

Sharott A, Marsden J, Brown P (2003) Primary orthostatic tremor is an exaggeration of a physiological response to instability. Mov Disord 18: 195-9.

Table of Contents

List of Figures

Chapter 3

Chapter 4

Table of Tables

Page

Abbreviations

6-OHDA	6-hydroxydopamine
ANOVA	Analysis of variance
BOLD	Blood-oxygen-level-dependent
BG	Basal ganglia
CCH	Cross correlation histogram
CL	Confidence limit
CP	Cerebral peduncle
CV	Coefficient of variation
DA	Dopamine
DBS	Deep brain stimulation
DF	Degrees of freedom
EEG	Electroencephalogram
ECoG	Electrocorticogram
ECG	Electrocardiogram
EMG	Electromyogram
EPSP	Excitatory post-synaptic potential
EP	Endopenduncular nucleus

FT	Fourier Transform
FFT	Fast Fourier Transform
GABA	Gamma amino butyric acid
GLM	General linear model
GP	Globus pallidus
GPe	Globus pallidus external segment
GPi	Globus pallidus internal segment
IC	Internal capsule
IPSP	Inhibitory post-synaptic potential
L-dopa	Levadopa
LFP	Local field potential
MAR	Multivariate autoregressive model
MEG	Magnetoencephalogram
MPTP	1-methyl-4-phenyl-1,2,3,6-tetrahydropyridine
MSN	Medium spiny neuron
NS	Non significant
PD	Parkinson's Disease
PPN	Pedunculopontine nucleus
PSTH	Post stimulation time histogram
RE	Reticular nucleus of the thalamus
SEM	Standard error of the mean
SD	Standard deviation
SN	Substantia nigra
SNr	Substantia nigra *pars compacta*
SNc	Substantia nigra *pars reticulata*
STN	Subthalamic nucleus
STR	Striatum
SWA	Slow wave activity
TAN	Tonically active neuron
TH	Tyrosine hydroxylase
TH-IR	Tyrosine hydroxylase-immunoreactive
Thal	Thalamus
ZIV	Zona incerta

Chapter 1: Synchronisation and the basal ganglia

Around 15 years ago the first comprehensive model of cortico-basal ganglia circuits was published (Albin et al, 1989; Delong, 1990). The model proposed that the main action of the basal ganglia was to increase or decrease activity in the motor thalamus and cortex. This regulation was postulated to occur through two anatomically distinct pathways, direct and indirect, which provided positive and negative regulation of the thalamocortical targets respectively. Crucially, the balance between the two pathways was thought to be mediated by dopamine, through the modulation of the rate of neurons in the different basal ganglia structures. The model provided the first truly mechanistic explanation for information flow in the basal ganglia and convincing explanations for several basal ganglia diseases and their treatments. Like many models in the natural sciences, although flawed, the deconstruction of the direct/indirect pathway model of basal ganglia function has provided real insight in to the true complexity of the system. In recent years, with the discovery of several new and potentially important anatomical projections, it is clear that the architecture of the system is more intricate than first thought. Perhaps even more importantly, the view that basal ganglia neurons influence each other only though positive and negative modulations of firing rate has been questioned. As with other brain areas, most notably the cerebral cortex and hippocampus, it is becoming apparent that synchronisation between both individual and populations of neurons may also be functionally important. In cortico-basal ganglia circuits the relative importance of synchronisation remains contentious. The aim of this work was to investigate whether synchronised population activity could provide an additional level of organisation in cortico-basal ganglia networks and whether the disruption of this putative organisation could underlie their pathology.

1.1 Anatomy of the Basal Ganglia.

The basal ganglia consist of a group of sub-cortical nuclei with heterogeneous cellular anatomy that are highly interconnected and form complex loops with the cerebral cortex and thalamus. In strict anatomical terms the basal ganglia refers to the large group of subcortical nuclei including the thalamus. Functionally, the term basal ganglia refers to the caudate nucleus and the putamen (collectively labelled the striatum (STR)), the globus pallidus internal and external segments (GPi and GPe respectively), the subthalamic nucleus (STN) and the substantia nigra pars reticulata (SNr) and pars compacta (SNc) (Kandel and Schwarz, 2000; see Figure 1.1). Recently the pedunculopontine (PPN) nucleus has also become frequently included amongst the main basal ganglia structures (Mena-Segovia et al, 2004). The basic chemo-architecture and connectivity between these structures is highly conserved between reptile, birds and mammals, suggesting that they contain circuits of fundamental importance to animal brain function and behaviour (Smeets et al, 2000).

Thus far, possible pathways of information flow through the various nuclei have mostly underpinned theories of basal ganglia function. This may be partly explained by the non-laminar arrangement of basal ganglia structures, which is unique amongst brain areas involved in so called higher functions. Instead, information is fed in to the basal ganglia primarily from cortical afferents to the striatum and subthalamic nucleus, which in turn project to the GPe, GPi and SNr. The GPi and SNr, collectively known as the output nuclei, send afferents to the ventral nuclei of the thamalus, which in turn project back to areas of the cortex. This anatomical arrangement is strongly suggestive that the majority of processing takes place not within the individual nuclei, but by the synaptic interactions between them (Bar-Gad et al, 2003). Before considering any functional hypotheses however, it is important to consider in detail the possible routes of information flow through these brain areas, which are likely to be determined in part by their anatomical connections and basic electrophysiological characteristics.

1.1.1 Cortico-basal-ganglia pathways

Anatomically, the striatum is the major input site for cortical afferents projecting to the basal ganglia. The striatum itself is composed mainly of medium spiny neurons (MSNs): GABAergic, spiny neurons, which account for 90-95% of the neuronal population in rats, cats and primates (Parent and Hazrati, 1995). At rest, MSNs are quiescent, firing at a frequency around 1Hz (Kimura, 1990; Kimura et al, 1996). MSNs can be subdivided in to two populations based on their pattern of connectivity and neurochemical characteristics (Smith et al, 1998). One subpopulation, expressing the neuropeptides substance P and dynorphin and the D1 dopamine receptor, project mostly to the output nuclei. The other expresses the neuropeptide enkephalin and the D2 dopamine receptor and project to the GPe. This organisation however is probably less clear-cut than at first thought (see below). MSNs receive afferents from the entire cortical mantle, which make glutamatergic synapses primarily on the heads of their dendritic spines (Kemp and Powell, 1971b; 1971c). The cortico-striatal projection is highly topographic and therefore imparts functional specificity on sub-populations of MSNs, which are at least partly preserved throughout the rest of the basal ganglia (Parent & Hazrati, 1995a; 1995b). For example, in humans and non-human primates the dorsolateral pre-frontal cortex projects most densely to the rostral striatum and is involved specifically in working memory tasks (Haber, 2003). It has also been extensively described that the membrane potential of striatal projection cells displays periodic shifts between polarised and depolarised potentials, which are dependent on cortical input and are sensitive to dopaminergic modulation (Murer et al, 2002). MSNs are more likely to fire action potentials during the depolarising phase, making striatal output highly dependent on cortical input (Murer et al, 2002).

The striatum contains several populations of interneurons, the most numerous of which are the so-called tonically active neurons (TANs), which are characterised by a tonic baseline firing rate of between 3-12Hz (Apicella, 2002). It is presumed, although hitherto unproven, that TANs (as defined

physiologically) correspond to the cholinergic interneurons described in the rodent striatum (Apicella, 2002).

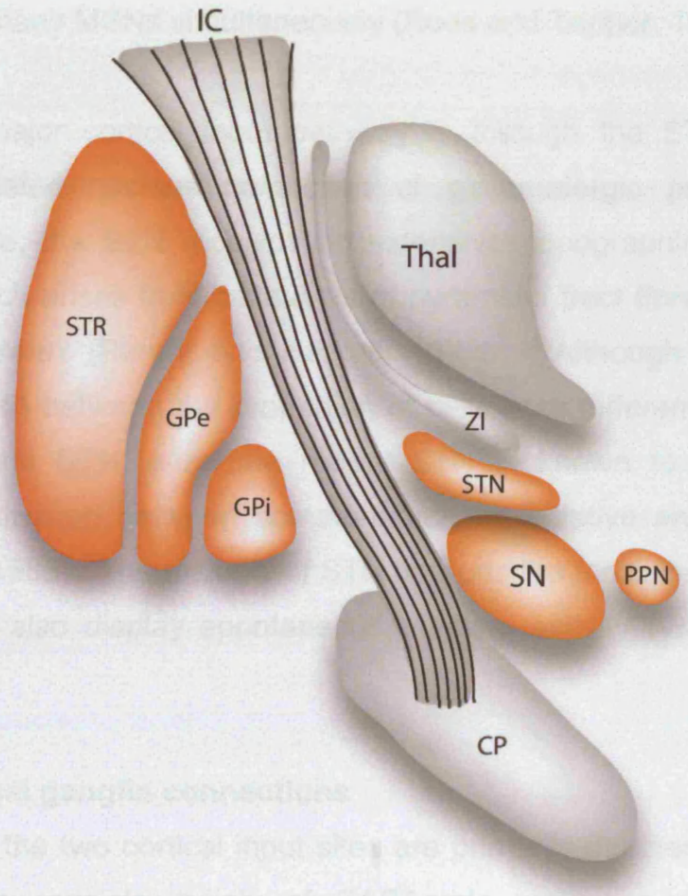

Figure 1.1 Macro-anatomy of the basal ganglia. Schematic representation of the gross anatomy of the nuclei commonly considered to belong to the basal ganglia (red) and there surrounding structures (grey) in the human. STR = striatum; GPe = globus pallidus external segment; GPi = globus gallidus internal segment; STN = subthalamic nucleus; SN = substantia nigra (*pars compacta* and *pars reticulata*); PPN = pedunculopontine nucleus; IC = internal capsule; CP = cerebral peduncle; Thal = thalamus. (Adapted from Hamani et al, 2004)

There are also several subtypes of GABAergic interneurons, which also receive extensive convergent input from both sensory and motor cortices (Ramanathan et al, 2002). Although these interneurons make up only a small percentage of the total striatal population, they are highly interconnected and can influence many MSNs simultaneously (Koos and Tepper, 1999)

The second major cortical input pathway is through the STN; a smaller, densely populated nucleus composed of glutamatergic projection cells. Despite its size, the STN receives an extensive, topographically organised projection, which arises from collaterals of pyramidal tract fibres in layer V of the cerebral cortex (Parent and Hazrati, 1995b). Although there is inter-species variation between the proportion of cells from different cortical areas projecting to the STN, even the rodent STN is known to have a crude functional subdivision between somato-motor, associative and limbic areas (Delong et al, 1985). The majority of STN neurons fire tonically at between 15 and 25Hz but also display spontaneous bursting activity (Wichmann et al, 1994).

1.1.2 Inter-basal ganglia connections

Afferents from the two cortical input sites are primarily directed to the globus pallidus, which consists mainly of GABAergic projection neurons. The pallidum is divided into external and internal segments that are separated by the internal capsule and have distinct patterns of connectivity. Neurons in both segments of the pallidum receive afferents from both the striatal MSNs and the STN (Parent and Hazrati, 1995b). As described above, separate populations of stratial cells innervate the two pallidal segments. Both segments also receive extensive subthalamic afferents, which form glutamatergic synapses though out the entire pallidum (Parent and Hazrati, 1995b). The SNr, which together with the GPi, or endopeduncular nucleus (EP) in the rat, form the basal ganglia output nuclei, also receives this pattern of innervation. The SNr and GPi/EP, will from this point often be considered together as the output nuclei unless otherwise stated. While the input connections of the GPe and output nuclei are similar, their efferent connections vary greatly. GPe neurons have reciprocal afferent projections to

both of the striatum and the STN (Parent & Hazrati, 1995b). In the striatum, some GPe axons synapse on MSNs, but primarily innervate GABAergic interneurons (Bevan et al, 1998). Axons from the GPe form extensive synapses throughout the STN, creating a highly symmetrical arrangement of connections between the two structures (Parent and Hazrati, 1995b). The same neurons that innervate the STN also project to the output nuclei (Bolam et al, 1993). The GPe is therefore in a position to simultaneously influence the entire basal ganglia network, making its neurons good candidates for controlling information flow (Parent & Hazrati, 1995b; Bolam et al, 2000). In contrast the output nuclei project predominantly to the ventral anterior and ventral lateral nuclei of the thalamus, which in turn project back to the cerebral cortex, completing the basal ganglia loop. These thalamo-cortical projections can either be reciprocal regarding the origin of cortical input, or project to other areas creating so-called "closed" or "open" loops, respectively (Haber, 2003; Kelly and Strick, 2004). Although there are some subtle differences in the baseline firing rates between GPe, GPi and SNr, the majority of cells recorded in the primate fire tonically at frequencies between 50 and 100Hz (Boraud et al, 2002). The output nuclei therefore provide constant inhibitory drive to the ventral thalamus.

1.1.3 The substantia nigra *pars compacta* and dopaminergic regulation

The SNc, one of the three groups of dopaminergic neurons found in the mesencephalon, sends thin, varicose axon fibres which form synapses throughout the striatum and, to a lesser extent, the pallidum and STN (Smith and Kieval, 2000). In the dorsal striatum, D1 and D2 receptors are most prevalent at nigrostriatal synapses, with D3 receptors confined mostly to the limbic parts of the striatum (Smith and Kieval, 2000). More than 90% of dopaminergric terminals form symmetric synapses with the spines and dendrites of MSNs and around 40% of spines on MSNs receive inputs from both cortical and dopaminergic neurons. This organisation is highly suggestive of dopaminegic regulation of cortico-striatal input (Smith et al, 1990; Smith and Keival, 2000). Dopamine neurons fire tonically at low frequencies (0.5-8Hz) maintaining a constant level of dopamine release in their target structures (Schultz and Romo, 1987; Schultz and Romo, 1990).

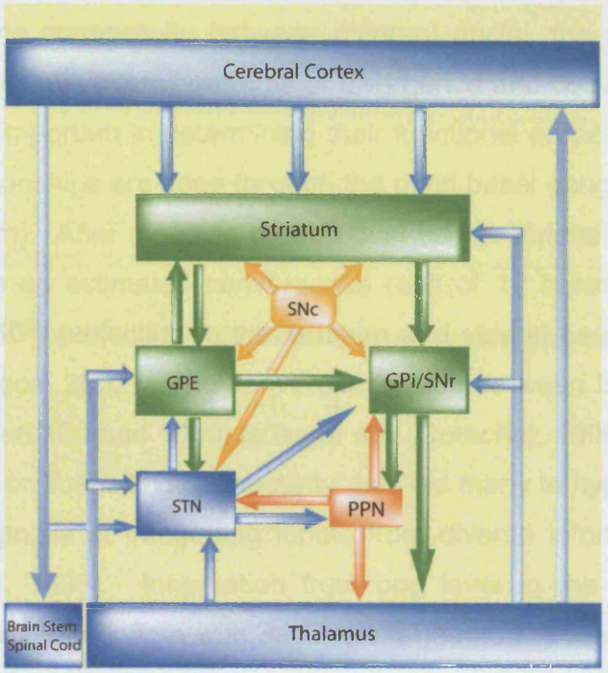

Figure 1.2 Micro-anatomy of cortico-basal ganglia circuits. The main brain areas classified as belonging to the cortico-basal ganglia circuits are represented by boxes and their axonal projections by arrows. The cerebral cortex, subthalamic nucleus (STN) and thalamus are composed mostly of glutamatergic neurons and send excitatory projections to their afferent targets (blue boxes and arrows). The striatum, globus pallidus external segment (GPe) and globus pallidus internal segment/substantia nigra *pars reticulata* (GPi/SNr) are composed mostly of GABAergic neurons and send inhibitory projections (green boxes and arrows). The cerebral cortex sends projections to both the striatum and the STN, which send excitatory and inhibitory projections respectively to both the GPe and GPi/SNr. The GPe makes significant reciprocal connections with both structures. The GPi/SNr, collectively known as the output nuclei, project mainly to the motor thalamus which projects back to the cerebral cortex, closing the cortico-basal ganglia loop. Neurons in the substantia nigra *pars compacta* (SNc, orange) are dopaminergic and send axons to all the basal ganglia nuclei, but the majority terminate in the striatum. The cholinergic neurons of the pedunculopontine nucleus (PPN, red) have reciprocal connections with the GPi and STN. The PPN is therefore often functionally grouped with the basal ganglia and may provide an additional output stream to the brainstem/spinal cord.

1.1.4 Convergence and divergence in basal ganglia loops

In addition to the connectivity between different nuclei, the anatomy of the basal ganglia displays overall patterns of divergence and convergence, which are likely to be important in determining their functional properties. The most consistent relationships are seen through the main basal ganglia axis (cortex-striatum-pallidum). After mapping of individual cortico-striatal arborisations in the rat, there is an estimated convergence ratio of 10 between the cortical neurons (17×10^6) projecting to the striatum and striatal neurons (17×10^6) (Zheng and Wilson, 2002). The convergence ratio between the striatum and pallidum, between 100 and 1000, is larger still (Oorschot, 1996). This pattern of convergence or "funnelling connectivity" has led many to hypothesise a role for the basal ganglia in integrating inputs from diverse information streams (Bergman et al, 1998). Innervation from one level to the next down the hierarchy is extremely sparse with each striatal neuron receiving inputs from around 0.01% of corticostriatal neurons and each pallidal cell receiving input from between 0.1-1% of the striatal neurons (Zheng and Wilson, 2002; Bar-Gad et al, 2003). In the striatum, this divergence is consistent with physiological data suggesting that many cortical inputs are necessary to elicit action potential firing in MSNs and is consistent with a role for striatal neurons in detecting activity in distributed cortical ensembles (Zheng and Wilson, 2002). There is little doubt, however, that a degree of parallel organisation also exists, whereby information streams from motor, cognitive or limbic areas remain anatomically segregated (Hoover and Strick, 1993; Parent and Hazrati, 1995a and see above). Recent anatomical models have stressed a role for both architectures in basal ganglia processing (Joel and Wiener, 1994; Haber, 2003). Taken together, anatomical studies of cortico-basal ganglia circuits suggest that their structural organisation is more complex than first thought. Investigation at the systems level will therefore be greatly enhanced by observing interactions across the network.

Aim 1: To make electrophysiological recordings from several basal ganglia nuclei simultaneously together with the cerebral cortex.

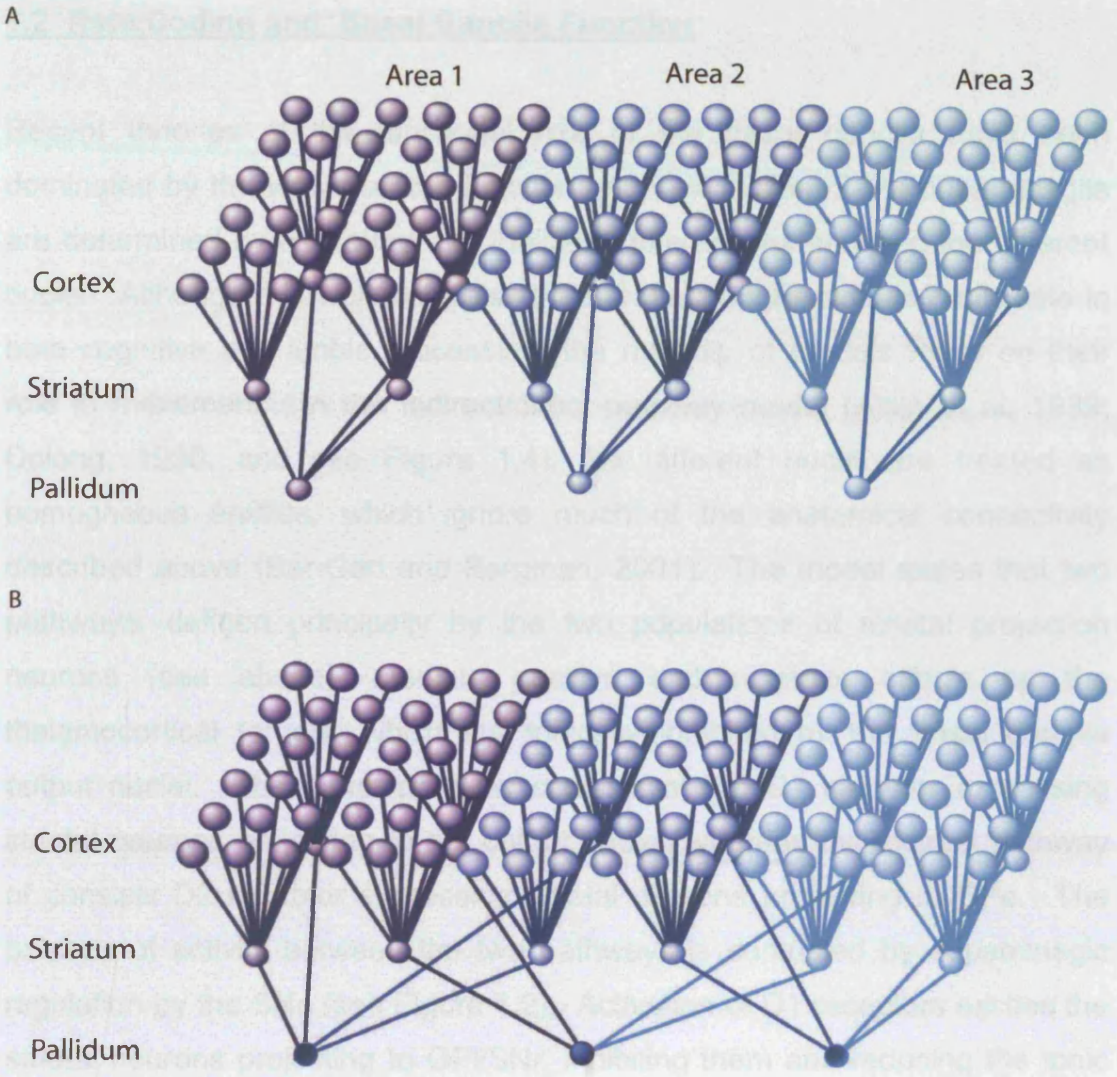

Figure 1.3 Information sharing versus segregation in cortico-basal ganglia circuits. ***A,B*** The number of neurons along the main axis of the cortico-basal ganglia circuits decreases by a ratio of around 10:1 from cortex to striatum and 100:1 from striatum to pallidum. This reduction in cell number suggests a large degree of convergence or "information funnelling" through the different layers of the circuits. Views differ as to the extent to which information from different cortical streams is shared across pallidal neurons. In the first view, ***A***, Inputs from specific cortical areas are funnelled though segregated parallel striato-pallidal circuits. In the second, ***B***, inputs from different cortico-stratial streams converge on the same pallidal neurons so that information is shared across the parallel channels. This type of divergent connection also exists at the level of the striatum. Cortico-basal ganglia circuits are likely to utilise both architectures. (Adapted from Bergman et al, 1998)

1.2 Rate Coding and Basal Ganglia Function

Recent theories of the functional role of the basal ganglia have been dominated by the view that the function and dysfunction of the basal ganglia are determined by excitatory and inhibitory interactions between the different nuclei. Although it is well recognised that basal ganglia circuits participate in both cognitive and limbic processing, the majority of models focus on their role in movement. In the indirect/direct pathway model (Albin et al, 1989; Delong, 1990. and see Figure 1.4), the different nuclei are treated as homogneous entities, which ignore much of the anatomical connectivity described above (Bar-Gad and Bergman, 2001). The model states that two pathways, defined principally by the two populations of striatal projection neurons (see above), mediate positive and negative effects on the thalamocortical targets, which are tonically inhibited by the basal ganglia output nuclei. The direct pathway consists of the D1 receptor expressing striatal neurons projecting to the output nuclei, whereas the indirect pathway of consists D2 receptor expressing striatal neurons projecting to GPe. The balance of activity between the two pathways is controlled by dopaminegic regulation by the SNc (see Figure 1.2). Activation of D1 receptors excites the striatal neurons projecting to GPi/SNr, inhibiting them and reducing the tonic inhibition of their thalamo-cortical targets. Activation of D2 receptors inhibits the striato-GPe neurons, which leads to an up regulation of the output nuclei's tonic inhibition of the thalamus, through the disinhibition of the excitatory STN-GPi/SNr projection. It is proposed that this up or down regulation of thalamo-cortical targets would then facilitate or inhibit movement respectively.

More recent theories of basal ganglia function have extended the direct/indirect model by proposing that it is the complex somatotopic arrangement of connections within and between basal ganglia nuclei, as opposed to the actions of the individual nuclei, which could allow the selection of some actions over others. These models vary in their complexity, from those that emphasise the selection process within the basal ganglia (Plenz, 2003), to those that treat the basal ganglia as part of a larger network involving the regulation of circuits in several brain areas (Mink et al, 1996;

Gurney et al, 2002). They also vary as to whether the key role of the basal ganglia is to actively select (Gurney et al, 2002; Mink, 1996) or inhibit (Berns and Sejnowski, 1996) competing motor programs (Bar-Gad et al, 2004). Both the original indirect/direct and more recent action selection models assume that neuronal interactions between the cerebral cortex and basal ganglia, and between the basal ganglia themselves, are mediated by rate coding. For a neuron to encode any parameter using spike rate, its target cell must operate an 'integrate and fire' principle, whereby excitatory and inhibitory post synaptic potentials are summed within a given time period or membrane constant, determined by the electrochemical properties of the cell membrane. An increase in the rate of the presynaptic neuron(s) will therefore make the postsynaptic neuron more or less likely to fire depending on whether its synapses are inhibitory or excitatory. In this way the postsynaptic cells can integrate the input of one or many cells, and encode the result in their own rate. Rate coding remains the dominant theory of information processing in neuroscience and its importance is supported by numerous studies showing variations in the rate of neurons in different brain areas with environmental changes, the dynamics of motor function and other neural computations (Shadlen and Movshon, 1999; Mazureck and Shadlen, 2002)

The models of basal ganglia function described above clearly hypothesise that under certain conditions, such as during movement, the rate of specific populations of basal ganglia cells should increase or decrease. The validity of these models has thus been explored by measuring changes in the firing rate of different basal ganglia neurons in response to tasks, particularly those involving movement. The vast majority of these studies have been carried out in the primate and rodent.

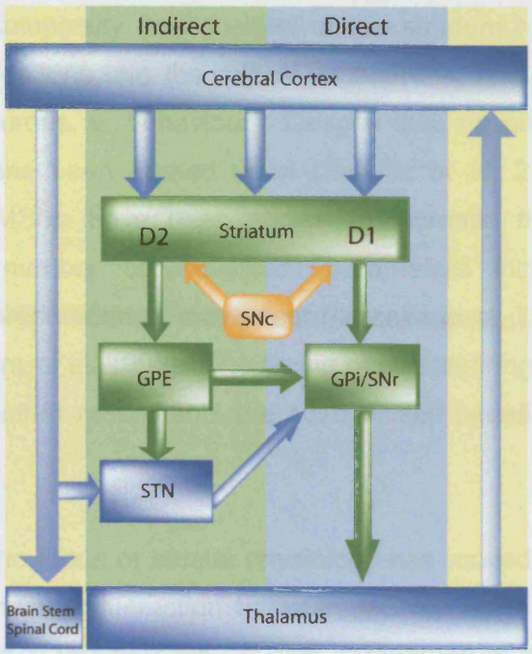

Figure 1.4 Direct/Indirect model of basal ganglia function.
The basal ganglia structures form the centre of loops between the cortex and thalamus. Structures with GABAergic cells and their inhibitory projections are green. Structures with glutamatergic cells and their excitatory projections are shown in blue. The key assumption of the model is that increased activity in the cortex and thalamus will lead to an increase in motor output through the brain stem and spinal cord, which is necessary for movement initiation. The role of the basal ganglia is to modulate this excitability, which is controlled by the level of dopamine release. When dopamine is released, activation of D1 receptors promotes activity in the direct pathway (blue background) by increasing the firing of inhibitory striatal medium spiny neurons projecting to the output nuclei (GPi/SNr). As the GABAergic neurons in the output nuclei fire tonically, this striatal inhibition leads to a disinhibition of thalamo-cortical targets. At the same time, activation of D2 receptors reduces activity in the indirect pathway (green background) by inhibiting the output of striatal neurons projecting to the GPe, increasing its tonic inhibition of the STN, the only excitatory projection to the output nuclei. The net effect of increased dopamine release is a disinhibition of the thalamus and cortex, which leads to an increased likelihood of movement initiation.

1.2.1 Striatum and Dopamine cell firing

The anatomical complexity and position of the striatum has led to a large number of investigations into the role of its neurons, and the dopaminergic input to those neurons, in behaviour. Despite this, no unifying concept for striatal function has been agreed upon (Schultz et al, 2003). In primate studies, striatal MSNs have been shown to increase their firing rate in response to a number of movement parameters including execution, expectation and preparation of movement (Apicella et al, 1992; Jaeger et al, 1993; 1995, Kimura et al, 1996). The timing of striatal firing may also change depending on whether movements are cued or self paced (Lee and Assad, 2003)

In recent years, the focus of striatal physiology has moved towards a role in motor learning and the interaction between MSNs, TANs and nigro-striatal dopaminergic cells in this process. A high percentage of dopamine neurons have been shown to give a phasic activation in response to rewarding stimuli in a large number of experimental paradigms (Schultz, 2003). Over a period of training, the magnitude of the dopamine response switches from being larger on presentation of an unexpected primary reward to the conditioning stimulus for that reward (Schultz, 2002). Thus, it has been hypothesised that the role of dopamine is to code for conditioned and unpredicted rewards, and the neurons can respond to either in consecutive trials (Schultz and Romo, 1990). In contrast TANs do not respond specifically in relation to reward but to behaviourally relevant events, which, lead to a pause in firing (Graybiel et al, 1994; Morris et al, 2004). The response of TANs increases in magnitude over training and is abolished by dopaminergic lesion (Graybiel et al, 1994). In primates, the firing of the TANs is highly predictive of whether a training stimulus will evoke a behavioural response (Blazquez et al, 2002). Coincident recordings of the two cell types confirm they carry distinct signals in relation to rewarding events (Morris et al, 2004). Both dopamine and acetylcholine (the putative transmitter of TANs) have been extensively shown to regulate plasticity in the rodent striatum (Calabresi et al, 2000; Centonze et al, 2001).

MSNs are more complex in their responses to reward tasks and different areas of the caudate/putamen are preferentially responsive to different cues in different sensory modalities (Schultz et al, 2003). In rodents performing a T-maze task, the timing of MSN firing changes with behavioural acquisition, eventually becoming maximal at the beginning and end of the task (Jog et al, 1999). In primates, responses also shift during learning between reward, task related and anticipatory increases in firing rate (Schultz et al, 2003). In summary, task related changes in the rate of striatal neurons are not consistently associated with movement, but are dynamic and appear to be specialised for reward associated learning.

1.2.2 STN

Investigations in to STN firing in the primate broadly support a role for STN neurons in movement, but provide limited insight into the precise role of STN neurons in the network. Early studies reported that increases in firing rate in STN neurons are related to the direction of movement more often and earlier than those in either pallidal segment (Georgopoulous et al, 1983). Changes in the firing rate of individual STN neurons were also found to be related to the active and passive movement of specific limbs (Delong et al, 1985). A later study also reported increased firing of the vast majority of STN cells around the time of movement of a single joint (Wichmann et al, 1994). Passive movement and somatosensory stimuli also activated a large number of cells. The fact that electrical stimulation of the STN did not elicit movement was seen as support for the role of the STN in the inhibition rather than in the activation of movement (Wichmann et al, 1994 and see above). Phasic changes in ventral STN neurons have also been linked with saccadic eye movements (Matsumura et al, 1992), with the majority of cells reaching maximum firing rate during maintained eye position. This study also supported the role of STN firing in stopping or suppressing unwanted movement (Mink, 1996).

1.2.3 Globus Pallidus and Substantia Nigra *Pars Reticulata*

Early studies of pallidal neurons in the primate showed evidence of a linear relationship between pallidal cell firing and movement parameters and ascribed a role in motor control to the GPi (Georgopoulous et al, 1983). Other studies of GPi neurons have found considerable variation in pallidal firing in relation to movement (Jaeger et al, 1995; Turner and Anderson, 1997; Gdowski et al, 2001). While all these studies supported an association between pallidal rate and movement, all concluded a more complex role for pallidal neurons, which could involve responses to sensory and contextual information.

Tonic SNr activity is highly correlated with motor activity in rodents and is reduced by dopamineregic stimulation (Gulley et al, 1999). In the primate, neurons in the SNr are thought to play a role in the generation of eye (Handel and Glimsher, 1999; Sato and Hikosaka, 2002) and limb (Wichmann and Klien, 2004) movements. Similarly, four populations of SNr cells could be characterised in relation to eye movements, two of which showed increased and two decreased firing (Handel and Glimsher, 1999). For limb movements, SNr firing was not consistently found to respond to passive or active movement (Wichmann and Klien, 2004). As with the pallidum, the lack of consistency in the maginitude and direction of responses improves markedly after reward-based learning (Sato and Hikosaka, 2002).

Despite these extensive investigations in to the rate changes predicted by the direct/indirect model of basal ganglia function, very few studies have looked at the interactions between nuclei. The studies described above, therefore, worked under the assumption that static anatomical connections define the interactions between neurons in the different basal ganglia nuclei. However, the physiological, and therefore functional, interaction between the nuclei under different conditions remains largely undefined. Moreover, despite the fact that the main input to the basal ganglia is the cerebral cortex, basal ganglia cortical activities have seldom been simultaneously recorded.

1.3 Rate coding in basal ganglia disease and lesions

In addition to investigating the task related activity of basal ganglia neurons in the healthy brain, important insights into the function of these brain areas have also been gained from recordings made in humans and experimental animals with basal ganglia damage.

1.3.1 Dopamine depletion and Parkinsons disease

The most common disease of the basal ganglia is Parkinson's disease (PD) affecting around 1% of adults over 60 years old. There are three cardinal features of PD. Tremor is often the first symptom recognised by sufferers, occurs at 3-5Hz and is most common in the hand. Secondly, most patients exhibit rigidity; the raised resistance noted during passive joint movement. The third and often most disabling symptom is bradykinesia; a slowness of movement which often manifests in difficulty with fine motor tasks. Postural instability and autonomic dysfunction are also common. Although tremor may not always develop, either bradykinisia of tremor must be present before a diagnosis of PD is made (Fahn and Sulzer, 2004, Samii et al, 2004). The underlying pathology in PD is principally the degeneration of dopaminergic neurons in the substantia nigra *pars compacta* projecting to the striatum (Ehringer and Hornykiewicz, 1960). Patients with established disease display a 60-80% loss of striatal dopamine in line with the reported loss of SNc neurons (Brooks, 2004). The cause of nigral degeneration in most cases is unknown, but multiple factors, including age, genetic susceptibility and environmental causes are thought to be involved (Fahn and Sulzer, 2004, Samii et al, 2004). PD can be treated effectively for a number of years using dopamine replacement therapy. Patients are often started on dopamine agonists before being given the dopamine precursor L-dopa, the most potent anti-parkinsonian drug. After 5 years, 25-50% of patients (90% of young onset patients) develop motor fluctuations, whereby the individual fluctuates between periods of high and low mobility, often described as on and off states respectively (Samii et al, 2004; Windnell, 2005). In addition, many patients develop dyskinesia over a period of months or years of L-dopa treatment,

which most commonly manifests as chorea during the 'on' state (Samii et al, 2004; Widnell, 2005). The effects of dopamine depletion have been investigated experimentally primarily in two models. In primates, systemic administration of the neurotoxin 1-methyl-4-phenyl-1,2,3,6-tetrahydropyridine (MPTP) causes bilateral, selective loss of nigral cells leading to bradykinesia and akinesia, although rarely tremor (Jenner, 2003). In the rodent model of PD, 6-hydroxydopmine (6-OHDA) is injected unilaterally in to the substantia nigra leading to relatively selective dopaminergic cell loss and a quantifiable motor deficit (Orth and Tabrizi, 2003).

1.3.3 Changes in Firing Rate following basal ganglia disease and lesion

The direct/indirect model predicts specific changes in the direction of rate in each basal ganglia structure following dopamine depletion, but the evidence for these changes is somewhat contradictory. Studies in the primate showed an increase in firing rate in both the STN and GPi after MPTP treatment, supporting the core predictions of the model (Filion and Tremblay, 1991; Wichmann et al, 1994; Bergman et al, 1994). These findings have not been fully supported by more recent studies, where reductions in GPi and SNr firing rate were found to be small or not significant (Wichmann et al, 1999). Other studies in the primate have shown more complex changes in rate, whereby GPi neurons switch from responding to passive movement around single to passive movement around multiple joints, in line with a deficit in action selection (Boraud et al, 2000).

Dopamine lesions in the rat were found to lead to a decrease pallidal activity, but net changes in the rate of endopenducular nucleus neurons were inconsistent compared to changes in pattern (Pan and Walters, 1988; Ruskin et al, 2002). In line with the Albin/Delong model, an increase in STN firing has also been observed, but this was found to be independent of the predicted disinhibition by the GP (Hassani et al, 1996). In cats, the spontaneous firing rate of motor thalamic cells is decreased after MPTP treatment (Schneider and Rothblat, 1996). This supports a correlation between dopamine depletion and loss of output from basal ganglia thalamus to its cortical targets. Reductions in firing rate after MPTP lesion have also been found in the pre-

supplementary and supplementary motor cortical areas, which are involved in movement initiation (Escola et al, 2003).

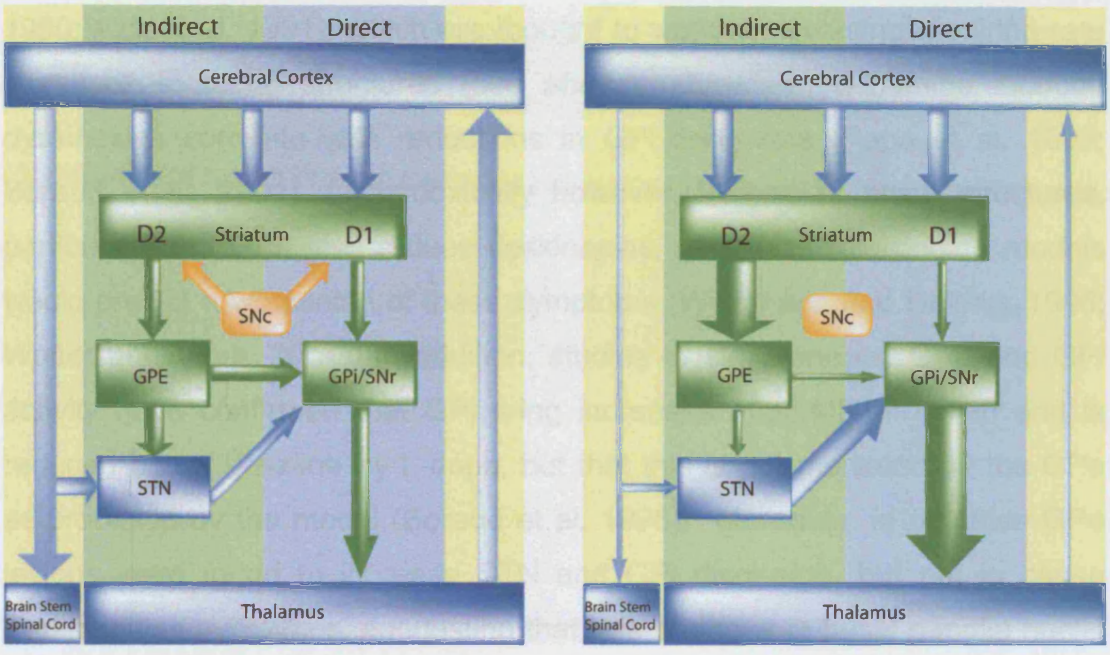

Figure 1.5 Rate coding models of basal ganglia dysfunction. ***A,*** In the healthy basal ganglia, dopamine release mediates the balance between the direct and indirect pathways (see Figure 1.3 for details). ***B,*** In Parkinson's disease, the removal of dopamine neurons in the SNc leads to increase in the firing of striatal neurons in the indirect pathway, usually inhibited by the D2 receptor activation. This leads to increased inhibition of the GPe, and in turn a dishibition of STN, leading to increased excitatory drive to the output nuclei (GPi/SNr). In addition, the striatial neurons in the direct pathway are inhibited due to the loss of activation by D1 receptors, leading to a reduction of their inhibition of the output nuclei. The net effect is increased inhibition of thalamocortical targets, which is hypothesised to cause Parkinsonian motor symptoms.

Evidence for dopamine replacement treatments for Parkinson's disease normalising the changes in firing rates predicted by the model is also mixed. The role of rate increases following dopamine depletion is supported by the amelioration of symptoms following lesions of the STN or GPi (Bergman et al, 1990; Aziz et al, 1991), which are thought to work by reversing the firing rate increases in those structures (see above). Moreover, dopamine induced dyskinesias correlate with reductions in GPi firing rate (Papa et al, 1999; Boraud et al, 2001). Paradoxically however, lesions to these structures, particularly the GPi, also reduce dyskinesias, where as rate coding models would predict a worsening of these symptoms (Wichmann and Delong, 1996; Walter and Vitek, 2004). In addition, studies of simultaneous GPe and GPi activity have confirmed that GPi firing increases after MPTP lesion and is reduced below baseline by L-dopa, but that this is not mediated by the GPe as predicted by the model (Boraud et al, 1998). Moreover, in primates GPe lesions were found to increase STN and GPi discharge, but not to cause Parkinsonian symptoms, suggesting that rate changes in basal ganglia nuclei alone cannot account for the motor symptoms of dopamine depletion (Soares et al, 2004).

1.3.4 Changes in Firing Pattern after dopamine depletion.

Several of the studies, including some of those described above, have reported that the pattern as well as the rate of activity of basal ganglia neurons is altered after dopamine depletion. In the primate after MPTP treatment, the number of pallidal and STN cells displaying bursting and/or oscillatory firing patterns significantly increases (Filion and Tremblay, 1991; Bergman et al, 1994; Wichmann et al, 1999; Raz et al, 2000). A similar propensity toward busting activity has been observed in the endopenducular nucleus, GP and STN of 6-OHDA treated rodents (Kriess et al, 1997; Ruskin et al, 2001). In primates, bursts in pallidal cells can be synchronous with MPTP induced tremor but the relationship between the two oscillations is dynamic (Raz et al, 2000). In addition to an increase in oscillatory activity, the synchronisation between pallidal cell pairs increases from around 5% to around 40% after MPTP treatment (Nini et al, 1995; Raz et al, 2000). An in

depth study of pallidal neurons in the healthy primate revealed that even in neighbouring neurons firing was very rarely correlated (Bar-Gad et al, 2003).

A similar increase in synchrony after MPTP treatment is seen in the synchronisation between pallidal cells and striatal TANs (Raz et al, 2001). In line with these subcortical results, MPTP-treatment causes a significant increase in synchrony between motor cortical neurons, completely independent of changes in mean firing rate (Goldberg et al, 2002). Administration of L-Dopa to MPTP treated monkeys almost completely reversed synchronisation between pallidal cells pairs to normal levels but also reduced the firing rate in both the GPi and GPe (Heimer et al, 2002). The effect of dopamine depletion on the pattern of neuronal activity will be discussed further below.

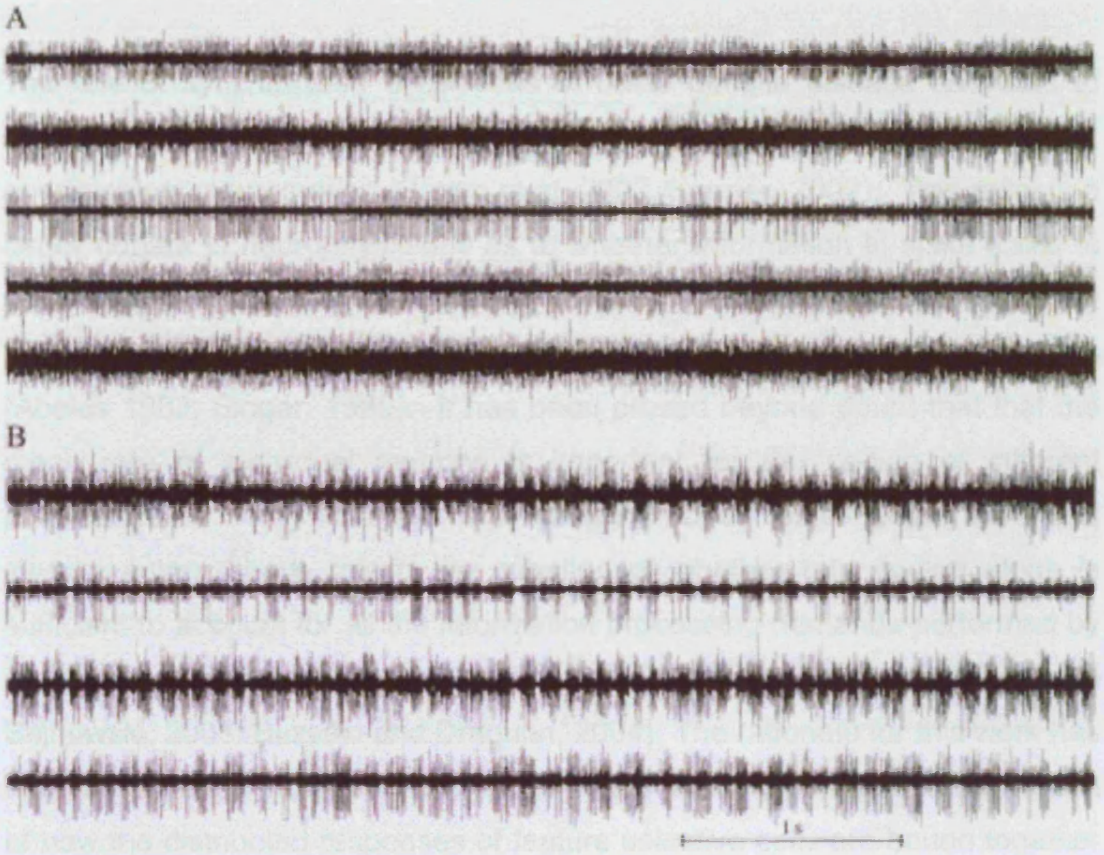

Figure 1.6 Changes in firing pattern after MPTP treatment in the monkey. ***A***, Recording of several units in the globus pallidus of a normal monkey. All units display high frequency, tonic firing which is unsynchronised across neurons. ***B***, Pallidal units in an MPTP treated monkey. Neurons display periodic bursting activity that is synchronised across units, which is not seen in the normal monkey (Taken from Raz et al, 2000).

1.4 Synchronisation, Oscillations and Temporal Coding in the Brain

The role of synchronised oscillations in basal ganglia disease has lead to speculation that they could be a pathological exaggeration of a functional, physiological phenomenon (Brown et al, 2003, Farmer, 2002). This reflects a larger debate in neurophysiology as to whether information in spike trains is coded primarily by noisy rate coding (Shadlen and Newsome, 1994) or by precise temporal relations between spikes in single or multiple channels (Abeles 1982; Singer, 1999). It has been proved beyond doubt that that the mean rate of individual neurons is important for the coding of different parameters in many different brain areas. Over recent years however, several authors have raised the question of whether rate coding alone is sufficient to account for all the information processing demands performed by neuronal networks (Singer, 1994; 1999; Bullock, 1997; Salinas and Sejnowski, 2001; Buzsáki and Draguhn, 2004). The rationale for this work has often been based around solving the so-called "binding problem;" the question of how the distributed responses of feature selective cells are bound together (Singer, 1994). The binding problem is most clearly illustrated when related to the sensory systems, where the perception of objects and events as being contiguous in space and time must involve neurons in different information streams. The most common view of how this problem is overcome is through "binding by convergence," whereby the axons carrying responses of feature specific cells converge on to a common target cell. At the level of processing, neurons would then be tuned to respond to a specific conjunction of afferent inputs, leading to greater feature specificity as the hierachy ascends (Singer,1999). This strategy certainly exists (Shadlen and Newsome, 1994), however it is expensive in terms of the number of cells needed to code for the infinite number of perceptual possibilities in the external environment that would need to be encoded by feature specific neurons (often described as the combinatorial explosion). Alternatively, it has been proposed that neurons which are synchronised in different processing streams could encode for one object, while remaining desynchronised from neurons responding to different objects (Singer, 1994; 1999; Nowak and Bullier, 2000). Any one neuron therefore can take part in different synchronous assemblies in response to

different stimuli and encode for different objects. The advantage of such a mechanism is that it removes ambiguity of response for a network of broadly tuned neurons, such as the cerebral cortex, while maintaining an inexhaustible processing capacity (Singer, 1999). This combination of properties is just as relevant in the sensory-motor system, where the number of sensory representations and motor programs that need to be associated is potentially massive (Roelfsema et al, 1997; Farmer, 1998).

The development of large scale recording systems, which are capable of recording hundreds or even thousands of individual neurons simultaneously, is increasingly moving the debate over rate versus temporal coding into the practical rather than theoretical domain (Buzsaki, 2004). The utilisation of temporal relationships is thought to involve populations or ensembles of neurons. To this end, the use of local field potential (LFP) recordings, which are thought to reflect the activity of large numbers of neurons simultaneously, has become an increasingly important tool (Bullock, 1997). Before discussing the relevance of these theories to the cortico-basal ganglia circuits, it is important to discuss the different types of synchronisation and temporal coding, and their utilisation in other brain areas.

1.4.1 Definitions, origins and the detection of synchronisation in the neural structures

The putative role of temporal coding in neural structures hinges on two central questions: whether neurons display synchronisation and whether this synchronisation is utilised to carry information. Defined most broadly, neurons or populations of neurons can be considered to display synchronisation if their electrical elements (spike trains, synaptic potentials and membrane potentials) share a common time or are time locked. This can encompass several detectable behaviours in neural circuits. Firstly, stochastic (non-rhythmic) elements can be synchronised in the time domain. This, non-oscillatory synchronisation is considered mostly for the action potentials of two or more individual neurons. Secondly, the electrical activities of oscillating neurons can be synchronised. This category of oscillatory synchronisation can be further subdivided. The membrane potentials or

action potentials of individual neurons can be phase locked to the same oscillation, whether through direct modulation of each other or through a common source. Although a single oscillating neuron gives no information about synchrony, a single oscillating population signal (such as a local field potential, see below) implies that the local electrical elements in a group of cells must be synchronised to produce that oscillation. Finally, two oscillating populations of cells can also be time locked, implying large scale synchronisation.

All of these neuronal behaviours have been proposed by some to carry information (Abeles, 1982: Singer et al, 1994; 1999; Bullock, 1997) and by others to be epiphenomena (Shadlen and Newsome, 1994; Shadlen and Movshon, 1999). In addition there is some disagreement as to what constitutes true synchronisation. When synchronisation occurs over a long time scale, where the correlation peak is broader than the average interspike interval of the two cells, the synchrony is often described as being due to covariations in firing rate and not purely temporal (Singer, 1999). In this case the temporal correlation is sometimes referred to as a noise correlation (Averbeck and Lee, 2004). It is clear however in many of these cases, such as slow oscillations in sleep, that synchronisation under these circumstances can have behavioural consequences and, therefore, must be involved in information processing (Steriade, 2000). In this section, all levels of synchronisation, as defined as temporal locking of neuronal elements, will be reviewed in relation to their detection, their underlying mechanisms and how they might contribute to information processing in neuronal networks.

1.4.2 Detecting synchronisation between single neurons.

The most common method of looking at synchronisation between the spike trains of two neurons (A and B) is the cross correlation histogram (CCH), which provides an estimate of the probability that neuron B will fire as a function of the time, before or since, a spike was fired by neuron A. The possible results of a CCH computed between two tonically firing neurons are shown in Figure 1.7. If the firing of the neuron A is not predictive of a spike in

neuron B the CCH will be flat, reflecting the independent nature of the two point processes. A sharp peak, displaced in relation to zero, indicates a possible monosynaptic connection between the two cells. If this is the case, the time interval from zero indicates the sum of the axon conduction and synaptic delay. A peak around zero in the CCH indicates that both cells are being driven from a common, third neuron at equal axonal and synaptic delays causing them to fire synchronously (Nowak and Bullier,2000). This situation can also arise through both neurons firing in response to a common stimulus. It was originally hoped that CCHs would allow the tracing of neuronal connections in vivo. The interpretation of CCHs however is too complex for this to be possible, mostly due to the influence of the local population of neurons on the ability of neuron A to elicit a single spike in neuron B (Nowak and Bullier, 2000; Ursrey, 2002). In the many brain areas (including the cerebral cortex and striatum, see Figure 1.3), sparse anatomical connectivity and week synaptic connections dictate that for one neuron to cause a spike in another, the membrane potential of the neuron B must be near threshold. If the activity in the population of neurons is low, the membrane potential in neuron B will not be high enough for neuron a to push it above threshold. Thus, a flat CCH may not necessarily indicate that two neurons are unconnected and the height of a peak will not indicate synaptic strength, as the population of neurons will contribute to the likelihood of firing.

The main use of CCHs has therefore moved to investigating functional connectivity between neurons during specific behaviour. To this end, post stimulation histograms (PSTHs) can be used to estimate the CCH averaged around a repeated motor task or external sensory event. However, spurious correlations can arise due to event related increases in firing rate in the two neurons (Villa, 2000; Brown et al, 2004a; Averbeck and Lee, 2004). Such correlations, labelled "noise correlations" by some authors, can be removed using the shift predictor method. For the shift predictor, the PSTHs computed between the two neurons recorded on separate trials are subtracted from the PSTH from the same trial, removing rate based correlations (Nowak and Bullier, 2000). Noise correlations may also have a role to play information processing (Averbeck and Lee, 2004).

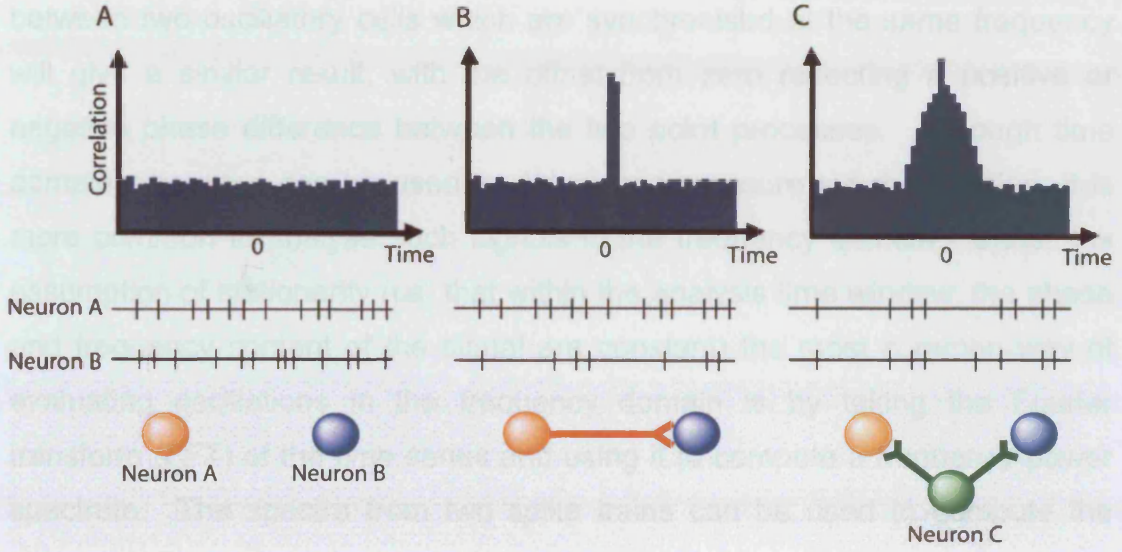

Figure 1.7 Detecting neuronal synchronisation. Synchronisation between the firing patterns of single neurons is most commonly detected using the cross correlation histogram (CCH) ***A***, A flat CCH indicates the firing of two neurons is completely independent ***B***, A sharp peak indicates a monosynaptic connection between two neurons. The displacement of the peak from zero is equal to the sum of the axonal and synaptic delay. ***C,*** A broad peak around zero indicates that the two neurons are being driven by a common third neuron.

1.4.3 Oscillations and synchronisation at the single neuronal level.

Oscillatory activity in and between single neurons can also be detected using the correlation techniques described above. An autocorrelogram (essentially a CCH where the cells spike train is both the input and the reference) of an oscillatory cell will show a series of peaks centred around zero, the intervals of which will reflect the period of the oscillation (See Figure 1.8). A CCH between two oscillatory cells which are synchronised at the same frequency will give a similar result, with the offset from zero reflecting a positive or negative phase difference between the two point processes. Although time domain measures can be used to detect and measure synchronisation, it is more common to analyse such signals in the frequency domain. Under the assumption of stationarity (i.e. that within the analysis time window, the phase and frequency content of the signal are constant) the most common way of evaluating oscillations in the frequency domain is by taking the Fourier transform (FFT) of the time series and using it to compute a frequency power spectrum. The spectra from two spike trains can be used to compute the cross spectrum or coherence (the normalised cross spectrum) - giving a measure of linear dependence between the two series in each frequency band. It is also possible that single neurons could show no individual synchronisation, while still contributing to oscillatory population synchrony (see Figure 1.8). In this case neither time domain nor frequency domain measures at the single neuronal level will reveal the synchronisation present at the level of the population. Details of frequency analysis methods can be found in Chapter 2.

1.4.4 Population Synchronisation: EEG, MEG and Local Field Potentials

Electroencephalography (EEG) measures the activity of a population of neurons as a change of potential at the surface of the skull. The closely related ECoG signal is essentially an invasive EEG signal measured above or below the dura, reducing the noise and filtering effects created by the skull. In humans, non-invasive recordings can also be made using magneto-encephalography (MEG), which records changes in the magnetic field rather than the voltage. MEG has several advantages over EEG in that it is reference free, records the magnetic field directly and records many different locations simultaneously (Niedermeyer and Lopes da Silva, 2005). Local field potentials (LFPs) are recorded using the same principal as EEG except that an electrode is placed directly into the brain tissue. LFP recordings therefore consist of summed electrical activity in the vicinity of the electrode, but are free of the signal filtering and distortion present in EEG (Niedermeyer and Lopes da Silva, 2005). LFP recordings have mostly been made in laminar structures (cerebral cortex and hippocampus) but are increasingly used in deeper, non-laminar structures. If a non-laminar arrangement of neurons leads to local, synchronous, electrical events "cancelling each other out," then the field potential should be featureless. LFPs recorded from the thalamus, basal ganglia and brainstem however all display oscillatory activity, albiet around 1/3 smaller than that seen at the cortex, suggesting that a strictly laminar arrangement of neuronal processes is not necessary to produce oscillatory activity that can be measured in the field potential (Niedermeyer and Lopes da Silva, 2005). LFPs have mostly been recorded in animal preparations, but surgical intervention for epilepsy, Parkinson's disease, dystonia and essential tremor have also allowed limited recordings in the cortex, hippocampus, cerebellum and basal ganglia of humans (Engel et al, 2005).

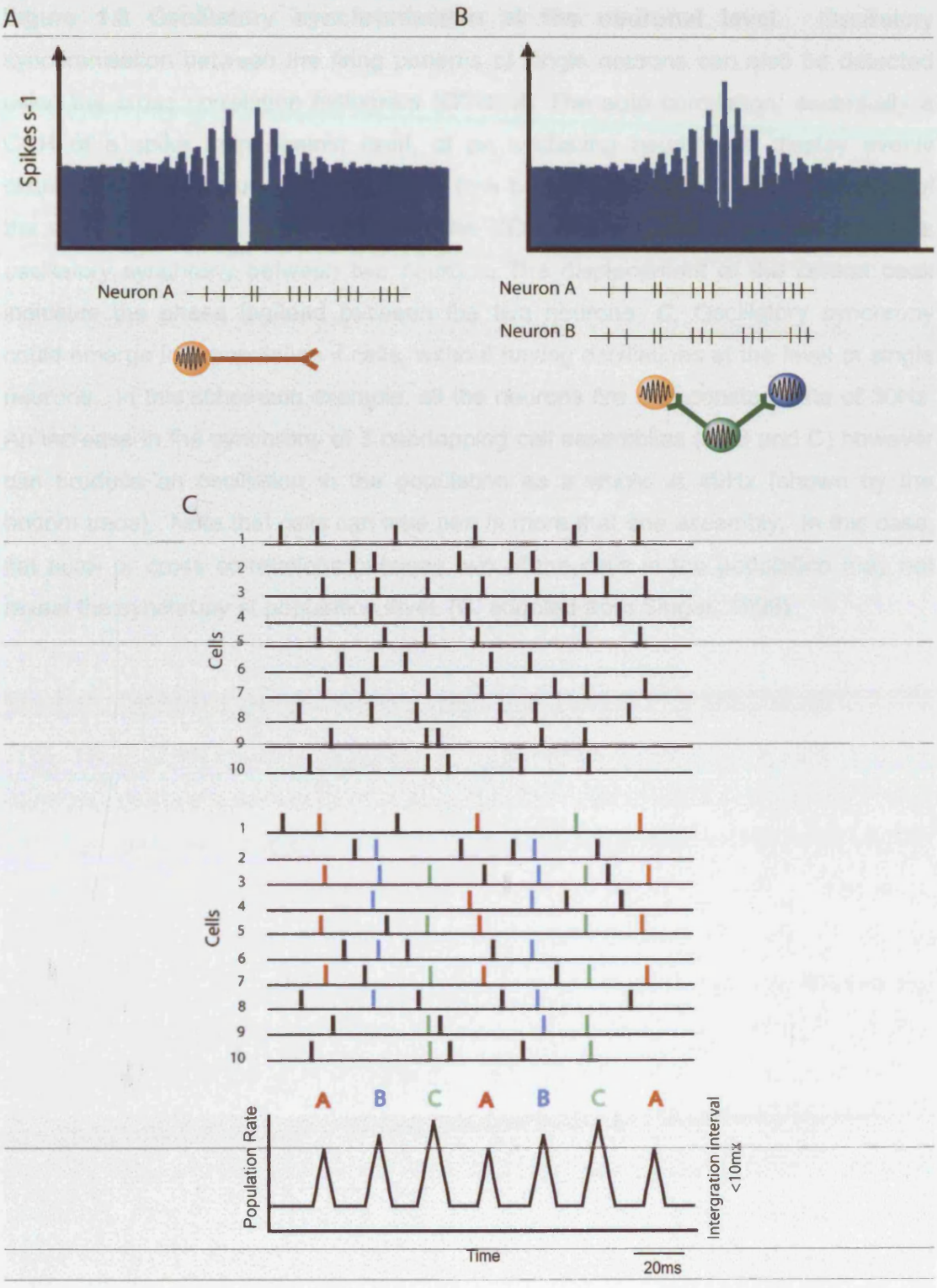
A
B
Spikes s-1
Neuron A
Neuron A
Neuron B
C
Cells
1
2
3
4
5
6
7
8
9
10
Cells
1
2
3
4
5
6
7
8
9
10
A B C A B C A
Population Rate
Intergration interval
<10ms
Time
20ms

Figure 1.8 Oscillatory synchronisation at the neuronal level. Oscillatory synchronisation between the firing patterns of single neurons can also be detected using the cross correlation histogram (CCH) ***A***, The auto correlation, essentially a CCH of a spike train against itself, of an oscillating neuron will display evenly distributed peaks around time zero. The time between peaks indicates the period of the oscillation. ***B,*** A similar result in the CCH between two processes indicates oscillatory synchrony between two neurons. The displacement of the central peak indicates the phase lag/lead between the two neurons. ***C***, Oscillatory synchrony could emerge in a population if cells, without having oscillations at the level of single neurons. In this schematic example, all the neurons fire at a constant rate of 30Hz. An increase in the synchrony of 3 overlapping cell assemblies (A, B and C) however can produce an oscillation in the population as a whole at 40Hz (shown by the bottom trace). Note that cells can take part in more that one assembly, In this case, flat auto- or cross correlations between two of the cells in the population may not reveal the synchrony at population level. (**C**, adapted from Singer, 1999)

1.4.5 Cellular basis of EEG, MEG and LFPs

Population activity, as recorded by the means described above, is the result of a complex interplay between the ionic currents of nerve cells and the cellular architecture of neuronal structures. The primary generators of the surface EEG signal are synaptic currents in the dendrites of pyramidal cells (see Figure 1.9). The polarity of the currents (EPSPs or IPSPs) and the layer in which these currents are initiated cause positive and negative deflections in the EEG (Kandel and Schwarz, 2000). The summation of these currents across a population of neurons will lead to an average positive or negative deflection at a given period of time. There is good evidence that the LFP activity recorded in the cortex is representative of aggregate or synchronous activity in local neuronal populations (Baker et al. 1997; Creutzfeldt et al. 1966; Donoghue et al. 1998; Frost 1968; Mitzdorf 1985; Murthy and Fetz 1992, 1996a; Steriade, 2000).

1.4.6 Oscillatory features in EEG, MEG and Local Field Potentials

EEG, MEG and LFP recordings from the cerebral cortex of both humans and animals contain numerous oscillations that are highly correlated with behavioural state. Oscillations with periods ranging from 2-120s have been recorded in animal preparations (Penttonen and Buzsaki, 2003). Ultra slow oscillations have been recorded in humans with periods as long as 20-30s seconds (Achermann and Boberely, 1997). Very slow oscillations may group and organise higher frequency activities (Penttonen and Buzsaki, 2003; Bullock, 1997). Slow (1Hz), delta (0.1-3.5) and spindle (around 12-18Hz in humans) oscillations occur in sleep and anaesthesia and are arranged in to K-complexes, consisting of a surface positive wave followed by a spindle sequence, which are a major element of sleep rhythms (Steriade, 2000). Theta (3-10Hz) oscillations are seen predominantly in the hippocampus and related structures, with the precise frequency varying with species and activation state (Penttonen and Buzsaki, 2003).

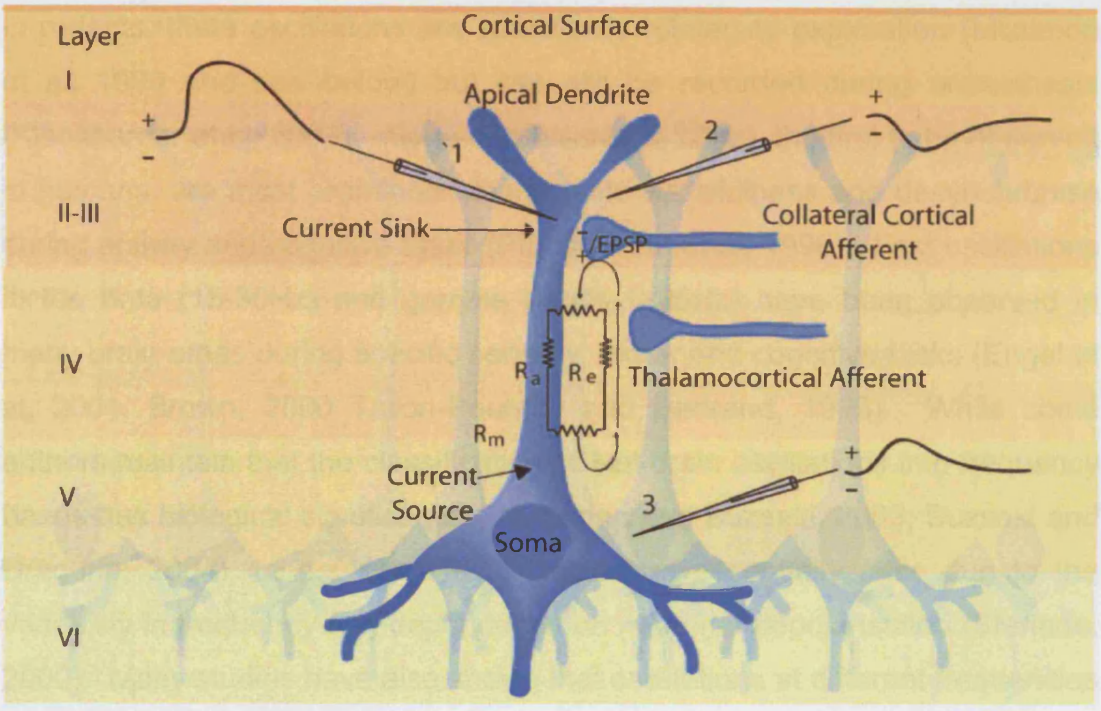

Figure 1.9 Biophysical Basis of EEG and LFPs in the Cerebral Cortex. The apical dendrites of pyramidal cells in the cerebral cortex are orientated perpendicular to the cortical surface and receive a variety of synaptic inputs. When an EPSP is elicited on the apical dendrite, current flows into the dendrite creating a current sink. In turn, the flow of current along the dendrite and back across the membrane at other sites creates a current source. The electrical resistance of the cell membrane (R_m) greatly exceeds that of the extracellular fluid (R_e), leading to a larger voltage deflection at the intracellular electrode (1) than the extracellular electrodes (2,3). At the site of current generation, the flow of current away from the extracellular electrode (2) leads to a negative deflection in voltage. These changes in current flow, across many neurons, due to synaptic currents are the basis of both the EEG and ECoG (Adapted from Kandel and Schwarz, 2000).

In rodents, theta oscillations are specifically related to exploration (Mizumori et al, 1990 and see below) but can still be recorded during anaesthesia (Klausberger et al, 2003). Alpha oscillations (8-12Hz), the first to be observed in humans, are most prominent during quite wakefulness and desynchronise during activity and cognitive tasks (Pfurtscheller et al, 1996). Fast oscillations in the beta (15-30Hz) and gamma bands (>35Hz) have been observed in many brain areas during specific sensory, motor and cognitive tasks (Engel et al, 2001; Brown, 2000 Tallon-Baundry and Bertrand, 1999). While some authors maintain that the classification of fast brain oscillations into frequency bands has biological significance (Penttonen and Buzsaki, 2003; Buzsaki and Draguhn, 2004), others see the distinction as essentially false due to the variability in frequency and dependence on neuronal depolarisation (Steriade, 2000). Many studies have also shown that oscillations at different frequencies are highly interrelated (Steriade, 2000; Penttonen and Buzsaki, 2003)

Aim 2: To use frequency based analysis of multi-site LFP recordings to investigate functional connectivity between the cortex and basal ganglia.

1.4.7 Cellular Mechanisms underlying network oscillations.

It has become clear that the brain rhythms described above are the result of a complex interplay of different populations of cells, often with their own oscillatory properties, that work together as a network. Mechanistically, the best-characterised oscillations are the slow oscillations generated by the thalamocortical networks. The cortical sheet has reciprocal connections with both the dorsal thalamic nuclei and the reticular nucleus of the thalamus (RE); a highly interconnected group of GABAergic neurons projecting to the relay nuclei. Slow wave (~1Hz) and spindle (~10Hz) activities are widespread in the thalamus and cortex during both deep sleep and anaesthesia (Conteras et al, 1995). Slow oscillations are highly coherent within the thalamus and

cortex, both at the neuronal and field potential level (Steriade 2000; 2001). The slow oscillation is of cortical origin, as evinced by its persistence after thalacotomy and absence in the thalamus after cortical deafferentation. Spindle oscillations on the other hand originate in the thalamus, specifically the RE, disconnection of which leads to the disappearance of the oscillation in thalamocortical cells (Conteras et al, 1996). The slow oscillation is generated by a complex interplay between intrinsic membrane currents and synaptic currents, which leads to a cyclic prolonged depolarisation and hyperpolarisation of cortical neurons. Slow oscillations however are also dependent on recurrent intracortical networks, which allow rapid synchronisation of the oscillation across large areas of thalamus and cortex. After decortication, spindle oscillations are still present in the thalamus, but the coincidence time across thalamic sites is disrupted (Conteras et al, 1997). This is due to the slow oscillations grouping the spindle oscillations by providing conditions under which the RE cells burst synchronously. The two oscillations are grouped into K-complexes, whereby each cortical slow oscillation leads to a series of thalamically generated spindle oscillations (Steriade 2000; 2001). Part of the delta oscillation (1-4Hz) is a result of the shape and duration of K-complexes. The slow oscillations, as seen in an intact brain, are therefore the result of a complex interaction between several ionic, synaptic and anatomical mechanisms throughout the network. In addition, fast oscillations (alpha, beta and gamma bands) are also seen during sleep and anaesthesia (Malony 1997; Steriade, 2000). During these states higher frequency rhythms are not continuous, as in the awake animal, but occur during the periods of depolarisation caused by the slow oscillations (Steriade, 2000, 2001).

The mechanism behind higher frequency oscillations is less well understood. A group of morphologically distinct pyramidal neurons that generate bursts at 5-15Hz, depending on stimulus intensity, have been recorded in the somatosensory and visual cortices of several species (Conners and Amitai, 1997). Another group of pyramidal neurons, often described as "chattering cells", produce bursts at 20-80Hz with inter-burst frequencies of up to 800Hz (Gray and McCormick, 1996). Investigations in cortical and hippocampal slice

preparations suggest that interconnected networks of fast spiking GABAergic interneurons are known to be important in the production of gamma oscillations (Traub et al, 1996). The precise time at which the projection neuron can fire action potentials will then be determined by this inhibitory oscillation (Lytton and Sejnowski, 1991), which could provide an important gating mechanism in neuronal processing. It has also been proposed that "induced" gamma oscillations recorded in EEG may be due to ring shaped distributions of dipoles, creating an LFP that does not reverse through the cortical depth (Tallon-Baudry and Bertrand, 1999).

1.4.8 Cellular mechanisms underlying the utilisation for synchrony in information coding

A key question as to whether any type of synchronisation is utilised in information processing is if individual neuronal networks possess the necessary equipment to utilise a temporal code. Central to the argument for the predominance of rate over temporal coding in the nervous system is the claim that the biophysical properties of neuron's and cerebral architecture are unsuited to temporal coding (Shadlen and Newsome, 1994; Shadlen and Movshon, 1999). The question of suitability of physical properties centres on the neurons membrane time constant; the timescale on which the voltage of the cell membrane can change as determined by its resistance and capacitance. A small time constant means the voltage can change rapidly.

For synchronous inputs to convey an advantage, neurons have to act as coincidence detectors, whereby the membrane constant must be small enough to confer an advantage on two or more inputs arriving within a short time window (Abeles et al, 1982). Although it has been convincingly shown that the neurons in the auditory brain stem can detect multiple inputs on a millisecond scale (Agmon-Snir et al, 1998), it has been argued that most neurons lack the electrophysiological properties to perform this type of computation (Reyes and Fetz, 1993; Reyes et al, 1996; Shadlen and Movshon, 1999). In vitro experiments however have shown that synchronous inputs increase postsynaptic output in hippocampal networks (Stevens and Zador, 1998), as have in vivo recordings in monkey motor cortex (Matsumura

et al, 1996). Numerous studies have shown that the computational properties of dendrites are highly non-linear due to a combination of structural and electrical properties (Singer, 1999, Salinas and Sejnowski, 2001). Moreover, the dendritic tree may not act as a whole, but integrate synaptic inputs locally, which would also increase computational capacity (Salinas and Sejnowski, 2001). In addition, synaptic currents can be boosted by voltage dependent currents, which could lead to supra-linear summation of synchronous or near synchronous inputs (Magee, 2000). In addition, the effect of correlated inputs is partly determined by the balance of excitatory and inhibitory afferents, with a balanced neuron being more sensitive to correlated input (Azouz and Gray, 2003). There is also evidence that some networks of cells in the cerebral cortex are connected by gap junctions, which could allow rapid detection and propagation of synchronous inputs (Galaretta and Hestrin, 1999).

The role of anatomical connectivity in producing/responding to correlated inputs adds further complexity to the issue. It has been claimed by some authors that the re-entrant architecture of the cortex favours a role for synchrony in thalamo-cortical processing (Sporns et al, 2000a; 2000b). Others maintain that the sparse connectivity between neurons is likely to make correlations ineffectual at driving postsynaptic output, while dense connectivity, as seen in cortical columns, will make correlations inevitable, but not necessarily meaningful (Shadlen and Movshon, 1999). Accordingly, investigations in sensory cortices, comparing information carried in the rate and temporal relations of neuronal populations, have suggested that only a small amount of information is represented by temporal coding (Aggelopoulos et al, 2005).

In conclusion the ability of a neuron to utilise correlated synaptic inputs is likely to be dependent on the biophysical properties of its dendritic tree, the structure of its synaptic inputs, the inhibitory/excitatory balance of those inputs and the cellular architecture in which it is embedded. There is evidence both for and against these conditions favouring temporal coding. Neurons may therefore be sensitive to and utilise correlations under some conditions but not others.

1.5 Temporal coding and behaviour

Many investigators have attempted to link the neuronal activities described above with behaviour. These studies can be roughly divided into two groups: 1) those that have correlated oscillatory activity with sensory and motor tasks and 2) those that have uncovered causal links between the temporal relations between neurons and the encoding of specific parameters.

1.5.1 Correlations between oscillations and behaviour

The vast majority of studies into a possible role for oscillations in neural processing have investigated the responses of single neuronal and population oscillations to sensory events. Oscillations related to sensory stimuli are divided in to those that are directly evoked by the stimulus and those that are internally generated or "induced" (Singer, 1999; Tallon-Baudry and Bertrand, 1999). Neurons in the cat and monkey visual cortex can follow high frequency oscillatory stimuli across several synapses, suggesting sensory neurons are capable of coding with high temporal precision (Singer, 1999). Binocular rivalry experiments in humans and cats have shown that synchronisation in visual areas and perception is highly correlated (Fries et al, 1997; Tononi and Edelman, 1998). Induced or internally generated oscillations, particularly in the gamma range (30-80Hz) are thought to be involved in attentional or "top down" sensory processing (Engel et al, 2001; Tallon-Baudry and Bertrand, 1999; Tononi and Edelman, 1998). In the primate, expectation related neuronal synchrony has been shown to be task dependent and independent of arousal (Fries et al, 2001a; 2001b). In addition there are many humans studies showing increased gamma responses during sensory tasks in humans (Engel, 2001; Tallon-Baudry and Bertrand, 1999). LFPs from different cortical areas (visual, parietal and motor) also show task dependent synchronisation with zero time lag, (Roelfsema et al, 1997; Von Stein et al, 2000) supporting the hypothesis that oscillations could bind disparate networks. Intracellular recordings from primate motor cortical neurons suggest that gamma synchronisation at both the unit and field potential levels are due to sub-threshold currents, which are synchronised across neurons (Lampl and Yarom, 1993).

In the motor system of humans and primates, prominent oscillations at a range of frequencies can be detected at all levels including cortex, basal ganglia, cerebellum and muscle (Farmer, 1998; Brown, 2000). In the motor cortex, cell pairs exhibiting synchronisation are significantly more likely to share muscle field, as determined by EMG, strongly suggesting a role for synchronisation in motor control (Jackson et al, 2003). Oscillations at beta frequency (15-30Hz) have been observed in motor cortical EEG, MEG, LFPs and contralateral EMG during sustained muscle contraction in humans and primates (Conway et al, 1995; Salanius et al, 1997; Baker et al, 1997). An increase in beta oscillation is also seen in response to movement cues and may therefore be related to movement preparation rather than movement itself (Sanes and Donoghue, 1993; Cassidy et al, 2002a). Higher frequency oscillations could therefore have an attentional role in the motor system analogous to that of the sensory system (Brown and Marsden, 1998). Directional analysis of multiple local field potentials in the sensory and motor cortices suggests that beta oscillations are involved in binding large-scale networks during motor behaviour (Brovelli et al, 2004). Modulation of gamma oscillations has also been observed in local field potentials in primates performing self paced grasping movements or visually guided reaching tasks (Murthy and Fetz, 1996a; 1996b). Modulations of alpha and beta frequency in human EEG related to different aspects of motor tasks have been extensively described (Neuper and Pfurtscheller, 2001).

In the hippocampus, oscillatory activity has been correlated with spatial memory related behaviour (O'Keefe, 1993). Field potential recordings from the hippocampus of humans, cats, rats and dogs reveal a prominent theta (4-8Hz) oscillation that is synchronised across the structure (O'Keefe and Burgess, 1999). In the rat, where theta has been best characterised, there are two types of theta rhythm. The first is directly coupled to the motor system and occurs during movement and exploration; the second is acetylcholine dependent and can occur independently of movement (O'Keefe and Burgess, 1999). Gamma oscillations (30-100Hz) are also prominent in the hippocampus and are modulated by theta activity and related behaviours (Csicsvari et al, 2003a). The mechanism of place coding mediated by

population oscillations is considered in detail below. In addition there are short bursts of higher frequency rhythms (120-200Hz) called ripples. Ripples occur mostly outside of the theta activity and are thought to mediate memory consolidation by "replaying" firing patterns that occur during exploration and optimise conditions for synaptic plasticity (Chrobak and Buzsaki, 1996)

1.5.2 Mechanistic evidence for temporal coding

Only a handful of studies have provided more than correlative evidence for the role of synchronised oscillations in neural processing. Within this group of studies the way in which the temporal qualities of the signal are utilised varies, but is always independent of a rate code (VanRullen et al, 2005).

Firstly, single neurons can code information by using the relation of their spikes to a global signal. In the hippocampus, place cells fire only when the animal is in a specific location in its environment or place fields (O'Keefe, 1993). The theta rhythm (see above) is synchronised across the hippocampus and its associated structures, binding them into a single processing module and providing systematic temporal relations for the firing of hippocampal pyramidal cells, irrespective of their anatomical location (O'Keefe and Burgess, 1999). In addition, as the animal moves through the place field, the spikes of a single place cell change their position in relation to the phase of the theta cycle (O'Keefe and Reece, 1993). This "phase progression" is highly predictive of the animal's position in the place field and is independent of rate coding.

A similar population phenomenon has been observed in the olfactory system of the locust (MacLeod et al, 1998; Lauren, 2002). The primary olfactory structure in locusts, equivalent to the olfactory bulb in mammals, is the so-called the antennal lobe and receives input from olfactory receptor neurons. Projection neurons in the antennal lobe send afferents to two downstream structures; the mushroom body and the lateral horn, which are connected by inhibitory projections from the lateral horn to the mushroom body (Lauren, 2002). The presentation of odours leads to synchronised oscillations at 20-

30Hz in the antennal lobe that are dependent on interconnected interneurons (Stopfer et al, 1997). Fast LFP oscillations at β-frequency arise from many antennal lobe spikes, only a fraction of which may be attached to a single cycle (Lauren, 2002). The same 20-30Hz oscillations can be recorded in the LFP of both the mushroom body and lateral horn, allowing the synchronisation of cells in all three structures to the same reference signal (Stopfer et al, 1997). The inhibitory neurons in the lateral horn fire around half a cycle later than the antennal lobe neurons. Both project to the Kenyon cells of the mushroom body, leading to post-synaptic EPSPs from the antennal cells half a cycle later by IPSPs from the lateral horn. This relationship creates a small time window in each cycle in which the Kenyon cells can intergrate the phase locked inputs from the antennal lobe (Perez-Orive et al, 2002). The Kenyon cells therefore act as coincidence detectors (see above), with the cycles of the fast oscillation providing a very short integration window, and will only respond when they receive all or most of their inputs (Lauren, 2002). Interruption of the fast oscillations, without affecting slow responses, using the GABAergic antagonist picrotoxin, disrupts odour discrimination (Perez-Orive et al, 2002). In both the hippocampus and the insect olfactory system the local field potential therefore provides the global reference signal. The locust olfactory system also utilises non-oscillatory synchrony for odour discrimination (Christensen et al, 2003).

Alternatively, sensory systems may utilise "first spike latency" rather than mean firing rate for information coding (VanRullen et al, 2005). The use of spike timing on the millisecond scale has been described in the auditory cortex of mammals for coding information on sound location (Alonso et al, 1996). A recent example of this mechanism was shown in different afferents in the human medial nerve of the upper arm during stimulation of the fingertip of varying force and shape. The first spike latency in these afferents yielded a reliable directional tuning curve that in two afferents did not correspond to that of firing rate (Johansson and Birznieks, 2004). Spike time and rate codes were therefore independent, but the temporal coding was 10-20ms faster. In these examples the reference signal is external but sensory systems could also use internal reference signals such as field potentials (VanRullen et al,

2005), which have been proposed by some authors to be a possible substrate for "top down" or Gestalt processing in sensory systems (Engel et al, 2001).

1.6 Oscillations in the Basal Ganglia

Compared to the cerebral cortex and hippocampus, the study of oscillations in cortico-basal ganglia circuits is in its infancy. As described above however the changes in rhythmicity seen following dopamine depletion have increased interest in such investigations. Recordings both *in vivo* and *in vitro* suggest that synchronised oscillations may play an important role in the organisation and function of these areas under both normal and pathological conditions.

1.6.1 Oscillations in the Healthy Basal Ganglia

The striatum displays rhythmic qualities at the level of subthreshold membrane potentials, single units and local field potentials. In anaesthetised animals, striatal medium spiny neurons display bistable membrane potentials (Stern et al, 1997), fluctuating between a depolarised "up state" and a hyperpolarised "down state" that are separated by 15-30mV. MSNs are more likely to fire in the up state, which is 3-5mV below the firing threshold. Cross-correlograms of the membrane potentials of spiny neurons show broad periodicity of around 1Hz corresponding to the up/down state transitions, where as the individual spikes remain asynchronous (Stern et al, 1998). In the ventral striatum the up states of MSNs are synchronous with the negative shifts in the local field potential, suggesting they represent the subthreshold oscillatory activity in the local population (Goto and O'Donnell, 2002). Striatal neurons therefore display population coherence at the subthreshold level, but retain the ability to display fine temporal patterns in their output. In the awake, behaving primate, oscillations at around 20Hz are seen in the striatal field potential that display zero phase lag across the structure (Courtemanche et al, 2004).

There is much evidence to suggest that the STN and the GPe have rhythmic properties and it has been suggested that these structures could act as a pacemaker for the cortico-basal ganglia networks (Plenz and Kitai, 1999; Bevan et al, 2002a). STN neurons display rhythmic activity even when isolated due to their intrinsic membrane properties. In slice preparations, STN neurons fire spikes in either tonic or bursting modes (Bevan et al, 2002a).

Tonic firing is independent of synaptic input and is the mode of STN discharge in the absence of afferent activity (Bevan et al, 2002a; Beurrier et al, 2000). A voltage gated, persistent sodium current, combined with a pacemaker depolarisation that brings the neuron back to firing threshold following the after-spike depolarisation, is known to be the mechanism behind this firing pattern (Beurrier et al, 2000). In contrast, burst firing is controlled by voltage dependent calcium currents and is sensitive to synaptic input (Song et al, 2000; Bevan et al, 2002b). Where as the electrophysiological properties of STN neurons are ubiquitous throughout the structure, in the GP there are several subtypes of neurons, which exhibit different morphological and electrophysiological characteristics (Stanford, 2003). Some of these neuronal subtypes also produce oscillatory activity in isolation (Stanford, 2003).

More complex oscillatory dynamics have been observed when the structures have been recorded simultaneously or by mimicking afferent input using electrophysiological or pharmacological means. Large, GPe mediated, IPSPs can reset the spontaneous STN oscillation, which is likely to lead to synchronisation (Bevan et al, 2002a), whereas smaller IPSPs lead to phase independent delays that could cause desynchronisation. Multiple IPSPs however can either inhibit the tonic STN output, or restore it through the initiation of a rebound depolarisation, via the activation of hyperpolarisation activated calcium currents, which can also lead to bursting activity (Bevan et al, 2002b). The effect of afferent pallidal input on STN neurons is highly non-linear and influenced not simply by rate but pattern of input and the polarisation of STN neurons, which will be determined by other afferent and neuromodulatory inputs (Bevan et al, 2002a; 2002b). However, studies using organotypic cell cultures have demonstrated that the STN and GPe cells can still produce oscillatory network activity when isolated from their major afferent inputs (Plenz and Kitai, 1999). Computer simulations of the STN/GPe network, based on both anatomical connectivity and ionic properties, have produced similar results (Terman et al, 2002).

1.6.2 Influence of cortical rhythms on basal ganglia network activity.

As described above, oscillations and synchrony are a ubiquitous property of the cortico-thalamic networks. Given that the basal ganglia are, anatomically massively connected to the thalamo-cortical system, it would be surprising if the same activities were not seen in those structures aswell. Several studies have shown the transfer of cortical rhythms to the basal ganglia input structures.

Oscillations in the striatum have a strong relationship to activity in the cortex. In vitro, where spontaneous cortical oscillatory activity is limited (Steriade, 2000; 2001), cortical stimulation evokes membrane potential oscillations in medium spiny neurons that resemble up/down state transitions (Vergara et al, 2003). Anaesthetised rodents have provided a particularly valuable model for investigating rhythmicity in cortico-basal ganglia networks. Under deep anaesthesia, the cerebral cortex displays a steady "slow wave" oscillation at around 1Hz, analogous to the delta oscillation seen during sleep (Streiade, 2000). The slow oscillation is seen in the membrane potential of both cortico-striatal neurons and medium spiny neurons suggesting that they oscillate synchronously (Stern et al, 1998). The up states of both cortico-striatal neurons and MSNs in the dorsal striatum are tightly coupled to the negative deflections of the slow wave activity in the frontal cortical EEG (Mahon et al, 2001; Kasanetz et al 2002; Tseng et al, 2001), where as those in the ventral striatum are strongly correlated with the slow rhythm in the hippocampus (Goto and O'Donnell, 2001).

Similar relationships to the cortical slow oscillation have been observed in extracellular recordings in the STN. Bursts of action potentials in STN neurons are highly correlated with, and dependent on, both cortical slow wave and spindle activities (Magill et al, 2000). After cortical activation, induced by sensory stimulation, STN neurons shift from bursting to tonic firing mode (Magill et al, 2000, 2001). The same shift in firing pattern has been observed in head restrained animals after the transition from slow wave sleep to wakefulness (Urbain et al, 2000). In the pallidum, some neurons also display coincident bursts with the EEG slow wave. Many neurons, however, continue

to fire tonically only showing variations in their mean firing rate, which becomes faster during cortical activation and wakefulness (Magill et al, 2000; 2001; Urbain et al, 2000). Single units in the SNr also fire tonically irrespective of the cortical slow wave (Belluscio et al, 2003).

Hitherto, recordings of basal ganglia oscillations in awake animals have been limited, but nevertheless provide some compelling evidence for a role in the organisation of basal ganglia networks. In the awake rat, dorsal/lateral striatal neurons were found to be entrained by cortical spindle oscillations, where as those in the ventral striatum were entrained by the hippocampal theta rhythm (Berke et al, 2004). Furthermore, putative local GABAergic interneurons fired at an earlier phase of the spindle oscillation than the medium spiny neurons suggesting a level of organisation between projection neurons and interneurons analogous to that of the hippocampus (Klausberger et al, 2003 and see above). In the primate, slow rate covariations between pairs of striatal TANs or pallidal neurons are predicted well by the local field potential on a third electrode, suggesting that as in the cortex, the LFP represents a mode of global dynamics reflecting local neuronal correlations (Goldberg et al, 2004). In addition, small areas of striatum have been observed to "pop out" of the widespread beta oscillations recorded there while primates perform saccade tasks (Courtmanche et al, 2003), suggesting an interaction between global and local dynamics is an important feature of striatal processing.

1.6.3 Studies in human subjects with deep brain electrodes

Until relatively recently, surgical treatments for basal ganglia diseases were limited to lesioning the STN or GPi. While these procedures were fairly successful in relieving motor symptoms in both Parkinson's disease and dystonia, the procedure lacks any flexibility in the site of action or reversibility. It was subsequently discovered in the MPTP primate that high frequency electrical stimulation of the STN achieved equally effective relief of motor symptoms as subthalamotomy (Benazzouz et al, 1993; Breit et al, 1994; Benabid et al, 1994). To this end, many surgical centres have since moved to deep brain stimulation (DBS), whereby macroelectrodes are implanted bilaterally in either the globus pallidus or subthalamic nuclei, which can

subsequently be used to deliver high frequency stimulation to the surrounding area after being connected to external stimulating units implanted under the skin. The location of the STN and/or GP is often estimated through a combination of strereotaxy and preliminary recordings through microelectrodes to try to detect STN and GP neurons.

DBS has contributed to the debate over the role of oscillations in the basal ganglia in two ways. Firstly, it is possible to record single units in the STN and GP intra-operatively using microelectrodes, and LFPs post-operatively using the macro (stimulating) electrodes. These studies have clear methodological difficulties. Firstly, in the case of post-operative LFP recordings, even with the highest resolution magnetic resonance imaging it is not possible to be certain of the location of the stimulating electrode. Secondly, with all human recordings, there is no opportunity to compare the results to the brain of a healthy individual. Nevertheless, studies of both single units and field potentials have provided invaluable insights into the basal ganglia structures and their role in the wider network. Microelectrode recordings of STN and GPi units, after administration of the non-selective dopamine agonist apomorphine, have confirmed that individual neurons in these structures do not follow the response to dopamingeric stimulation predicted by the direct/indirect model (Levy et al, 2001). Although the mean rate of GPi units increased, there was no change in the rate of units in the STN. Action potentials from single units in the STN do however display prominent bursting at beta frequency (15-30Hz) that is coherent between pairs of STN cells and is reduced by voluntary movement and dopaminergic medication (Levy et al, 2002a; 2002b). Oscillatory activity has been investigated more thoroughly using LFP recordings from the macroelectrode. LFPs from both the STN and GPi from patients off medication show prominent oscillations at beta frequency that are coherent between the two structures (Brown et al, 2001). After medication, the coherent beta activity is significantly decreased and a higher frequency peak at around 70Hz emerges (Brown et al, 2001, Cassidy et al, 2002a). In the STN, beta oscillations in the subthalamic nucleus are coherent with those in the sensorimotor cortical EEG and EMG in the wrist muscles (Marsden et al, 2001a). Dopaminergic

medication also decreases intermuscular coherence in the beta band (Marsden et al, 2001b). Together these results suggest that beta oscillations are highly coupled in widespread areas of the cortico-basal ganglia circuits and musculature in parkinsonian patients. The finding that they are reduced with both medication and movement is highly suggestive that they are mechanistically important in PD pathology (Brown, 2003; Farmer, 2002). LFPs recorded from the pallidum of dystonic patients have significantly less beta power than PD patients on medication, suggesting that increased beta oscillations are specific to the effects of dopamine depletion (Silberstien et al, 2003). In addition, power in the 4-10Hz band was higher in dystonic patients than PD patients off or on medication, suggesting synchronised activity in that band may contribute specifically to dystonic symptoms (Silberstein et al, 2003).

It is unclear to what extent oscillations are present in the basal ganglia of the healthy human, but their modulation during movement tasks suggests they may still be involved in the execution of motor tasks. Coherent oscillations between the EEG and the STN and/or GPi are consistently modulated before or at the time of movement with a decrease and increase in the beta and high gamma (around 70Hz) bands, respectively (Cassidy et al, 2002). Several studies have shown that beta oscillations in the STN desynchronise in response to a cue to move (Williams et al, 2002; 2003; Kuhn et al 2004). Moreover, the reaction time to cued movement negatively correlates with the power of STN beta power (Williams et al, 2003). Although it is impossible to say whether desynchronisation of beta oscillations related to movement are physiological, similar findings in the cortical activity of healthy humans and non-human primates suggests they may not be a de novo feature of the pathological process (Kilner et al, 1999, Baker et al, 1997).

Secondly, the therapeutic mechanism of DBS has lead to questions over whether it is a disruption of oscillatory activity that leads to the therapeutic effect. It was originally thought that, given their similar therapeutic outcomes, DBS at high frequency simply produced a "virtual lesion" of STN or pallidal cells, probably by causing a depolarisation block. Evidence from in vitro

experiments suggests that this is at least partly the case (Garcia et al, 2005), although whether these preparations are suitable for studying the manipulation of a network phenomenon in a human brain is questionable. Other studies in both human and animal experiments have found evidence to suggest otherwise. Stimulation of the subthalamic area at 20Hz exacerbates LFP oscillations at beta frequency; where as stimulation at 70Hz (around therapeutic frequency) reduces them (Brown et al, 2004b). These results are more consistent with the action of DBS being more akin to that of dopaminegic medication on oscillations, than of a complete block of subthalamic activity. A recent study showed similar improvements in parkinsonian symptoms following both L-dopa and high frequency DBS along with increased desynchronisation in the sensorimotor cortex, supporting the premise that it is alterations in network rhythmicity that underlies the amelioration of Parkinsonian symptoms (Silberstein et al, 2005). Further support for a modulation of oscillations rather than inhibition is provided by experiments in MPTP-treated primates demonstrating that in the STN and pallidum, local high frequency stimulation can reduce oscillations in single STN neurons (Meissner et al, 2006) and reshape the temporal structure of neuronal activity in the pallidum (Bar-Gad et al, 2004). In addition, high frequency stimulation of the rodent STN leads to patterns of SNr neuron firing suggestive of STN activation, rather than inhibition (Maurice et al, 2003). Although a lesion could have the same effect by breaking the oscillatory loop in the network, this does not mean that DBS works by the same mechanism. The studies described above suggest that DBS may actually restore oscillations that promote dynamic movement as opposed to just breaking up the pathological activities (Brown, 2003). All studies based on human recordings however have been limited by the lack of a healthy brain against which to compare the effects of both disease and therapy.

Aim 3: To investigate the differences in cortico-basal ganglia population oscillations in the healthy and dopamine depleted brain.

1.7 Aims

The common aim throughout this thesis will be to combine simultaneous electrophysiological recordings from the cerebral cortex and basal ganglia with frequency domain analysis to investigate connectivity between these structures at a systems level. These techniques will be used to test the following specifc hypotheses regarding cortico-basal ganglia circuits in normal and pathological conditions, in anaesthetised and awake rats respectively.

Normal conditions: Hypotheses

1. **Populations of neurons in the cortex and basal ganglia, as measured by ECoG and LFPs display functional connectivity**
2. **Inter basal ganglia connectivity is dependent on brain state, as indicated by changes in the oscillatory activity.**

Pathological conditions: Hypotheses

1. **Dopamine depletion leads to changes in the oscillatory activity of cortico-basal ganglia circuits in specific frequency bands.**
2. **Dopamine replacement leads to a reversal in these pathological oscillatory activities to those of the healthy animal.**

Chapter 2: Methods

This chapter contains a description of the experimental and analytical methods that are common to the investigations described in chapters 3-6. The vast majority of experimental methods are described within these individual chapters, due to the difference in recording techniques and different laboratories in which the studies were carried out. The focus of this chapter will therefore be the signal analysis and statistical methods that were used across the separate investigations and how they can be used in conjunction to investigate the basal ganglia at a systems level.

2.1 Electrophysiological Recording

Experiments were performed at one of two laboratories. All experiments described in Chapter 3 were performed at Charité Virchow-Klinikum, Humboldt University, Berlin, Germany, in collaboration with Drs Daniel Harnack and Wassilios Meissner. All experiments described in Chapters 4-6 were performed at the Medical Research Council Anatomical Neuropharmacology Unit, University of Oxford, Oxford, in collaboration with Dr Peter Magill and Prof. Paul Bolam.

Three types of electrophysiological signals were recorded; single unit activity and local field potentials (LFPs) from sites in the basal ganglia and the electocorticogram (ECoG) from the frontal cortex. Details of the exact recording locations, electrodes and acquisition systems used to record these activities can be found in the appropriate chapters.

All electrophysiological signals were recorded as analogue signals and converted to digital representations for acquisition. Amplifiers and low- and high-pass filters were used to condition the signals before sampling. The sampling rate of all signals was more than twice that of the highest frequency contained in the analogue signal. This eliminates "aliasing;" the appearance of

high frequencies as aliased frequencies in the examined range, which is caused by the time intervals between data points being too low (Gotman, 1990). Filter design is an important consideration. In chapters 3-5 the filters used for all signals were of a simple 2-pole 'Resistor-Capacitor' (RC) design, with 12dB octave attenuation above and below the selected frequency values for both low and high cutoffs (NL-106 AC-DC Amp, Digitimer Ltd., Welwyn Garden City, UK). In chapter 6, ECoG was filtered using modules with a one-pole Bessel filter and a 6 dB octave attenuation above and below the selected frequency values for both low and high cutoffs (DPA-2FS filter/amplifier: Scientifica Ltd., Harpenden, UK). Depth channels in chapter 6 were recorded using filter modules of a Butterworth design with a 12dB octave attenuation above and below the selected frequency values for both low and high cutoffs (Lynx-8: Neuralynx, Tucson, AZ, USA). Different filter designs vary in their ability to smoothly attenuate signal around the cutoff frequency and their propensity to cause 'ringing' i.e., unwanted oscillations introduced by the filtering process. The cutoff frequencies used in these experiments were generous in that they were far removed from the frequency domains of interest, in turn suggesting that spurious influences on the data from such artificacts were highly unlikely. Details of specific filtering parameters can be found in the appropriate chapters. In addition to aliasing, a common problem with electrophysiological recording is the presence of 50Hz 'noise' and associated harmonics that originate from mains power supplies and can distort the signals of interest and their subsequent data analysis. Notch filters, band stop filters for frequencies around 50Hz, used either online of offline, may lead to the loss of true biological signal of around 50Hz and may also distort signal phase. To avoid this, we used HumBug™ units (Quest Scientific, Vancouver, Canada), which construct a real-time replica signal of the mains noise and continuously subtract it from the input signal. This technique has the advantage of only removing the noise element of the signal, leaving physiological activity around these frequencies intact, without causing signal distortion. These characteristics are particularly important if the phase relations between signals are of interest (see Chapters 3 and 5).

2.2 Mathematical basis of frequency and time domain analysis

The following section contains a description of the analytical techniques used for the analysis of electrophysiological signals in the time and frequency domains. The techniques described have been extensively used to investigate problems in neurophysiology and have been previously described in detail (Halliday et al, 1995: Rosenberg et al, 1998; Halliday and Rosenberg, 1999; Cassidy and Brown 2002b; Korzeniewska et al, 2003). All signal analyses were performed with Spike 2 (version 4; Cambridge Electronic Design Ltd., Cambridge, UK), Matlab (version 6.5, Mathworks Inc.) or Neuro (a suite of programs written by D. Halliday, Department of Electronics, University of York).

2.2.1 Fast Fourier Transform

The Fourier transform is computed by multiplying a signal independently by the cosine and sine values of the frequencies of interest. The sine and cosine coefficients can be used to derive a number of frequency domain based analyses. The discrete Fourier transform refers to this transformation as applied to digital (non-continuous) signals, such as the electrophysiological data used in all experimental chapters. The Fast Fourier Transform (FFT) is used to calculate the discrete Fourier transform for a time series divided into disjoint segments. To obtain the FFT, all time series were divided into disjoint segments of length T (either 512 or 1024 data points in all standard analysis and 256 or 512 data points for time evolving analysis in Chapter 3). The number of segments, defined as L, varies with record length (R), such that R=LT. For a time series a(t), the discrete Fourier transform was performed on the l^{th} segment at frequency λ, defined as:

$$d_a^T(\lambda,l) = \int_{(1-l)T}^{lT} a(t)e^{-\lambda t}dt \approx \sum_{t=(l-1)T}^{lT-1} e^{-i\lambda t}x_t$$

Equation 2.1

, where $i=\sqrt{-1}$ and $e^{it} = \cos(t) + i\sin(t)$.

This can be adapted for a point process, N1 :

$$d_{N1}^{T}(\lambda,l)=\int_{(l-1)T}^{lT} e^{-i\lambda t}\,dN(t)\approx\sum_{(l-1)T\le tj\le lt} e^{=i\lambda tj}$$

Equation 2.2

Where t_j are the times of the events, N1. For any given parameter, $\hat{z}$, an estimate is derived with a variance $(\mathrm{var}\{\hat{z}\})$. Under the assumption of a normal distribution, the 95% confidence limits are given by:

$$\hat{z}\pm 1.96x\sqrt{(\mathrm{var}\{\hat{z}\})}$$

Equation 2.3

2.2.2 Cross Spectrum and the auto and power spectrum

The simplest measures derived from the FFT are the cross-spectrum and auto-spectrum. The cross spectrum measures the correlations between two time series, with respect to phase and amplitude, where as the autospectrum measures the amount of energy present at a specific frequency band in a single process. The cross spectrum between time series a(t) and b(t) at frequency λ is given by:

$$\hat{f}_{ab}(\lambda)=\frac{1}{2\pi LT}\sum_{l=1}^{L} d_a^T(\lambda,l)\overline{d_b^T(\lambda,l)}$$

Equation 2.4

where $\overline{}$ indicates a complex conjugate. The products of the discrete Fourier transform and the complex conjugated discrete Fourier transform were averaged across sections 1 to L. This leads to smoothing of the

variability that would result from performing the analysis on non-segmented data. The autospectrum of one time series, for example *faa* for a(t), is derived by replacing b with a in the equation above. The power spectum, giving the strength of the signal in each frequency bin, is derived from taking the square of the magnitude of the complex coefficients, and discards phase information. In some analyses/plots, the power spectrum was logarithmically transformed in order to stabilise the variance. Where power spectra were performed on ECoG/LFP time series, the raw power may be highly variable between subjects due to variations in recording parameters. In these cases, the power at each frequency was converted to a percentage of total power at all the frequencies of interest to allow comparison across subjects (Silberstein et al, 2003 and see Chapter 3)

2.2.3 Coherence and Partial Coherence

The cross- and autospectra from two time series can be combined to give the coherence; a measure of the degree to which one can linearly predict change in one signal given a change in another signal (Brillinger 1981; Halliday et al, 1995; Rosenberg et al, 1989). Coherence is essentially a correlation coefficient that relates the covariance of two parameters with their autovarience. It is without units and it is bounded from 0 to 1, with a coherence of 0 indicating non-linearly related signals and a value of 1 signifying two linearly identical signals. All time series were assumed to be realisations of stationary, zero-mean time series (Brillinger 1981). Spike trains were assumed to be realizations of stationary, stochastic point processes (Perkel et al. 1967). All processes were further assumed to satisfy a mixing condition, whereby sample values widely separated in time were independent (Brillinger 1981). A Hanning window filter was used for all spectral analyses. Spectra were estimated by averaging across these discrete sections (Halliday et al. 1995). For the two time series a(t) and b(t) coherence is given by:

$$\left|\hat{R}_{ab}(\lambda)\right|^2 = \frac{\left|\hat{f}_{ab}(\lambda)\right|^2}{\left|\hat{f}_{aa}(\lambda)\hat{f}_{bb}(\lambda)\right|}$$

Equation 2.5

where λ denotes the frequency, f_{aa} and f_{bb} are the autospectra and $f_{ab}(\lambda)$ is the cross spectrum between series a and b. Because coherence is a measure of the linear association between two signals, the ECoG/LFP waveforms must be phase-locked (temporally-coupled) and their amplitudes must have a constant ratio to be coherent at any given frequency. At low coherence values, estimates for the variance are poor leading to inaccurate confidence limits. To this end, confidence limits, shown as horizontal lines on all coherence plots, were based on the number of segments used and were independent of frequency. The 95% confidence limit was defined as:

$$1-(0.05)^{1/(L-1)}$$

Equation 2.6

Partial coherence can be used to evaluate the dependence of a third time series on the coherence between two others. The first order partial coherence measure $\left|R_{ab/c}(\lambda)\right|^2$ is equivalent to a partial correlation which removes the common linear effects of the third process, c(t), from the coherence between time series a(t) and b(t) and is given by:

$$\left|R_{ab/c}(\lambda)\right|^2 = \frac{\left|R_{ab}(\lambda) - R_{ac}(\lambda)R_{bc}(\lambda)\right|^2}{(1-\left|R_{ac}(\lambda)\right|^2)(1-\left|R_{bc}(\lambda)\right|^2)}$$

Equation 2.7

Partial coherence is also a normalised measure bounded between 0 and 1. In this case however a coherence of zero indicates that any coherence between a(t) and b(t) can be fully predicted by their individual relationships with c(t). To compare the coherence and partial coherence within and between signals, the variance of the modulus of the coherency (given by the square root of the coherence) was normalized using a Fisher transform (Rosenberg et al, 1989).

2.2.5 Cumulant Density

The cumulant density provides a general measure of statistical dependence between random processes and, like coherence, will assume the value zero if the processes are independent (Halliday et al, 1995). The cumulant density differs from coherence however in that it is a non-normalised measure and there is no upper limit should there be a perfect linear relationship between processes. Although it is derived from Fourier based measures, the cumulant density is similar to a cross-correlogram when comparing two zero-mean time series or a spike-triggered average when comparing a stochastic point process with a zero-mean time series. As with a cross correlation histogram (see Figure 1.7), peaks/troughs in the cumulant density at time zero indicate positive/negative correlation between the two processes at zero lag. Peaks/troughs deviating from time zero can be thought of in the same way except that one channel (the input) is shifted in respect to the other (the reference) by the time indicated by the x-axis. The cumulant density, is derived from the inverse Fourier spectrum of the cross spectrum:

$$\hat{q}_{ab}(u) = \frac{2\pi}{T} \sum_{|j| \leq T/2w} \hat{f}_{ab}(\lambda_j) e^{i\lambda j u}$$

Equation 2.8

where u represents the considered time lag, j = 1,2,3,,,,,,,,$T/2w$, and $\lambda_j = 2\pi/T$ were the frequencies considered up to the Nyquist limit (half the sampling rate) in bin widths of w. Although the cumulant density calculates relationships across the frequency range as defined above, the result will

mostly reflect the dominant oscillatory processes at lower frequencies, which generally have larger amplitudes. Local field potentials were digitally low-pass filtered at 80 Hz for cumulant density estimates, and further high pass filtered when multiple oscillatory frequencies were present (see Chapter 4). For ease of interpretation, the y-axes of cumulant density estimates were scaled in 'correlation strength' (derived from the cross-correlograms between two time series or spike-triggered averages between time series and point processes). Unlike a conventional cross correlogram, the calculation of cumulant density derived from FFT based spectral analysis allows estimation of the variance and, therefore, a confidence limit. Values lying outside the confidence limits can be considered significantly linearly associated. Confidence limits were derived by:

$$\mathrm{var}\{\hat{q}_{ab}(u)\} \approx \left[\left(\frac{2\pi}{R}\right)\left(\frac{2\pi}{T}\right)\sum_{j=1}^{t/2} 2\hat{f}_{aa}(\lambda_j)\hat{f}_{bb}(\lambda_j)\right]^{1/2}$$

Equation 2.9

Where $\lambda_j = 2\pi \ \ j/T$, T = segment length and R = record length.

2.2.6 Phase

If the coherence between two time series is significant, the phase difference between two time series can be used to calculate the time delay between two time series over a given frequency range. The phase spectrum, in radians, between two time series is given by the argument of the cross spectrum:

$$\hat{\Phi}_{ab}(\lambda) = \arg\{\hat{f}_{ab}(\lambda)\}$$

Equation 2.10

Over frequency ranges with significant coherence, the time lag/lead between two signals can be calculated from the slope of the phase estimate, having

fitted a line by linear regression. A significant positive or negative gradient indicates a lag or lead by the input channel respectively relative to the reference channel, at a latency given by:

$$\frac{\Delta\phi}{\Delta frequency \times 2\pi}$$

Equation 2.11

2.2.7 The Directed Transfer Function (DTF)

The directed transfer function (DTF) investigates any possible asymmetry in the flow of coherent activity between regions (Kaminski & Blinowska, 1991). To this end, the multiple autoregressive (MAR) model that best describes the signals coming from the two regions of interest is determined. The MAR methodology is essential for the DTF, as the DTF is built directly from the MAR coefficients. In contrast, the methods described thus far have all been based on the FFT. These measures produce and use coefficients within discrete disjoint or overlapping data segments of the signal. Alternatively, if a model can be fitted to the whole signal, it can be transformed into the frequency domain instead, producing a continuous spectrum. The most common method of achieving this is by using autoregressive (AR) modelling. The AR model is formed using coefficients constructed by autocorrelation, whereby a value at time t is based on a linear combination of prior values. The model therefore measures the ability to predict the value of time t based on the previous values. The number of previous values that are incorporated into the coefficient at each time point is described by the model order. Where as the frequency resolution of FFT-based spectra is determined primarily by the number of data points in each window, the frequency resolution of AR based spectra is determined by the model order. Following the procedure detailed in Cassidy and Brown (2002b), a Bayesian methodology was applied to estimate the parameters of the autoregressive model. This approach is desirable in that it provides full probabilistic distributions for all of the model parameters. In addition, the complexity of the model (i.e. the most

appropriate number of spectral peaks) is determined objectively and automatically based on the data supplied to the model. The Bayesian update equations for the MAR coefficients are similar in form to the standard maximum likelihood equations, but additionally incorporate a prior precision term, α, and are given by:

$$\hat{\Sigma} = (\Lambda \otimes XTX + \alpha I_K) - 1$$

Equation 2.12

$$\hat{a} = \hat{\Sigma}(\Lambda \otimes XTX) a_{ml}$$

Equation 2.13

They are given by the normal distribution $N(a \mid \hat{a}, \hat{\Sigma})$, Λ is the noise precision, X is a matrix containing the regressors, a_{ml} is the usual maximum likelihood solution for the coefficients, I_k is the identity matrix and $k = pd^2$, where p is the model order and d is the number of channels, while $\otimes$ denotes the Kronecker product. For further details, the reader is referred to Cassidy and Brown (2002b, 2003). The autoregressive coefficients can be used to construct a bounded normalised measure (the DTF) that provides information on the effective direction of coupling. The off-diagonal MAR coefficients indicate the temporal coupling between one site and another and (depending on whether they are upper or lower off-diagonal) the direction of that coupling. By squaring and normalising the MAR coefficients, the DTF is obtained, as described by Kaminski and Blinowska (1991). Standard coherence analysis can also performed using the same autoregressive model as that used for the DTF and was utilised in Chapter 5 so that methodology was consistent for all spectral analyses in that Chapter.

2.3 Application of frequency and time domain methods to electrophysiological data.

The functional connectivity between networks of neurons may be inferred from the synchronisation of their respective activities (Glaser and Ruchkin, 1976; Thatcher et al., 1986; Thatcher et al., 1987; Fein et al., 1988; Rappelsberger and Petsche, 1988; Lopez da Silva et al., 1989; Nunez, 1995; Andrew and Pfurtscheller, 1996; Shen et al., 1999). This is regardless of whether synchronisation is a consequence of common inputs to each neuronal group (Halliday et al., 1995), or the result of self-organization into synchronized networks for optimal interaction (see reviews by Engel et al., 2001; Buzsáki and Draguhn, 2004), as both may effectively define functional connectivity. Synchronisation in electrophysiological data can be analysed using a variety of methods in the time and frequency domains. In the following chapters the techniques described in the section above are used to analyse the relationships between ECoG and LFP recordings from the cerebral cortex and multiple basal ganglia structures. In this section, these methods will be outlined in terms of how they are related and can be used in conjunction to make inferences about fuctional connectivity between different brain areas. The figures in this section are given in the context of ECoG and basal ganglia LFPs to aid the interpretation of Chapters 3-6, but could be applied to any similar data series.

2.3.1 Auto correlation, cross Correlation and the Fast Fourier Transform (FFT)

Electophysiological signals can be divided into two categories of data series; point processes and time series. A point process is a series of ordered events, which in this context always corresponds to the times of action potentials or spikes. Time series describe the fluctuation of a variable at successive time intervals, in the case of ECoG/LFPs this the potential difference between recording and reference electrodes. Time and frequency domain analysis techniques can be used to detect temporal consistencies within and between these signals, which can be used to infer information about the neurons (point processes) and populations of neurons (time series)

being recorded. The foundation of time domain analysis is the cross correlation, which describes the relative timing of one data series (the input) with respect to another (the reference). The autocorrelation is computed by using the same data series as both the input and reference and reveals repetitive events (such as oscillations) within a single data series. The result of the cross correlation between two time series is the cross correlation histogram (CCH), which has been extensively used to investigate relations between single neurons (see Chapter 1). For two point processes, the cross correlation has the advantage of detecting both non-oscillatory and oscillatory synchronisation, both of which are common at the single neuronal level (see Chapter 1). This thesis will be mostly concerned with the relations between spike trains (point processes) and ECoG/LFPs (time series) and to a greater extent between ECoG/LFPs recorded from different brain areas. The cross correlation of spike trains and ECoG/LFPs gives the spike triggered average (STA): a measure of the mean ECoG/LFP amplitude around the time of each action potential. Similarly the waveform average, the correlation between two time series, gives a simple measure of the covariance of two ECoG/LFP signals. While these techniques have also been extensively used, they are highly biased towards high amplitude features in the time series. For spontaneous (as opposed to stimulus locked) ECoG/LFP data, the activities of interest are oscillatory in nature (see Chapter 1). Using time domain methods, both the classic cross-correlograms (Abeles, 1982; Perkel et al, 1967) and the FFT derived cumulant density estimate (see below), it may be difficult to resolve correlated activity of more than one frequency. Indeed, large amplitude common elements at low frequencies tend to dominate (Challis and Kitney 1990). The same is true for the autocorrelation where different frequencies within the signal may be missed. In addition, time domain analyses are often used without a measure of the variance of the signal, making them statistically weak. Although it is possible to detect higher frequencies through filtering (see Chapter 4), a more efficient and accurate way to analyse signals in the frequency domain is through spectral analysis, which is most commonly derived from the FFT. The auto- or power spectrum measures the energy across discrete frequencies using statistical parameters based on the variance of the signal at those frequencies. In the case of

ECoG and LFPs, the power spectrum can therefore reveal the frequency of locally synchronised electrical events and measure the statistical strength of this synchronisation. The cumulant density (equivalent to a cross correlation) can be derived from the inverse FFT to give information in the time domain without loosing statistical power. Methods derived from the FFT can be applied to all combinations of time series and point processes and, as such, the type of data series will not be referred to specifically (see Halliday et al, 1995 and Halliday and Rosenberg, 1999 for review)

2.3.2 Cross Spectra and Coherence

Auto/power spectra give valuable information regarding local synchronisation, but if two signals from different brain areas have identical power spectra this cannot be used to infer that the two series are related (see Figure 2.2). As described above, cross correlations can be used to detect relations between data series, but will not reveal temporal relations across the multiple frequencies seen in neurophysiological data. The most common and accurate measure of synchronisation between network activities can be measured by their coherence, a normalized measure that describes the distribution of synchronisation across frequencies (Halliday et al, 1995; Nunez et al, 1997; Nunez et al, 1999). For two signals coherence is derived from a ratio of the two autospectra and their cross spectra, and essentially measures the consistency of the phase and amplitude of the two signals across frequencies. Coherence will give a measure of the linear dependence between two data series, which can be used to infer functional connectivity between the areas from which the data was recorded (Thatcher, 1986; Christakos, 1997 and see Figure 2.1).

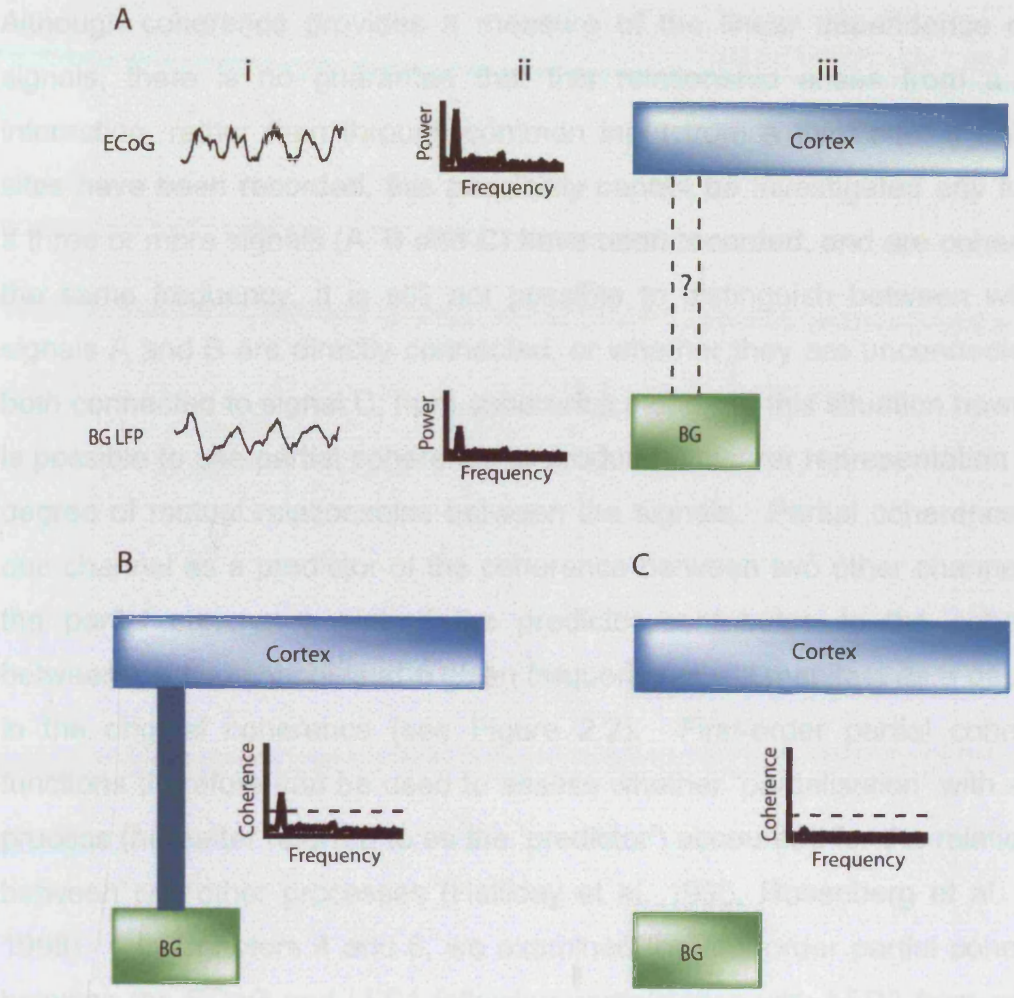

Figure 2.1 Application of power and coherence measures to the investigation of function connectivity between brain structures. ***A,*** In this theoretical example, an ECoG signal has been recorded from cortex with a coincident LFP signal from a basal ganglia nucleus (BG). Both signals have a peak in the power spectrum at the same frequency. As this gives no information regarding the temporal relations between the oscillations at each site, no inference can be made about connectivity between the two sites. ***B,*** If there is significant (above the dotted confidence limit) coherence between the two signals, then they can be described as functionally connected (blue bar). ***C,*** If there is no significant coherence then the two oscillations are independent and the signals from the two structures are unrelated in the frequency domain.

2.3.3 Partial Coherence Analysis

Although coherence provides a measure of the linear dependence of two signals, there is no guarantee that this relationship arises from a direct interaction, rather than through common input from a third site. If only two sites have been recorded, this possibility cannot be investigated any further. If three or more signals (A, B and C) have been recorded, and are coherent at the same frequency, it is still not possible to distinguish between whether signals A and B are directly connected, or whether they are unconnected but both connected to signal C, from coherence alone. In this situation however it is possible to use partial coherence to produce a clearer representation of the degree of mutual relationships between the signals. Partial coherence uses one channel as a predictor of the coherence between two other channels. In the partial coherence plot, if the predictor contributes to the coherence between the two channels at a given frequency, it will manifest as a decrease in the original coherence (see Figure 2.2). First-order partial coherence functions therefore can be used to assess whether 'partialisation' with a third process (hereafter referred to as the 'predictor') accounted for the relationship between two other processes (Halliday et al. 1995; Rosenberg et al. 1989, 1998). In Chapters 4 and 6, we examined the first-order partial coherence between the ECoG and LFP1 following partialisation with LFP2 from another site as the predictor. If LFP2 contributes to coherence between ECoG and LFP1, then the partial coherence will show a clear reduction in magnitude when compared with the ordinary coherence estimate between ECoG and LFP1 over the relevant frequencies (see Figure 2.2). As with coherence, the partial coherence function is based on the assumption of linearity, so that failure in the partial coherence to drop compared to the ordinary coherence does not exclude non-linear interactions between the different signals. Example applications of first-order partial coherence functions to problems in neuroscience are given in Spauschus et al (1999), Halliday et al (1999), Kocsis et al (1999) and Korzeniewska et al (2003).

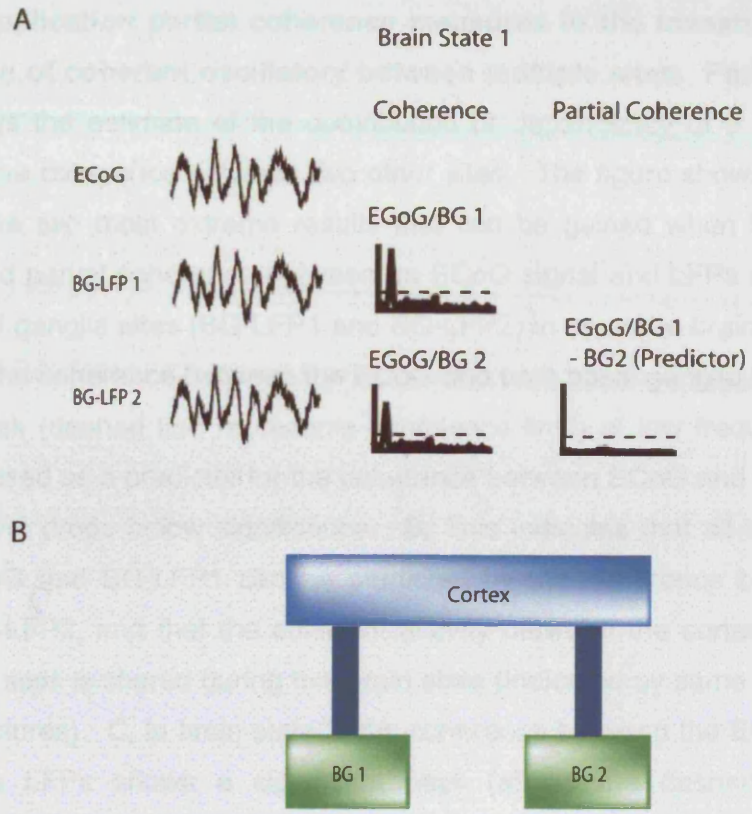
A
Brain State 1
Coherence
Partial Coherence
ECoG
EGoG/BG 1
BG-LFP 1
EGoG/BG 1
- BG2 (Predictor)
EGoG/BG 2
BG-LFP 2
B
Cortex
BG 1
BG 2
C
Brain State 2
Coherence
Partial Coherence
ECoG
EGoG/BG 1
BG-LFP1
EGoG/BG 1
- BG2 (Predictor)
EGoG/BG 2
BG-LFP2
D
Cortex
BG 1
BG 2

Figure 2.2 Application partial coherence measures to the investigation of the independence of coherent oscillatory between multiple sites. Partial coherence analysis allows the estimate of the contribution or dependency of a third site (the predictor) to the coherence between two other sites. The figure shows a schematic example of the two most extreme results that can be gained when looking at the coherence and partial coherence between an ECoG signal and LFPs recorded from different basal ganglia sites (BG-LFP1 and BG-LFP2) in separate brain states. ***A,*** In brain state 1 the coherence between the ECoG and both basal ganglia LFPs shows a significant peak (dashed line represents confidence limit) at low frequency. When BG-LFP 2 is used as a predictor for the coherence between ECoG and BG-LFP1, the coherence level drops below significance. ***B,*** This indicates that all the coherence between ECoG and BG-LFP1 can be predicted by the coherence between those sites and BG-LFP2, and that the coherent activity between the cortex and the two basal ganglia sites is shared during this brain state (indicated by same coloured bars between structures). ***C,*** In brain state 2, the coherence between the ECoG and both basal ganglia LFPs shows a significant peak (above the dashed line) higher frequency. This time however when BG-LFP2 is used as a predictor for the coherence between ECoG and BG-LFP1, there is no reduction in the coherence at the higher frequency. ***D,*** This result indicates that the coherent activity between cortex and the basal ganglia sites is independent during brain state 2 (indicated by different coloured bars).

2.3.4 Phase and the Directed Transfer Function (DTF)

Coherence and partial coherence can be used to give detailed information regarding the linear dependence of multiple signals, but give no information about the time delay or direction between those signals. Time domain measures allow a direct measure of the phase difference through the measurement of a central peak or trough from zero, giving the time lag/lead of the input signal in relation to the reference. In addition to the problems with time domain analysis described above however, the central peak/trough of and oscillatory activity may be ambiguous leading to a spurious estimate. The phase difference between two signals can also be derived from the FFT, but is ambiguous at individual frequencies. When coherence is strong across a given frequency band, the phase lag/lead between two signals can be calculated by using the slope of the phase estimate (radians/Hz) across the coherent frequency range, with a positive or negative gradient indicating the input is lagging or leading the reference respectively. The phase estimate, while useful, may also lead to spurious results as it may reflect a mixture of coherent activities with both lags and leads (see Chapter 5 for further detail). The directed transfer function (DTF), derived not from the FFT but an autoregressive model of the two signals, can overcome this problem by providing information about coherent activity in both directions, giving a result which reflects the relative strength of coherence in each direction, rather than an absolute lag or lead.

Although the DTF can theoretically be used on point processes, its use thus far has been restricted to time series. Given two time series A and B, the DTF gives two coherence plots which reflect the coherence directed from A to B and from B to A. Where the DTF of coherent activity at two recording sites is symmetric, no one 'effective direction of coupling' predominates, either because phase delays of mixed coherent activities are balanced or there was genuine synchronisation with zero phase (and time) difference (see Cassidy and Brown, 2003 and Figure 1*A*, *B*). Where the DTF of coherent activity at two recording sites is asymmetric, the 'effective direction of coupling' predominates in one direction and coherent activity or activities in one population of neurons tend to lead in time (Figure 2.3). It should be noted,

however, that an asymmetrical DTF does not necessarily imply a direct connection between the two areas in which activity was recorded. Thus, information can be transferred indirectly between recorded structures, via one or more unrecorded structures, or indeed, activity in both recorded structures may be driven by a third unrecorded structure (Figure 2.4 *C*, *D*). The relative time delays between different structures and intermediate relays may also influence the effective direction of coherent activity (Figure 2.4 *D*). As such, the interpretation of the DTF has to be informed by evidence of anatomical connectivity and/or other sources of evidence for functional connectivity, particularly partial coherence (Korzeniewska et al, 2003 and see Chapters 5 and 6). Example applications of the DTF on neurophysiological time series are given in Serrien et al (2003; 2004), Korzeniewska et al (2003), Astolfi et al (2004) and Brovelli et al (2004).

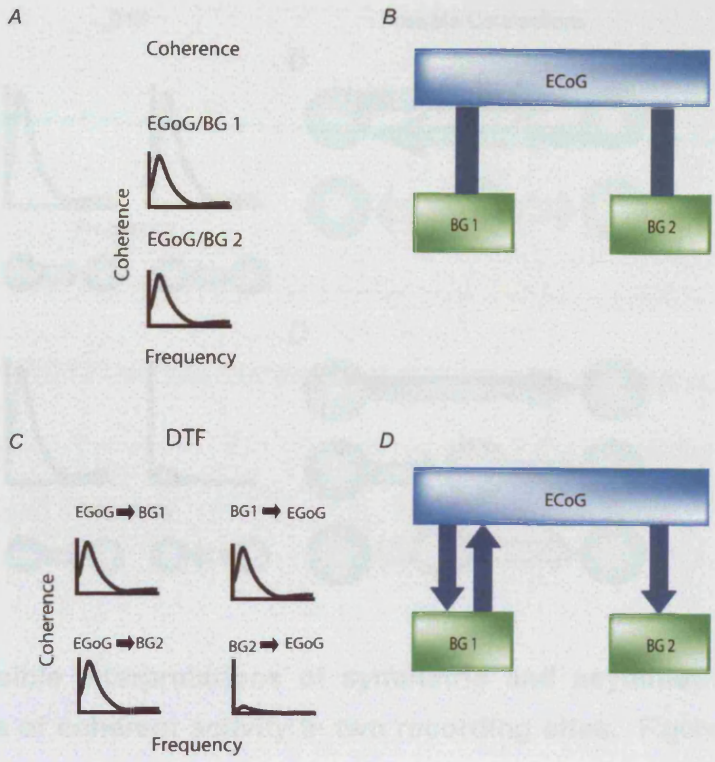

Figure 2.3 Application directed transfer function (DTF) measures in the investigation of the direction of coherent activity between multiple sites. Coherence gives an estimate of the linear coupling in between two signals but gives no information regarding the direction of this coupling. The figure shows a schematic example of the two most extreme results which can be gained when looking at the DTF between for the LFPs recorded at two basal ganglia sites and the ECoG. ***A,*** The basal ganglia LFPs (BG1 and BG2) are equally coherent with the ECoG at the same frequency. ***B,*** This result shows only that the BG sites are coupled to the ECoG, but nothing about the direction of coherent activity and are therefore shown as bars with no direction assigned (see also Figures 2.1 and 2.2). The bars are given the same colour in the absence of partial coherence analysis, but there independence/dependence cannot be assumed. ***C,*** The DTF gives two plots for each pairing, with the proportion of coherence in each direction between the two sites. For ECoG and BG1 the two DTF plots are symmetric, indicating an equal coherence in each direction between the two recording sites. For EGoG and BG2 the DTF is completely asymmetric, with all the coherence in the direction of ECoG to BG2. ***D,*** With this additional information, the bars from ***B*** can be replaced with arrows indicating the differences in direction in coherence between the cortex and the two basal ganglia sites. (Arrows in ***B*** and ***D*** show only the simplest interpretations of DTF results. More complex explanations are shown in Figure 2.4)

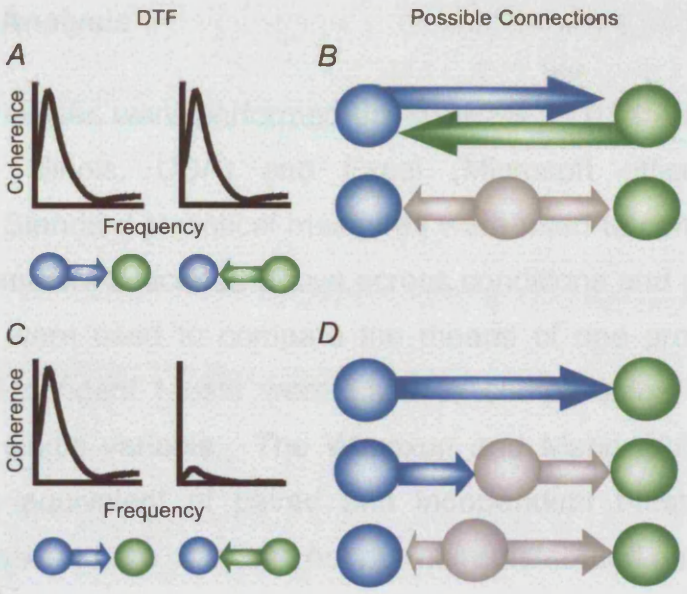

Figure 2.4. Possible interpretations of symmetric and asymmetric directed transfer functions of coherent activity in two recording sites. Figure 2.3 shows a simplified version of the possible interpretation of the DTF, which is in reality more complex than Figure 2.3. ***A, B,*** Symmetric DTFs and possible underlying connections. ***A,*** The two DTF graphs are identical, indicating that the net flow of coherent activity between recording sites 1 (blue circle) and 2 (green circle) is equal. Arrows represent direction of coherent activity detected by DTF analysis. ***B,*** Identical DTF graphs could be produced by an equal and direct flow of coherent activity between the two recording sites (top). Alternatively, information could be transferred indirectly between recording sites from a third connecting structure (grey; not recorded). ***C, D,*** Asymmetric DTFs and possible underlying connections. ***C,*** Dissimilar DTF graphs show that the flow of coherent activity from site 1 to site 2 is significantly greater than the flow from site 2 to site 1. ***D,*** Asymmetries could indicate that activity at site 2 is directly driven by activity at site 1 (top). This dependence, however, might not be due to a direct influence, but may involve feed-forward propagation via a third site (middle). Alternatively, coherent activity at recording sites may be driven by a third site (bottom). If the latency of propagation from the third site to recording site 1 is shorter than the latency to site 2, then site 1 will have a larger DTF and thus, will apparently drive site 2 (bottom).

2.4 Statistical Analysis

All statistical analyses were performed using SPSS 11.0 for Windows (SPSS Inc., Chicago, Illinois, USA) and Excel (Microsoft office 2000 SR-1 Professional). Standard statistical measures were used to compare time and frequency parameters described above across conditions and groups. Paired student t-tests were used to compare the means of one group across two variables. Independent t-tests were used to compare the means of two groups with a single variable. The Wilcoxon and Mann-Whitney tests, the non-parametric equivalent of paired and independent t-tests respectively, were used in cases where data was not normally distributed as determined by the Kolmogorov Smirnov test. Where multiple t-tests where used, the Bonferroni correction was applied. Linear regression was used to determine the strength and the direction of the relationship between two variables.

Repeated measures general linear models (GLMs) of analysis of variance (ANOVA) were used to compare multiple variables within groups. ANOVAs allow the investigation of the effects of each variable, or factor, individually and the interaction between factors. The ANOVA relies on the sphericity (equal variance across time) of the dependant variables. The Huynh-Feld correction for non- sphericity was incorporated where this assumption was violated as assessed by the Mauchly sphericity test. Post-hoc t-tests were used were necessary to further investigate significant factors and interactions identified by ANOVAs.

Further details of statistical measures are given in Chapters 3-6.

Chapter 3 : Dopamine depletion increases the power and coherence of β-oscillations in the cerebral cortex and subthalamic nucleus of the awake rat

Excessive synchronisation of neuronal activity in the basal ganglia is increasingly recognised as a critical functional change accompanying the parkinsonian state (see reviews by Brown and Marsden, 1998; Bergman et al, 1998; Bevan et al, 2002; Brown, 2003). Such synchronisation is evident at the levels of pairs of neurons or larger neuronal populations. Hitherto, studies in parkinsonian animal models have concentrated on investigations of synchronisation between single neurons within the monkey pallidum, largely assessed through cross-correlation analysis (Bergman et al, 1998; Boraud et al, 2002 and see Chapter 1). These studies emphasise the role of pathological activity that is synchronized at frequencies under 15 Hz, including those frequencies associated with parkinsonian tremor (Nini et al, 1995; Raz et al, 2000; Heimer et al, 2002; Goldberg et al, 2004). In contrast, studies of synchronized activity in patients with Parkinson's disease (PD) have assessed both the pallidum and subthalamic nucleus (STN) and have explored the synchronisation of population activity in these structures and the cerebral cortex, an important source of input to the basal ganglia. The synchronisation of the activities of single neurons (Levy et al, 2000, 2001, 2002b), as well as the synchronisation within and between the rhythmic activities of local populations of neurons, as evinced by oscillations in local field potentials, have been investigated (Marsden et al, 2001a; Brown et al, 2001; Priori et al, 2002; Williams et al, 2002; Silberstein et al, 2003). Collectively, these investigations in parkinsonian humans suggest synchronisation preferentially occurs at 15-30 Hz, in the so-called β-frequency band, and is ameliorated, together with motor symptoms, by dopaminergic medication. Although these and other studies suggest that the dopamine-dependent modulation of synchronized activity in cortico-basal ganglia circuits is a prerequisite for normal function, the exact nature of this modulation is not known.

The aims of this chapter were twofold. First, to test whether activity within and between frontal cortex and STN is synchronized in the β-frequency band in the unilateral 6-OHDA-lesioned rodent model of PD, and whether synchronized activity is reduced or otherwise different in the non-lesioned animal. Second, to determine the temporal evolution of the effects of dopamine receptor stimulation on oscillatory activity in the 6-OHDA-lesioned rat, thereby further characterising the nature of dopaminergic modulation of synchronized population synchrony in the cortico-basal ganglia circuits.

3.1 Methods

Experimental procedures were carried out on 26 adult male rats (HsdCpb:WU strain; Wistar-Winkelmann, Germany), and were conducted in accordance with the European Communities Council Directive (86/609/EEC) for care of laboratory animals and with the Society for Neuroscience policy on the use of animals in research.

3.1.1 Unilateral lesion of dopaminergic neurons and electrode implantation

Unilateral 6-OHDA injections were carried out on 16 rats. Control (vehicle) injections were performed in another 10 rats (age-matched). Sixty minutes before the injection of 6-OHDA, all animals received a bolus of desipramine (25 $mgkg^{-1}$, i.p.; Sigma, Germany), to minimise the uptake of 6-OHDA by noradrenergic neurons, and pargyline (50 $mgkg^{-1}$, i.p.; Sigma), to maximise the toxic effects of 6-OHDA on dopaminergic neurons (Schwarting and Huston, 1996a). Anesthesia was induced and maintained with chloral hydrate (400 $mgkg^{-1}$; i.p.; Sigma, Germany). Animals were then placed in a stereotaxic frame (David Kopf Instruments, Tujunga, CA), a small craniotomy was made over the left substantia nigra, and the overlying dura mater removed. The neurotoxin 6-OHDA (hydrochloride salt; Sigma) was dissolved immediately before use in ice-cold 0.9% w/v NaCl solution containing 0.1% w/v ascorbate to a final concentration of 8 $mgml^{-1}$. Then 1.0 µl of 6-OHDA solution (or vehicle in controls) was injected at a rate of 0.5 $\mu lmin^{-1}$ through a steel cannula (0.2 mm outside diameter) attached to a 10 µl Hamilton microsyringe (Cole-Parmer, London, UK) into the region adjacent to the median forebrain bundle (A: –4.2 mm; L: 1.1 mm; V: –7.6 mm). Stereotaxic coordinates were calculated from the atlas of Paxinos and Watson (1986). The cannula was left in place for 5 min before being withdrawn.

Animals were implanted with recording electrodes 4 weeks (± 3 days) after the injection of 6-OHDA or saline. Rats were anesthetized with chloral hydrate (400 $mgkg^{-1}$; i.p.) and placed in a stereotaxic frame (David Kopf

Instruments). A concentric, bipolar 'semi-microelectrode' (customized SNE-100; Rhodes Medical Instruments, USA) was implanted in the left STN under stereotaxic conditions (A: 3.8 mm; L: 2.5 mm; V: –7.6 mm), as previously described (Brown et al, 2002). Semi-microelectrodes were constructed from stainless steel cannulae and wires, which were insulated with epoxylite (except at the two electrode contacts). The outer contact was 100 μm in length and had a diameter of 150 μm. The inner contact had a diameter of 25 μm (only the tip of the inner wire was exposed). The two recording contacts were separated by 100 μm. Stainless steel screws (1 mm diameter) were positioned above each frontal cortex (A: -2.7 mm; L: +/-2.0 mm), each cerebellar hemisphere (A: –12.0 mm; L: +/-2.0 mm) and centrally over an area of thickened nasal bone rostral to the cerebral cortex (A: -5.7 mm; L: 0.0 mm). Thereafter, the microelectrode and screws were fixed to the skull with dental cement (Technovit; Heraeus-Kulzer GmbH, Germany). Animals were allowed at least 72 hours to recover from the surgery before recording began.

3.1.2 Electrophysiological recording and behavioural testing

The extent of the 6-OHDA lesion was assessed 4 to 5 weeks after toxin injection by challenge with apomorphine (Hudson et al, 1993; Schwarting and Huston, 1996b). Following a 15 min period in the recording chamber, animals received a single bolus of apomorphine (0.05 mg $mgkg^{-1}$, s.c.; Sigma) and were returned to the chamber for observation. The numbers of contraversive and ipsiversive turns were then counted. As single doses of dopamine agonists 6-OHDA lesioned animals have been reported to lead to complex changes in the striatum at the genetic level (Berke et al, 1998), apomorphine testing was always conducted after all electrophysiological recording.

During recordings of spontaneous and apomorphine-induced activity patterns, animals were placed in a plexiglas bowl within a Faraday cage. Residual mains artifact (50 Hz) was minimised by the use of 'Humbugs' (Quest Scientific, Canada). The electrocorticogram (ECoG) was recorded from the screw above the left frontal cortex (ipsilateral to STN recording) or right frontal cortex. Screws in the nasal bone and above the cerebellum were used as the

ground and the ECoG reference for differential recording, respectively. Subthalamic nucleus LFPs were recorded from the concentric semi-microelectrode in a bipolar (differential) configuration. Signals were recorded in the active animal through the use of a commutator. Raw STN and ECoG signals were AC-coupled, amplified (x1000-5000) and then band-pass filtered (0.1-100 Hz; Neurolog 100AK and 104A modules: Digitimer, UK). Conditioned signals were sampled at 512 Hz using a 12-bit A-D card (PCM-DAS16S, ComputerBoards, Middleboro, MA 02346, USA) and a portable computer running a custom-written program. Subsequent off-line signal processing was performed using commercial software (Spike2 software; Cambridge Electronic Design, Cambridge, UK). Data traces were digitally high-pass filtered off-line (cut-off at 0.5 Hz; Spike2) before analysis (see below). Recordings were made during rest and movement periods. During rest periods animals were completely still but alert. Movement recordings were defined as periods of sustained motor activity involving walking and exploring. Behavioural states were identified and noted by continuous visual inspection by one or two of the experimenters. Movement periods lasting 10-30 s were concatenated to produce epochs of 60 s for comparison with rest periods of 60 s duration. Periods of grooming and other stereotyped behaviour were excluded from analysis due to artefacts and the possibility that they contain their own distinctive neuronal activities (Aldridge and Berridge, 1998).

3.1.3 Histological processing

After recording, animals were transcardially-perfused under deep anesthesia with 30 ml 0.1 M phosphate-buffered saline, followed by 100 ml 4% w/v paraformaldehyde in 0.1 M phosphate buffer. Brains were removed and post-fixed in 4% w/v paraformaldehyde for at least 24 hours before being sectioned at 20 μm intervals in the coronal plane. Cresyl violet staining was performed on coronal sections for histological verification of all recording sites. Only animals with correct placement of the recording electrode in the subthalamic nucleus were included in the analysis (see Figure 3.1*F*). Furthermore, free-floating serial sections (20 μm) of mesencephalon were cut and processed for

tyrosine hydroxylase (TH) immunohistochemistry and then counterstained with cresyl violet in order to perform stereology-based counting of TH immunoreactive (TH-IR) neurons (described in Meissner et al, 2003). Cell counts were done using a computer-based image analyser (Visioscan v4.12, Biocom, San Diego, CA, 92121, USA). Unbiased stereological techniques (Gundersen et al, 1988; West and Gundersen, 1990; West, 1999) were used to estimate cell number in the substantia nigra *pars compacta* (SNc). Every four sections, the boundaries of the SNc were delineated by examining the size and shape of the different TH-IR neuronal groups, their cellular relationship to axonal projections and nearby fiber bundles (German et al, 1996; Paxinos and Watson, 1986). The volume of SNc, V(SNc), was calculated using the formula: $V(\text{SNc}) = \Sigma S\, td$; where ΣS is the sum of surface areas, t is the average section thickness (12 µm after immunohistochemistry processing) and d is the distance between the sections (Theoret et al, 1999). Eight sections, the first being randomly chosen, were used and optical disectors were distributed using a systematic sampling scheme. Disectors (50 µm length, 40 µm width) were separated from each other by 30 µm (x) and 20 µm (y). In these disectors, the nuclei of the neurons being in focus were counted (Gundersen et al, 1988). To be included in the count, the cell body of a neuron had to be entirely in the disector, or at least cross the disector border by more than half its surface (Gundersen et al, 1988). Only two consecutive borders (of four) of the disectors were considered (Gundersen et al, 1988). The following formula was used to estimate the number of TH-IR neurons: $N = V(\text{SNc})\ (\Sigma Q^- / \Sigma V(\text{dis}))$; where N is the estimation of cell number, V(SNc) is the volume of the SNc, ΣQ^- is the number of cells counted in the disectors and ΣV(dis) is the total volume of all the dissectors (Theoret et al, 1999). The mean estimated number of neurons and S.E.M. were then calculated.

3.1.4 Data analysis

Rhythmic neuronal activity was characterized by calculating power spectra (Fast Fourier Transform with Hanning window function; block size of 512 data points, giving 1.0 Hz resolution) using Spike2 software. Power was expressed as % total power over 5-45 Hz and 55-100 Hz to normalise the

data across animals. Power at very low frequencies (<5 Hz) was excluded so as to minimize the contribution of movement artefact and 'DC drift', and that at ~50 Hz was excluded to avoid inclusion of residual mains artefact. Data were analysed in the frequency domain as described in Chapter 2.

All standard power and coherence comparisons were performed on 60 s of data for each animal in each condition (rest or movement). Significant peaks in coherence were defined as 3 contiguous bins above the 95% CL. Two frequency bands were selected for comparison between groups based on the most prominent activities in the mean transformed coherence between STN-LFPs and ECoGs in the lesioned and control animals. The first band was 5-11 Hz, representing the three bins either side of the peak at 8 Hz, while the second was 22-32 Hz, representing the five bins either side of the peak at 27 Hz. Differences in power and transformed coherence between behavioural conditions and between lesioned and control animals were evaluated with paired and unpaired two-tailed t-tests as appropriate

The phase relationships between cortical and STN activity were determined for lesioned animals from 60 s recordings made during rest. Phase estimates were derived from spectral analysis using blocks of 1024 data points (0.5 Hz resolution). Linear regression was performed on a frequency range of 10 Hz (10 bins), centred on the peak coherence above 15 Hz in individual spectra.

Time-evolving power and coherence spectra were constructed from overlapping windows of data and plotted for rest periods and post-apomorphine periods (Matlab 6.5, Mathworks Inc.). Power spectra (1 Hz resolution) were constructed using 10 s windows with 5 s overlap. Coherence spectra (2 Hz resolution) were constructed using the same window size and overlap. For histograms and statistics, spectral analysis was performed on three 20 s epochs recorded before apomorphine administration, nine 20 s epochs recorded after apomorphine but before rotation, and lastly, three 20 s epochs recorded during rotation. Raw power (as opposed to % total power) or transformed coherence in the β-frequency range was averaged across all

animals to give a single value at each 20 s time point. In the case of coherence plots, coherence values below the level of significance (95% CL) were given values of zero. The 20 s epochs of data were used to compile histograms of power and coherence of activity in the β-frequency range throughout the period after injection with apomorphine as a percentage of levels present before injection (see below). For statistical analysis, groups of three consecutive 20 s epochs were averaged to give five 60 s periods covering 60 s of activity before injection, 180 s after injection but before the first rotation, and 60 s immediately following onset of rotation behaviour. General linear models were used to compare differences between these time periods. Changes in β-frequency activity after apomorphine injection as compared to rest were further examined using *post hoc* paired *t*-tests.

Linear regression was used to examine the correlations between the frequencies at which peak power and coherence occurred and their temporal relationship with respect to the onset of apomorphine-induced rotation behaviour. The frequencies of the peak power and coherence between 20 and 44 Hz were averaged across the spectra from all relevant animals. This broad band was chosen to allow for increases in the frequencies of activity over time, as described in the results. Regression was performed on each of the 20 s time points in the 180s preceding the first rotation. P values of ≤ 0.05 were considered significant. All group data are expressed as mean ± S.E.M. unless stated otherwise.

3.2 Results

3.2.1 Verification of recording sites and 6-hydroxydopamine lesions.

Histological analyses confirmed that both poles of the bipolar electrodes were outside of STN in 11 of 26 animals implanted and recorded. Data derived from these animals were not considered further because the recording electrodes varied greatly in location. Thus, only animals with correct placement of the recording electrode in the STN (see Figure 3.1F) were included in the analysis. Ten animals with electrodes implanted in STN had previous intracerebral injections of 6-OHDA, and 5 successfully implanted animals were injected with saline. The extent of the 6-OHDA lesion was assessed in each animal 4 to 5 weeks after toxin injection (after recording drug-free, spontaneous activity) by challenge with apomorphine (0.05 mg $mgkg^{-1}$; s.c.). The lesion was considered successful in those animals that made at least 90 net contraversive rotations in 20 min (Hudson et al, 1993; Magill et al, 2001). The mean number of contraversive rotations exhibited by those animals that were both successfully lesioned and implanted in STN (n = 10) was 175 ± 18.8. In good agreement with this, the same lesioned animals showed a dramatic decrease in the number of TH-IR neurons in the SNc of the lesioned hemiphere, as compared to the contralateral SNc (62 ± 51 and 12,562 ± 562 neurones, respectively). Control animals that received intracerebral injections of saline did not exhibit rotational behaviour after administration of apomorphine.

3.2.2 Oscillations in the β-frequency range are increased by dopamine depletion

Oscillations at around 20-30 Hz were clearly observable in the raw LFPs recorded in frontal cortex (i.e. the ECoG) and STN of most 6-OHDA-lesioned animals at rest, but not control animals at rest (Figure 3.1*A* and *B*). The power spectra derived from ECoG and STN recordings in both lesioned and control animals at rest displayed peaks within the range of 5-11 Hz (Figure 3.1*C* and *D*).

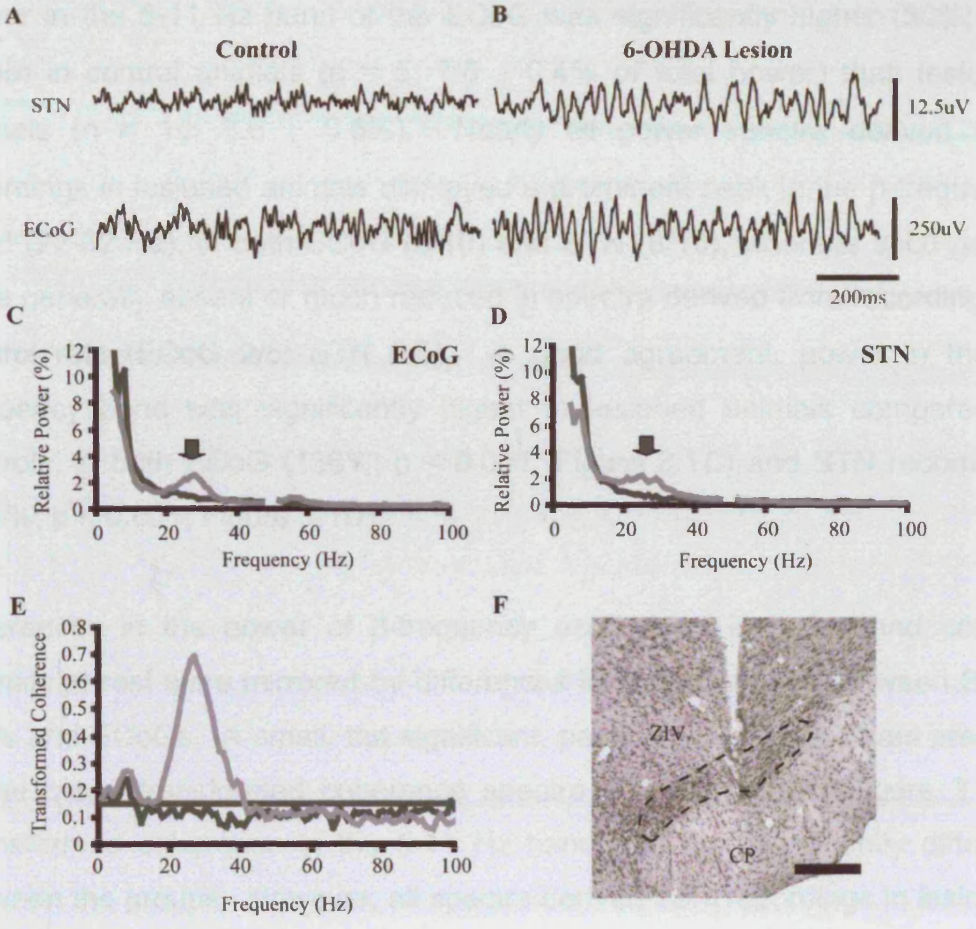

Figure 3.1 6-hydroxydopamine lesions increase the power and coherence of β (22-32 Hz) oscillations in the cerebral cortex and subthalamic nucleus of the awake rat. ***A***, ***B***, Local field potentials recorded in the subthalamic nucleus (STN) and ipsilateral frontal cortex (ECoG) of 6-OHDA-lesioned animals at rest (***B***) were dominated by β-range oscillations that were not present in controls at rest (***A***). ***C***, ***D***, Mean power spectra of both ECoG (***C***) and STN (***D***) activity recorded from lesioned animals (n = 10; grey lines) had clear peaks in the β-frequency range (arrows) that were absent in control animals (n = 5; black lines). Power at mains artefact frequency has been omitted. (***E***) Mean transformed coherence spectrum between STN and ECoG in lesioned animals (n = 10; grey line) displayed a large, significant peak between 20-35 Hz, which was not seen in the spectrum of control animals (n = 5; black line). (***F***) Electrode placement in the STN (borders indicated by dashed line) was confirmed with light microscopy. CP, cerebral peduncle; ZIV, ventral division of zona incerta. Horizontal calibration bar is 300 μm.

Power in the 5-11 Hz band of the ECoG was significantly higher (50%; $p < 0.005$) in control animals ($n = 5$; $7.8 \pm 0.4\%$ of total power) than lesioned animals ($n = 10$; $3.6 \pm 0.6\%$). Nearly all power spectra derived from recordings in lesioned animals displayed a prominent peak in the β-frequency band (22-32 Hz), in both ECoG (9/10) and STN (8/10), whereas such peaks were generally absent or much reduced in spectra derived from recordings in control rats (ECoG 2/5; STN 0/5). In good agreement, power in the β-frequency band was significantly higher in lesioned animals compared to controls, in both ECoG (136%; $p < 0.001$; Figure 3.1*C*) and STN recordings (200%; $p < 0.001$; Figure 3.1*D*).

Differences in the power of β-frequency oscillations in lesion and control animals at rest were mirrored by differences in the coherence between STN-LFPs and ECoGs. A small, but significant, peak at around 8 Hz was present in the mean transformed coherence spectra of both groups (Figure 3.1*E*). Transformed coherence in the 5-11 Hz band was not significantly different between the groups. However, all spectra derived from recordings in lesioned animals ($n = 10$) also had a large (mean peak transformed coherence of 0.8 ± 0.1), broad (mean 17.3 ± 2.4 Hz width) and highly significant peak in coherence between 23 and 31 Hz (26.4 ± 2.8 Hz; Figure 3.1*E*). Accordingly, mean transformed coherence in the β-frequency band (22-32 Hz) was significantly higher in lesioned animals compared to controls ($p < 0.001$). Nevertheless, the majority of healthy animals (4/5) did have significant peaks of coherence between cortex and STN in the beta-frequency band. However, these peaks were relatively small (mean peak transformed coherence 0.23 ± 0.02) and narrow (mean 3.0 ± 0.0 Hz width) and varied in frequency across the beta-frequency band (24.5 ± 2.8 Hz), such that a clear peak was not visible in the spectrum of mean transformed coherence derived for all five control animals (Figure 3.1*E*). Significant phase relationships were found in the β-frequency band for 8 of 10 lesioned animals; 3 animals showed ECoG leading STN ($4.6 \text{ ms} \pm 0.8 \text{ ms}$), while 5 animals showed STN leading ECoG (7.9 ± 0.8 ms).

In the above assessments, the ECoG was referenced to a screw over the cerebellum, raising the possibility that the ECoG signal was biased towards cerebellar activity rather than cerebral cortical activity. To test for this possibility, we reconfigured the ECoG electrodes to register the differential between the frontal cerebral cortices of both hemispheres. Differences in ECoG power and ECoG-STN coherence between control and lesioned animals were robust and persisted after changing the ECoG recording configuration. There was a prominent peak in the β-frequency band (mean peak frequency of 25.5 ± 1.0 Hz) in power spectra derived from bipolar ECoG recorded between the ipsilateral and contralateral cortices of lesioned rats (n = 5). Power in the β-frequency band was significantly higher ($p < 0.001$) in the reconfigured bipolar ECoG from lesioned animals (n = 5; 2.8 ± 0.20%) as compared to control animals (n = 6; 1.6 ± 0.11%). Coherence spectra derived from the bipolar ECoG and STN recordings in lesioned animals also displayed a peak in the β-frequency band (23.8 ± 0.9Hz; n = 5). Transformed coherence in this frequency band was significantly higher ($p < 0.05$) in lesioned animals (0.38 ± 0.1; n = 5) than in control animals (0.07 ± 0.004; n = 4). Taken together, these experiments confirm that the ECoG was generated by the underlying cortex and thus, was not related the use of a cerebellar reference electrode.

There were no significant differences in either the 5-11 Hz band or the β-frequency band between rest and movement conditions in control or lesion animals when analyses were carried out using data averaged over 60 s periods. However, time-evolving coherence analysis over 10 s time windows revealed a small increase in the frequency of coherent activity in lesioned animals over periods where movement was recorded (Figure 3.2). The peak frequency of coherent activity above 15 Hz was significantly higher (Paired t-test < 0.02) during these movement periods (32.2 ± 1.0 Hz) than during randomly selected periods of rest (29.3 ± 0.9 Hz). The magnitude of peak coherence during these periods however was not significantly different between movement and rest.

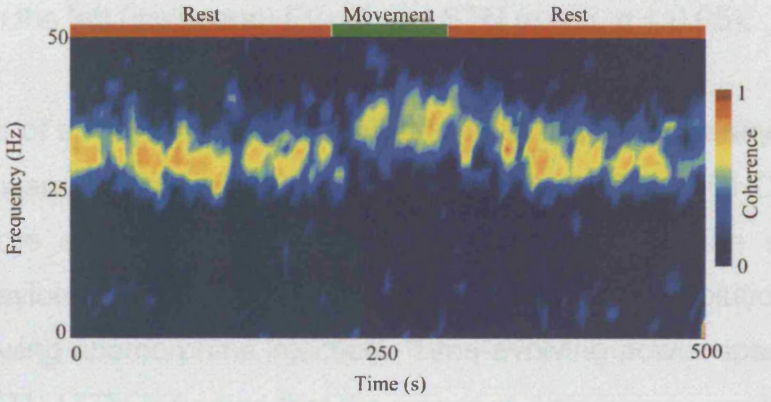

Figure 3.2 Time-evolving coherence spectrum recorded during periods of rest and movement. Coherence plot was derived from 10 s overlapping windows of data recorded in one lesioned animal. At rest (red bars), sustained coherence between ECoG and STN-LFP was seen at 25-30 Hz. A period of continuous exploratory movement (green bar) was associated with a distinct increase (~ 5 Hz) in the frequency of coherent activity.

Coherent activity in cortex and STN of lesioned animals was also dependent on the laterality of the ECoG recording site. Mean transformed coherence between the right (contralateral) ECoG and STN was significantly lower than that between the left (ipsilateral) ECoG and STN ($n = 5$, $p < 0.05$).

3.2.3 Effects of apomorphine on oscillations in the β-frequency range

Recordings were made free of movement artefact in five 6-OHDA-lesioned animals before and after apomorphine administration and the subsequent rotation behaviour. In these we investigated the temporal evolution of power spectra following apomorphine injection. Time-evolving power spectra of both ECoG and STN-LFPs indicated that the power of β-frequency oscillations (22-32 Hz) decreased preceding rotation (Figure 3.3*A*). To investigate this phenomenon in more detail, spectral analysis was performed on each 20 s epoch in the 180 s before the first rotation and compared to each 20 s epoch in the 60 s period preceding apomorphine injection and in the 60 s period immediately following first rotation. Histograms of power in the 22-32 Hz range in both ECoG and STN recordings suggested a drop in β-frequency activity before rotation, as compared to the activity present before the injection (Figure 3.3*B*). A general linear model of raw power in this frequency band determined from the five 60 s periods described above (60 s of rest; 180 s to 0s before rotation, and the first 60 s of rotation) confirmed a main effect of time for ECoG activity ($F(4,16) = 14.173$; $p < 0.0001$) but not STN. *Post hoc* Bonferroni-corrected t-tests showed that both 60 s periods immediately before and after the first rotation had significantly less power in the ECoG in the β-frequency range compared to that at rest ($p < 0.01$).

Apomorphine administration also induced changes in the coherence of activity present at 22-32 Hz in ECoGs and STN-LFPs; these changes were similar in their evolution to the changes in power described above (Figure 3.4*A* and *B*). A general linear model of transformed coherence in this frequency band also confirmed a main effect of time ($F(4,14) = 9.878$; $p < 0.0005$).

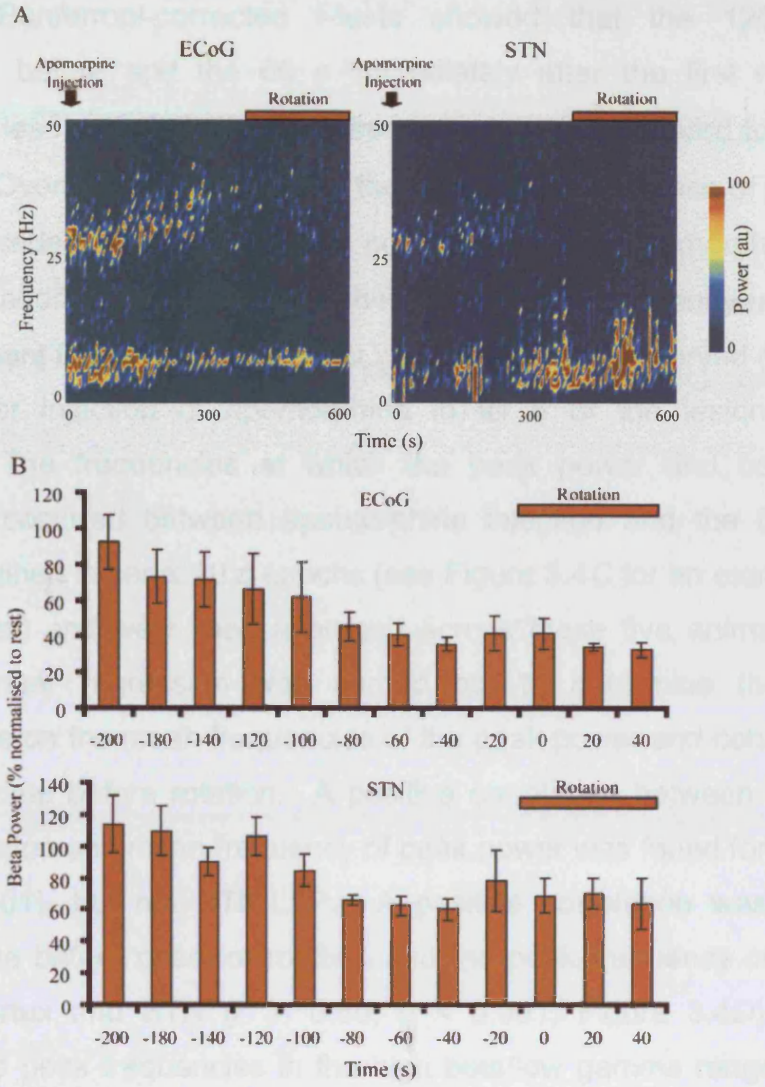

Figure 3.3 Power of β (22-32 Hz) oscillations in the cortex and subthalamic nucleus of 6-hydroxydopamine-lesioned rats is decreased by apomorphine. ***A,*** Time-evolving power spectra of ECoG and STN-LFP activity simultaneously recorded from a lesioned animal recorded after injection of apomorphine. Power of prominent β-frequency oscillations remains high in both channels immediately after injection (t = 0 s; arrows) but begins to decrease after ~100 s, and is much reduced by the time of onset of rotation behaviour. A gradual increase in the frequencies of the oscillatory activity above 15 Hz in both cortex and STN is also clearly visible. ***B,*** Histograms of average power (± S.E.M.s; power normalised with respect to rest) of ECoG and STN activity over 22-32 Hz across all lesioned animals (n = 5). Reductions in power precede the rotations, although this was only found to be statistically significant for ECoG. In these histograms, times indicate timing with respect to the first rotation in each animal (time = 0), rather than with respect to time of injection.

Post hoc Bonferroni-corrected t-tests showed that the 120 s period immediately before and the 60 s immediately after the first rotation had significantly less coherence in the β-frequency range compared to that at rest ($p < 0.01$). Overall, the reductions in the power and coherence of β-frequency activity preceded and thus, were not caused by, apomorphine-induced rotation. In addition to the drop in coherence in the β-frequency range, a shift in the dominant frequency of coherent activity was also observed (Figure 3.4*A* and *C*) after injection of apomorphine in all 5 of the lesioned animals recorded. The frequencies at which the peak power and coherence of oscillations occurred between apomorphine injection and the first rotation were determined in serial 20 s epochs (see Figure 3.4*C* for an example from a single animal) and were then averaged across these five animals for each epoch. Linear regression was carried out to determine the effect of apomorphine on the mean frequencies of the peak power and coherence as a function of time before rotation. A positive correlation between time before onset of rotation and mean frequency of peak power was found for ECoG ($r^2 = 0.6$, $p < 0.01$), but not STN-LFP. A positive correlation was also seen between time before onset of rotation and the peak frequency of coherence between cortex and STN ($r^2 = 0.80$, $p < 0.001$; Figure 3.4*D*). In some animals, two peak frequencies in the high beta/low gamma range (30-45Hz) were present in the coherence of ECoG and the STN-LFP immediately prior to rotation (see Figure 3.4A). A shift in the original beta frequency however, was seen in all cases.

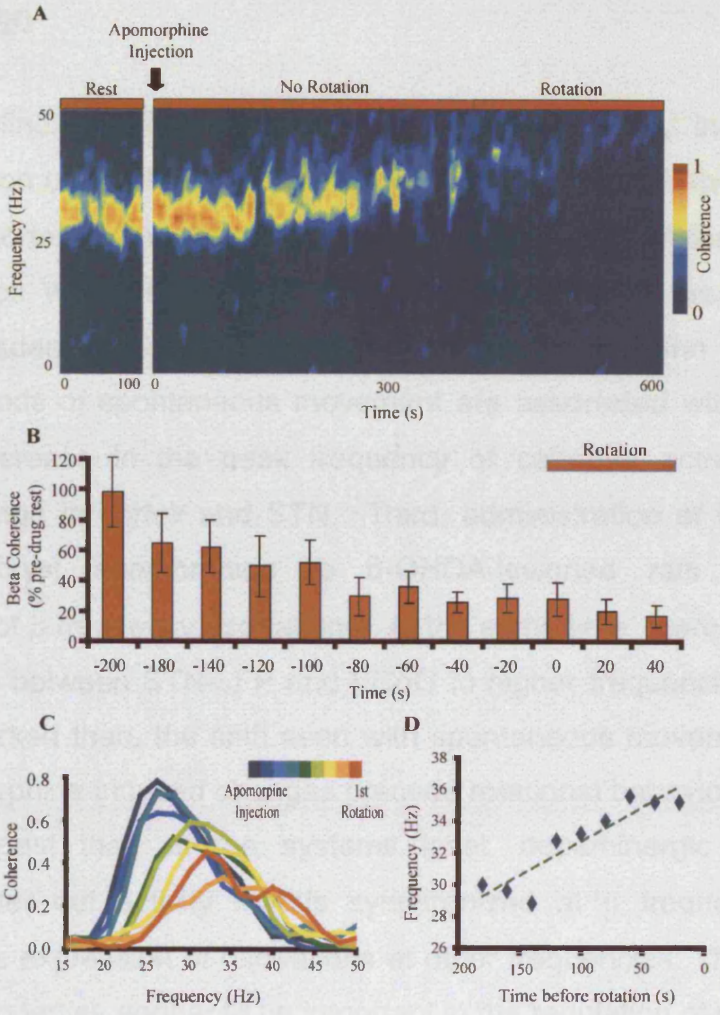

Figure 3.4 Magnitude and dominant frequency of coherent activity in the cortex and subthalamic nucleus of 6-hydoxydopamine-lesioned rats is altered by apomorphine. ***A,*** Time-evolving coherence spectrum recorded before and after injection of apomorphine in the same lesioned animal as seen in Figure 3.3. Coherence between ECoG and STN-LFP is dominated by β-frequency activity at rest. As with power spectra, coherence at β frequencies decreases and also shifts to higher frequencies during the time between injection and the onset of rotations. ***B,*** Histogram showing mean transformed coherence (± SEMs; normalised with respect to rest) over 22-32 Hz across all lesioned animals (n = 5). ***C,*** Coherence in 20 s epochs in a single lesioned animal recorded after injection of apomorphine. Colour changes from dark blue to red indicate chronological order of 20s epochs from injection (dark blue) to first rotation (red). A gradual shift in peak coherence to higher frequencies and lower magnitude is evident after injection. ***D,*** Regression analysis of the mean frequency of peak coherence (5 lesioned animals) in each 20s epoch before the first rotation (time = 0 s) induced by apomorphine administration.

3.3 Discussion

The central findings of this chapter are threefold. First, the preferential synchronisation of oscillatory population activity within and between the STN and frontal cortex in the β-frequency band in the 6-OHDA-lesioned rodent closely agrees with the patterns of activity prevalent in the parkinsonian human (Marsden et al, 2001a; Williams et al, 2003; Kühn et al, 2004). Second, periods of spontaneous movement are associated with a small but significant increase in the peak frequency of coherent activity in the β-frequency range in cortex and STN. Third, administration of the dopamine receptor agonist apomorphine to 6-OHDA-lesioned rats leads to a suppression of β-frequency oscillations. At the same time, there is also a shift of coherence between STN-LFP and ECoG to higher frequencies, similar to, but more marked than, the shift seen with spontaneous movement. Both of these apomorphine-induced changes precede rotational behaviour. The latter findings suggest that, at the systems level, dopaminergic mechanisms effectively filter out activity that is synchronized at β frequencies, whilst promoting the expression of oscillations at other frequencies. These changes in network properties appear to be important in the regulation of movement.

3.3.1 Interpretation of local field potential recordings

Before considering our findings in greater detail we should explore some of the limitations and assumptions of our experimental approach. First, it is possible that increased coherence between ECoGs and STN-LFPs in the 6-OHDA-lesioned animal is a mere by-product of local increases in the power of synchronized activity in the β-frequency band in STN and cortex. However, this is unlikely because increases in the power of non-correlated activities would have been expected to decrease, rather than increase, coherence. Thus, for coherence to increase, there must have been a correlated increase in the amplitude of phase-locked activity at both recording sites (Florian et al, 1998). Second, the question arises as to what extent the coherence between STN-LFPs and ECoG was due to the temporal coupling of local oscillatory activity in STN and cortex, or the volume conduction of synchronous cortical

activity to STN. We used a bipolar recording configuration, thereby avoiding a common reference that may sometimes lead to contamination of STN-LFPs with cortical activity (see Wennberg and Lozano, 2003). In addition, there was a temporal (i.e. phase) difference between the cortical and STN signals in 80% of animals. Although the phase relationship between cortical and subthalamic activities varies, presumably as a result of small relative differences in the cortical areas and STN domains recorded in different animals, temporal differences were nevertheless significantly different to zero and therefore incompatible with volume-conducted activity. Third, we assume that the oscillations present in STN-LFPs and ECoGs reflect the synchronized activity of local neuronal populations. There is much evidence from studies of laminated structures, such as the cortex, that LFPs are representative of the aggregate activity of local neuronal populations (Creutzfeldt et al, 1966; Frost, 1968; Murthy and Fetz 1996a; Baker et al, 1997; Donoghue et al, 1998). The basal ganglia do not share the laminar structure seen in the cortex, but nevertheless, there is evidence to support the notion that LFPs recorded in these nuclei also reflect synchronized aggregate activity (Levy et al, 2002a; Berke et al, 2004; Goldberg et al, 2004; Magill et al, 2004a). Cortical stimulation produces highly synchronized responses in STN neurons that are, in turn, reflected in the field potential (Magill et al, 2004a). The fact that cortical stimulation elicits a stereotypical LFP within STN, but not neighbouring areas, also argues that the population activity reflected in the STN-LFP is dominated by current flow in STN neurons (Magill et al, 2004a). Furthermore, *in vivo* recordings from rat nucleus accumbens show that low-frequency oscillations in LFPs are a consequence of synchronous fluctuations in the membrane potentials of principal cells (Goto & O'Donnell, 2001). Specifically, temporal coupling in the β-frequency band has been demonstrated between single units and LFPs in the striatum of healthy monkeys (Courtemanche et al, 2003) and the STN of parkinsonian patients (Levy et al, 2002a). Moreover, β-frequency oscillations in STN-LFPs are coupled to LFPs recorded in distant, but connected sites, such as the globus pallidus and cerebral cortex, suggesting that they are at least partly associated with synchronized pre-synaptic and/or post-synaptic effects

(Brown et al, 2001; Marsden et al, 2001a; Williams et al, 2002). Thus, β-frequency oscillations in STN-LFPs may be informative about the aggregate or population activity of local neuronal elements. Finally, it should be stressed that the coherence in the beta-frequency band between STN and cortex, as seen predominantly in the 6-OHDA-lesioned animal, was well above the frequency of any periodic motor phenomena, such as walking or whiskering, and was clearly observed when the animals were alert but resting.

3.3.2 Dopamine depletion and synchronisation of activity in the β-frequency band

Is synchronisation of activity in the β-frequency band in parkinsonism an exaggeration of physiological activity in STN or a *de novo* pathological activity? Although we found no evidence of a discrete β-frequency peak in the power spectrum of the STN-LFP of healthy non-lesioned animals, we did find low coherence between ECoGs and STN-LFPs in this frequency band. In contrast, animals with successful and widespread 6-OHDA lesions of neurons in SNc displayed greatly exaggerated power within, and coherence between, the cortex and STN in the β-frequency band. Reductions in the power and coherence of β-frequency oscillations were clearly observed in these animals after administration of the dopamine receptor agonist apomorphine. Note that decreases in β-frequency power and coherence occurred well before the onset of apomorphine induced rotation and could not therefore be ascribed to movement-related decreases in β-frequency activity, as reported when STN-LFPs from parkinsonian patients are averaged around phasic movements (Cassidy et al, 2002a; Levy et al, 2002a; Priori et al, 2002; Kühn et al, 2004; Williams et al, 2003). The decrease in β-frequency power and coherence was found in every animal tested, supporting the idea that these and other changes in network activity may be important in the regulation of movement. It is possible that the observed reductions in β-frequency network activity were associated with changes in alertness, muscle tone, or other non-motor activities involving STN, before rotation (Chudasama et al, 2003). Although non-motor activities were not specifically addressed in the present study, they are presumably of significance for movement initiation anyway and, as such,

the suggestion that changes in β-frequency network activity are important in the regulation of movement is still valid. Although administration of apomorphine decreased the power and coherence of activity in the β-frequency band, it did not affect the weaker coherent activity between cortex and STN at around 6-12 Hz, which may be associated with whisker movements and exploratory behaviour (Moore et al, 1999). Collectively, the above suggest that the dopaminergic mechanisms activated by apomorphine effectively serve to band-pass filter input to, and activity in, the STN in the β-frequency band. Such input is, at least in part, likely to be cortical in origin (Magill et al, 2001, Chapter 4 and 5), whether direct (via cortico-subthalamic pathway) or indirect (via trans-striatal and trans-thalamic pathways), and appears to have greater functional impact in the 6-OHDA-lesioned animal (also see Magill et al, 2001). Because apomorphine was systemically administered, and because we recorded activity at only two areas, cortex and STN, the exact site(s) of action of apomorphine are unknown. Dopamine itself has multiple presynaptic and postsynaptic actions throughout the basal ganglia (see reviews by Greengard et al, 1999; Nicola et al, 2000; Smith and Kieval, 2000), including the STN (Cragg et al, 2004). Nevertheless, our data provide important new insights in the context of the influences of 'dopaminergic tone'.

The effects of dopaminergic stimulation were, however, not limited to a systems-level band-pass filtering of β-frequency activities. Indeed, apomorphine administration also promoted synchronized oscillatory population activity at higher frequencies. This observation is in line with studies in parkinsonian humans showing an increase in oscillations of higher frequency after dopaminergic medication (Brown et al, 2001; Williams et al, 2002), particularly when movements are performed following treatment (Cassidy et al, 2002a). The steady shift in the dominant frequency of activity over time following apomorphine is also consistent with a *dose-dependant* band-pass filtering effect on activity synchronized at β frequencies. A similar, albeit much less pronounced, increase in the frequency of coherence between STN and cortex was seen in lesioned animals during spontaneous

movements, as compared to rest. This intrinsic modulation may relate to dopamine release (for review, see Hauber, 1998) from the remaining few ipsilateral dopamine neurons, and/or may involve an indirect effect of dopaminergic influences originating in the contralateral non-lesioned hemisphere. The role of coherent oscillations at the higher frequencies recorded during movement or after apomorphine is unclear, but it is of interest that these activities were most marked post-apomorphine in the period between injection and florid hyperkinesia (rotation); an intermediate state may be the closest to "normal" function in the lesioned animals. The increase in the frequency of rhythmic population activity with dopamine receptor stimulation observed in the present study contrasts with the ability of dopamine receptor agonists to reduce the firing rates of single STN neurons in the 6-OHDA-lesioned animal (Kreiss et al, 1997). The opposite direction of these effects underscores the complex relationship between synchronized population activity and single unit activity (Bullock, 1997; Engel et al, 2001 and see Chapter 7).

3.3.3 Functional Implications

These results indicate that rhythmic and synchronised population activity in the STN is likely to be strongly coupled to that in cortex, which provides an important excitatory input to the STN (Magill et al, 2000, 2001, 2004a). The findings presented here, together with those showing that the excessive synchronisation of β-frequency activity in STN in PD patients is reversed with dopaminergic medication (Brown et al, 2001; Levy et al, 2001, 2002a), suggest that the function of dopamine is to modulate not only the degree of synchronisation of activity within the basal ganglia, and the synchronisation between the cortex and basal ganglia, but also its frequency. Modulations of oscillatory activity are increasingly being recognised as potentially valuable measures of drug action (Whittington et al, 2000). Given the growing evidence for the importance of synchronized activity in PD pathology (Bergman et al, 1998; Boraud et al, 2002; Brown, 2003), the reduction of activity synchronized in the β-frequency band in basal ganglia and/or cortex in

the 6-OHDA-lesioned rat could prove a highly predictive model for the efficacy of novel anti-parkinsonian therapies (see Chapter 7).

3.4 Chapter 3: Summary

- 6-hydroxydopamine (6-OHDA) lesions of midbrain dopamine neurons are associated with significant increases in the power and coherence of β-frequency oscillatory activity present in LFPs recorded from frontal cortex and STN of awake rats, as compared to the healthy animal.

- The pattern of synchronisation between population activity in the STN and cortex in the 6-OHDA-lesioned rodent model of Parkinson's disease closely parallels that seen in the parkinsonian human. The peak frequency of coherent activity in the β-frequency range was increased in lesioned animals during periods of spontaneous and sustained movement.

- Administration of the dopamine receptor agonist apomorphine to lesioned animals suppressed β-frequency oscillations, and increased coherent activity at higher frequencies in cortex and STN, before producing the rotational behaviour indicative of successful lesion.

- Taken together, these results support a crucial role for dopamine in the modulation of population activity in cortico-basal ganglia circuits, whereby dopaminergic mechanisms effectively filter out synchronised, rhythmic activity at β-frequencies at the systems level, and shift temporal couplings in these circuits to higher frequencies. These changes may be important in regulating movement.

A Sham Lesion

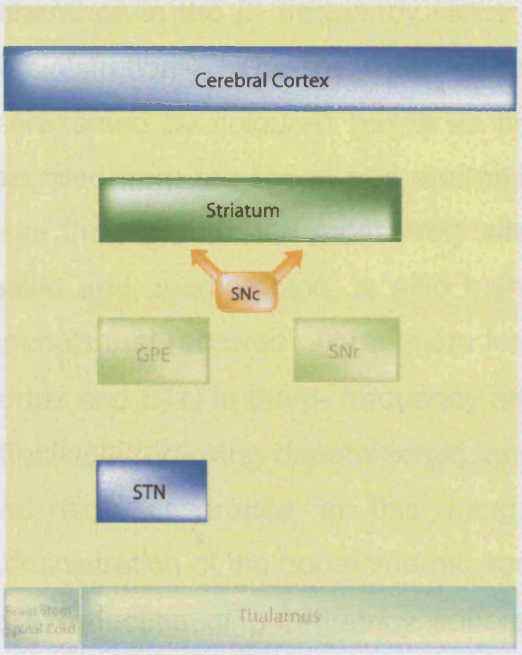

B 6-OHDA lesion

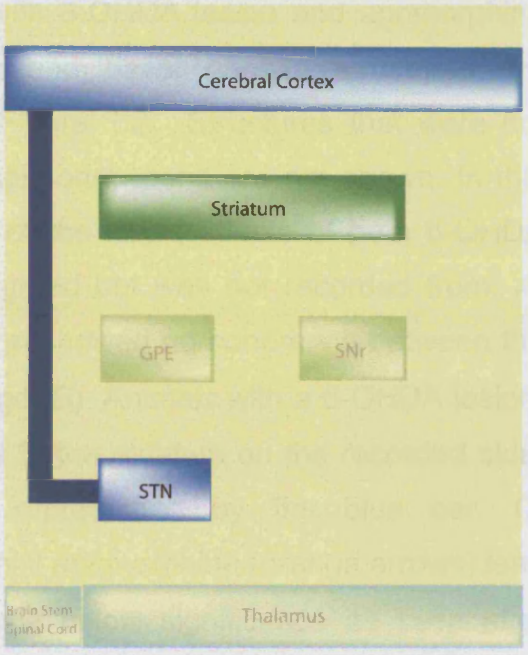

C 6-OHDA lesion + Apomorhine

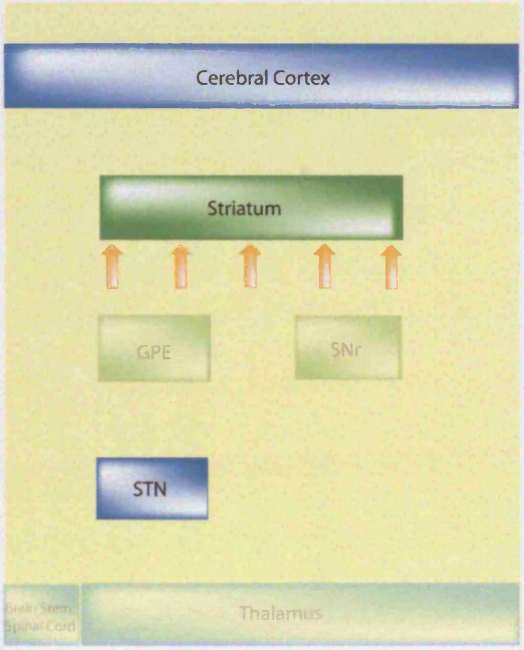

Figure 3.5 Summary diagram showing changes in cortico-subthalamic coherence in the β- frequency range with 6-OHDA lesion and apomorphine administration. The cerebral cortex and basal ganglia structures are represented by coloured boxes as in Figure 1.2. Structures that were not recorded from are faded and anatomical connections are not shown. In this case the striatum, the most likely site of the direct effects of both 6-OHDA lesion and apomorphine, is also highlighted but was not recorded from. *A*) Animals that received only a sham lesion showed no coherence between the cortex and STN in the β- frequency range. *B*) Animals with a 6-OHDA lesion, effectively removing dopaminergic input to the striatum on the recorded side, had high coherence in this band, represented by the blue bar. *C*) Administration of the dopaminergic agonist apomorphine (orange arrows) lead to a reduction of β-frequency coherence below significance as seen after sham lesion. The striatal position of the orange arrows indicates the most likely site of action for apomorphine (see Section 3.3.2), but due to the systemic administration used, this may also occur at other sites.

Chapter 4: Brain state-dependence of coherent oscillatory activity in the cerebral cortex and basal ganglia of the rat

Although much is known about the anatomy of cortico-basal ganglia circuits and the integration of cortical information at the level of single striatal and STN neurons (Gerfen and Wilson 1996; Nambu et al, 2002; Smith et al, 1998), the way in which the activities of large populations of cortical and basal ganglia neurons are coordinated, *i.e.* the "functional organization" of these circuits, remains obscure. Single units alone are inadequate for investigating population activity because they represent only one level of functional organization of a given brain area and thus, reflect only a limited part of the information processing (Bullock 1997; Pesaran et al, 2002). This may be of particular relevance in the basal ganglia, where the output nuclei and their efferent partners receive highly-processed information converging from multiple cortical and subcortical loops (Alexander and Crutcher 1990; Smith et al, 1998 and see Figures 1.2 and 1.3). Recordings of local field potentials (LFPs), which better reflect coordinated population activity (Hubbard et al, 1969; Mitzdorf 1985), and single units from multiple sites have proved useful for investigating the functional organization of the neocortex, thalamus and hippocampus (Buzsáki 2002; Contreras et al, 1997; Engel and Singer, 2001; Engel et al, 2001). Data from humans implanted with deep brain electrodes for the treatment of Parkinson's disease (PD) suggest that these techniques will also be informative in basal ganglia circuits (Brown 2003; Levy et al, 2002a; Liu et al, 2002). Indeed, coherent or temporally-coupled LFPs are often observed in sensorimotor cortex and basal ganglia during behaviour (Brown 2003). Moreover, the coherence and frequency profiles of oscillatory LFPs recorded from the cortex and basal ganglia of PD patients vary with movement and levodopa treatment, suggesting that the population activity reflected in the LFP may be functionally significant (Brown et al, 2001; Cassidy et al, 2002a; Kuhn et al, 2004; Levy et al, 2002a; 2002b; Marsden et al, 2001a; Williams et al, 2002).

The recording sites available in the human are necessarily limited to therapeutic targets, such as the STN, and recordings can only be performed in patients with abnormal movement control. The overall objective of the this chapter was to investigate functional connectivity using simultaneous recordings from the cortex and other strategic basal ganglia sites of healthy animals in different brain states. To this end, LFP and unit recordings were made in the urethane-anesthetized rat, a good model for determining the impact of extremes of cortical activity on the basal ganglia (Magill et al, 2000, 2001), enabling us to test the dependence of coherent activity on brain state. Changes in LFPs were investigated using frequency analysis techniques that favour the demonstration of oscillatory rather than stochastic synchronisation (Halliday et al, 1995; Rosenberg et al, 1998), although the latter may also exist in cortico-basal ganglia circuits.

Three key hypotheses were tested. First, that there is extensive temporal coupling between the ECoG and basal ganglia LFPs. Second, such coupling varies with frequency and depends on brain state. Third, that the pattern of coupling is also dependent on the precise site of LFP recording in basal ganglia, compatible with a relative functional segregation between different elements of the cortico-basal ganglia circuitry.

4.1 Methods

4.1.1 Electrophysiological recordings and labeling of recording sites

Experimental procedures were carried out on adult male Sprague-Dawley rats (Charles River, Margate, UK) and were conducted in accordance with the Animals (Scientific Procedures) Act, 1986 (UK) and the APS's *Guiding Principles in the Care and Use of Animals*.

Electrophysiological recordings were made in 12 rats (200-320 g). Anesthesia was induced with isoflurane (Isoflo™, Schering-Plough Ltd., Welwyn Garden City, UK) and maintained with urethane (1.3 gkg^{-1}, i.p.; ethyl carbamate, Sigma, Poole, UK), and supplemental doses of ketamine (30 $mgkg^{-1}$, i.p.; Ketaset™, Willows Francis, Crawley, UK) and xylazine (3 $mgkg^{-1}$, i.p.; Rompun™, Bayer, Germany), as described previously (Magill et al, 2000, 2001). All wound margins were infiltrated with the local anesthetic, bupivacaine (0.75% w/v; Astra, Kings Langley, UK) and corneal dehydration was prevented with application of Hypromellose eye drops (Norton Pharmaceuticals Ltd., Harlow, UK). Animals were then placed in a stereotaxic frame. Body temperature was maintained at 37 ± 0.5°C with the use of a homeothermic heating device (Harvard Apparatus Ltd., Edenbridge, UK). Anesthesia levels were assessed by examination of the ECoG (see below), and by testing reflexes to a cutaneous pinch or gentle corneal stimulation. Electrocardiographic (ECG) activity and respiration rate were also monitored constantly to ensure the animals' well being (see below). Mineral oil or saline solution (0.9% w/v NaCl) was applied to all areas of exposed cortex to prevent dehydration.

The ECoG was recorded via a 1 mm diameter steel screw juxtaposed to the dura mater above the right frontal cortex (AP: –4.5 mm, ML: –2.0 mm [Paxinos and Watson 1986], which corresponds to the medial agranular field of the somatic sensorimotor cortex [Donoghue and Wise 1982]) and referenced against an indifferent electrode placed adjacent to the temporal musculature (Figure 4.1*A*). This and adjacent regions of cortex project to both

striatum and STN, as demonstrated in anatomical and electrophysiological studies (Fujimoto and Kita 1993; Kolomiets et al, 2003; Magill et al, 2004; Smith et al, 1998), and thus, activity in these regions is of direct functional relevance. Raw ECoG was band-pass filtered (0.1-150 Hz, -3 dB limits) and amplified (2000×, NL104 preamplifier; Digitimer Ltd., Welwyn Garden City, UK) before acquisition. The ECG was differentially recorded via two silver wires inserted into the skin of the ipsilateral forelimb and hindlimb. Raw ECG was band-pass filtered (10-100 Hz) and amplified (5000×, NL104; Digitimer) before acquisition. The chest movements accompanying respiration were recorded using a miniature accelerometer (AP19, Bay Systems Ltd., Somerset, UK) and charge amplifier (Type 5007; Kistler Instrumente AG, Winterthur, Switzerland). The signal from the accelerometer allowed the depth and rate of respiration to be accurately assessed on- and off-line.

Extracellular recordings of LFPs and action potentials in the ipsilateral GP, STN and SNr were simultaneously made with glass electrodes (6-12 MΩ measured at 10 Hz *in situ*, tip diameters of 2.5-3.0 μm; see Figure. 4.1*A*) that were filled with a 0.5 M NaCl solution containing 1.5% w/v Neurobiotin™ (Vector Labs, Peterborough, UK). Extracellular signals from the three electrodes were amplified (10×) through the active bridge circuits of two Axoprobe-1A amplifiers (Axon Instruments, Foster City, CA), bifurcated, and then differentially filtered to extract LFPs and unit activity. The LFPs were recorded after further amplification (100×; NL-106 AC-DC Amp, Digitimer) and low-pass filtering (between d.c. and 150 Hz; NL125 filters, Digitimer). Single units were recorded following AC-coupling, further amplification (100×; NL-106, Digitimer), and band-pass filtering (between 0.4 and 4 kHz; NL125, Digitimer). The monopolar glass electrodes were independently referenced via wires inserted into the skin at the top of the neck. Three HumBug™ units (Quest Scientific, Vancouver, Canada) were used in place of traditional 'notch' filters to eliminate mains noise or 'hum' at 50 Hz (Brown et al, 2002). Action potentials were typically between 0.3 and 0.8 mV in amplitude and always exhibited an initial positive deflection. Recordings of spontaneous activity typically lasted for 20-40 min.

Activity was recorded, first, during slow-wave activity (SWA), which accompanies deep anesthesia and is similar to activity observed during natural sleep, and secondly, during episodes of sensory-evoked 'global activation', which contain patterns of activity that are more analogous to those observed during the awake, behaving state (see review by Steriade (2000) and references therein). Sensory stimulation and subsequent global activation were elicited by pinching the hindpaw for 15 s with serrated forceps that were driven by a standard pneumatic pressure, as described previously (Magill et al, 2000, 2001). The animals did not exhibit either a marked change in ECG/respiration rates or a hindpaw withdrawal reflex in response to the pinch.

After the recording sessions, all recording locations were marked by discrete, extracellular deposits of Neurobiotin™ (100 nA anodal current; 1 s [50%] duty cycle for 60 min; Magill et al, 2001, 2004). Following a period of 1-2 hr for the uptake and transport of the Neurobiotin™ by neurons and glia at the recording sites, animals were given a lethal dose of ketamine anesthetic and perfused via the ascending aorta with 100 ml of 0.01 M phosphate-buffered saline at pH 7.4 (PBS), followed by 300 ml of 0.1% glutaraldehyde and 4% paraformaldehyde in 0.1 M phosphate buffer, pH 7.4, and then by 150 ml of the same solution without glutaraldehyde. Brains were then post-fixed in the latter solution at 4°C for at least 12 hr before sectioning.

4.1.2 Histochemistry

Standard techniques were used to visualize the Neurobiotin™ deposits (see Magill et al, 2001). Briefly, the fixed brain was cut into 60 μm thick sections in the parasagittal plane on a vibrating blade microtome (VT1000S: Leica Microsystems, Milton Keynes, UK). Sections were washed in PBS and incubated overnight in avidin-biotin peroxidase complex (ABC *Elite*; 1:100; Vector) in PBS containing 0.2% Triton X-100 and 1% bovine serum albumin (Sigma). After washing, the sections were incubated in hydrogen peroxide (0.002% w/v; Sigma) and diaminobenzidine tetrahydrochloride (0.025% w/v;

Sigma) in the presence of nickel ammonium sulphate (0.5% w/v; Sigma) dissolved in Tris buffer (0.05 M, pH 8.0) for 15-30 min. Neurobiotin™-filled neurons and glia were intensely labelled with an insoluble, black/blue precipitate (Figure 4.1*B-D*). Finally, sections were dehydrated, cleared and mounted for light microscopy using standard techniques (Bolam 1992). The precise locations of all recording sites in the basal ganglia were histologically verified. The central and medial two thirds of the GP, and all regions of STN and SNr were sampled in this study (Figure 4.1*B-D*).

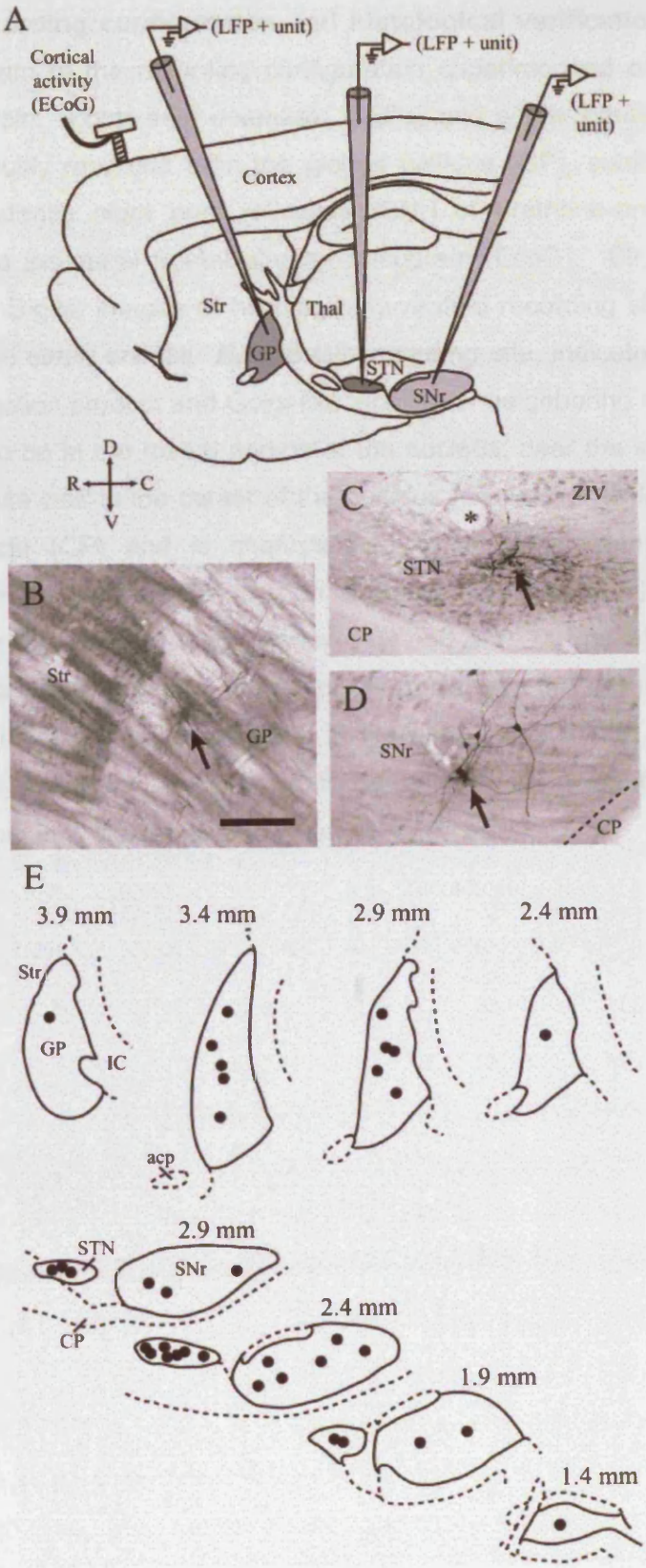
A
(LFP + unit)
(LFP + unit)
(LFP + unit)
Cortical activity (ECoG)
Cortex
Str
Thal
GP
STN
SNr
D
R
C
V
B
Str
GP
C
ZIV
STN
CP
D
SNr
CP
E
3.9 mm
3.4 mm
2.9 mm
2.4 mm
Str
GP
IC
acp
2.9 mm
STN
SNr
CP
2.4 mm
1.9 mm
1.4 mm

Figure 4.1 Recording configuration and histological verification of recording sites. ***A,*** Diagram of the recording configuration superimposed on a parasagittal section of rat brain. Local field potentials (LFPs) and single neuron (unit) activity were simultaneously recorded from the globus pallidus (GP), subthalamic nucleus (STN) and substantia nigra pars reticulata (SNr) of urethane-anesthetized rats, together with the ipsilateral frontal electrocorticogram (EcoG). Str, striatum; Thal, thalamus. ***B-D,*** Digital images of histologically-verified recording sites in GP, STN and SNr from the same animal, ***B,*** The GP recording site, indicated by an intense spot of black reaction product and Golgi-like labeling of neighboring neurons (arrow), was confirmed to be in the rostral portion of the nucleus, near the striatum. ***C,*** The STN recording site was in the center of the nucleus (arrow), which lies dorsal to the cerebral peduncle (CP) and is characterized by a higher density of neurons compared to the overlying ventral division of the zona incerta (ZIV). A large blood vessel (*) lies on the border between dorsal STN and ZIV. ***D,*** The SNr recording site was centrally placed in the lateral portion of the nucleus (arrow), which lies dorsal to the CP (border indicated by dashed line). ***E,*** Recording sites in GP, STN and SNr in all 12 animals. Numbers above sections correspond to the distances lateral of midline. Scale bar in B also applies to C and D = 200 μm.

4.1.3 Data acquisition and analysis

Local field potentials and unit activity were sampled at 400 Hz and 10 kHz, respectively. The ECoG, ECG and respiration signals were each sampled at 400 Hz. All biopotentials were digitized on-line with a PC running Spike2™ acquisition and analysis software (version 4; Cambridge Electronic Design Ltd., Cambridge, UK). Data from the recording session were first scrutinized for ECG and respiration artifacts. LFP data contaminated with ECG artifact were rejected. The occasional influence of a respiration artifact (1.5-2.5 Hz; see also Hu et al, 2002) in the LFPs was negated by partialisation of coherence measures with the respiration waveform as the 'predictor' (see below). Artifact-free data were then visually inspected and epochs of robust cortical slow-wave activity (see Figure 4.2) or global activation (see Figure 4.3) were identified (Magill et al, 2000, 2001). Portions of the concurrently recorded spike trains composed of 250 spikes were isolated and used for statistical analysis of spontaneous unit discharge. The coefficient of variation of the interspike intervals (CV), a value used widely as an indicator of regularity in point processes (Johnson 1996), was calculated (the lower the CV value, the more regular the unit activity). Mean firing frequency was calculated from the reciprocal of the mean interspike interval, Statistical comparisons of unpaired data were performed using the Mann-Whitney *U* test. Statistical comparisons of paired data (*i.e.* firing rates or CVs before and during global activation) were performed using the Wilcoxon Signed Rank test. Multiple statistical comparisons of unit discharge in GP, STN and SNr were performed using a One-Way ANOVA, with a *post hoc* Bonferroni test, or when not appropriate (in cases of inhomogeneous variance; Levene test), using the Kruskal-Wallace *H* Test, together with a *post hoc* Dunn test for further definition (SPSS; SPSS Inc., Chicago, IL). The criterion for significance was the 95% level (unless stated otherwise). Data are expressed as mean ± standard deviation (SD). Auto- and cross-correlograms of action potentials (between 250 and 1200 per neuron) were calculated and normalized according to standard methods and a bin size of 1, 5 or 10 ms (Abeles 1982; Perkel et al, 1967).

The connectivity between the cortex and basal ganglia across conditions was investigated primarily using coherence and partial coherence analysis. A detailed description of the foundation and application of these methods in neurophysiology can be found in Chapter 2. Briefly, in the context of these recordings the partial coherence can be viewed as representing the fraction of coherence between, for example, ECoG and STN-LFP that is not shared with a third signal, say GP-LFP. Thus, if sharing of the signal between ECoG, STN-LFP and GP-LFP were complete, then partialisation of the coherent activity between ECoG and STN-LFP with GP-LFP as the predictor would lead to zero coherence. It follows that if the coherent activity between ECoG and STN-LFP were kept completely separate from GP, partialisation with GP-LFP as the predictor would have no effect on the coherence between ECoG and STN-LFP signals.

Coherence and partial coherence analyses were performed on two data segments of activity during robust SWA episodes, as identified by assessing ECoG activity (see above), and one data segment of pinch-evoked activity per animal. All data segments were 80 s in length. Single data segments of pinch-evoked activity were derived by splicing together multiple recordings made during and immediately after (up to 5 s) four hindpaw pinches. The variance of spectral power estimates was stabilized by logarithmic transformation (Halliday et al, 1995). Group analysis of transformed coherence data was performed by repeated measures General Linear Models (GLMs) as described in the Results. A Greenhouse-Geisser correction for non-sphericity was used where necessary and significance was set at $p \leq 0.01$ to correct for the multiple GLMs. *Post hoc* testing was by two-tailed paired *t*-tests.

4.2 Results

4.2.1 Distinct patterns of cortical activity during SWA and global activation

Cortical activity, as assessed from the ECoG, was the primary indicator of brain state. Two states were identified, slow-wave activity (SWA) and 'global activation'. As described previously (Magill et al, 2000, 2001), urethane anesthesia was accompanied by regularly occurring slow-waves of large amplitude (> 450 μV), with a mean frequency of 0.89 ± 0.12 Hz (n = 12), in the frontal ECoG (Figure 4.2; see *inset* of figure 4.4*A*). Higher frequency (7-12 Hz), smaller amplitude (< 200 μV) spindle activity was often superimposed on the crests of the slow-waves (Figure 4.2). Sensory stimulation by hindpaw pinch resulted in a marked loss of the power (*i.e.*, rhythmicity and amplitude) of oscillatory activity in the slow- and spindle-frequency ranges in the ECoG (Figure 4.3), indicative of global activation of the forebrain. This was paralleled by an increased presence of high frequency, small amplitude (< 200 μV) oscillations in the β- (15-30 Hz) and γ- (30-60 Hz) frequency ranges (Figure 4.3).

4.2.2 Distinct patterns of basal ganglia LFPs during SWA and global activation

Slow-waves in the ECoG were associated with similar slow oscillations of large amplitude (> 400 μV) in the LFPs recorded from ipsilateral STN (mean peak frequency of 0.90 ± 0.12 Hz; n = 12), GP (0.89 ± 0.16 Hz) and SNr (0.90 ± 0.13 Hz), as shown in Figure 4.2 and *insets* of Figure 4.4*A, E,* and *I*.

Cumulant density estimates of ECoG and LFP activities confirmed that during SWA, the LFP and ECoG activities were correlated (Figure 4*A*, *E*, and *I*) and were dominated by a significant, rhythmic feature with a period of ~ 1 s (*i.e.* ~ 1 Hz oscillation). The surface-positive active components of the cortical slow oscillation were phase-locked, at small time lags, with deflections of negative polarity in all basal ganglia LFPs (Figure 4*A*, *E*, and *I*; also see epoch marked by dashed box in Figure 4.2).

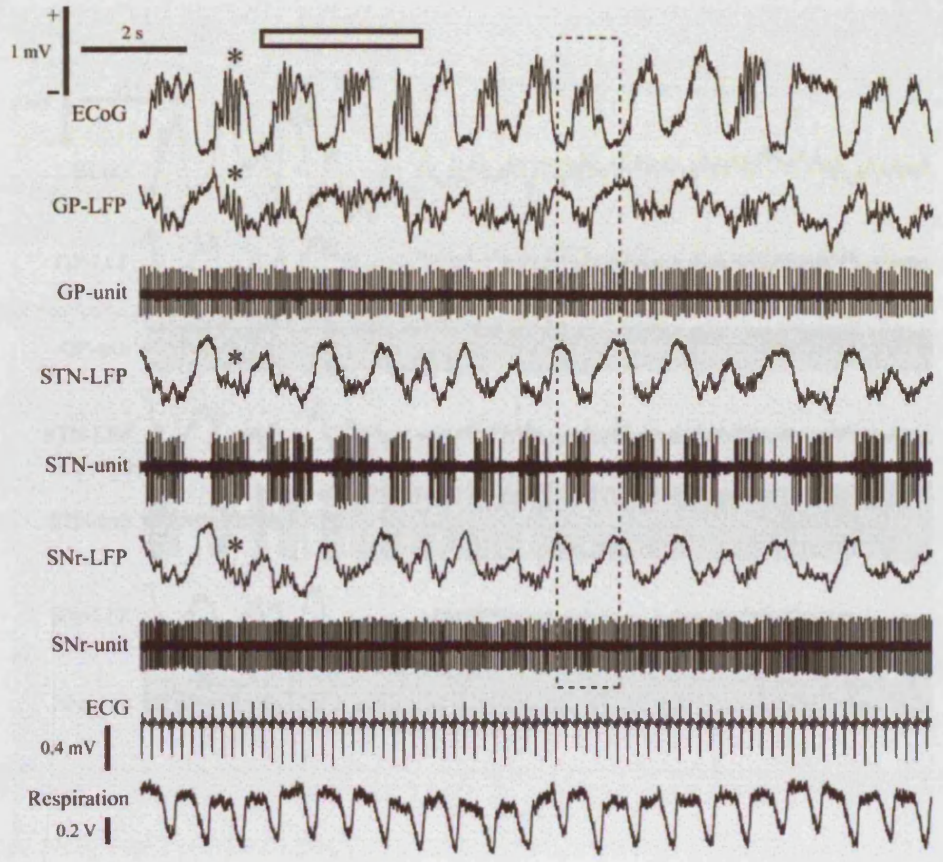

Figure 4.2 Simultaneous recordings of activity patterns in the cerebral cortex and basal ganglia during robust slow-wave activity. The ECoG was dominated by a large-amplitude, slow oscillation (~1 Hz) and spindle activity (7-12 Hz; one spindle is indicated by asterisks) during SWA. Concomitantly recorded LFPs in GP, STN and SNr displayed similar oscillatory phenomena, but with reversed polarities compared to cortical activity (see dashed box for a clear example). Note that the LFP in GP did not reflect the cortical slow oscillation as faithfully as did LFPs in STN and SNr (see epoch under white bar for a clear example of this dissociation of signals). Neurons in STN exhibited low-frequency oscillations in firing and thus approximated a bursting type of activity. Such activity was closely related to the slow-wave activity in the ECoG and LFPs. Neurons in GP and SNr discharged at higher frequencies in a more regular manner, and the relationship between unit activity and ECoG/LFPs was not as clear as that in STN. The ECoG and LFPs were not related to either electrocardiogram (ECG) or respiration. Calibration bars for ECoG apply to all basal ganglia recordings. Calibration bar for time also applies to ECG and respiration.

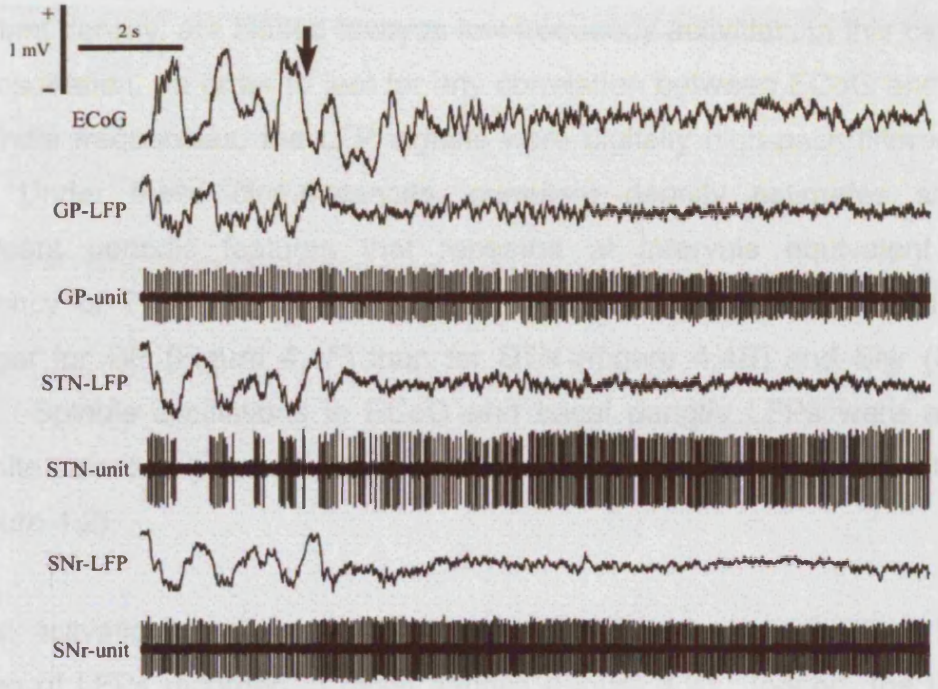

Figure 4.3 Simultaneous recordings of activity patterns in the cerebral cortex and basal ganglia during global activation. Same recording sites and neurons as in Figure 4.2. Global activation of the forebrain following pinch onset (arrow) was exemplified by a loss of slow-wave and spindle oscillations in the ECoG, and a shift to oscillatory activity of smaller amplitude and higher frequency. Local field potentials in GP, STN and SNr displayed similar shifts in oscillatory phenomena. During global activation, the pattern of unit activity in STN switched from low-frequency oscillatory firing to tonic, regular/irregular firing at a higher frequency (CV of unit shown was reduced from 1.22 to 0.46; increase in firing to 180 % of firing rate during SWA). Although the firing patterns of the GP unit and the SNr unit did not significantly change during activation, the firing rates of the neurons significantly increased (to 156% and 126% of firing rates during SWA, respectively). Calibration bars apply to all panels.

Spindle events in the ECoG were also reflected by similar oscillations in basal ganglia LFPs. As discussed in Chapter 2, time domain methods including the cumulant density, are biased towards low frequency activities, in this case the slow oscillation. In order to test for any correlation between ECoG and LFPs at spindle frequencies, the LFP signals were digitally high-pass filtered at 5 Hz. Under these circumstances, cumulant density estimates showed significant periodic features that repeated at intervals equivalent to a frequency of 7-12 Hz (Figure. 4.4*B*, *F*, and *J)*. These correlations were stronger for GP (Figure 4.4*F*) than for STN (Figure 4.4*B*) and SNr (Figure 4,4*J*). Spindle oscillations in ECoG and basal ganglia LFPs were also of opposite polarities (Figure 4.4*B*, *F*, and *J*; also see epoch marked by asterisks in Figure 4.2).

Global activation was always associated with time-locked changes in the profiles of LFPs recorded in basal ganglia (Figure 4.3). Indeed, the loss of cortical SWA and the adoption of high-frequency, small-amplitude oscillatory activity in ECoG during sensory stimulation were effectively mirrored by similar shifts in the activity patterns of STN-LFPs, GP-LFPs and SNr-LFPs (Figure 4.3). Low-frequency, large-amplitude oscillatory activity in basal ganglia LFPs only resumed when SWA reappeared in the ECoG (data not shown).

4.2.3 Coherence between ECoG and basal ganglia LFPs differs across brain states and frequencies

Spontaneous activity in cortex and basal ganglia was significantly coherent in the slow oscillation and spindle-oscillation frequency ranges during SWA (Figure 4.4*C*, *G*, and *K*; also see Figure 4.5*A-C*). Coherence analysis also confirmed that spontaneous activity in cortex and basal ganglia was significantly coherent at high frequencies that broadly encompassed β- and γ–band oscillations (15-60 Hz) during the activated brain state (Figure 4.6*A-C*), mirroring the loss of SWA and the adoption of high-frequency, small-amplitude activity in ECoG.

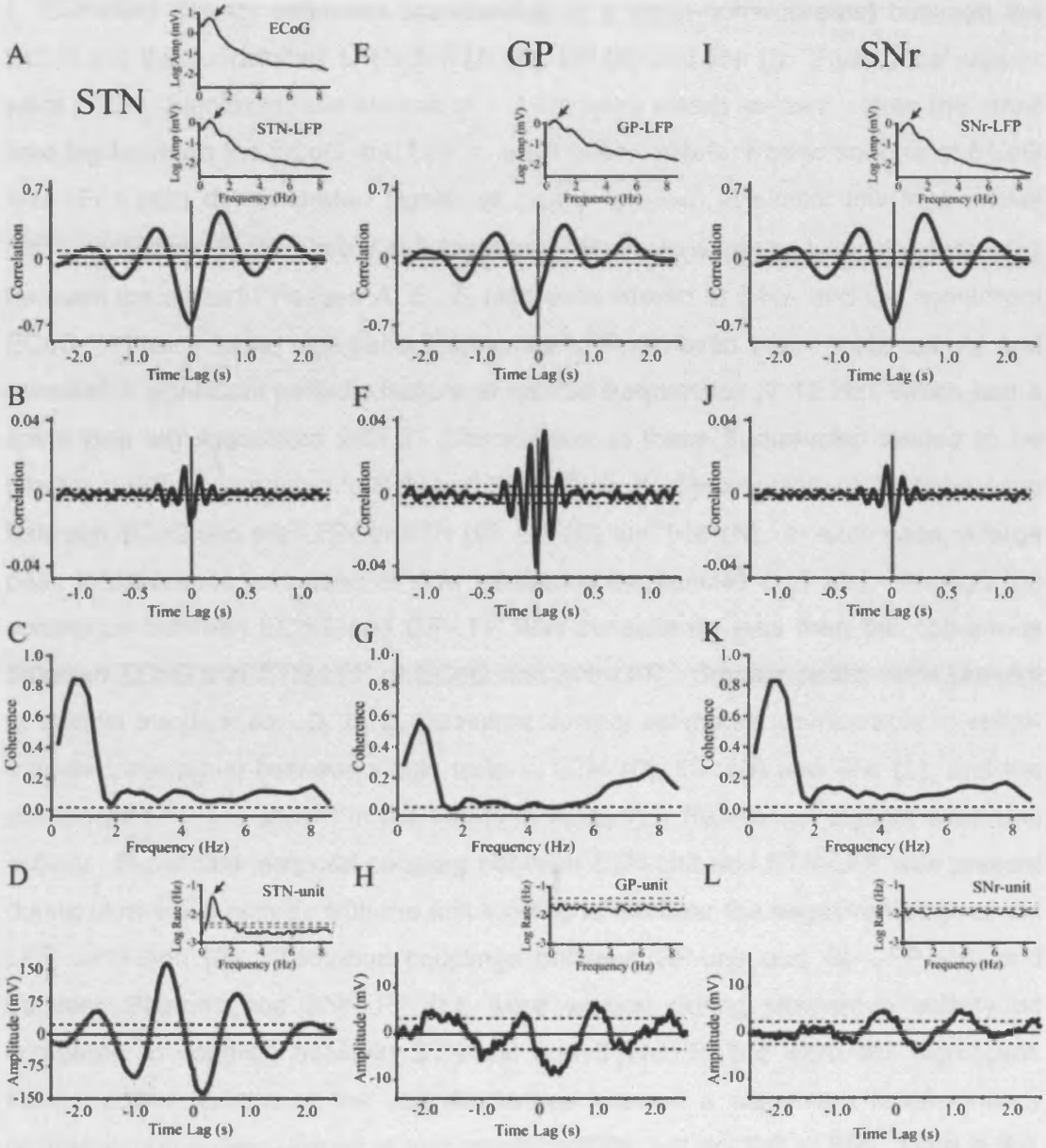
A
STN
ECoG
STN-LFP
Log Amp (mV)
Frequency (Hz)
Correlation
Time Lag (s)
B
C
Coherence
D
STN-unit
Log Rate (Hz)
Amplitude (mV)
E
GP
GP-LFP
F
G
H
GP-unit
I
SNr
SNr-LFP
J
K
L
SNr-unit

Figure 4.4 Oscillations in basal ganglia LFPs are temporally coupled to both ECoG activity and single unit discharge during robust slow-wave activity. ***A, E, I,*** Cumulant density estimates (comparable to a cross-correlograms) between the ECoG and the concomitant LFPs in STN (***A***), GP (***E***) and SNr (***I***). 'Reference' signals were LFPs. Significant correlations at ~ 1 Hz were clearly evident. Note the small time lag between the ECoG and LFP in each case. *Insets:* Power spectra of ECoG and LFPs both demonstrated significant peaks (arrows) at similar low frequencies (95% confidence limits were $\leq$ 0.2 log mV^2). ***B, F, J,*** Cumulant density estimates between the same LFPs (see ***A, E , I***), high-pass filtered at 5 Hz, and the concurrent ECoG. In each case, high-pass filtering the LFP removed the ~ 1 Hz activity and revealed a significant periodic feature at spindle frequencies (7-12 Hz), which had a small time lag associated with it. Correlations at these frequencies tended to be greater in GP as compared to STN and SNr. ***C, G, K,*** Typical plots of the coherence between ECoG and the LFPs in STN (***C***), GP (***G***) and SNr (***K***). In each case, a large peak in coherence was seen at slow oscillation frequencies (~ 1 Hz), although the coherence between ECoG and GP-LFP was consistently less than the coherence between ECoG and STN-LFP or ECoG and SNr-LFP. Smaller peaks were present at spindle frequencies. ***D, H, L,*** Cumulant density estimates (comparable to spike-triggered averages) between single units in STN (***D***), GP (***H***) and SNr (***L***), and the concurrent LFP (as shown in the insets in ***A, E, I***). 'Reference' signals were unit activity. Significant temporal coupling between STN-unit and STN-LFP was present during slow-wave activity, with the unit tending to fire near the negative trough of the LFP oscillation (***D***). Temporal couplings between GP-unit and GP-LFP (***H***), and between SNr-unit and SNr-LFP (***L***), were weaker during slow-wave activity as compared to coupling between STN-unit and STN-LFP, but were still significant. *Insets:* power spectra of the unit discharges showed a significant low-frequency oscillatory component (arrow) of unit activity in STN, but not GP or SNr. Data in ***A-L*** were taken from the same epoch of slow-wave activity (306 s of data, block size of 4096 data points, frequency resolution of 0.24 Hz); ECoG, LFPs and units were simultaneously recorded. The dashed lines in the coherence spectra, cumulant density estimates and single unit power spectra are the 95% confidence limits.

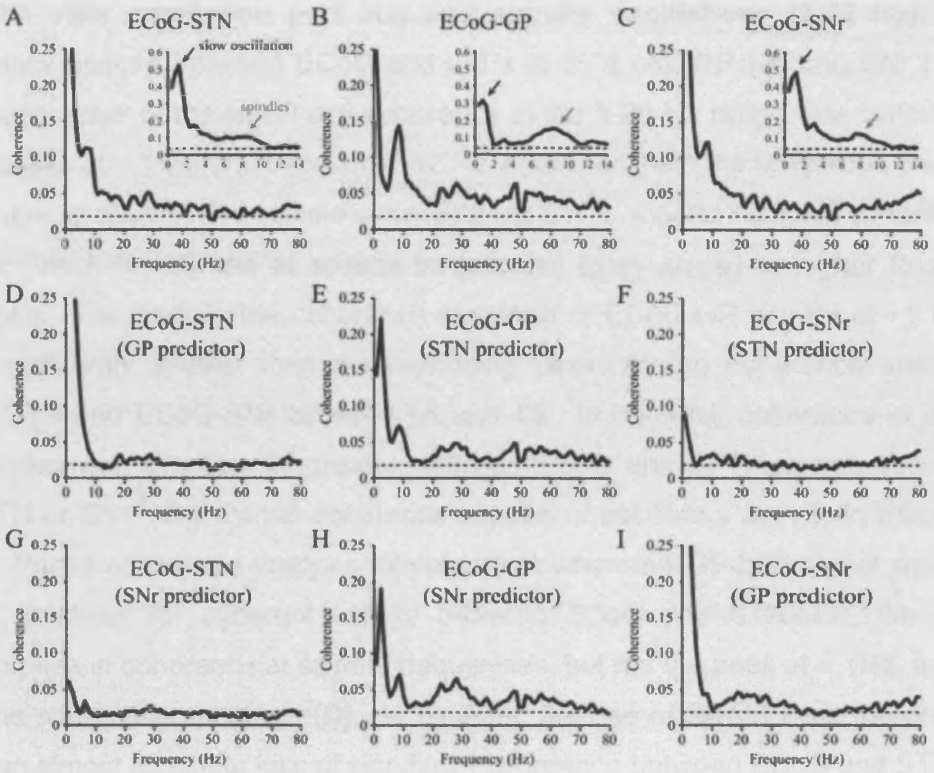
A
ECoG-STN
slow oscillation
spindles
B
ECoG-GP
C
ECoG-SNr
D
ECoG-STN
(GP predictor)
E
ECoG-GP
(STN predictor)
F
ECoG-SNr
(STN predictor)
G
ECoG-STN
(SNr predictor)
H
ECoG-GP
(SNr predictor)
I
ECoG-SNr
(GP predictor)
Coherence
Frequency (Hz)

Figure 4.5 Coherent oscillatory population activity in cortex and basal ganglia during robust slow-wave activity is largely confined to frequencies associated with the slow oscillation (~ 1 Hz) and spindle oscillations (7-12 Hz). ***A-C,*** Coherence spectra between ECoG and LFPs in STN (***A***), GP (***B***) and SNr (***C***). In each case, most of the significant coherence in the 0-80 Hz range was contained in major peaks at ~ 1 Hz and between 7-12 Hz, consistent with the ubiquitous presence of the slow oscillation and spindle activity during SWA. *Insets:* Peaks in coherence at ~ 1 Hz (black arrow) and at spindle frequencies (grey arrow) at higher frequency resolution. The peak in the coherence spectrum of ECoG-GP activity at ~1 Hz (***B***) was significantly smaller than corresponding peaks in the coherence spectra of ECoG-STN and ECoG-SNr activities (***A*** and ***C***). In contrast, coherence at spindle frequencies was significantly greater between ECoG and GP than between ECoG and STN or SNr. ***D-I,*** Partial coherence spectra of oscillatory activity in ECoG and LFPs. Partial coherence analysis revealed that when the GP-LFP signal was used as the predictor for coherent activity between ECoG and STN-LFP, the clearly defined peak in coherence at spindle frequencies, but not the peak at ~ 1Hz, was lost from the coherence spectrum (***D***). In contrast, the use of SNr-LFP as the predictor led to an almost complete loss of significant coherence between ECoG and STN-LFP (***G***). The STN-LFP (***E***) and SNr-LFP (***H***) signals were not effective predictors of coherence between ECoG and GP-LFP, as shown by the relatively small changes in the coherence plot following partial coherence analysis. In agreement with findings in STN and GP, the coherent activity in ECoG and SNr-LFP was much more sensitive to the use of STN-LFP as a predictor (***F***) compared to GP-LFP as a predictor (***I***). Main spectral plots in *A* to *I* are grand averages from the 12 animals that were computed using data from two 80 sec epochs of slow-wave activity per animal (512 data points per FFT block; 0.78 Hz resolution). Insets in *A-C* are higher resolution spectra (1024 data points; 0.39 Hz resolution) derived from the same data. *Dashed lines* indicate 95% confidence levels.

A general linear model (GLM) incorporating basal ganglia nucleus, frequency band and brain state as the main effectors of activity relationships was used to assess differences in coherence between cortex and basal ganglia. There was no significant effect for nucleus correlated to ECoG (three levels; STN, GP and SNr), but there were significant effects for brain state (two levels; SWA and global activation) and frequency (two levels; 0.8-1.5 Hz and 15-60 Hz). In addition, there were significant interactions between nucleus and frequency, and between brain state and frequency. There was no second-order interaction between nucleus and state, and no third-order interaction between nucleus, frequency and state. *Post hoc* paired *t*-tests confirmed that coherence in the 0.8-1.5 Hz band was significantly greater during SWA than during global activation for STN, GP and SNr (compare Figures 4.5 and 4.6), which is in good agreement with differences in the distribution of power of oscillatory activity in the two states. The average strength of coherence between LFPs and ECoG over the 0.8-1.5 Hz frequency band was greater for both STN and SNr than GP (Figure 4.5*A-C insets*). Coherence in the 15-60 Hz band was significantly larger for all basal ganglia nuclei during activation than during SWA (compare Figures 4.5 and 4.6). Furthermore, the magnitude of coherence with cortex over the 15-60 Hz range was significantly greater for both STN and GP than SNr (Figure 4.6*A-C*).

During robust SWA, there was also significant coherence between oscillatory activity in cortex and basal ganglia at frequencies associated with spindling (7-12 Hz; Figure 4.5*A-C*). Most of the coherence at spindle frequencies was lost during global activation (Figure 4.6*A-C*). A separate GLM was used to investigate whether there were any differences in coherence between ECoG and basal ganglia LFPs at slow-wave and spindle frequencies. The main factors were nucleus (three levels; STN, GP and SNr) and frequency band (two levels; 0.8-1.5 Hz and 7-12 Hz). Frequency was the only significant main effect, but there was also an interaction between nucleus and frequency. *Post hoc t*-tests showed that coherence with ECoG at spindle frequencies was greater in GP than STN or SNr, which both had similar levels (Figure 4.5*A-C*), in congruence with the cumulant density estimates of LFP and ECoG activities (Figure 4.4). In general agreement with previous studies showing

that β and γ rhythms are often present during the active components of the cortical slow oscillation (Steriade 2000), there was low, but statistically significant, coherence between cortex and basal ganglia in the 15-60 Hz range during SWA (Figure 4.5*A-C*). In summary, coherence between cortex and basal ganglia was relatively frequency-selective. Differences in spectral power mirrored differences in coherence (Figure 4.4), demonstrating that changes in coherence were not due to modulations in non-linearly related frequency components (Florian et al, 1998).

4.2.4 Pattern of coherence between ECoG and basal ganglia LFPs varies with recording site during SWA

Partial coherence analysis was used to further define the functional organization of coherent activity between cortex and basal ganglia nuclei. During robust SWA, partialisation of ECoG-STN coherence with the SNr signal as predictor (Figure 4.5*G*) and partialisation of ECoG-SNr coherence with the STN signal as predictor (Figure 4.5*F*) markedly attenuated coherence at slow-wave frequencies (0.8-1.5 Hz), the dominant band of coherence. In contrast, partialisation of either ECoG-STN coherence or ECoG-SNr coherence with GP acting as the predictor led to little change in coherence in this frequency band (Figure 4.5*D* and *I*).

Partialisation of ECoG-GP coherence with either STN (Figure 4.5*E*) or SNr (Figure 4.5*H*) had a paradoxical effect in that coherence at slow-wave frequencies shifted, with a significant peak appearing at 2-3 Hz that was not evident in the standard mean ECoG-GP coherence spectrum (Figure 4.5*B*). This occurs because ECoG-STN coherence and ECoG-SNr coherence are stronger than ECoG-GP coherence at slow-wave frequencies (compare Figure 4.5*A-C*) and implies that there is little temporal coupling of this component between STN/SNr and GP. Under these conditions, removal of the STN/SNr effect by partialisation is equivalent to eliminating a 'noise term' from the ECoG-GP coherence (Lopes da Silva et al 1980). Removing this noise term leads to a relative increase of the frequency components shared by ECoG and GP, which appear at a slightly higher frequency.

In summary, the partial spectra in Figure 4.5*D-I* suggest that, during robust SWA, the cortex, STN, and SNr are temporally-coupled at low frequencies in functional loops, which together form an axis of coherence that is largely independent of GP, which has its own independent activity coherent with cortex. Interestingly, this distinction between the cortex-STN-SNr and cortex-GP axes was less acute at spindle frequencies (7-12 Hz), where, for example, partialisation of ECoG-SNr coherence or ECoG-STN coherence with the GP signal reduced coherences in this band, despite having little effect on coherences over the 0.8-1.5 Hz range (see Figure 4.5*D* and *I*, respectively).

4.2.5 Pattern of coherence between ECoG and basal ganglia LFPs varies with recording site during global activation.

During global activation, ECoG-STN coherence and ECoG-SNr coherence, which were mainly confined to the 15-60 Hz band, were significantly reduced following partialisation with the GP-LFP as predictor (Figure 4.6*D*, *I*, respectively). However, the converse was not true; partialisation of ECoG-GP coherence with STN or SNr as the predictors led to only modest changes in coherence at these high frequencies (Figure 4.6*E* and *H*, respectively). Partialisation of ECoG-SNr coherence with STN as predictor and partialisation of ECoG-STN coherence with SNr as predictor both led to significant reductions in coherence (Figure 4.6*F* and *G*, respectively). Thus, in marked contrast to coherence during SWA, the partial spectra in Figure 4.6*D-I* imply that, during the activated state, prevalent activity in the cortex-STN-SNr axis is shared with GP, although, again, some coherent activity in the loop between cortex and GP was not shared with either STN or SNr.

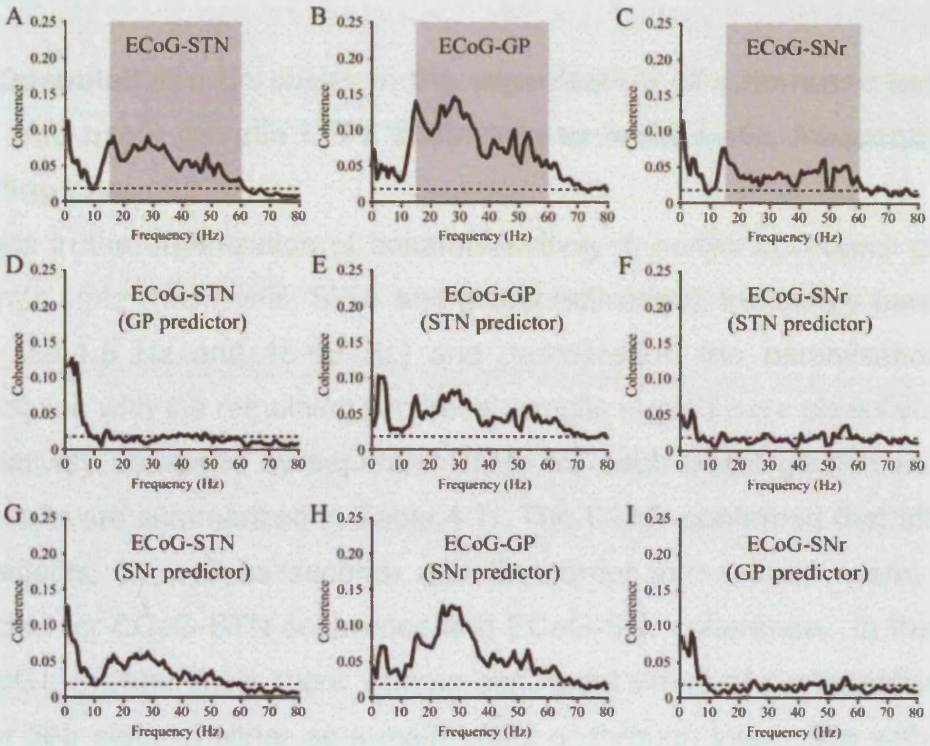

Figure 4.6 Coherent oscillatory population activity in cortex and basal ganglia during global activation is largely confined to β- (15-30 Hz) and γ- (30-60 Hz) range frequencies. ***A-C,*** Coherence spectra between ECoG and LFPs in STN (***A***), GP (***B***) and SNr (***C***). In each case, much of the significant coherence in the 0-80 Hz range was contained in the β- and γ-frequency bands (light grey boxes in *A-C*), consistent with the obliteration of slow-wave activity and the increased presence of high-frequency oscillations during global activation. Note, however, that coherence between ECoG and SNr-LFP (***C***) at these high frequencies was lower compared to ECoG-STN and ECoG-GP couplings (***A*** and ***B***). ***D-I,*** Partial coherence spectra of oscillatory activity in ECoG and LFPs. Partial coherence analysis revealed that the use of the GP-LFP as a predictor (***D***), but not the use of SNr-LFP as the predictor (***G***), led to an almost complete loss of significant coherence between ECoG and STN-LFP in the β- and γ-frequency bands. Similarly, the STN-LFP (***E***), but not the SNr-LFP (***H***), was an effective predictor of coherent activity between ECoG and GP-LFP at these high frequencies. The temporal coupling of high frequency activity in ECoG and SNr-LFP was sensitive to the use of either STN-LFP (***F***) or GP-LFP (***I***) as a predictor of activity. Spectral plots in *A* to *I* are grand averages from the 12 animals that were computed using one 80 s data segment of pinch-evoked activity per animal (512 data points per FFT block; 0.78 Hz resolution). *Dashed lines* indicate the 95% confidence levels.

4.2.6 Quantitative differences in the organization of coherence between ECoG and basal ganglia LFPs according to brain state, frequency and recording site

Changes in the organization of coherent activity in cortex and basal ganglia with brain state (two levels; SWA and global activation), frequency band (two levels; 0.8-1.5 Hz and 15-60 Hz) and partialisation (no partialisation and partialisation with the remaining two basal ganglia nuclei) were objectively and quantitatively assessed by separate GLMs for each basal ganglia nucleus. The results are summarized in Table 4.1. The GLMs confirmed that all three main effects, as well as second- and third-order interactions, were highly significant for ECoG-STN coherence and ECoG-SNr coherence. In the case of ECoG-GP coherence, there was no significant effect of partialisation with STN or SNr signals, either as a main effect or through interaction with other factors (although note that the slow-wave band used tended to exclude some of the coherent activity between cortex and GP during SWA; see above). The other main effects and the interaction between brain state and frequency band were significant.

Post hoc t-tests verified that partialisation of the SWA-related coherence (0.8-1.5 Hz) between ECoG and STN and between ECoG and SNr with, respectively, SNr and STN predictors, significantly reduced coherence in both cases (Figure 4.7*A* and *C*, respectively). In contrast, partialisation with GP as predictor had no effect on this low-frequency coherence (Figure 4.7*A* and *C*). Furthermore, STN and SNr were not efficient predictors of ECoG-GP coherence (Figure 4.7*B*), confirming that the coherence loop between cortex and STN and the loop between cortex and SNr were functionally related, yet apparently independent of the coherence loop between cortex and GP. During global activation, the high-frequency coherence (15-60 Hz) between ECoG and STN was significantly reduced by partialisation with both SNr and GP predictors (Figure 4.7*D*), while the high-frequency coherence between ECoG and SNr was significantly reduced by partialisation with STN and GP as predictors (Figure 4.7*F*). This adds further weight to the finding that some of the activity in the cortex-STN-SNr axis is shared with GP during activation,

when coherence is limited to higher frequencies. Under these circumstances, partialisation with a GP predictor reduces ECoG-STN coherence to a greater extent than partialisation with a SNr predictor (Figure 4.7*D*). Moreover, much of the coherence within the cortex-GP loop remains independent of temporally-coupled activity in STN and SNr during activation, as indicated by the lack of significant effects of predictors of ECoG-GP coherence (Figure 4.7*E*). In short, during activation, coherent activity in the cortex-STN-SNr axis may be shared with GP, but the bulk of coherence between cortex and GP remains restricted to this loop. Note that there were no differences following the use of predictors in the high frequency bands during robust SWA or the low frequency band during global activation (results not shown).

4.2.7 Changes in the pattern of basal ganglia LFPs with brain state are associated with alterations in local unit activity

The firing properties of single units in GP, STN and SNr during SWA and global activation are summarized in Table 4.2, and are similar to those reported by Magill et al, (2001). Unit activity in STN was closely related to ongoing LFP oscillations, with discharge primarily occurring near the negative troughs of the ~ 1 Hz oscillation in the LFP (Figure 4.2). Although STN neurons predominantly fired during the negative phases of the slow oscillation in the LFP, discharges also occurred rarely during positive peaks (Figure 4.2). All STN neurons exhibited a significant low-frequency oscillation in their spike trains (*inset* of Figure 4.4*D*). In contrast, GP neurons and SNr neurons exhibited more regular (tonic) firing patterns during SWA (Figures 4.2, *insets* of 4*H* and *L*), as shown by significantly lower CVs, so that the relationship between single unit activity and ongoing LFP oscillations was less marked than in STN.

Changes in the activity profiles of the ECoG and LFPs following sensory-evoked global activation were immediately reflected at the single cell level by alterations in the rate and pattern of unit activity in basal ganglia (compare Figures. 4.2 and 4.3). On average, the firing rate of STN units was significantly increased and the firing pattern became significantly more regular during global activation (Table 4.2).

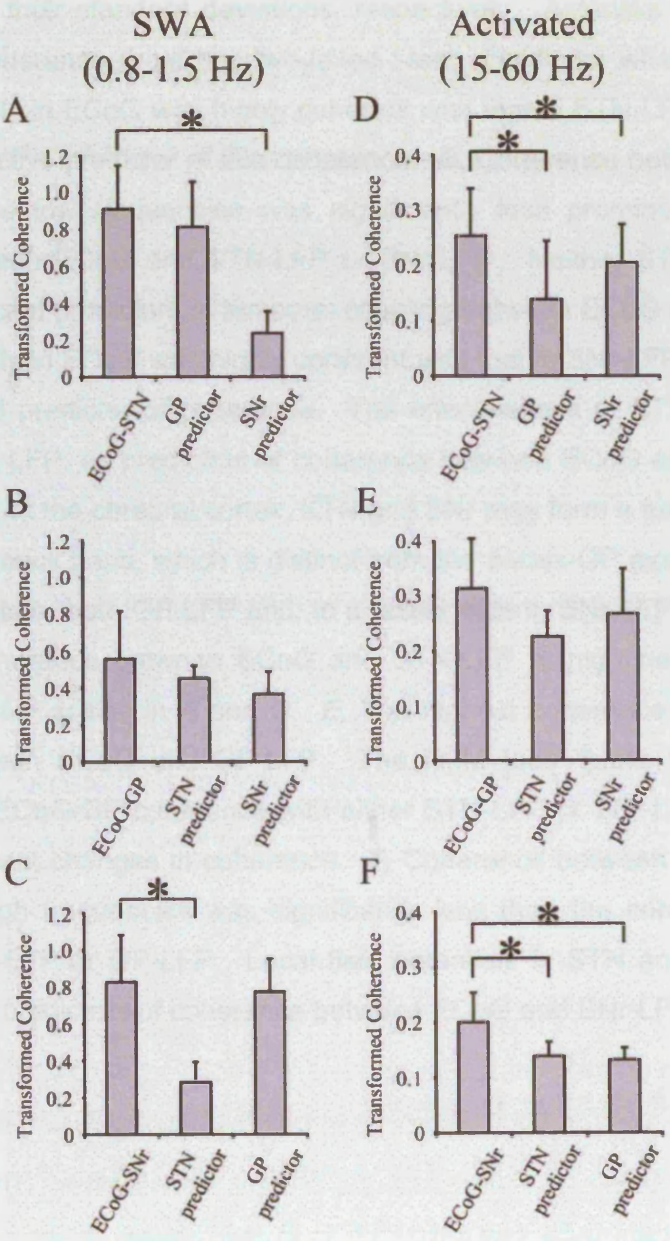
SWA
(0.8-1.5 Hz)
Activated
(15-60 Hz)
A
B
C
D
E
F
Transformed Coherence
ECoG-STN
GP predictor
SNr predictor
ECoG-GP
STN predictor
ECoG-SNr
*

Figure 4.7 Summary of changes in coherent activity in the cortex and basal ganglia in the slow-wave frequency band (0.8-1.5 Hz) during robust SWA (*A, B, C*), and in the combined β- and γ- frequency bands (15-60 Hz) during global activation (*D, E, F*). Bar charts and error bars represent mean Fisher-transformed coherences and their standard deviations, respectively. Asterisks show significant differences in coherence (*post hoc* two-tailed *t*-test; significant when $p < 0.01$). ***A,*** Slow-wave activity in ECoG was highly coherent with that in STN-LFP, but only SNr-LFP was an effective predictor of this coherence. ***B,*** Coherence between ECoG and GP-LFP at these low frequencies was significantly less prominent compared to coherence between ECoG and STN-LFP or SNr-LFP. Neither STN-LFP nor SNr-LFP were significant predictors of temporal coupling between ECoG and GP-LFP. ***C,*** Slow-wave activity in ECoG was highly coherent with that in SNr-LFP, and only STN-LFP was a good predictor of coherence. The effectiveness of STN-LFP and SNr-LFP, but not GP-LFP, as predictors of coherence between ECoG and basal ganglia LFPs suggests that the cerebral cortex, STN and SNr may form a functionally related axis in this frequency band, which is distinct from the cortex-GP axis. ***D,*** During the activated brain state, both GP-LFP and, to a lesser extent, SNr-LFP were significant predictors of coherence between ECoG and STN-LFP at high frequencies (15-60 Hz). Note different scales in *A* and *D*. ***E,*** The highest coherence in the 15-60 Hz band was between ECoG and GP-LFP. The GLM (see Table 1) indicated that partialisation of ECoG-GP coherence with either STN-LFP or SNr-LFP as predictors led to no significant changes in coherence. ***F,*** Coherence between ECoG and SNr-LFP at these high frequencies was significantly less than the coherence between ECoG and STN-LFP or GP-LFP. Local field potentials in STN and GP were both equally effective predictors of coherence between ECoG and SNr-LFP.

Table 4.1 Repeated measures general linear model (GLM) of changes in coherence between ECoG and basal ganglia LFPs.

	STN		GP		SNr	
	F [DF]	*p* value	F [DF]	*p* value	F [DF]	*p* value
Partialisation	49.7 [2,20]	<0.001	3.9 [2,20]	(NS)	28.7 [2,20]	<0.001
State	16.0 [1, 10]	0.009	25.3 [1,10]	0.003	58.6 [1,10]	<0.001
Frequency	63.9 [1,10]	<0.001	15.7 [1,10]	0.009	97.7 [1,10]	<0.001
Partial x State	41.8 [2,20]	<0.001	1.4 [2,20]	(NS)	11.8 [2,20]	0.009
Partial x Frequency	34.8 [2,20]	<0.001	1.4 [2,20]	(NS)	24.6 [2,20]	<0.001
State x Frequency	33.4 [1,10]	<0.001	43.3 [1,10]	<0.001	47.7 [1,10]	<0.001
Partial x Frequency x State	32.6 [2,20]	<0.001	3.2 [2,20]	(NS)	21.5 [2,20]	0.001

Three main effects were considered: partial coherence (three levels: no partialisation, and partialisation with the remaining two basal ganglia recording sites), brain state (two levels: SWA and global activation) and frequency band (two levels: slow-wave oscillations [0.8-1.5 Hz] and high-frequency oscillations [15-60 Hz]). Separate models were run for coherence between cortex and STN, cortex and GP, and between cortex and SNr. Differences were considered significant when $p \leq 0.01$. DF, degrees of freedom. NS, not significant.

The firing rates of both GP and SNr units were also significantly increased during global activation; alterations in firing pattern were minor and were evident as small changes in CVs (Table 4.2). In agreement with previous studies (Magill et al, 2000; Ryan et al, 1992), correlations of STN, GP and SNr unit activities on the low millisecond time scale (< 10 ms) were not observed during either SWA or global activation.

4.2.8 Single unit activity and LFPs in the basal ganglia are correlated during SWA

Changes in LFPs were accompanied by changes in the discharge pattern of single units. This circumstantial association between LFPs and single unit discharge pattern could be strengthened by the demonstration of a linear relationship between these variables. However, with one important exception, the utility of analyses of the correlation or coherence between units and LFPs recorded through the same electrode is limited by overlaps in the frequency content of the two signals, which may lead to the spurious detection of temporal coupling. The exception is the low-frequency activity (~1 Hz) evident in LFPs during SWA. In this case, cumulant density estimates of single unit and LFP activities demonstrated an unambiguous correlation between unit activity and LFPs in STN (Figure 4.4*D*), and, to a lesser extent, GP and SNr (Figure 4.4*H* and *L*). The relatively weak correlations between units and LFPs in GP and SNr might have been a persistent feature throughout the record or may have arisen because of the inclusion of periods of weak low-frequency oscillations in the spike trains of neurons, as sometimes seen after supplementary doses of ketamine, which promotes the emergence of low-frequency, oscillatory activity (Magill et al, 2000). Our analysis cannot distinguish these two possibilities, but nevertheless, these results serve to show that, during SWA, single unit activity in GP and SNr can be temporally coupled, albeit weakly or episodically, to ongoing LFP oscillations, while single unit activity in STN remains strongly coupled to LFP oscillations.

Table 4.2 Firing properties of single units in basal ganglia during slow-wave activity and global activation

	STN		GP		SNr	
	SWA	Activation	SWA	Activation	SWA	Activation
Total number of neurons[a]	11	11	9	9	11	11
Number of LFO neurons[b]	11	0	0	0	0	0
Firing rate (spikes/s^{-1})	8.4 ± 3.7	14.6 ± 6.1*	21.9 ± 6.3§	30.1 ± 8.0*§	27.0 ± 11.1§	37.2 ± 13.2*§
Coefficient of variation	1.28 ± 0.34	0.53 ± 0.10*	0.25 ± 0.05§	0.21 ± 0.07§	0.24 ± 0.05§	0.23 ± 0.06§

[a]The same neurons were compared in both activity states. [b]Low-frequency oscillatory (LFO) neurons were defined as such when their firing displayed a significant, low-frequency (< 1.5 Hz) oscillatory component. *Significantly different compared to activity of same type of neurons during SWA. §Significantly different compared to activity of STN neurons during same brain state. Data are expressed as mean ± SD.

4.3 Discussion

The main findings of this chapter are that coherent oscillations are present in LFPs recorded in cortico-basal ganglia circuits. The frequency of coherent oscillations in cortico-basal ganglia circuits depends on brain state and varies across basal ganglia nuclei.

4.3.1 The interpretation of LFP activity in the basal ganglia

The principal aim of the current chapter was to gain insight into the nature of functional connectivity between neuronal populations in cortico-basal ganglia circuits. As such, our conclusions depend on whether LFPs can be considered to represent the synchronized activity of local populations of pre- and/or post-synaptic neuronal elements. There is good evidence that the LFP activity recorded in the cortex is representative of aggregate or synchronous activity in local neuronal populations (Baker et al, 1997; Creutzfeldt et al, 1966; Donoghue et al, 1998; Frost 1968; Mitzdorf 1985; Murthy and Fetz 1992, 1996a; Steriade 2000). The basal ganglia do not share the laminar structure seen in the cortex, but nevertheless there is evidence that LFPs recorded in these nuclei may also reflect synchronized population activity (Courtemanche et al, 2003; Goto and O'Donnell 2001; Levy et al, 2002a; Magill et al, 2004, Goldberg et al, 2004). Two aspects of the present results lend further support to this. First, oscillatory LFPs were clearly coherent in distant, but connected sites, such as STN and cortex, suggesting that they are at least partly associated with synchronized pre- and/or post-synaptic effects. Similar arguments have been made with respect to LFPs recorded in the basal ganglia of humans (Brown et al, 2001; Marsden et al, 2001a; Williams et al, 2002). Second, in SWA, where action potential-LFP correlations are unambiguous, unit activity was phase-locked to the LFP in STN, and to a lesser extent in GP and SNr (also see Magill et al, 2004).

It is unlikely that LFPs recorded in the basal ganglia were contaminated by the volume conduction of cortical potentials, which would lead to inflated measures of the coherence between cortex and basal ganglia, for several

reasons. During SWA, units were correlated with LFPs, indicating that local currents are timed to elicit phase-locked variations in the firing of neurons. In addition, under similar conditions, it has been demonstrated cortical stimulation leads to a pattern of amplitude changes in STN LFPs that closely resemble fluctuations in the rate of single units (Magill et al, 2004). Futhermore, LFPs evoked in cortex and STN by cortical stimulation are not closely related (Magill et al, 2004). Consistent with the small temporal offsets of the cumulant density estimates illustrated in Figure 4.4, directed transfer function between cortical and basal ganglia activity involves asymmetrical driving (Chapter 5), rather than the symmetrical effects that would be expected from volume-conducted potentials. Asymmetrical directed transfer function effects are particularly insensitive to volume conducted activity (Cassidy and Brown, 2003; Korzeniewska et al, 2003), and therefore provide strong evidence that the coherent activities described here are due to neuronal synchronisation.

4.3.2 Neural basis of coherent oscillatory activity in cortex and basal ganglia

The ECoGs of anesthetized rats were dominated by a slow oscillation (~1 Hz) that grouped higher frequency rhythms, including prominent spindle oscillations, and was similar to that previously described in naturally sleeping or anesthetized rats, cats and humans (Magill et al, 2000, 2001; Steriade 2000; Urbain et al, 2000). This slow oscillation is generated by synchronous and rhythmic depolarizing and hyperpolarizing events in principal cortical neurons (Steriade 2000; Stern et al, 1997; Chapter 1.4.7). It is important to note that a mixed urethane and ketamine/xylazine anaesthetic regime was used in this study, rather than pure ketamine anaesthesia. The former has a distinct advantage over the latter in that neural activity patterns observed in the basal ganglia more closely resemble those present in the unanaesthetised state (Urbain et al, 2000). For example, STN neurons tend to fire in a bursting manner during SWA present under urethane anaesthesia and during natural non-REM (slow-wave) sleep (Magill et al, 2000; Urbain et al, 2000). Spontaneous or sensory-driven global activation in anesthetised animals is

associated with a shift in STN activity from busting to tonic/irregular firing, just as occurs in the STN in unanaesthetised animals during the shift from natural slow-wave sleep to wakefulness (Magill et al, 2000; Urbain et al, 2000). In contrast to STN, neurons in GP tend to fire in a regular tonic manner irrespective of brain state and sleep-wake cycle in both the urethane-anesthetised animal and unanaesthetised animal, respectively (Magill et al, 2000; Urbain et al, 2000). The same cannot be said for activity under pure ketamine anaesthesia because GP neurons fire in a bursting mode during SWA (Magill et al, 2000; Magill et al, 2001; Goldberg et al, 2004). LFPs in the STN, GP and SNr have not been similarly studied across the natural sleep-wake cycle. However, because the single-unit activity is qualitatively similar in urethane-anesthetised and unanaesthetised states, it is not unreasonable to assume that that the LFPs will also be similar across preparations.

During SWA, the active components of low-frequency cortical rhythms were closely associated with the burst-like discharges and low-frequency oscillations of single STN neurons. It is thus likely that rhythmic and synchronized cortical input to the STN resulted in periodic depolarization of (and hence, increased discharge of) many STN neurons in unison. Indeed, the firing of neighbouring STN neurons has been shown to be synchronously phase-locked during SWA (Magill et al, 2000; Ryan et al, 1992). Because LFPs reflect synchronized, subthreshold post-synaptic currents better than action currents (Hubbard et al, 1969; Mitzdorf 1985), the prominent negative deflections in STN LFPs were probably the result of the synchronized depolarization of neurons by cortical inputs. These periodic depolarizations resulted in the phase-locked discharges of STN neurons. In agreement, distinct LFPs evoked in the STN by cortical stimulation are phase-locked to, but are not dependent on, the discharges of neighboring neurons (Magill et al, 2004).

In contrast to observations in STN, unit activity in GP and SNr was more regular in nature and was less strongly entrained by concurrent cortical SWA. This is despite the fact that both sites receive inputs from STN and striatum, neurons, which often fire in phase with SWA (Goto and O'Donnell 2001;

Magill et al, 2000, 2001; Stern et al, 1997). The translation of pre-synaptic activity into post-synaptic discharge in GP/SNr is therefore complex and partly non-linear (Hanson and Jaeger 2002 and see Chapter 7). Accordingly, the LFPs in these structures could either reflect pre-synaptic current flows or, more likely, summated post-synaptic currents that manifest as oscillations in the LFP but which fail to elicit more than minor fluctuations in firing rate (Hubbard et al, 1969; Mitzdorf 1985). In support of this, it has recently been shown that the dendrites of GP neurons receiving subthreshold inputs are functionally uncoupled from the somata of the same neurons (Hanson et al, 2004).

Global activation was associated with a reduction in low-frequency rhythms and increases in the power and coherence of high-frequency oscillations in β- and γ-frequency ranges in the ECoG and LFPs. The effects of global activation were similar to those elicited by the midbrain reticular activating system, which is known to increase cortical activity and promote synchronous, high-frequency oscillations (Munk et al, 1996; Steriade 2000). Thus, as with SWA, changes in activity in the basal ganglia may be driven, at least in part, by the cortex, although excitatory subcortical afferents may also contribute to responses (see Magill et al, 2001). These changes were reflected in single unit activity in basal ganglia as increases in the mean firing rates of all neurons and the abolition of low-frequency oscillatory firing of STN neurons. However, it proved impossible to unambiguously determine whether high-frequency LFP activity was correlated with local unit activity recorded through the same electrode because of the overlapping frequency bands of action potential discharge and high-frequency LFP oscillations.

While unit activity and LFPs both changed upon activation, suggesting a relationship, evidence of strict temporal correlations between units was not apparent. A lack of correlations on the low millisecond time scale (< 10 ms) suggests that the recorded neurons were not monosynaptically connected (Abeles 1982). Evidence for correlations on a longer time scale is often not forthcoming in the absence of a strong sensory input, a clear behavioural

context, or disease. Studies in awake and anesthetized animals have shown that high-frequency oscillations can be effete and focal in nature, especially in sensorimotor systems (Donoghue et al, 1998; MacKay 1997; Murthy and Fetz 1992, 1996a). Indeed, correlations between units, or between units and LFPs, are sometimes elusive, perhaps as a consequence of the rapid recruitment of neurons to, and release from, the population oscillation (Donoghue et al, 1998; Murthy and Fetz 1992, 1996b). For these reasons, current statistical methods may neglect subtle or dynamic correlations.

4.3.3 Organization of coherent oscillatory activity in cortex and basal ganglia

The topography and preferred frequency of coherent activity in the cortex and basal ganglia was dynamic, exhibiting a strong dependence on brain state. It was not possible using these analyses to ascribe direction to the coherence described here (but see Chapter 5). The coherence between cortex and basal ganglia nuclei is therefore described in terms of distributed and shared 'loops'. Coherence and partial coherence analyses showed that, during SWA, cortex was temporally coupled to the STN and SNr in highly coherent loops that formed a single functional axis. Cortex was also tightly coupled to the GP, but in an axis distinct from that containing the more strongly coupled STN and SNr. During global activation, cortex was temporally coupled to the STN, GP and, to a lesser extent, the SNr via loops that formed a single functional axis. In addition, the cortex was closely coupled to the GP alone in another, functionally distinct axis.

The results are compatible with two major conduits of cortical influence over the basal ganglia. During SWA, the STN and SNr were temporally coupled at low frequencies to cortex, but not to the GP, suggesting that, in accordance with past studies of unit activity (Magill et al, 2000, 2001), the STN and SNr may be predominantly driven through the direct cortico-subthalamic projection during SWA. During global activation, high-frequency oscillatory activities in the STN, SNr and cortex were coherent with one another and with activity in the GP, which raises the possibility that activity of higher frequency may reach the basal ganglia predominantly via the cortico-striatal projection to the GP.

Indeed, this may also be true of the spindle activity recorded during SWA, which seemed to be shared between the cortex, STN, SNr and GP, in contrast to the activity at around 1 Hz. It is of particular interest that the distribution of spindles in the basal ganglia differed from that of SWA, given the close relationship between the generation and sychronisation of these activities in the thalamocortical system (Steriade, 2002 and see Section 1.4.7). Although the origin of SWA in the STN and GP is known to be cortical (Magill et al, 2000;2001), spindle activities, which are generated in the thalamus (Steriade, 2002), could also be propagated through direct thalamo-basal ganglia pathways (Parent and Hazrati 1995a; Bolam et al, 2000), leading to subtle differences in inter-basal ganglia relationships between the two activities.

At first glance, it seems paradoxical that the GABAergic (presumably inhibitory) projection neurons in the GP could be involved in the propagation of high-frequency activity. However, GABAergic neurons can be as important as excitatory neurons in driving and sculpting population oscillations, both within the basal ganglia and in other regions of the brain (Bevan et al, 2002; Klausberger et al, 2003; Whittington and Traub 2003; Section 1.6.1). The division of cortico-basal ganglia information flow into trans-subthalamic and trans-striatal pathways, which thereafter converge at the level of the output nuclei, has already been suggested based on single unit recordings (Fujimoto and Kita 1992, 1993: Kolomiets et al, 2003; Maurice et al, 1999; Nambu et al, 2000, 2002). It is important to note, however, that the relationships described here may not hold for all cortical areas. Indeed, relationships may depend on the relative influences of trans-striatal and trans-subthalamic pathways, the latter of which is more restricted in terms of contributing cortical regions (Smith et al, 1998). With this caveat in mind, the current data still serve to highlight important new relationships between the basal ganglia and a region of frontal cortex that projects directly to both striatum and STN (Fujimoto and Kita 1993; Kolomiets et al, 2003; Magill et al, 2004; Smith et al, 1998).

In summary, the data suggest the existence of two major pathways underlying cortical influence over the basal ganglia. Although these pathways have

partly overlapping spheres of influence, each favours activities of different frequency. This hypothesis merits further investigation, particularly through simultaneous recordings of LFPs in STN and striatum during SWA and cortical activation. Equally, the role of synchronisation in cortico-basal ganglia circuits in behaviour has yet to be firmly established. Nevertheless, it is of interest that γ oscillations have recently been demonstrated in the STN of the alert and mobile rat (Brown et al, 2002), whereas task-related β oscillations are known to occur throughout the striatum of awake monkeys (Courtemanche et al, 2003). Moreover, the frequency range of coherent activity during global activation is similar to that of (levodopa-responsive) EEG-STN and EEG-GPi coherence in patients with Parkinson's disease (Marsden et al, 2001a; Williams et al, 2002).

4.3.4 Implications for information processing in cortico-basal ganglia circuits

The present data show that the basal ganglia oscillate together with the cortex, and that coherent oscillatory activity in cortico-basal ganglia circuits is dynamically and complexly organized. As such, these findings support an extension to classic models of basal ganglia function, which posit that simple changes in the rates of firing of neurons underlie behaviour (Albin et al, 1989; DeLong 1990 and see Chapter 1.1). The existence of complex, brain state-dependent synchronisations of neuronal ensembles in different frequency bands raises the possibility that synchronisation itself may be mechanistically important in the organization of basal ganglia function, paralleling its putative roles in cortex (Engel and Singer 2001; Engel et al, 2001; MacKay 1997; Pesaran et al, 2002). Synchronisation at subthreshold and suprathreshold levels might provide complex 'carrier signals' utilized by populations of basal ganglia neurons to process, encode and disseminate information. In addition, functional coupling of cortico-basal ganglia circuits through coherent oscillations may facilitate the binding together of distributed neural assemblies during, for example, sensory-motor integration (Cassidy et al, 2002a; Engel and Singer 2001; Engel et al, 2001; MacKay, 1997; Pesaran et al, 2002; Roelfsema et al, 1997). It follows that dysfunctional coupling of appropriate

and/or inappropriate oscillatory population activity may underlie, or at least contribute to dysfunction in basal ganglia diseases. In support of this, aberrant functional couplings and abnormal oscillatory activities have been frequently observed in cortico-basal ganglia circuits in Parkinson's disease and its models (Bergman et al, 1998; Bevan et al, 2002; Boraud et al, 2002; Brown 2003; Levy et al, 2000, 2002; Liu et al, 2002; Marsden et al, 2001a; Wichmann and DeLong 1996; Williams et al, 2002; Chapter 3).

4.4 Chapter 4: Summary

- The coherence between ECoG and LFPs simultaneously recorded from subthalamic nucleus (STN), globus pallidus (GP) and substantia nigra pars reticulata (SNr) was largely confined to slow- (~1 Hz) and spindle- (7-12 Hz) frequency oscillations during slow-wave activity (SWA).

- In contrast, during cortical activation, coherence was mostly restricted to high-frequency oscillations (15-60 Hz).

- The coherence between ECoG and LFPs also depended on basal ganglia recording site. Partial coherence analyses showed that, during SWA, STN and SNr shared the same temporal coupling with cortex, thereby forming a single functional axis.

- Cortex was also tightly, but independently, correlated with GP in a separate functional axis. During activation, STN, GP and, to a lesser extent, SNr shared the same coherence with cortex as part of one functional axis. In addition, GP formed a second, independently-coherent loop with cortex.

- These data suggest that coherent oscillatory activity is present at the level of LFPs recorded in cortico-basal ganglia circuits, and that synchronized population activity is dynamically organized according to brain state, frequency and nucleus. These attributes further suggest that synchronized activity should be considered as one of a number of candidate mechanisms underlying the functional organization of these brain circuits.

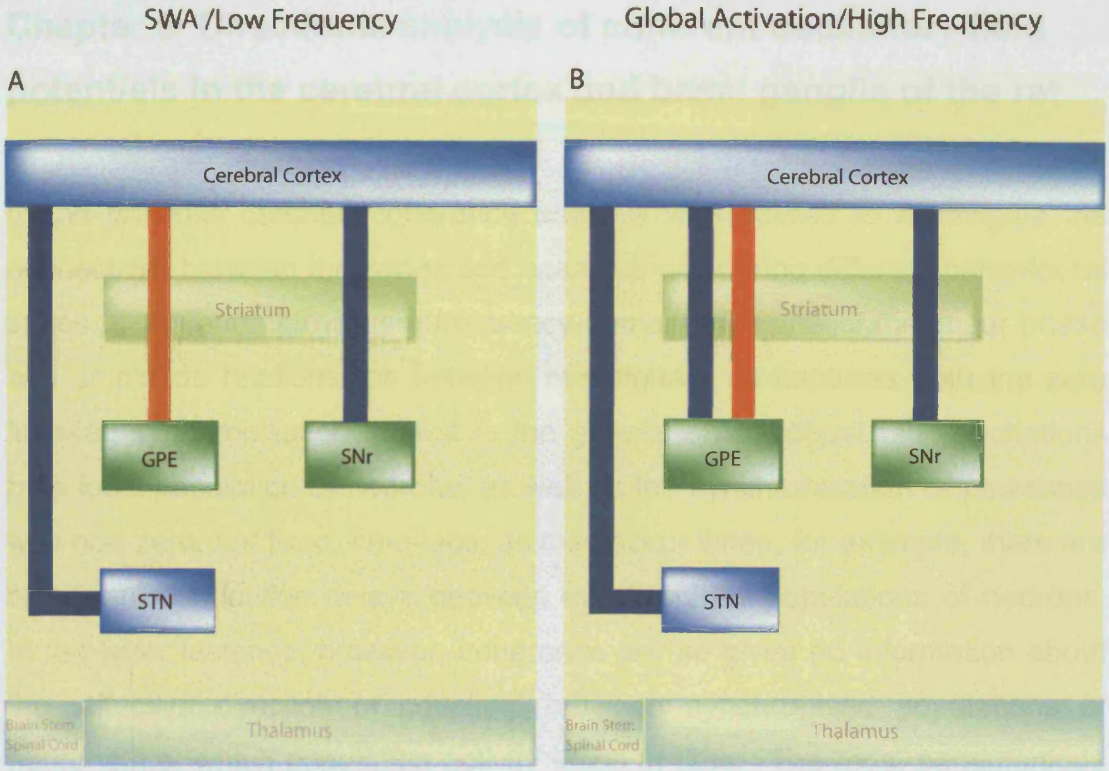

Figure 4.8 Summary diagram of oscillatory connections between cortex and basal ganglia during SWA and global activation shown by coherence and partial coherence analysis. The cerebral cortex and basal ganglia structures are represented by coloured boxes as in Figure 1.2. Structures not included in recordings are faded. The coloured bars between boxes represent significant coherence between the cortex and the LFP recorded from that structure (bars are used as direction cannot be inferred at this stage). The colour of the bars shows whether coherence between the cortex and the different structures is shared (same colour) or independent (different colours). Magnitude of coherence is not represented here to improve clarity. ***A,*** During SWA, coherence with cortex in the low frequency range is shared by STN and SNr (blue bars), but not GP which is in an independent loop (red bar). ***B,*** Following global activation, induced by pinch, coherence with cortex at higher frequencies (15-60Hz) is shared between all three basal ganglia structures (blue bars). Additionally however, there is still a significant portion of cortex-GP coherence that remains independent from the STN and SNr (red bar).

Chapter 5: Directional analysis of coherent oscillatory field potentials in the cerebral cortex and basal ganglia of the rat

In the previous chapter, coherence analysis was utilised to investigate the connectivity between the cortex and basal ganglia during different behavioural states. Coherence provides a frequency-domain measure of the linear phase and amplitude relationships between two signals. It captures both the zero time-lag synchronisation implicit in the generation of robust LFP oscillations by a local population of neurons, as well as the synchronisation of processes with non-zero, but fixed, time-lags, as may occur when, for example, there are significant conduction delays between synchronised populations of neurons. In the latter instance, however, coherence *per se* gives no information about the 'effective direction of coupling' between synchronised populations of neurons, i.e. which population activity leads in time. The most parsimonious explanation for such a relationship between two coherent population activities is that the leading population actually drives the lagging population of neurons. However, this may not be the only explanation for such a relationship (see Chapter 2 and Discussion), and hence, the term 'effective direction of coupling' is used to describe a pattern of temporal relationships rather than a unique state of connectivity. One measure, closely related to coherence, commonly used to estimate the effective direction of coupling is the phase spectrum, which describes the phase and hence, time delay, between two coherent signals in a specific frequency band (Halliday et al, 1995). However, paradoxical phase estimates can arise when different coherent activities have overlapping frequency components. In these cases, the phase estimate is, in reality, a mixture of distinct phases, each of which is associated with a different coherent activity (Cassidy and Brown, 2003). A good example of this is the afferent and efferent couplings between cortex and muscle (Mima et al, 2001). Mixtures of activities with different phase relationships are particularly likely in highly interconnected circuits, such as the cortico-basal ganglia loops.

The directed transfer function (DTF) provides an alternative method of assessing the effective direction of coupling between brain regions (Kaminski and Blinowska, 1991; Cassidy and Brown, 2003; Chapter 2). Importantly, the DTF is able to separate coherent activities that have overlapping frequency components, but which differ in their phase relationships (Kaminski and Blinowska, 1991; Cassidy and Brown, 2003). Accordingly, the DTF can provide information about the effective direction of coupling of the predominant coherent activity. In this chapter, the DTF is used to analyse the effective direction of coupling between the different BG nuclei described in Chapter 4, and between these nuclei and the cortex, during two different brain states in the urethane-anaesthetised rat. The DTF results obtained in the present study, when taken in the context of those previously obtained from Chapter 4, are used to elucidate further the functional organisation of oscillatory population activity in these circuits.

5.1 Methods

5.1.1 Electrophysiological recordings and verification of recording sites

Techniques for the electrophysiological recordings and the labelling and histological verification of recording are described in Chapter 4.

5.1.2 Data Analysis

A detailed description of the methodology and principles of the directed transfer function (DTF) can be found in Chapter 2. Recordings from 10 animals were suitable for DTF analysis. Data from two animals used for fast Fourier transform (FFT)-based spectral analysis (Chapter 4) were excluded due to ambiguity in the selection of the MAR model order (see Chapter 2). For each animal, data were organised so as to consist of separate pairs of recording sites. All the pairs were modelled and analysed separately. This bivariate approach gave a more detailed spectral picture than the simultaneous analysis of the multivariate data. Selection of the model order for each pairing is discussed above. Separate analyses were performed on recordings made during slow-wave activity and global activation in all animals.

An 80 s epoch of the cortical and BG activity present during deep anaesthesia with robust cortical slow-wave activity (described in Chapter 4) was selected for each animal. To better model low-frequency activity, these data segments were down-sampled to 20 Hz (after appropriate low-pass filtering to avoid aliasing). The fact that activity at frequencies of < 10 Hz dominated these data segments had already been established using FFT methods (see Chapter 4). For cortex-basal ganglia pairings, statistical analysis was performed on frequencies between 0.1 Hz and 2 Hz, a range that encompasses the bulk of the coherent activity present in this brain state, as verified by both DTF (see Figure 5.1*A-C*), and FFT methods (Chapter 4). Statistical analysis for basal ganglia-basal ganglia pairings during slow-wave activity were analysed using a smaller range (0.1-1 Hz) because the DTFs displayed narrower peaks as compared to the DTFs of cortical-basal ganglia pairings (see Figure 5.1*D-F*). To investigate activity present during sensory stimulation-evoked global activation, three data segments (20 s each)

recorded during (15 s) and immediately after (5 s) hindpaw pinches were analysed separately and then averaged to give single values for each animal, Before DTF analysis, these files were down-sampled to 200 Hz (after appropriate low-pass filtering to avoid aliasing) to detect coherence below 100 Hz and statistical analysis was performed on values between 15 Hz and 60 Hz. Again, this frequency range contains much of the coherent activity present in cortex and BG during global activation (Magill et al, 2004b). Standard coherence analysis was also performed using the same autoregressive model as that used for the DTF on all channel pairings, in both brain states, to confirm that there was significant coherent activity in these bands. For each frequency range (0.1-2 Hz, 0.1-1 Hz and 15-60 Hz), the DTF values for each direction of each recording site pairing were averaged in each animal. Student's paired t-tests were then performed on all pairings to determine whether coherence was consistently greater in one direction across all ten animals.

The above analyses investigated the effective direction of coupling in averaged data. Time-evolving DTF analysis was used to confirm that any changes in effective direction of coupling between structures associated with brain state could be seen in a single record. Time-evolving DTF plots (see Figure 5.3) were constructed using DTF coherence values calculated in consecutive 10 s windows (with 5 s overlap). For each window, the coherence values in one direction (e.g. effective direction of coupling from GP to STN) were made negative and summed with those in the opposite direction (e.g. effective direction of coupling from STN to GP). This resulted in a single coherence value in each frequency bin, with the direction of asymmetry represented by the sign (e.g. negative when effective direction of coupling is from GP to STN, and positive when effective direction of coupling is from STN to GP), and the magnitude of that asymmetry represented by the coherence value (e.g. a value of +1.0 would represent: (1) all activity in that frequency bin being completely coherent; and (2) coherent activity being completely asymmetric and all coupling is in the direction of STN to GP). Coherence at low frequencies (30 Hz sampling rate, 0.3 Hz bins) and high frequencies (100 Hz sampling rate, 1 Hz bins) was analysed separately at sampling rates that

maximised detection of these activities. In this case, analysis of low-frequency activity was performed using a 30 Hz sampling rate (rather that 20 Hz as in other analyses) to increase data points within the 10 s windows. The frequency bins displayed (Figure 5.3) have been chosen to approximately match those used in the main statistical analysis (see above).

5.2 Results

5.2.1 DTF of activity present during robust cortical slow-wave activity

We have previously shown that during the robust slow-wave activity prevalent under urethane anaesthesia, oscillatory activity in frontal ECoG and basal ganglia LFPs is dominated by low-frequency rhythms at ~ 1 Hz (see Chapter 4 and Figure 5.1). Analysis of the standard coherence between cortex and basal ganglia LFPs, and between basal ganglia LFPs themselves, confirmed strongly coupled activity at low frequencies across animals, with lower 95% CL that were well above zero (see Table 5.1). Directed transfer function analyses of the coherent activity present in the cortex and basal ganglia during this brain state were performed to detect asymmetries in the directed coherence at low frequencies. The highest directed coherence between activity in cortex and basal ganglia was seen between 0.1 and 2 Hz (see Figure 5.1*A-C*). The mean coherence at 0.1-2 Hz in the DTFs of the basal ganglia recording sites was used to assess the effective direction of coupling to, and from, the cortex. Coherence between cortex and basal ganglia was asymmetrical, with significantly more low-frequency coherence being directed from cortex to STN, GP and SNr than vice versa (Figure 5.1*A-C* and Table 5.1). The highest coherence in all pairings between STN, GP and SNr was at ~ 1 Hz, but there was also coherence at slightly higher frequencies, which was most clearly seen in the DTF between STN and SNr (Figure 5.1 *D-F*). The DTF between basal ganglia sites was narrower than that between cortex and basal ganglia sites, so statistical analysis was performed on values between 0.1 and 1 Hz (see Figure 5.1*D-F* and Table 5.1). Directed coherence in this range between all basal ganglia pairings was asymmetrical, There was significantly more coherence directed from SNr to both STN and GP, and from STN to GP (Table 5.1).

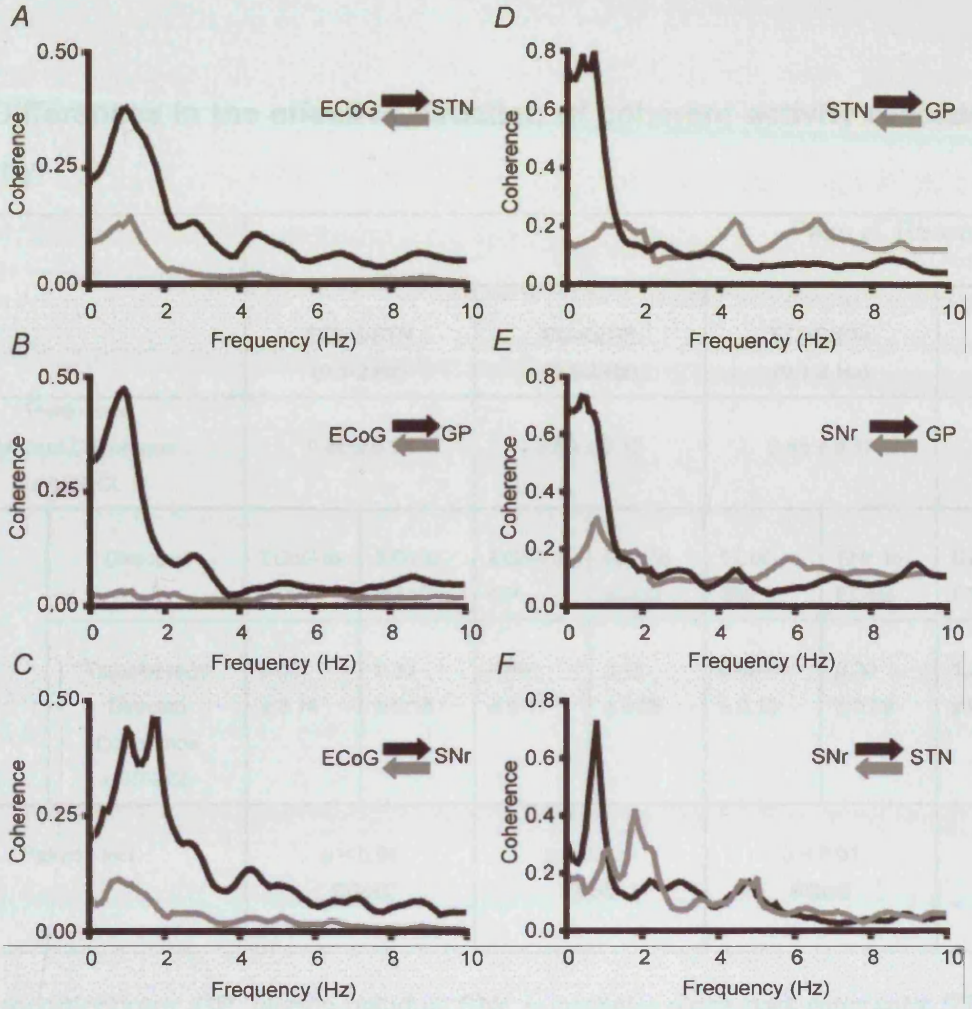

Figure 5.1 Directed transfer function analysis of local field potentials recorded in cortex and basal ganglia during robust slow-wave activity. Plots were constructed using the mean coherence in each direction for each individual recording site pairing (n = 10 animals). Coherence in all pairings was confined mostly to 0.1-2 Hz and, in nearly all cases, peaked at around 1 Hz. ***A, B, C,*** Coherence between cortex and all three basal ganglia recording sites was asymmetric, with the effective direction of coherent oscillatory activity being from cortex to the basal ganglia (black) rather than vice versa (grey). ***D,*** Coherence between STN and GP was asymmetrical, with the effective direction of coherent oscillatory activity at ~ 1 Hz being from STN to GP (black) rather than vice versa (grey). ***E, F,*** Coherence between SNr and GP and between SNr and STN was asymmetrical, with more coherent activity being directed from SNr. Note different y-axis scales for cortex-basal ganglia and basal ganglia-basal ganglia pairings.

Table 5.1 Differences in the effective direction of coherent activity recorded in the corte wave activity.

		Pairs of Recording Sites								
		ECoG/STN (0.1-2 Hz)		ECoG/GP (0.1-2 Hz)		ECoG/SNr (0.1-2 Hz)		STN/GP (0.1-1 Hz)		
Tranformed Standard Coherence ± 95% CL		0.86 ± 0.13		0.60 ± 0.12		0.88 ± 0.13		1.25 ± 0.26		
DTF	Direction	ECoG to STN	STN to ECoG	ECoG to GP	GP to ECoG	ECoG to SNr	SNr to ECoG	STN to GP	GP to STN	
	Transfor-med Directed Coherence ± 95% CL	0.63 ± 0.14	0.33 ± 0.13	0.68 ± 0.17	0.16 ± 0.06	0.68 ± 0.13	0.30 ± 0.09	1.36 ± 0.41	0.42 ± 0.09	
Paired t-test		$p < 0.04$ **ECoG**		$p < 0.001$ **ECoG**		$p < 0.01$ **ECoG**		$p < 0.01$ **STN**		

ECoG, electrocorticogram; GP, globus pallidus; SNr, substantia nigra *pars reticulata*; STN, subthalamic n
coherence values have been Fisher transformed. Significance for confidence limits (CL) of the mean an
For t-test results, the leading structures where the DTF is asymmetric are shown in bold.

5.2.2 DTF of activity present during global activation.

Recordings of activity present during global activation were analysed specifically to detect directed coherence at higher frequencies (15-60 Hz), i.e. the frequency band containing the dominant coherent activities as previously recorded in anaesthetised rats (see Chapter 4 and Figure 5.2) and showing significant standard coherence between cortex and basal ganglia LFPs and between basal ganglia LFPs themselves (see Table 5.2). Some coherent low-frequency activity (<5 Hz) was still present from all recording site pairings, although this was reduced relative to activity in robust slow-wave activity (Chapter 4). Coherence spectra derived from some animals had clear peaks at higher frequencies, particularly at around 20 Hz and 50 Hz. However, such clear peaks were not consistently found, such that coherence was best described as 'broadband' when considered across the whole experimental population (Figure 5.2). Nevertheless, coherence at 15-60 Hz was significantly higher during global activation compared to slow-wave activity (Chapter 4). In all but one pairing, that between SNr and STN, the DTFs showed at least some degree of asymmetry (Figure 5.2*A-F*). Cortico-basal ganglia relationships at these high frequencies were similar to those at low frequencies (compare Figure 5.1 and 5.2), with significantly more coherence directed from cortex to all the basal ganglia sites (Fig. 5.2*A-C* and Table 5.2). In contrast, the relationships between different basal ganglia sites were profoundly different from those evident during slow-wave activity. There was significantly more high-frequency coherence directed from GP to both STN and SNr (Figure 5.2*D,E* and Table 2) than vice versa, while the coherence between STN and SNr across animals became symmetrical (Figure 5.2*F*). Global activation thus produced a selective reversal in the effective direction of coupling in those pairings involving GP.

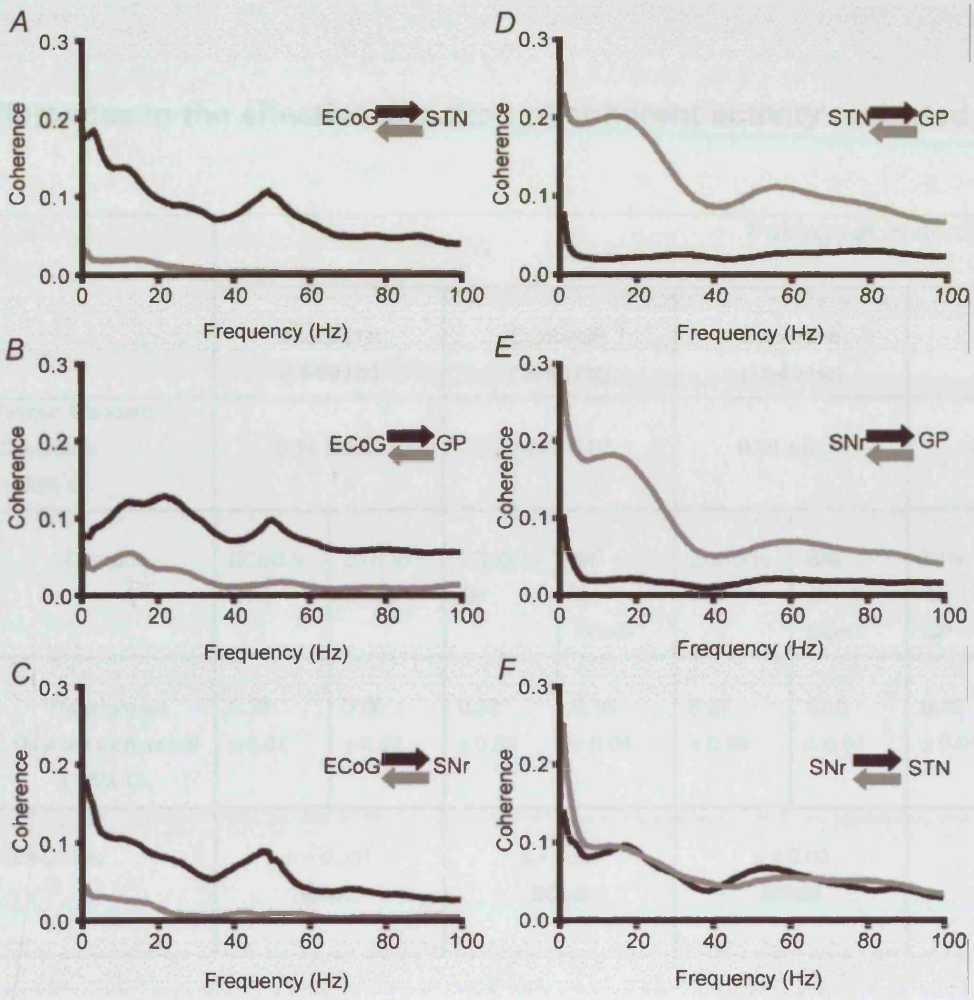

Figure 5.2 Directed transfer function analysis of local field potentials recorded in cortex and basal ganglia during global activation. Plots were constructed using the mean coherence in each direction for each individual recording site pairing (*n* = 10 animals; same as shown in Figure 5.1). Coherence was seen over a broad range of frequencies between 15-60 Hz. ***A, B, C,*** Coherence between cortex (ECoG) and the basal ganglia (STN, GP and SNr) was asymmetric, with the effective direction of coherent oscillatory activity being from cortex to the basal ganglia (black) rather than vice versa (grey). ***D, E,*** Directed coherence at 15-60 Hz was significantly higher from GP to both STN and SNr (grey) than from either STN or SNr back to GP (black). ***F,*** In contrast, STN and SNr had symmetrical coherence at these high frequencies. Note different y-axis scale as compared to Figure 5.1.

Table 5.2 Differences in the effective direction of coherent activity recorded in the corte activation

		Pairings of Recording sites							
		ECoG/STN (15-60 Hz)		ECoG/GP (15-60 Hz)		ECoG/SNr (15-60 Hz)		STN/GP (15-60 Hz)	
Transformed Standard Coherence ± 95% CL		0.34 ± 0.06		0.44 ± 0.07		0.26 ± 0.04		0.71 ± 0.10	
DTF	Direction	ECoG to STN	STN to ECoG	ECoG to GP	GP to ECoG	ECoG to SNr	SNr to ECoG	STN to GP	GP to STN
	Transformed Directed Coherence ± 95% CL	0.30 ± 0.07	0.08 ± 0.03	0.32 ± 0.09	0.14 ± 0.04	0.27 ± 0.08	0.10 ± 0.04	0.15 ± 0.04	0.37 ± 0.07
Paired t-test		p < 0.001 **ECoG**		p < 0.02 **ECoG**		p < 0.02 **ECoG**		p < 0.001 **GP**	

ECoG, electrocorticogram; GP, globus pallidus; SNr, substantia nigra pars reticulata; STN, subthalan coherence values have been Fisher transformed. Significance for confidence limits (CL) of the mean an t-test results, the leading structures where the DTF is asymmetric are shown in bold. NS, not significant.

Time-evolving DTF analysis was used to confirm that the changes in the direction of coherence between STN and GP associated with global activation could be seen in a single record (Figure 5.3). During spontaneous slow-wave activity, as assessed from the ECoG, periods of asymmetric low-frequency coherence, in which the effective direction of coupling from STN to GP dominated, were interspersed with periods of asymmetric high-frequency coherence, in which the effective direction of coupling from GP to STN dominated. During and after the induction of global activation by hindpaw pinch, high-frequency coherence directed from GP to STN increased in magnitude and became more sustained, while the low-frequency coherence reversed its asymmetric pattern so that most activity was directed from GP to STN rather than from STN to GP. Thus, the highly dynamic relationship between STN and GP could be observed in single recording sessions.

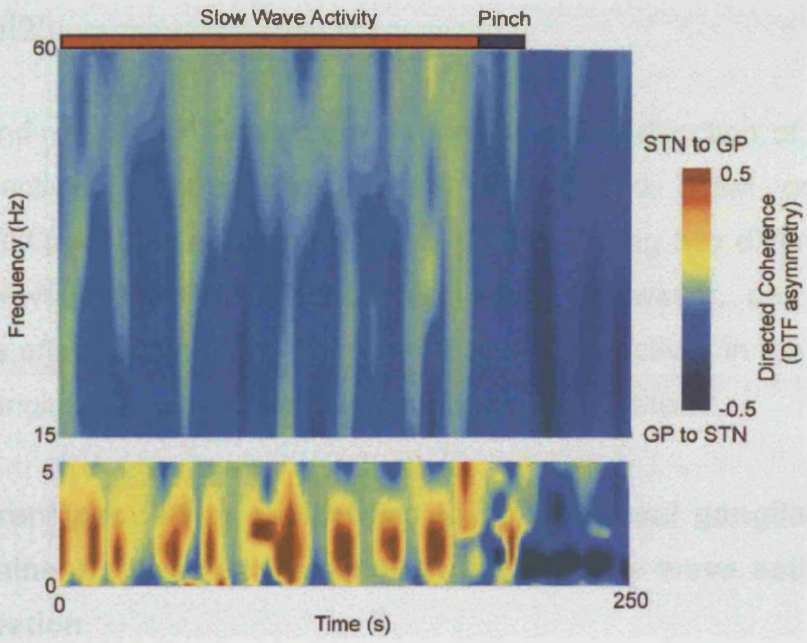

Figure 5.3 Time-evolving directed transfer function analysis of local field potentials recorded in subthalamic nucleus and globus pallidus. Plot was constructed from data acquired during a single contiguous recording. Low and high frequencies have been analysed at different sampling rates and are therefore separated. Two frequency blocks have been chosen to show the dominant activities most clearly; 0-5 Hz and 15-60 Hz. The colour scale represents the relative asymmetry of coherent activity in either direction. During spontaneous slow-wave activity, periods of asymmetric low-frequency coherence, with more activity directed from STN to GP, were interspersed with periods of asymmetric high-frequency coherence, with more activity directed from GP to STN. During and after the induction of global activation by a 15 s hindpaw pinch, high-frequency coherence directed from GP to STN increased and became more sustained, while the low-frequency coherence reversed direction so that most activity was directed from GP to STN rather than from STN to GP.

5.3 Discussion

The main findings of this chapter are that the effective direction of coherent oscillatory activity between the cerebral cortex and basal ganglia is predominantly from the cortex to the basal ganglia during two different brain states, slow-wave activity and global activation. However, and in stark contrast, the effective directions of coherent oscillatory activity in the nuclei of the basal ganglia are dynamic and dependent on brain state.

5.3.1 Coherent population oscillations in cortico-basal ganglia circuits are predominantly directed from cortex during slow-wave activity and global activation

In both brain states investigated, the effective direction of coupling was from cortex to basal ganglia rather than *vice versa*, at least as far as activity in the predominant frequency bands was concerned (Figure 5.4). As with cross correlation or phase analysis, there is no assurance that directed coherence from one recording site to another indicates a direct connection between the two sites. However, it is known, at the single-neuron level, that the slow oscillation (at ~ 1 Hz) present in the cortex during anaesthesia drives low-frequency oscillations in the STN, via direct connections, and, to a lesser extent, GP and SNr via indirect routes (Magill et al, 2000, 2001, 2004b). The DTF analysis presented here suggests that this is also true of local field potentials.

Cortico-basal ganglia connections are not functionally homogeneous. In the previous chapter, FFT-based analyses showed that coherent cortical SWA is shared more strongly between STN and SNr than GP (Magill et al, 2004). The coherence between cortex and GP may therefore reflect a relatively independent loop of activity during SWA. The reasons for this are not known. Given that LFPs may largely reflect synaptic input (for reviews, see Hubbard et al, 1969; Mitzdorf, 1985), an explanation for independent loops of coherent activity could be that the GP is more sensitive to slow oscillatory input from striatal neurons, which are also entrained by the cortical slow oscillation (Stern et al, 1997; Tseng et al, 2001; Kasanetz et al, 2002). In contrast, the

STN, which is tightly coupled with SNr, is most likely driven directly by the cortico-subthalamic pathway (Magill et al, 2001) and thus, is relatively independent of the GP in this brain state (Magill et al, 2000; Urbain et al, 2000). Irrespective of the pathway(s) subserving temporal coupling between cortex and GP or cortex and SNr, i.e. trans-subthalamic and/or trans-striatal pathways, the fact remains that the cortex provides the major driving force for low-frequency oscillations in LFPs recorded from these basal ganglia nuclei. That said, it should be noted that a small proportion of coherent activity was consistently directed from the basal ganglia to the cortex, which may reflect the looping architecture of the cortico-basal ganglia circuits (Alexander and Crutcher, 1990; Haber, 2003; Kelly and Strick, 2004).

Sensory stimulation led to a suppression of slow-wave activity in the ECoG, i.e. global activation, and an increase in coherence between the cortex and basal ganglia at higher frequencies, as previously reported (Chapter 4). From the present DTF results, however, it is clear that the effective direction of coherent oscillatory activity is unchanged during global activation, being principally driven by the cortex.

5.3.2 The effective direction of coherent population oscillations in the basal ganglia is dependent on brain state and recording location

Two questions that remain are why the effective direction and sharing of coherent oscillatory activity between basal ganglia nuclei changes with brain state, and why might this phenomenon be of importance? The interpretation of activity relationships within the basal ganglia is more challenging given the highly interconnected nature of the constituent neuronal networks (Smith et al, 1998; Bolam et al, 2000). This is well illustrated by the directed coherence between STN and SNr. Partial coherence analysis suggests that the oscillatory activities in STN and SNr that are coherent with cortical oscillations are bound together tightly in a single functional axis (Chapter 4). Given that the anatomical connections between STN and SNr are thought to be limited to projections from the former only (Smith et al, 1998), it might be expected that the DTFs would be asymmetric, with coherence being directed primarily from STN to SNr. During global activation however, coherent activity between the

two sites was found to be symmetrical. There could be several reasons why this was the case in the present experiments. The first possibility is that volume conduction between the two electrodes led to spurious symmetrical coupling. If this were the case, then the DTFs would be expected to be symmetrical for all individual subjects. However, the DTFs derived from individual animals were often asymmetrical between STN and SNr; the direction of the asymmetry was inconsistent across animals, thereby leading to apparent symmetry in the population average. Moreover, volume conduction would have been expected to lead to symmetrical directed coherence regardless of brain state, and this was not so. Alternatively, the inconsistent asymmetry of the DTFs may have been a reflection of two functionally distinct axes of coupling between STN and SNr. However, because data were necessarily pooled for statistical analysis, the existence and significance of such axes remain to be verified. The asymmetrical nature of individual DTFs raises the second possibility that the STN and SNr were being driven by a third site with equal or unequal time delays, which in turn, would depend on recording location and the topography of underlying neuronal circuits, thus creating inconsistencies in direction (see Figure 2.4*D*). An obvious candidate for a third site would be GP because the effective direction of coherent oscillatory activity from GP to both structures dominated over that in the reverse direction during global activation (Figure 5.4*B*). Of course, the demonstration of a direct projection from SNr to STN might help explain the symmetry apparent in the mean DTFs and, in fact, preliminary anatomical studies suggest that this projection may exist (J.M. Deniau, personal communication). Finally, it is also possible that the DTF estimates may have become unreliable due to the small conduction delays between STN and SNr (Cassidy and Brown, 2003).

A surprising result was also seen during slow-wave activity, when there was significantly more coherent activity directed from SNr to STN. This again raises the possibility of a direct connection from SNr to STN, preferentially showing activity of low frequency during slow-wave activity. Note however that there are two peaks in the DTF of activity between SNr and STN. The DTF over 0.1 to 1 Hz showed a predominant effective direction of coherent

oscillatory activity from SNr to STN, but the DTF at a slightly higher frequency of around 2 Hz demonstrated the expected direction from STN (Figure 5.1*F*). Of course, we cannot rule out the possibility that a third (unrecorded) site provides an important functional interface between SNr and STN (see Figure 2.4*D*). Two key contenders for such an interface are the intralaminar thalamic nuclei and the pedunculopontine tegmental nucleus; both of these brain areas receive extensive inputs from SNr and in turn project to STN (Mena-Segovia et al, 2004; Smith et al, 2004). Overall, the pattern of directed coherence between basal ganglia sites during slow-wave activity suggests that the full complexity and subtlety of their interconnections have yet not been fully established.

The most dramatic changes in the effective direction of information flow to accompany shifts in brain state were seen in paired recordings involving GP. During SWA, directed coherence between STN and GP was asymmetrical, with flow mostly going from STN to GP. Low-frequency oscillations in STN are known to be driven by cortex and are clearly seen at the levels of units, pairs of units, and LFPs (Magill et al, 2000, 2001 and Chapter 4). Local field potentials recorded in GP are less strongly coupled to the cortical oscillations at low frequencies, in agreement with the finding that similar oscillations do not manifest readily in single unit recordings (Chapter 4). Thus, low-frequency oscillations in STN are unlikely to be driven by GP (also see Magill et al, 2000; Urbain et al, 2000). Furthermore, standard coherence analysis has suggested that temporal coupling of cortex with STN (and SNr) during SWA is not shared with GP, which may rely more heavily on striatal inputs (Chapter 4). As the cortico-subthalamic pathway is considerably faster than the cortico-striato-pallidal pathway in transmitting cortical information to the basal ganglia (Nambu et al, 2000, 2002; Magill et al, 2004), it is possible that the asymmetry between STN and GP could be due to the time difference between these input pathways (Figure 2.4*D*).

During global activation, the effective direction of coherent oscillatory activity was predominantly from both cortex and GP to STN and SNr, suggesting that subthalamic and nigral LFP oscillations are partly derived from the cortex via

the pallidum. Given that the STN and GP (or the external segment of GP in primates) are reciprocally connected (Shink et al, 1996; Bevan et al, 2002), the GP may play an important role in driving high-frequency oscillatory activity in STN. Consistent with the above, coherence and partial coherence analyses have shown that during global activation, all high-frequency coherent activity between cortex and STN (and SNr) is shared with that between cortex and GP (Chapter 4). In addition, the synchronous responses of STN neurons to cortical stimulation are partly due to interconnections with both cortex and GP (Magill et al, 2004). The axons of GP neurons collateralise locally, as well as in STN and SNr (Kita and Kitai 1994; Bevan et al, 1998; Sato et al, 2000). Furthermore, up to 40% of GP cells also project to the striatum (Bevan et al, 1998; Sato et al, 2000; Kita and Kita, 2001). The GP is therefore in an ideal position to synchronise activity across the whole of the basal ganglia neuronal networks, and indeed, the present results suggest that this may in fact occur, particularly at the higher frequencies predominating in the activated brain state. Thus, under these circumstances, GP could provide a critical link between, or interface for, the cortico-subthalamic and cortico-striatal input pathways (Nambu et al, 2002).

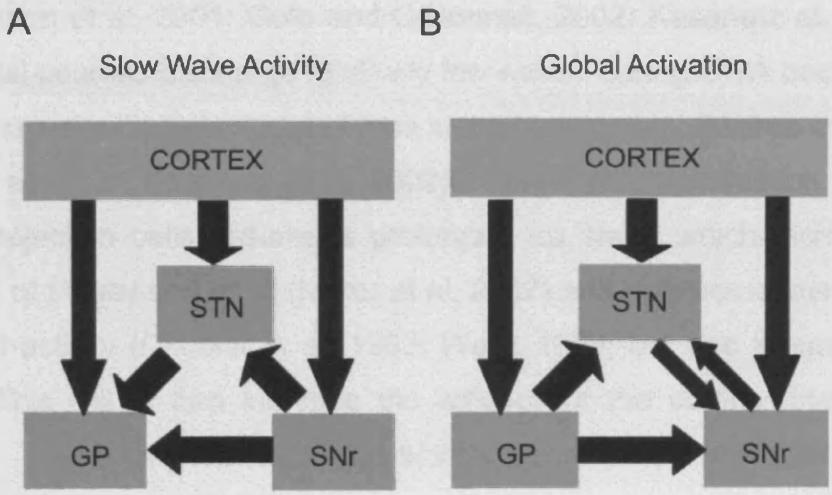

Figure 5.4 Summary diagrams showing directions of coherent activity present in cortico-basal ganglia circuits during slow-wave activity and global activation. Predominant coherence was found at 0.1-2 Hz during slow-wave activity (***A***) and at 15-60 Hz during global activation (***B***). Arrows represent the effective direction of coherence between recording sites. Single arrows represent pairings where the effective direction of coherence was significantly larger in that direction. Identical arrows between sites indicate that there was no significant asymmetry in the directed coherence. Note that the relationships between the basal ganglia sites are dynamic and dependent on brain state.

What might underlie the shift in the impact of the cortico-striatal pathway during global activation? It is well documented that that the 'up states' of striatal projection neurons, which need to be achieved before firing can occur, are entrained by cortical slow rhythms during anaesthesia (Stern et al, 1997, 1998; Mahon et al, 2001; Goto and O'Donnell. 2002; Kasanetz et al, 2002). Yet, striatal neurons discharge relatively few spikes during SWA because they also spend a significant amount of time in the 'down state' (Mahon et al, 2001; Tseng et al, 2001; Kasanetz et al, 2002). During global activation, however, striatal projection cells assume a prolonged up state, which increases the likelihood of striatal unit firing (Murer et al, 2002) and may sometimes result in increased activity (Chudler et al, 1993; West, 1998; but see Kasanetz et al, 2002). This will in turn increase the efficacy of the cortico-striato-pallidal pathway. The finding that coherent activity between GP and STN is led by GP during cortical activation, but not during slow-wave activity, is strongly suggestive of a switch in the relative dominance of the cortico-subthalamic and cortico-striatal-pallidal pathways according to the ongoing brain state. The functional state of the striatum, which provides the densest input to GP (Smith et al, 1998; Bolam et al, 2000), may partly explain this switch. Bi-directional coherence at high frequencies between STN and SNr could also be due to both structures receiving pallidal input (see above). This explanation is consistent with recent hypotheses about the functional role of the two cortico-basal ganglia pathways in the active brain (Nambu et al, 2002; Kolomiets et al, 2003).

5.3.3 Role of synchronised population activity in cortico-basal ganglia circuits.

The results presented in this chapter establish the principle that synchronous population activity within cortico-basal ganglia circuits can be dynamic, consistent with a functional role for synchronisation of activity at different frequencies in large-scale integrative processes during sleep and wakefulness. Synchronisation of activity, however fleeting, potentially facilitates the appropriate selection, assembly and disassembly of neural networks, according to processing demands, and may be an important

organisational principle in cortico-basal ganglia circuits (Graybiel, 1995; Bar-Gad et al, 2003a). In line with this, oscillatory LFPs recorded in the striatum of awake monkeys and rats (Courtemanche et al, 2003; Berke et al,, 2004), the STN of alert rats (Brown et al, 2002), and the STN of parkinsonian patients (Cassidy et al, 2002a; Williams et al, 2002; Kühn et al, 2004) are modulated in a task-dependent manner. However, further studies involving simultaneous recordings of population oscillations in striatum, GP and STN are critical to test the hypothesis that the STN and output nuclei are engaged through the cortico-striato-pallidal route or cortico-subthalamic pathway, according to the state of cortical or forebrain activation and the frequency of interaction. Nonetheless, the apparent dynamic nature of functional connectivity within cortico-basal ganglia circuits, in which both the components of a given circuit and the net direction of interaction may change, serves to illustrate the need for models of basal ganglia function that are not solely based on fixed and/or unidirectional influences.

5.4 Chapter 5: Summary

- The directed transfer function (DTF) was used to investigate the direction in which coherent activity is effectively driven in cortico-basal ganglia circuits.

- Directional analysis was performed on recordings made during robust cortical slow-wave activity (SWA) and 'global activation'.

- During SWA, there was coherence at ~ 1 Hz between ECoG and basal ganglia LFPs, with much of the coherent activity directed *from* cortex *to* basal ganglia. There were similar coherent activities at ~ 1 Hz within the basal ganglia, with more activity directed *from* SNr *to* GP and STN, and *from* STN *to* GP rather than vice versa.

- During global activation, peaks in coherent activity were seen at higher frequencies (15-60 Hz), with most coherence also directed *from* cortex *to* basal ganglia. Within the basal ganglia, however, coherence was predominantly directed *from* GP *to* STN and SNr.

- Together, these results highlight a lead role for the cortex in activity relationships with the basal ganglia, and further suggest that the effective direction of coupling between basal ganglia nuclei is dynamically organised according to brain state, with activity relationships involving the GP displaying the greatest capacity to change.

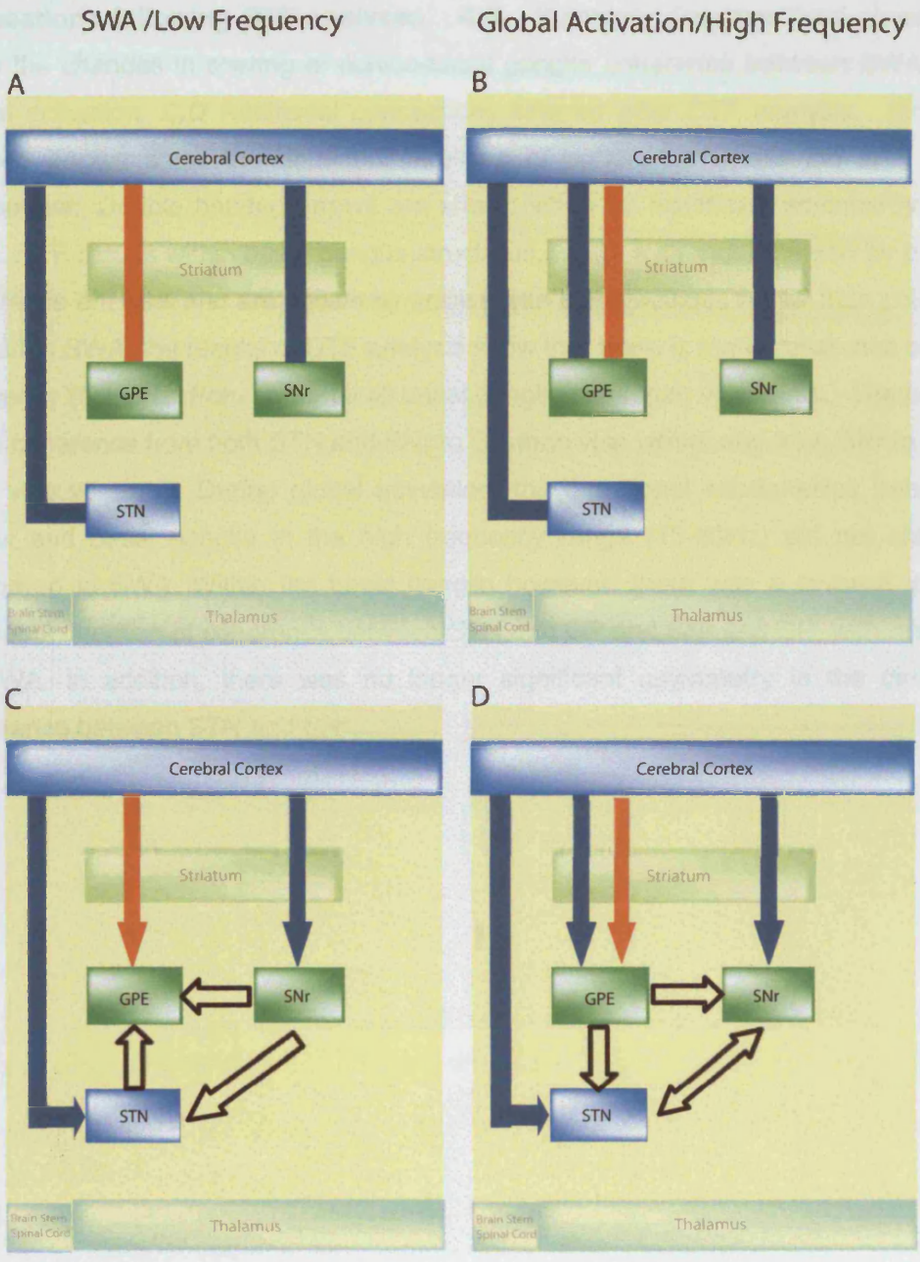
SWA /Low Frequency
Global Activation/High Frequency
A
B
C
D
Cerebral Cortex
Striatum
GPE
SNr
STN
Thalamus
Brain Stem
Spinal Cord

Figure 5.5 Summary diagram of showing additional information on oscillatory connections following DTF analyses. ***A,B,*** Summary diagrams from chapter 4 show the changes in sharing of cortico-basal ganglia coherence between SWA and global activation. ***C,D*** Additional connections inferred after DTF analysis. Singled headed arrows show the dominant direction of coherence where the DTF was asymmetric. Double headed arrows are shown when no significant asymmetry was seen. DTF results within basal ganglia structures, which were not informed by partial coherence analysis and are shown by arrows with black outlines rather than colours. ***C,*** During SWA, the results of DTF analysis show that there is more coherence at low frequency (0.1-2Hz) from cortex to all basal ganglia sites than vice versa. There was more coherence from both STN and SNr to GP than vice versa, and from SNr to STN than vice versa. ***D,*** During global activation, the directional relationships between cortex and basal ganglia in the high frequency range (15-60Hz) did not change compared to SWA. Within the basal ganglia however, there was a reversal in the dominant direction of coherence between STN and GP and SNr and GP, with respect to SWA. In addition, there was no longer significant asymmetry in the directed coherence between STN and SNr.

Chapter 6: Interdependence of coherent oscillatory activity between the cerebral cortex, striatum and globus pallidus.

In the two preceding chapters it has been demonstrated that the transmission and direction of cortical oscillations to and between the basal ganglia is brain state dependant. In addition, it was hypothesised that the differences in coupling between the globus pallidus and other basal ganglia sites may be due to the relative dominance of the trans-striatal and trans-subthalmic pathways. Slow oscillations in the cortical EEG can be seen in the membrane potentials and action potentials of the striatal neurons (Stern et al, 1998; Goldberg et al, 2003) and oscillations of several higher frequencies have been recorded in the field potentials of awake animals (Courtmanche et al, 2003: Berke et al, 2005). In the anaesthetised rat the slow oscillations recorded at the level of the cortical EEG and striatal membrane potential are also coupled to slow oscillations seen in the firing of single pallidal neurons (Goldberg et al, 2003). Hitherto, no investigation has observed the propagation of high frequency (β and γ) oscillations along the cortico-striato-palldial axis. In this chapter, the preliminary findings from multi-contact silicon probe recordings from many striatal and pallidal sites with co-incident ECoG in the aneasthetised rat are presented. The recordings demonstrate that, as with the other basal ganglia nuclei, oscillations in striatal LFPs are coherent with the ECoG over a range of frequencies in both deep anaesthesia and global activation. Partial coherence analysis is used to demonstrate that coherent low and high frequency oscillations between the cortex and GP are highly dependant on those in the striatum. These results support a role for the trans-striatal, over the trans-subthalamic, pathway in driving STN and SNr activity during global activation. Hitherto, multiple unit recordings have rarely been employed in the investigation of cortio-basal ganglia circuits. Although only preliminary data are presented here, future analyses and the potential use of silicon probe technologies to investigate the role of synchrony in cortico-basal ganglia are also discussed.

6.1 Methods

6.1.1 Electrophysiological recordings

Experimental procedures were carried out on adult male Sprague-Dawley rats (Charles River, Margate, UK) and were conducted in accordance with the Animals (Scientific Procedures) Act, 1986 (UK).

Electrophysiological recordings were made in 8 rats (280-330 g). Anaesthesia was induced with 4% v/v isoflurane (Isoflo™, Schering-Plough Ltd., Welwyn Garden City, UK) in O_2, and maintained with urethane (1.3 gkg^{-1}, i.p.; ethyl carbamate, Sigma, Poole, UK), and supplemental doses of ketamine (30 $mgkg^{-1}$, i.p.; Ketaset™, Willows Francis, Crawley, UK) and xylazine (3 $mgkg^{-1}$, i.p.; Rompun™, Bayer, Germany), as described previously (Chapter 4). All wound margins were infiltrated with the local anaesthetic, bupivacaine (0.75% w/v; Astra, Kings Langley, UK) and corneal dehydration was prevented with application of Hypromellose eye drops (Norton Pharmaceuticals Ltd., Harlow, UK). Animals were then placed in a stereotaxic frame (Kopf, Tujunga, CA, USA). Body temperature was maintained at 37 ± 0.5°C with the use of a homeothermic heating device (Harvard Apparatus Ltd., Edenbridge, UK). Anaesthesia levels were assessed by examination of the electrocorticogram (ECoG; see below), and by testing reflexes to a cutaneous pinch or gentle corneal stimulation. Supplemental doses of ketemine/xylazine (30/3 $mgkg^{-1}$) were given as and when necessary (typically, once per hour). Electrocardiographic (ECG) activity and respiration rate were also monitored constantly to ensure the animals' well being (see below).

The ECoG was recorded via a 1 mm diameter steel screw juxtaposed to the dura mater above the right frontal cortex (AP: –4.5 mm, ML: –2.0 mm [Paxinos and Watson 1986], which corresponds to the medial agranular field of the somatic sensorimotor cortex [Donoghue and Wise 1982]) and was referenced against a screw implanted in the skull above the ipsilateral cerebellar hemisphere. Raw ECoG was band-pass filtered (0.3-1500 Hz, -3 dB limits) and amplified (2000×; DPA-2FS filter/amplifier: Scientifica Ltd.,

Harpenden, UK) before acquisition. The ECG was differentially recorded via two silver wires inserted into the skin of the ipsilateral forelimb and hindlimb. Raw ECG was band-pass filtered (5-500 Hz) and amplified (5000×; DPA-2FS filter/amplifier) before acquisition. The chest movements accompanying respiration were recorded using a miniature accelerometer (AP19, Bay Systems Ltd., Somerset, UK) and charge amplifier (Type 5007; Kistler Instrumente AG, Winterthur, Switzerland). The signal from the accelerometer allowed the depth and rate of respiration to be accurately assessed on- and off-line.

Discrete crainotomies (4 mm^2) were performed above the striatum, and the dura mater removed for insertion of recording electrodes. Mineral oil and/or saline solution (0.9% w/v NaCl) was applied to all areas of exposed cortex to prevent dehydration. Extracellular recordings of local field potentials (LFPs) and unit activity in the ipsilateral striatum and GP were simultaneously made using 'silicon probes' (1cm100-400s: NeuroNexus Technologies, Ann Arbor, MI, USA). Each probe had 16 recording contacts arranged in a single vertical plane, with a contact separation of 100 μm (Figure 6.1). Each contact had an impedance of 0.9-1.3 MΩ (measured at 1000 Hz) and an area of 400 μm^2. Probes were manually lowered into the brain under stereotaxic control (Paxinos and Watson, 1986), using an angle of 15° to the vertical to maximize the spread of recording contacts across the striato-pallidal axis (Figure 6.1). Extracellular signals from the silicon probe were amplified (1000×-2000×) and low-pass filtered (0-6000 Hz) using computer-controlled amplifiers (Lynx-8: Neuralynx, Tucson, AZ, USA). The ECoG and probe signals were each sampled at 17.5 kHz. The ECG and respiration signals were sampled at 400 Hz and 64 Hz, respectively. All biopotentials were digitised 'on-line' using a Power1401 Analogue-Digital converter (Cambridge Electronic Design Ltd., Cambridge, UK) and a PC running Spike2™ acquisition and analysis software (version 5; Cambridge Electronic Design).

In most cases (6 of 8 animals), putative recording locations were identified using established electrophysiological characteristics of neurons during

urethane anaesthesia: striatal projection neurons typically have low firing rates (<5 Hz) and phasic activity patterns, whilst pallidal neurons have relatively high firing rates (15-30 Hz) and tonic activity patterns (Magill et al. 2000, 2001; Kasanetz et al. 2002 and see Chapter 1). The recording strategy was to have an even spread of probe contacts across the striato-pallidal axis, with contacts 1-8 in the GP and contacts 9-16 in the striatum. In two of the animals, recording locations were additionally verified using histological procedures (see below).

As in Chapters 4 and 5, recordings were made during slow-wave activity (SWA), which accompanies deep anaesthesia and is similar to activity observed during natural sleep, and during episodes of sensory-evoked 'global activation', which contain patterns of activity that are more analogous to those observed during the awake, behaving state. Sensory stimulation and subsequent global activation were elicited by pinching the hindpaw for 15 s with serrated forceps that were driven by a standard pneumatic pressure, as described previously (Chapter 4). The animals did not exhibit either a marked change in ECG/respiration rates or a hindpaw withdrawal reflex in response to the pinch.

6.1.2 Histology

In addition, recording locations were histologically verified in two animals. Before recordings, the silicon probe was coated with a red dye, DiI (1,1'-dioctadecyl-3,3,3',3'- tetramethylindocarbocyanine perchlorate; Molecular Probes; Eugene, OR, USA), by immersion of the probe in a 80 $mgml^{-1}$ DiI solution (in 50/50% acetone/methanol) under microscopic control. No differences in recording quality (signal:noise ratio) or neuronal activity were observed when the probe was coated with DiI. Because DiI is non-toxic to neurons and highly lipophylic, it is taken up into cell membranes and white matter tracts when the probe is in situ.

After the recording sessions, the animals were given a lethal dose of ketamine anaesthetic and perfused via the ascending aorta with 100 ml of 0.01 M phosphate-buffered saline at pH 7.4 (PBS), followed by 300 ml of 0.1% w/v

glutaraldehyde and 4% w/v paraformaldehyde in 0.1 M phosphate buffer, pH 7.4, and then by 100 ml of PBS. Brains were then left in the latter solution at 4°C until sectioning 24-72 hours later. The fixed brain was cut into 60 μm thick sections in the parasagittal plane on a vibrating blade microtome (VT1000S: Leica Microsystems, Milton Keynes, UK). Sections were then washed in PBS and viewed on a light microscope using 10x objective. Probe locations were indicated by discrete red/pink staining of the tissue (Figure 6.1). Images of sections were captured using a digital camera (Photometrix CoolSnap: Roper Scientific, Tucson, AZ, USA) and associated imaging software (OpenLab: Improvision Ltd., Coventry, UK).

6.1.3 Data Analysis

Data from the recording session were first scrutinized for ECG and respiration artifacts. LFP data contaminated with ECG artifact were rejected. Artifact-free data were then visually inspected and epochs of robust cortical slow-wave activity or global activation were identified (Chapter 4). One animal was rejected due to continuous artefact in the ECoG channel.

In this chapter, analysis was performed only on ECoG and basal ganglia LFPs. Units were used only for verification of recording sites and will be analysed in future studies. Prior to all analysis, LFPs were down-sampled to 1167Hz after appropriate low-pass filtering to avoid aliasing, (Spike 2. version 5; Cambridge Electronic Design). Coherence and partial coherence analyses were performed on one data segment recorded during robust SWA episodes, as identified by assessing ECoG activity, and one data segment of pinch-evoked activity per animal. All data segments were 80 s in length. Single data segments of pinch-evoked activity were derived by splicing together multiple recordings made during and immediately after four hindpaw pinches. For each animal, LFPs were included in coherence analysis only if they displayed clear striatal or pallidal action potentials. Between 2 and 7 pallidal LFPs (3.8 ± 1.6) and 4 and 8 striatal LFPs (5.4 ± 1.8) were used for each animal (n=7). It is probable that LFPs which did not display identifiable units

were also striatal or pallidal, but these were not considered in the current analysis due to the possibility that at some point the electrode was outside these areas.

Coherence, partial coherence and DTF analyses were performed on all unit containing channels. For detailed explanations of these methods please see Chapters 2, 4 and 5. For each animal the coherence for each ECoG/STR-LFP and each ECoG/GP-LFP pairing was calculated. Partial coherence was used to test the specific hypothesis that the striatal LFP is an effective predictor for ECoG/GP coherence. To this end, for each animal the partial coherence was calculated for all individual ECoG/GP pairs with each of the striatal channels as a predictor. These partial coherence values were averaged to give a mean value for each ECoG/GP pair with the striatum as the predictor, which was compared to the mean ECoG/GP coherence. DTF analysis was performed only on SWA episodes, which were further down-sampled to 20Hz to maximise the detection of the slow oscillation. DTF analysis was only performed only to rule out volume conduction by establishing a significant asymmetry

To compare the coherence between signals, the variance of the modulus of the coherency (given by the square root of the coherence) was normalized using a Fisher transform (Rosenberg et al. 1989). Group analysis of transformed coherence data was performed by repeated measures General Linear Models (GLMs) as described in the Results. A Greenhouse-Geisser correction for non-sphericity was used where necessary and significance was set at $p \leq 0.01$ to correct for the multiple GLMs. *Post hoc* testing was by two-tailed paired *t*-tests. DTF asymmetry was evaluated using two-tailed paired *t*-tests to compare coherence in each direction as described in Chapter 5.

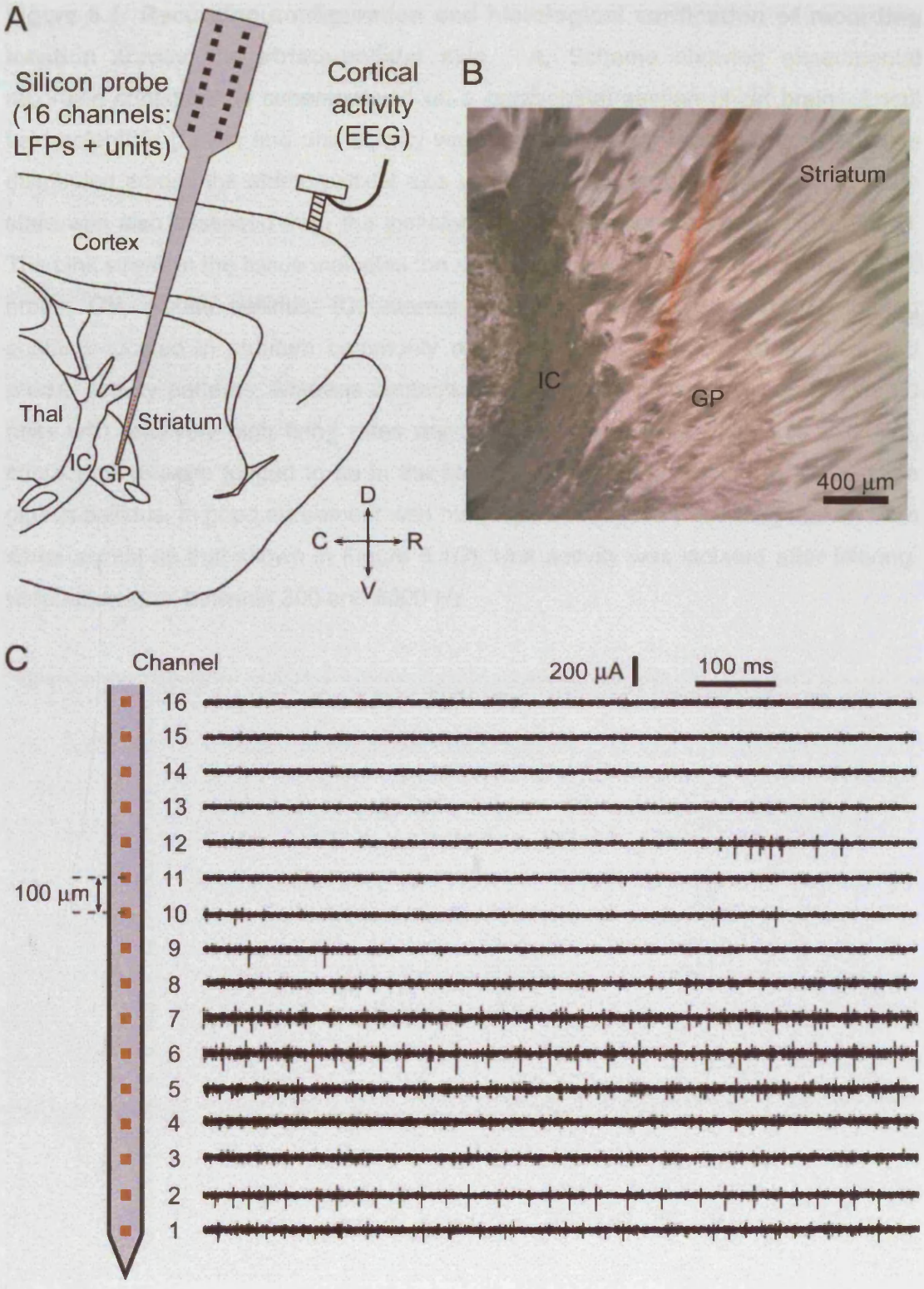
A
Silicon probe
(16 channels:
LFPs + units)
Cortical
activity
(EEG)
Cortex
Thal
Striatum
IC
GP
D
C
R
V
B
Striatum
IC
GP
400 µm
C
Channel
200 µA
100 ms
16
15
14
13
12
11
10
9
8
7
6
5
4
3
2
1
100 µm

Figure 6.1 Recording configuration and histological verification of recording location across the striato-pallidal axis. ***A,*** Scheme showing experimental recording configuration superimposed on a parasagittal section of rat brain. Local field potentials (LFPs) and unit activity were simultaneously recorded from 16 sites distributed across the striato-pallidal axis using a silicon probe. The ongoing brain state was also assessed from the ipsilateral frontal electrocorticogram (ECoG). ***B,*** The pink streak in the tissue indicates the recording position of the dye-coated silicon probe. GP, globus pallidus; IC, internal capsule; Thal, thalamus. ***C,*** Recording contacts located in striatum commonly registered units with low firing rates and phasic activity patterns, whereas contacts located in the globus pallidus registered units with relatively high firing rates and tonic activity patterns. In this example, contacts 9-16 were judged to be in the striatum, whereas contacts 1-8 were in the globus pallidus, in good agreement with histological analyses (recordings taken from same animal as that shown in Figure 6.1*B*). Unit activity was isolated after filtering. wideband signal between 300 and 6000 Hz.

6.2 Results

6.2.1 Identification of brain states and conformation of recording sites.

Cortical activity, as assessed from the ECoG, was the primary indicator of brain state. Slow-wave activity (SWA) and 'global activation states were detected as described in Chapter 4. In all animals it was possible to confirm by unit identification that several contacts in the dorsal 8 contacts of the probe were in the striatum and that several contacts in the ventral 8 contacts were in the pallidum (see Figure 6.1)

6.2.2 Coherence between ECoG and basal ganglia LFPs is not due to volume conduction

DTF analysis was used to investigate the directional relationship between the ECoG and basal ganglia local field potentials. Analysis were performed only on SWA periods under the rationale that demonstrating a significant asymmetry between the highest amplitude oscillations should negate the possibility of volume conduction between all lower amplitude, higher frequency activities. These analyses were performed purely for methodological reasons, rather than to investigate function as in Chapter 5. DTF analysis confirmed that there was more coherence in the slow range (0-1.5Hz) from ECoG to both striatum and GP (see Figure 6.2). Only in the case of the STR-LFPs however there was a significant asymmetry (paired t-test, $p < 0.05$). These results indicate that highest amplitude coherent oscillations between cortex and basal ganglia were not the result of volume conduction from the ECoG.

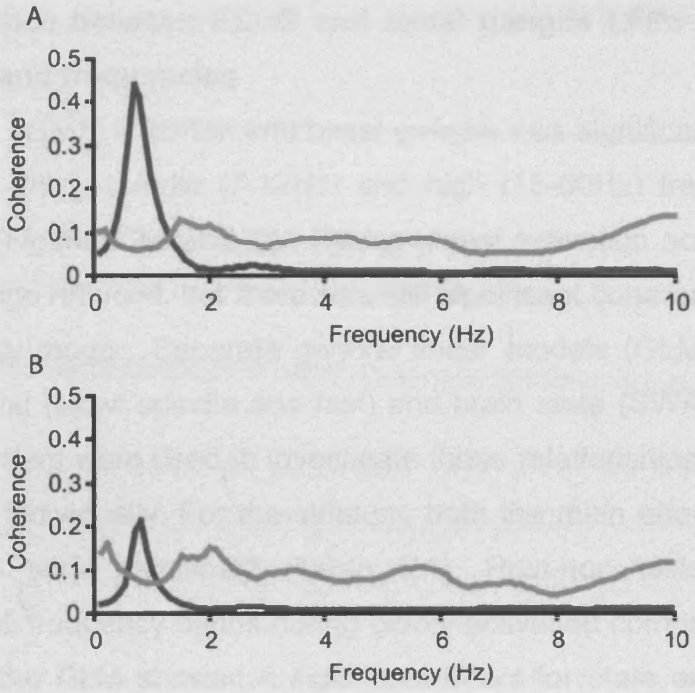

Figure 6.2 Directed transfer function analysis of local field potentials recorded in cortex and basal ganglia during robust slow-wave activity. ***A,B*** Directed transfer function analysis confirmed greater coherence in the direction of EEG to basal ganglia (black lines) than from basal ganglia to EEG (Grey lines) in the low frequency range (around 1Hz). This asymmetry was statistically significant for the striatum (***A***) but not GP (***B***).

6.2.3 Coherence between ECoG and basal ganglia LFPs differs across brain states and frequencies

Spontaneous activity in cortex and basal ganglia was significantly coherent in the slow (0.1-2Hz), spindle (7-12Hz) and high (15-60Hz) frequency ranges during SWA (Figure 6.3*A* and *C*). During global activation activity in the low frequency range reduced, but there was still significant coherent activity in the high frequency range. Separate general linear models (GLM) incorporating frequency band (slow: spindle and fast) and brain state (SWA and pinch) as the main effectors were used to investigate these relationships in the striatum and pallidum individually. For the striatum, both the main effects and second order effects were significant (Table 6.1). Post-hoc tests confirmed a decrease in all frequency bands during global activation compared with SWA. For the GP, the GLM showed a significant effect for state and a significant second order interaction for state and frequency (see Table 6.1). Post-hoc tests showed a significant decrease in the slow and spindle frequency during global activation compared to pinch, but no significant change in the high frequency range between states.

In Chapter 4, there was a significant increase in ECoG to GP-LFP in the 15-60Hz band during activation (see Figure 4.6). Although there was no significant increase in this range for these data, the mean coherence plots (Figure 6.3*A-D*) seemed to suggest specific changes in β- and γ- bands. To investigate this further, the peak frequency (the frequency with the highest coherence) in the 15-60Hz band was calculated for each animal in each condition. For ECoG to GP-LFP coherence the peak frequency during SWA (32.9 ± 4.1 Hz) was significantly higher than during pinch (24.9 ± 2.0 Hz). The coherence was then re-analysed using 10Hz bands made up of the 5Hz either side of these mean peak values. There was a significant increase in activity in the 20-30Hz band, corresponding to β-frequency in the awake rat (see Chapter 3) during pinch compared to rest. No significant difference was seen over higher frequencies (27-37Hz) more prominent during SWA. As described above, for ECoG to STR-LFP coherence there was actually a significant decrease in the high frequency range. A significant decrease in the peak

frequency of the high frequency range during SWA (39 ± 4.1 Hz) compared to pinch (26.2 ± 2.2) was also observed for ECoG to STR-LFP coherence. Although there were trends toward higher beta coherence (22-32 Hz) and lower coherence above this range (29-39Hz), these comparisons were not significant.

6.2.4 Coherence between ECoG and GP is dependant on the Striatum

In Chapter 5, it was hypothesised that coherent activity between ECoG and GP, which was not shared with STN and SNr, could be dependant on the cortico-striatal pathway. To test this hypothesis, partial coherence analysis was used specifically to assess the effectiveness of the striatal LFPs as a predictor for the coherence between ECoG and GP-LFPs. Partialisation resulted in a decrease in coherence in all frequencies across both states (see Figure 6.3*E* and *F*). A GLM incorporating partialization (coherence and partial coherence), brain state (SWA and pinch) and frequency (0-2Hz and 15-60Hz) confirmed a main effect for partialisation and a third order interaction between partialisation, state and frequency (Table 6.2). Post-hoc tests showed significant reductions in coherence in the low frequency range during SWA and the high frequency range during global activation. There was however still some low frequency coherence following partialisation (see Figure 6.3*E*). DTF analysis suggested that basal ganglia LFPs were not due to volume conduction from cortex (see above). This does not rule out the possibility however that volume conduction between contacts could be responsible for the effects of partialisation. This would be unlikely however if the frequency contents of coherent activity between STN and GP with ECoG are different, suggesting that the coherent activities are independent (ie. a significant effect of nucleus). To this end, separate general linear models were performed on recordings in each state with nucleus (STR and GP) and frequency (0-2Hz, 7-12Hz and 5-60Hz) as the main effects (Table 6.3). During SWA, there were significant main effects were found for nucleus and frequency, and a significant interaction between the two variables (Table 6.3). Post-hoc t-tests confirmed that coherence was higher in all frequency bands between ECoG and STR than ECoG and GP. No significant effects were found during

activation. If volume conduction were responsible for shared coherence between contacts in the striatum and ECoG, such differences between nuclei would not be expected during any state.

Table 6.1 Repeated measures general linear model (GLM) of changes in coherence between ECoG and STR/GP LFPs across state and frequency

	STR		GP	
	F [DF]	*p* value	F [DF]	*p* value
State	75.7 [1,5]	<0.001	25.6 [1,5]	0.006
Frequency	12.2 [2,5]	0.002	4.7 [2,5]	NS
State x Frequency	19.2 [2,5]	<0.001	16.1 [2,5]	<0.009

Two main effects were considered: brain state (two levels: SWA and global activation) and frequency band (two levels: slow-wave oscillations [0.8-1.5 Hz] and high-frequency oscillations [15-60 Hz]). Separate models were run for coherence between cortex and STR and cortex and GP. Differences were considered significant when $p \leq 0.02$. DF, degrees of freedom. NS, not significant.

Table 6.2 Repeated measures general linear model (GLM) of changes in coherence between ECoG and GP after partialisation.

	F [DF]	*p* value
Partialization	48.3 [1,5]	0.001
State	12.5[1,5]	0.02
Frequency	5.8 [1,5]	NS
Partial x State	3.4 [1,5]	NS
Partial x Frequency	2.0 [1,5]	NS
State x Frequency	73.4 [1,5]	<0.001
Partial x Frequency x State	17.3 [1,5]	0.009

Three main effects were considered: partial coherence (two levels: no partialisation, and partialisation of EEG/GP with the STR recording sites), brain state (two levels: SWA and global activation) and frequency band (two levels: slow-wave oscillations [0.8-1.5 Hz] and high-frequency oscillations [15-60 Hz]). Differences were considered significant when $p \leq 0.02$. DF, degrees of freedom. NS, not significant.

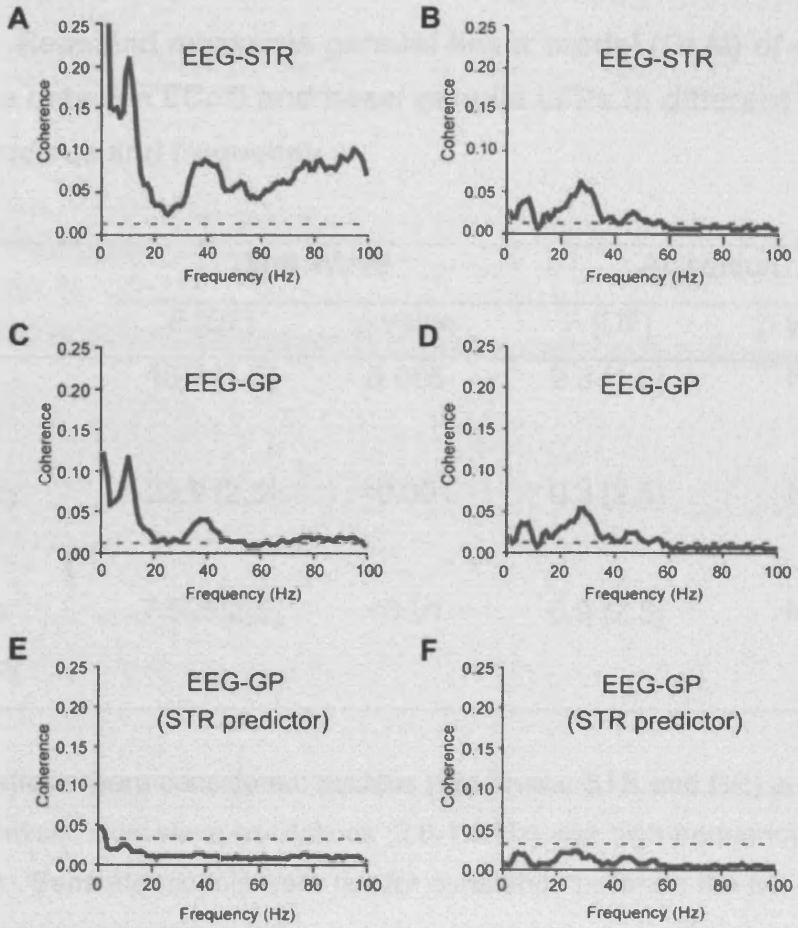

Figure 6.3 Coherence and partial coherence analysis of local field potentials recorded in cortex and basal ganglia during SWA and global activation. ***A,*** Coherent oscillatory activity between ECoG and local field potentials in the striatum occurred across a large range of frequencies during SWA. In addition to the slow, spindle and β\γ ranges, there was also significant coherence above 60Hz. ***B,*** After paw pinch ECoG-STR LFP coherence became focused in the β\γ range with some significant coherence around 8Hz. ***C,*** Coherent oscillatory activity between ECoG and GP-LFPs was seen in the slow, spindle and β\γ range during SWA. **D,** Activity in the slow and spindle ranges decreased after forepaw pinch, but β\γ range activity was unchanged. ***E, F*** Partialsation of coherence between ECoG and GP-LFP using STR LFP as a predictor, lead to a decease in coherence across all frequency ranges in both SWA (***E***) and global activation (***F***). Spectral plots in *A* to *F* are grand averages from all unit displaying channels across the 7 animals. Coherence was computed using one 80 s data segment of SWA (***A, C, E***) and pinch-evoked activity (***B, D, F***) per animal (1024 data points per FFT block; 1.13 Hz resolution). *Dashed lines* indicate the 95% confidence levels.

Table 6.3 Repeated measures general linear model (GLM) of changes in coherence between ECoG and basal ganglia LFPs in different brain state across nucleus and frequency

	Slow Wave		Activation	
	F [DF]	*p* value	F [DF]	*p* value
Nucleus	18.7 [1,5]	0.005	2.3 [1,5]	NS
Frequency	23.9 [2,5]	<0.001	0.3 [2,5]	NS
Nucleus x Frequency	7.525[2,5]	<0.01	0.9 [2,5]	NS

Two main effects were considered: nucleus (two levels: STR and GP) and frequency band (two levels: slow-wave oscillations [0.8-1.5 Hz] and high-frequency oscillations [15-60 Hz]). Separate models were run for coherence between the two brain states (SWA and global activation). Differences were considered significant when $p \leq 0.02$. DF, degrees of freedom. NS, not significant.

6.3 Discussion

The main findings in this chapter are that there is coherent oscillatory activity between ECoG and striatal LFPs which is brain state and frequency dependant. In addition, the striatal LFPs are effective predictors of low and high frequency coherence between the ECoG and GP-LFPs. These results support the hypothesis put forward in Chapter 5, that high frequency oscillatory activity is propagated to the STN and SNr though the cortico-striato-pallidal pathway.

6.3.1 The advantages and limitations of multi-contact silicon-based electrodes

The use of silicon-based electrodes to record from multiple channels is a relatively new development in systems neuroscience. The ultimate goal of electrophysiological recording should be to maximise the number of recording sites while causing minimal damage to the surrounding tissue (Csicsvari et al, 2003a; Buzsaki et al, 2004). The development of silicon probes was designed to improve this ratio by reducing the size of the electrode tip compared to a conventional tetrode, while still providing multiple recording contacts. Hitherto, silicon electrodes have enabled recordings of hundreds of hippocampal neurons simultaneously (Csicsvari et al, 2003a; 2003b), but have not been used in basal ganglia structures. In the recordings presented here, up to six pallidal and six striatal units could be detected simultaneously. Future analysis of multiple single units together with LFPs recorded from different electrodes has the potential to provide insights in to these brain areas that are impossible with conventional recording set ups (see Chapter 7 for further discussion).

In Chapters 4 and 5, several arguments are presented as to why the results are unlikely to be the result of volume conduction. The latter is a particular concern when monopolar signals are analysed as here. The DTF results provide conclusive evidence that the striatal LFPs lag the cortical ECoG at low frequency. This result makes the possibility of volume conduction from the cortex to the electrode, leading to spurious coherence, highly unlikely even for

the very high amplitude SWA. This is also supported by differences in the coherence and DTF between the striatum and pallidum with the ECoG, suggesting that the LFP signals were local to those structures. In addition, differences between the coherence between contacts in each nuclei and ECoG provide evidence that the results of partialisation are not the result of volume conduction between contacts.

6.3.2 Potential confounds across experiments

Before discussing the relevance of the results presented in this chapter it is important to note that some results here disagree with those presented in the previous two chapters. Most notably, no increase in coherence was seen in ECoG-GP coherence following paw pinch in the 15-60Hz range. A significant increase was detected however when only the β-range (20-30Hz) was taken. This range was in fact where the majority of coherence was found between ECoG and GP in Chapters 4 and 5 (see Figures 4.6 and 5.2). It is unclear why there was not a significant increase over the whole 15-60Hz range in these recordings. A methodological origin cannot be totally ruled out given the different electrode types, although this seems unlikely given that the entire range of frequencies from 1-100Hz was detected over the two structures and brain states. Alternatively, there may have been some difference in the recording site due to the necessity to straddle STR and GP, which could account for the difference to the previous recordings. In addition, the level of pinch induced activation may have differed between experiments.

An interesting, albeit speculative explanation for the relatively specific increase in β-activity during pinch observed in this chapter could be that it is dopamine related. The same pinch stimulus has been shown to inhibit dopaminergic neurons in the VTA (Ungless et al, 2004). If this is true across the population of midbrain dopaminergic neurons, the results presented in Chapter 3 would predict an increase in the β-range. Given that pinch induced cortical activation involves many structures and neuronal populations, further experiments would be necessary to confirm this. Cortico-striatal coherence was also seen in the high gamma range (<60Hz) at rest, but not during

activation (see Figure 6.3). High gamma activity has been described in a variety of structures during anaesthesia (Steriade, 2000: Penttonen and Buzsaki, 2003). The state dependence of this range and its specificity to the striatum suggests it is a genuine activity that requires further investigation.

6.3.3 Implications of the dependence of cortico-pallidal coherence on striatum.

In Chapter 4, coherence and partial coherence analyses showed that, during SWA, cortex was temporally coupled to the STN and SNr in highly coherent loops that formed a single functional axis. Cortex was also tightly coupled to the GP, but in an axis distinct from that containing the more strongly coupled STN and SNr. During global activation, cortex was temporally coupled to the STN, GP and, to a lesser extent, the SNr via loops that formed a single functional axis. In addition, the cortex was closely coupled to the GP alone in another, functionally distinct axis. In Chapter 5, DTF analyses showed that in both states the majority of coherent activity was directed from the cortex to the basal ganglia. Within the basal ganglia however, the predominant direction of coherent activity differed between brain states. Most notably, there was more low frequency coherence directed from STN to GP than vice versa during SWA, but more high frequency activity directed from GP to STN during pinch than vice versa. These results lead to the hypothesis that slow oscillatory activity was propagated through the cortico-subthalamic pathway to the SNr but not the GP, whereas coherent high frequency activity was propagated to the STN and SNr from the cortico-striatal pathway via the pallidum.

The results of coherence and partial coherence analysis presented in this chapter provide strong support for this hypothesis. The striatal channels were effective predictors of cortico-pallidal coherence across state and frequency. The propagation of cortical SWA via the trans-striatal rather than trans-subthalamic pathway would explain the independent loops at low frequency during this brain state, presented in Chapter 4. It is important to consider however that the DTF results in Chapter 5 demonstrate that there is coherent

activity between STN/SNr and GP at low frequencies, the predominant direction of which is from STN and SNr to GP. These results are not mutually exclusive given that the results in Chapter 4 consider only the oscillations coherent with the ECoG, where as the DTF analysis measures all coherent oscillations between the basal ganglia structures. Therefore the results imply that from a given area of cortex, oscillatory activities, even those as widespread as the slow oscillation, can be independent at the level of the basal ganglia input structures. The coherence directed from STN/SNr to GP described in Chapter 5 may be driven by another cortical or thalamic area, but as a whole the results still demonstrate the presence of independence in relation to the cortical area recorded along the cortico-basal ganglia axis. This finding could be explained by anatomical separation of the trans-subthalamic and trans-striatal pathways, or even simply by segregated cortico-basal ganglia loops (see Figure 1.2). During activation however, oscillations from the same cortical area are shared by all structures and are driven mostly from the GP. The effectiveness of the striatum as a predictor for high frequency coherence during activation strongly suggests this change in the sharing of oscillations between brain states is caused by oscillations in the ECoG being transmitted to the STN and SNr though the cortico-striatal-pallidal axis, rather than the cortico-subthalamic pathway.

Although we cannot fully generalise these findings to awake behaving animals, they may nevertheless give much insight in to information flow through cortico-basal ganglia networks. As discussed in Chapter 1, with the exception of a handful of recent studies (Berke et al, 2004; Courtemanche et al, 2004, Goldberg et al, 2004), the predominant view of the organisation of basal ganglia networks has been in terms of anatomical connections and changes in the rate of individual neurons. The results presented here, and in the previous chapters suggest that oscillations could provide a level of organisation in cortico-basal ganglia networks that is highly dynamic and dependant on brain state.

6.4 Chapter 6: Summary

- LFPs and single units were simultaneously recorded from striatum (STR) and globus pallidus (GP) using multi-contact silicon probes, with simultaneous ECoG.

- Characteristic single and multi-unit activity allowed the identification of multiple striatal and pallidal LFPs simultaneously.

- DTF analysis showed that coherence between ECoG and LFPs recorded from the probe was not volume conducted.

- During SWA Coherence between ECoG and STR-LFPs was seen at both low and high frequencies. During activation low frequency coherence decreased between ECoG and basal ganglia LFPs. An increase at higher frequencies was seen only in the beta band for ECoG to GP coherence during pinch.

- STR-LFPs were highly effective predictors of ECoG to GP-LFP coherence during both SWA and activated brain states, for low and high frequencies, respectively.

- These data support the hypothesis that during the activated state, cortical high frequency oscillations are propagated to the STN and SNr via the trans-striatal-pallidal pathway.

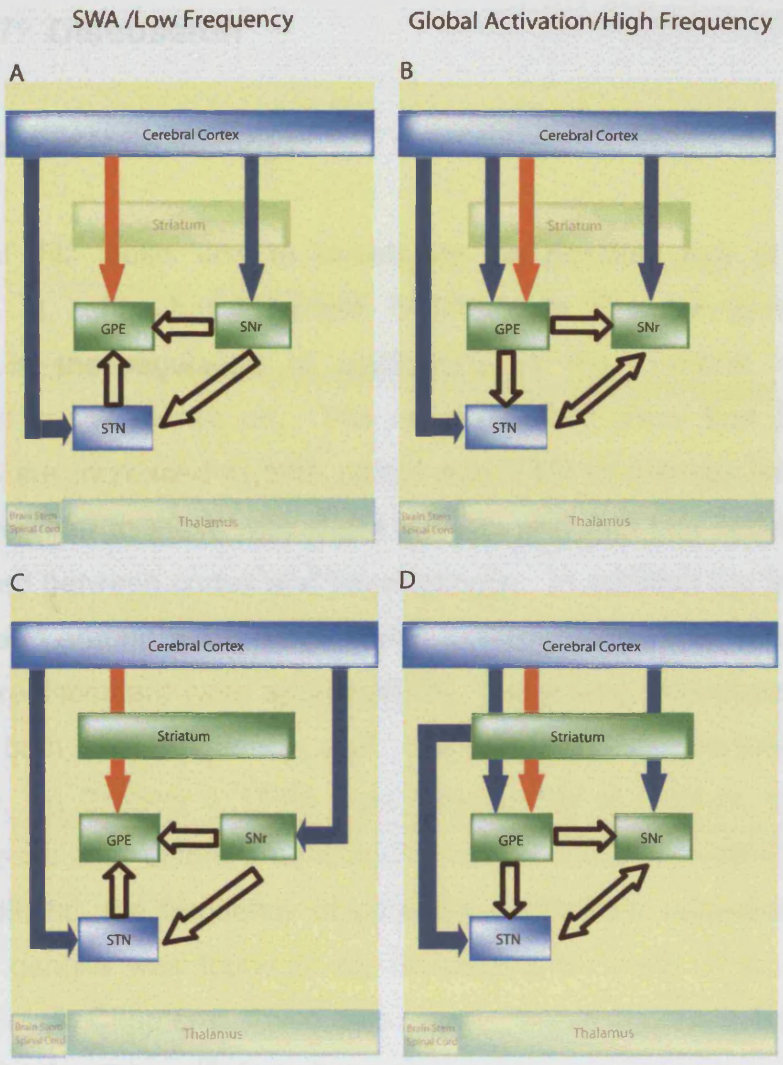

Figure 6.4 Summary diagram synthesising results of all analyses performed on ECoG and basal ganglia LFPs. ***A,B,*** Summary diagrams from chapter 5 showing oscillatory connections following coherence, partial coherence and DTF analysis of cortex, GP, STN and SNr. ***C,D,*** Additional connections after effective partialisation of cortex to GP coherence with striatum as a predictor. ***C,*** The independent coherence between the cortex and GP at low frequency during SWA is dependant on striatum. As coherence between cortex with STN and SNr was not shared with GP, it can be inferred that these connections are not dependant on striatum. ***D,*** All high frequency coherence between cortex and the basal ganglia during pinch was shared with GP. Coherence between cortex and GP was dependant on striatum, so it can therefore be inferred that high frequency coherence between cortex and STN and SNr is also dependant on the striatum.

Chapter 7: Discussion

7.1 Summary of Main Findings

The aim of this thesis was to investigate the possible role of population oscillations in cortico-basal ganglia circuits. In Chapter 3, the role of dopamine in the regulation of oscillations in the cerebral cortex was investigated in the awake rat. The results clearly show that β-frequency oscillations are increased in both cortex and STN in animals with 6-OHDA lesions compared to those with sham lesions, and that this activity is highly synchronised between cortex and basal ganglia. In addition the frequency of activity in and around the β-range varied systematically with movement and dopamine replacement (with apomorphine), suggesting that dopamine could modulate both the frequency and magnitude of cortico-basal ganglia oscillations. In Chapter 4, LFPs were investigated at multiple cortico-basal ganglia sites during different behavioural states under anaesthesia. Under these conditions, the frequency of coherent oscillations between the cortex and basal ganglia was found to be dependent on brain state and varied across nuclei. In Chapter 5, these data was further analysed to show that the direction of coherent oscillations between the basal ganglia, but not between the cortex and basal ganglia, is also dependent on brain state. The results for these two chapters together lead to the hypothesis that coherent oscillations between the cerebral cortex and the GP are propagated through the striatum. In Chapter 6, partial coherence analysis of multiple LFP recordings from the striatum and GP confirmed this hypothesis. In this chapter, both the implications and limitations of these findings will be discussed. In addition, the putative role of population oscillations in both the healthy and dopamine depleted basal ganglia will be considered.

7.2 The use of EEG and Local Field Potential Recordings to investigate population activity in the healthy brain.

How is the local field potential generated and what can it tell us about neuronal processing?

In laminar structures, it is generally agreed that LFPs are generated from synaptic potentials, which are summed due to the consistent orientation of the dendritic field (Creutzfeldt et al, 1966; Mitzdorf, 1985; Bedard et al, 2004 and see Chapter 1). In addition, LFPs in cortex can have constant relationships with single neuronal activity (Murthy and Fetz, 1996a; Donoghue et al, 1998; Steriade, 2000). The debate becomes more complex when the LFP is recorded from non-laminar structures such as the basal ganglia nuclei. Recent evidence suggests however that LFPs in the STN (Magill et al, 2004; Kuhn et al, 2005; Levy et al, 2002) and the striatum (Berke et al, 2004: Fujii and Graybiel, 2005) are highly correlated with single unit activity. The recordings in chapter 4 suggest that basal ganglia LFPs are generated from summed synaptic activity, rather than being a representation of spiking activity. STN neurons displayed prominent bursting in time with the EGoG slow oscillation, which was also highly coherent between the ECoG and the STN-LFP (see also Magill et al, 2001). In contrast, SNr neurons show virtually no significant locking to the slow oscillation, despite having similar ECoG/local field potential coherence (see also Belluscio et al. 2004). In the GP, the neurons show some locking to the ECoG slow oscillation (see also Goldberg et al, 2003), but the LFP shows significantly less coherence with the EEG than the other two structures. These findings are inconsistent with a linear relationship between the firing of action potentials and parameters derived from basal ganglia LFPs, especially those in STN and SNr where coherence with the ECoG is shared but action potential firing differs greatly (see Fig. 7.1). These findings could be explained by the LFP being generated by pre- and post-synaptic potentials, which may not be represented in the spike train. SNr/GPi neurons are not reliant on synaptic input to fire, due to their intrinsic membrane properties, where as STN neurons are highly sensitive to cortical afferent input (see Chapter 1), which may explain this difference.

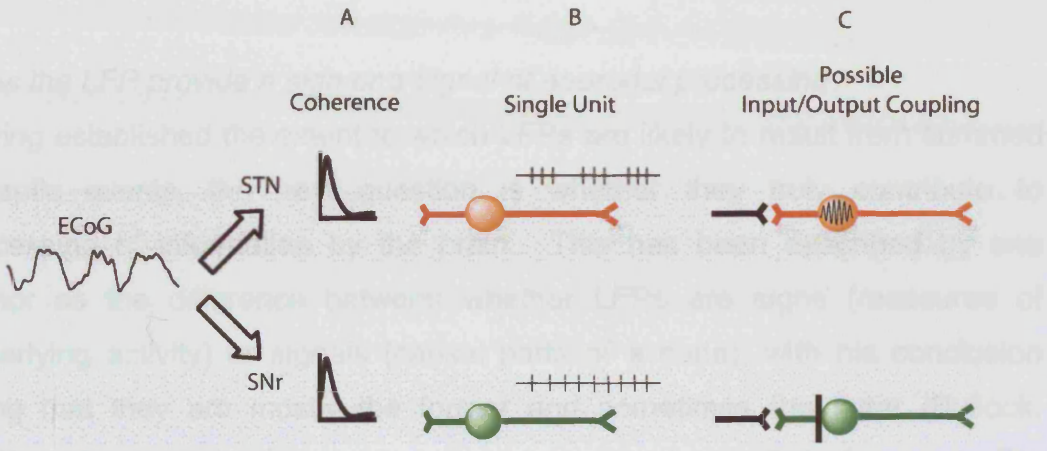

Figure 7.1 Relationships between LFP coherence and the temporal properties of action potential firing. ***A,*** LFPs from both STN and SNr were highly coherent with the slow oscillation in the ECoG, indicating the oscillatory properties of local electrical elements could be highly predicted from those in the cortex. ***B,*** The firing of STN neurons can also be predicted from the cortical slow oscillation with great accuracy. This is not the case for single SNr neurons, which fire tonically and show little or no locking to the slow oscillation. ***C,*** These results indicate that the action potential firing of STN neurons is highly sensitive to its synaptic input. SNr neurons however maintain the non-oscillatory firing (at least at low frequency) despite oscillations in their LFP. This finding suggests that despite having oscillations at the level of pre/post synaptic potentials (believed to underlie the LFP), SNr neurons can maintain non-oscillatory firing.

These results illustrate that the LFP may not provide information about the aggregate spiking activity in the recorded structure, but when used together with single neuronal activity can provide a powerful tool for looking at the relationships between synaptic and spiking activities under different conditions.

Does the LFP provide a sign or a signal of neuronal processing?

Having established the extent to which LFPs are likely to result from summed synaptic events, the next question is whether they truly contribute to processing of information by the brain. This has been described by one author as the difference between whether LFPs are signs (measures of underlying activity) or signals (causal parts of a code); with his conclusion being that they are mostly the former and sometimes the latter (Bullock, 1997). Answering this question is not as simple as it first seems. For example, the BOLD measure used in fMRI is highly predictive of both spiking activity and behaviour (Logothetis and Wandell, 2004), but blood flow (and oxygenation) is clearly not a causal part of neural code. Conversely, many neurons provide tonic input to their efferent targets. Much of the time, responses elicited by these tonic inputs are not coding any specific parameter, may not cause changes in the target neuron's firing rate or code for any easy definable behavioural parameter. The synaptic potentials elicited by these neurons provide more subtle modulation of the environment under which the neuron is processing other inputs (Cavelier et al, 2005), but they would clearly be categorised as signals. It is worth expanding this definition further to say that a neural code is a system of rules and mechanisms used by the brain (deCharms and Zador, 2000). The issue as to whether the LFPs recorded in previous chapters represent signs or signals can be further divided into two questions. Firstly, as coherence between the ECoG and basal ganglia was brain state dependent, what is the significance of brain states in neural processing *per se*? Secondly, as changes in brain state lead to changes in the coupling and direction of oscillatory activities between basal ganglia nuclei, what significance could these changes have within the cortico-basal ganglia network?

What is the significance of brain states?

Brain states are characteristic patterns of oscillatory activity encompassing widespread areas. The frequency and synchronisation of these states across different brain areas is determined by reciprocally connected thalamic and cortical networks under the influence of brainstem modulatory systems (Steriade, 1997; 2000). Many brain states are characterised by several different oscillations. For example, in deep sleep there are prominent oscillations at both low (slow wave), intermediate (spindle) and high (gamma) frequencies (Maloney et al, 1997; Steriade, 2000). As well as having characteristic frequencies, a crucial part of what defines different brain states is the degree to which these oscillations are themselves synchronised. This can be considered in at least two dimensions. Firstly, there are differences in the relationship between the different types of oscillations. For example, during sleep the timing of gamma oscillations is tightly bound by the slow oscillation (Maloney et al, 1997), but during alert wakefulness it can be associated with specific sensory stimuli (Tallon-Baudry and Bertrand, 1999; Engel et al, 2001). Secondly, the temporal coupling within and between brain areas varies between states. For example, in quiet wakefulness large cortical areas exhibit coherent alpha oscillations, where as during high levels of vigilance/attention the coherence between gamma oscillations is relatively local (Steriade, 2000).

There is no question that the synchronised neuronal activity that characterises brain states can be used to predict the gross behavioural state, such as widespread slow/spindle rhythms and sleep, posterior alpha oscillations and quiet wakefulness, etc. (see Chapter 1). Thus, brain states can certainly provide a sign of the level of information processing and subsequent behaviour. From this viewpoint, the more synchronised the brain activity, the lower the level of processing, ranging from widespread synchronisation grouped by slow oscillations during sleep, to more local synchronisation or complete desynchronisation during complex behaviour. Viewed as just a sign, the oscillations in the ECoG do not actually contribute in any way to the coding of information by the brain and can be seen in a similar way to the BOLD signal; a useful way of knowing that something is happening in part, or

often all, of the brain. To be considered as more than a sign, firstly, brain states must be a direct result of neuronal elements and, secondly, the patterns of synchronisation that define brain states must be used by the brain for information processing.

As discussed in Chapter 1, at a cellular level, the oscillations which characterise different brain states are the result of several factors: anatomical connections, intrinsic ion currents and synaptic interplay between different neuronal pools amongst others. The fact that there is not a neat unit of information however, such as a spike or EPSP, should not prevent the evaluation of whether they are causal parts of neural code. Local oscillations which act as reference signals and, together with related single unit activity, have a clear relationship to a particular parameter (e.g. theta oscillations and location in the rat or beta oscillations in the olfactory system of the locust: see Chapter 1) are also the result of multiple neuronal processes. In fact, these examples highlight the utilisation of neuronal circuitry to utilise temporal information that could not be transmitted by individual neurons alone.

Brain state synchronisations are clearly not coding for an easily definable parameter or to put it another way, they are unlikely to form representations. If we refer back to the previous definition of neural code, a system of rules and mechanisms used by the brain, a representation can be thought of as a message that uses these rules to carry information (deCharms and Zador, 2000). Into this category can go the examples whereby temporal relations are used to code a specific parameter such as phase progression in the hippocampus of the rodent, odour representation in the locust and the general putative role for synchronous unit coding in sensory "binding" (see Chapter 1). However, the changes in oscillations and synchronisation seen between brain states occur across the whole forebrain, over areas in which single neurons receive and process diverse types of information (Gervesoni et al, 2004). It might be more accurate, therefore, to think of brain states as defining the rules under which representations can be formed. Importantly, it is not always advantageous for all parts of the brain to be involved in processing information at any one time. Although brain states may not code specific

information, they may determine where and how information is processed. For example, at the far ends of the scale, the collection of rhythmic activities seen during sleep may optimise conditions for "off line processing" and memory consolidation, where as fast oscillations could maximise the processing of ongoing environmental events and the response to these stimuli (Steriade, 2000; Fell et al, 2003; Gervesoni et al, 2004). This would be achieved principally through controlling the level of synchronisation of synaptic inputs: a high level of synchronisation (as in sleep) will lower the entropy of the system, reducing the amount of information that can be processed and vice versa (de Charms, 1998). If this is the case, as is becoming increasingly proposed (Steriade, 2000; Engel et al, 2001; Varella et al, 2001; Gervesoni et al, 2004), brain states would meet the criteria of a signal. This view however involves an acceptance that not all neural processing can be reduced to individual action and synaptic potentials, which remains highly contentious.

Whether the oscillations in the LFP are themselves a signal is more debatable, given that they are the result of only part, albeit a crucial part, of the phenomenon (synchronised synaptic potentials). The absolute content of LFPs is also defined to a large extent by the recording parameters (see Figure 7.2). They are at least, however, a direct and highly informative sign of brain states and, in some circumstances, of part of a representational code (e.g. hippocampal theta and see below). In addition, it should be remembered that by reflecting synchronised synaptic activity, the LFP gives separate information from the spike train or membrane potential of single neurons (see Figure 7.1).

What is the significance of brain state dependence to information coding in the basal ganglia?

In Chapter 1 the weakness of rate coding models of the basal ganglia was addressed. It is clear that, as in the rest of the brain, rate coding is utilised by basal ganglia neurons. However, it seems increasingly clear that it is changes in the pattern, and not the rate, of populations of neurons that lead to pathological basal ganglia activity (Farmer et al, 2002). The question

addressed by the current work is whether population synchronisation may provide another level of organisation utilised by these structures under normal conditions. The first important conclusion is that the changes in brain state observed in the cortex are seen throughout the basal ganglia. While it is well known that cortical slow wave oscillations are transmitted to the striatum and STN, this is the first demonstration that higher frequencies are also propagated to those structures. This implies that all the hypothesised roles for beta and gamma oscillations in the cerebral cortex (Chapter 1) may also apply to basal ganglia circuits. Given the massive cortical input into the basal ganglia, it is possible that this could merely be a secondary view of cortical processes. The results presented in Chapters 4-6, however, suggest that brain state transitions also modulate the flow of information within the basal ganglia network. Firstly, cortical oscillations can remain independent between structures in one state and shared in another (Chapter 4 and 6). Secondly, the prominent direction of information flow between basal ganglia structures can change dramatically with brain state (Chapter 5 and see Figure 6.5). These results suggest that changes in oscillatory synchronisation across the cortex (and probably the whole forebrain) also lead to changes within basal ganglia processing on a macro scale, which cannot be addressed by the recording of single neurons. As discussed above, while not coding for a specific parameter, the population dynamics that define brain states may provide organisation across disparate networks. Specifically, rapid changes in the dominance of the cortico-subthalamic and cortico-striatal pathways could allow rapid, widespread changes in information flow, related to incoming information (i.e. SWA and hindpaw pinch). The proposed mechanisms would not in any way be expected to be alternative to rate coding, but as another level of organisation that could be complementary to it, and possibly necessary for normal information processing. Brain state dependency could even be one cause of the inconsistency of many studies investigating the correlations between single units and behavioural parameters (see Chapter 1). The relative importance of these findings, however, cannot be properly evaluated until similar recordings are made in the awake, behaving animal.

7.3 The role of dopamine in the modulation of cortico-basal ganglia oscillations

The results presented in Chapter 3, together with previous studies in human patients, provide considerable evidence that the removal of dopaminergic cells in the substantia nigra leads to dramatic changes in the oscillatory properties of the cortex and basal ganglia. These results raise several general issues about the role of LFPs in detecting and understanding pathology, the significance of the specific frequencies of oscillations in the LFP and the effect of dopamine on cortico-basal ganglia circuits.

Why is there an increase of oscillatory activity following dopamine depletion at beta frequency and what is its significance to PD?

Transient beta oscillations are normal, probably functional, phenomena in the healthy brain. In the primate, beta oscillations have been extensively described in the primary motor cortex, both at the local field potential and unit level (Murthy and Fetz, 1996a; 1996b; Baker et al, 1997; Donoghue et al, 1998; Brovelli et al, 2004). Similarly, beta oscillations have been described in the motor cortical EEG of healthy human subjects (Pfurtscheller et al, 1997, Kilner et al, 1999; Salenius et al, 1997) and are likely to be cortically generated, as they are GABA dependent (Baker and Baker, 2003). There has been less work on beta oscillations in the healthy rat, but the limited studies have produced similar results (van Leir, et al, 2004). Many of these studies have provided strong evidence that beta oscillations are task related, specifically it has been postulated that the function of motor cortical beta activity is to produce sustained muscle contraction (Baker et al, 1997; Salenius et al, 1997; Pfurtscheller et al, 1997; Kilner et al, 1999). The findings described above have led to a duel hypothesis that the beta activity seen in Parkinson's disease is a pathological exaggeration of a healthy activity and underlies akinesia and rigidity (Brown et al, 2001; Farmer, 2002). There is undoubtedly much evidence linking pathological oscillations to parkinsonian motor symptoms (see Chapter 1). Moreover, if motor cortical beta oscillations are responsible for sustained contraction or "holding" behaviour in the motor system, an exaggeration of these rhythms could reasonably be expected to

cause rigidity and akinisia. In the rodent, dopaminergic antagonists administered directly in to the striatum lead to an increase in muscular rigidity (Helmsley et al, 2001), supporting a correlation between dopaminergic tone and parkinsonian symptoms in rodents. The results in Chapter 3 confirm that in that in the rat dopamine depletion and beta oscillations are also linked, suggesting the 6-OHDA-lesioned rat may closely mimic the parkinsonian human.

In other models however, dopamine depletion leads to synchronisation at other frequencies. In the primate, it is oscillations around 10Hz that are the cardinal feature following MPTP treatment (Nini et al, 1995; Goldberg et al, 2004). An increase in 3-10Hz is also seen in the LFPs of PD patients (as well as that of beta), but it is unclear whether this is independent of tremor oscillations (Brown, 2003). The difference in primates could well be the timescale and severity of the MPTP lesion, which bilaterally depletes all the nigral dopamine neurons on a timescale of days (Meissner et al, 2003b). For the majority of PD patients however, the loss of dopamine neurons and appearance of symptoms is progressive over a period of years. The increased severity of the lesion could push the oscillatory frequency to lower frequencies, in the opposite way to the gradual increase in frequency following apomorphine treatment in Chapter 3. The hemi-lesion used in rats may therefore lead to pathology more similar to that of the human. In the anaesthetised rat the changes observed have mostly related to changes in the synchronisation of basal ganglia neurons and membrane potentials to the slow oscillation (see Murer et al, 2002 for review). This raises the possibility that the dominant frequency of synchronisation may relate to the brain state of the animal. Beta oscillations may, therefore, be specific to the level of dopamine depletion and alertness found in human patients, which is mimicked relatively well by the 6-OHDA-lesioned rat.

What is the origin of widespread oscillatory synchronisation following dopamine depletion?

Dopaminergic terminals are found in all the major basal ganglia structures, including the subthalamic nucleus (Smith and Kieval, 2000). It is the striatum

however that is the major site of dopamine terminal loss, and is therefore most likely to underlie pathology (Obeso et al, 2000; Smith and Kieval, 2000). In chapter 3, the oscillations in the cortex and STN were shown to be coupled, but changes in oscillations and synchronisation have also been found across the cortico-basal ganglia network following dopamine depletion, including the GPe, GPi, SNr and thalamus (see Chapter 1). How then does the pathology of a specific transmitter system in one structure lead to widespread oscillations that affect many others? As most widespread oscillations are generated by the thalamo-cortical loops, it has been proposed that they are the origin of the oscillatory activity. Indeed, there is reasonable evidence to suggest that dopamine depletion increases the entrainment of striatal neurons to cortical oscillations (Murer et al, 2002). Although the phase analysis in Chapter 3 was inconclusive, similar analysis of human data suggests that cortical beta oscillations lead those in the STN (Williams et al 2003; Fogelson et al, 2005). An alternative, but not mutually exclusive, hypothesis is that the reciprocal connections between GPe and STN are the key structures in producing pathological oscillations. This proposal comes mostly from *in vitro* studies suggesting that the GPe/STN network has pacemaker properties (Bevan et al, 2004a and see Chapter 1). While this needs further investigation *in vivo,* the success of STN lesions in reducing parkinsonian symptoms suggests that the STN is in some way necessary for pathological synchronisation. Finally, an interesting question is the possible role of feedback from the basal ganglia to the cortex. The looping architecture of basal ganglia loops has been extensively described in terms of anatomy, but physiological evidence for the effect of the output nuclei/motor thalamus on the cortex remains sparse. The possible importance of resonance in PD has yet to be investigated in detail. This is probably partly due to the difficulty of analysing the evolution of resonance in a complex system (Pikovsky et al, 2001; 2004). DTF analysis of LFPs recorded at several points of the cortico-basal ganglia-thalamus axis could help to resolve this issue. In conclusion, the widespread oscillatory phenomena therefore seem likely to be a complex result of the interaction between structures across the network (Leblois et al, 2006).

Do oscillations in the LFP following dopamine depletion represent a sign or signal?

It is clear from the results in Chapter 3 that sustained beta oscillations are highly predictive of dopamine depletion. Studies in humans have also suggested that the magnitude of beta oscillations is predictive of parkisonian symptoms (Silberstien et al, 2003) and the ability of patients to initiate movement (Cassidy et al, 2002a). There seems little doubt that abnormally high beta oscillations in the cortex or STN, or abnormally high coupling between the structures are an accurate sign of dysfunction in the nigro-striatal pathway. As described above, the dominant frequency of the oscillations appears to relate to the species of animal, level of dopamine depletion and whether the animal is anaesthetised. The general trend towards oscillation and synchronisation across diverse brain areas caused by dopamine depletion can be thought of in similar terms as brain states; a system of rules and mechanisms used by the brain. In fact, the control of oscillation and synchronisation relating to brain states is also highly dependent on ascending monoaminergic and cholinergic pathways (Munk et al, 1995; Rodriguez et al, 2004; Steriade, 2000) that are not dissimilar from the nigrostriatal pathway. The argument as to whether widespread synchronisation at different frequencies acts as a signal is therefore more or less the same as that above for brain states. If beta oscillations in the motor cortex and basal ganglia are an exaggeration of a normal activity with a specific purpose (sustained muscle contraction), as described above, they could even fit the definition for a representation: a message that uses the rules of neural code to carry information. This may be a pathological signal, but by determining movement parameters it must count as a signal nonetheless.

7.4 Future Perspectives

Multi-site recording and synchrony in the basal ganglia?

A central issue as to the significance of population oscillations and synchronisation in the basal ganglia is how these activities relate to the spiking of single neurons. These questions cannot be investigated fully using the type of recordings used in Chapters 3-5, which are limited by having a maximum of one unit from each structure. The preliminary results presented in Chapter 6 demonstrate that multi-contact electrode recording techniques could provide a highly effective method for investigating information coding in these areas.

In the vast majority of studies, a maximum of two or three basal ganglia neurons have been recorded simultaneously. This allows synchrony to be detected in only hyper-synchronous states, such as dopamine depletion, where the locking of many individual units to global dynamics will increase the chance of finding a synchronous unit pair (Goldberg et al, 2004). Given that these states lead to a loss of function, any synchronous process used in information processing must operate on a lower level of synchronisation. Only when many units have been simultaneously recorded will it be possible to evaluate the level of synchrony present in the healthy brain at the action potential level. Analysis of this number of single neurons may reveal locking to higher frequency rhythms seen in the LFP that cannot be detected using single units (see Chapter 4). This may be particularly valuable the striatum, where single neurons have a low firing rate. It would be interesting to investigate whether assemblies of striatal neurons can carry oscillatory signals, without displaying them on an individual neuronal level (Figure 1.8). This may be of particular relevance to the link between dopamine depletion and the propagation of oscillations to the rest of the basal ganglia (see above). Multi-site probes could also greatly enhance the utilisation of LFP signals. A single contact electrode allows no control as to the size of the field potential. Offline bipolar and multipolar derivation between the contacts could be used to manipulate the scale of the LFP (see Figure 7.2).

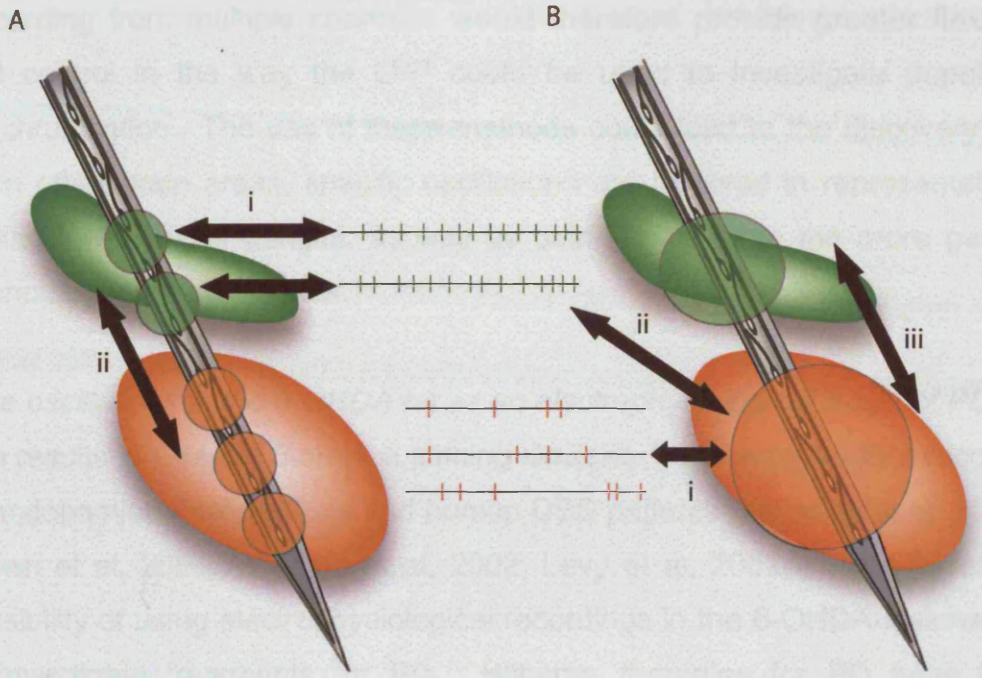

Figure 7.2 Future analysis possibilities provided by using multi-site recording in basal ganglia structures. The results presented in Chapter 6 represent only a small range of possible analyses that can be performed on such data. In this schematic representation, recordings from two nuclei (green and red) are considered in relation to using bipolar (***A***) and multi-polar derivations (***B***) of monopolar LFPs and coincident single units recorded from each contact. ***A***, Bipolar derivations of the LFPs (small circles) allow the measurement of population activity from subsection of the nucleus. ***Ai***) This allows the relationship between LFP and units to be examined on a purely local scale. ***Aii***) Similarly, coupling can be investigated between local populations in each nucleus. ***B***) Alternatively derivations can be taken between more distant electrodes (larger circles), allowing population signals which can encompass the whole nucleus (depending on its size and the resistance of the electrode) with greater control than by using a monopolar recording. ***Bi***) By using multi-polar derivations, the population activity across the nucleus can be related to the activity of multiple units from the same structure or, ***Bii***) another structure. ***Biii***) LFP signals can be used to investigate population activity on a nuclear level. Comparisons between these different parameters may be particularly informative for elucidating relationships between oscillatory synaptic activities, as measured by the LFP, and the activity of many single units.

Recording from multiple channels would therefore provide greater flexibility and control in the way the LFP could be used to investigate population synchronisation. The use of these methods could lead to the discovery that, as in other brain areas, specific oscillations are involved in representational coding in the basal ganglia, as well as being involved in the more general phenomenon of brain states.

Beta oscillations in the 6-OHDA rat as an electrophysiological mode of PD

The results in Chapter 3 show a striking similarity between the LFPs recorded from dopamine depleted rats and human DBS patients (Marsden et al, 2001a, Brown et al, 2001, Williams et al, 2002; Levy et al, 2002a). This raises the possibility of using electrophysiological recordings in the 6-OHDA-lesioned rat to investigate treatments for PD. Hitherto, therapies for PD have been evaluated in the 6-OHDA rodent using motor symptoms and apomorphine rotation to measure efficacy. Although this has proved a valuable early screening tool for possible pharmacological therapies, both the 6-OHDA rodent and the MPTP primate have recently been criticised, mainly for not mimicking the progression and extent of the disease fully (Meissner et al, 2003b and see above). In the rat model, the method of detection of a successful lesion, i.e. apomorphine rotation (see Chapter 3), will only give a positive result if there is a substantial loss of cells and is essentially a measure of compensation for dopamine depletion, rather than dopamine depletion itself (Linazasoro, 2004). In humans the reduction of beta activity after successful surgical and pharmacological treatment is well documented. Using ECoG and/or local field potential recordings could greatly improve the model by giving a more direct electrophysiological measure of pathological processing. Measuring beta activity as well as motor activity may allow more subtle changes in progressive models of the disease to be seen and more detailed observation of the effect of possible therapies at these earlier stages. Moreover, as an electrophysiological measure, synchronisation of neuronal activity appears to be far more predictive of PD pathology and successful treatment than the rate of any cell group.

References

Abeles M (1982) Quantification, smoothing, and confidence limits for single-units' histograms. J Neurosci Methods 5: 317-325.

Achermann P, Borbely AA (1997) Low-frequency (< 1 Hz) oscillations in the human sleep electroencephalogram. Neuroscience 81: 213-22.

Aggelopoulos NC, Franco L, Rolls ET (2005) Object perception in natural scenes: encoding by inferior temporal cortex simultaneously recorded neurons. J Neurophysiol 93: 1342-57.

Agmon-Snir H, Carr CE, Rinzel J (1998) The role of dendrites in auditory coincidence detection. Nature 393(6682): 268-72.

Albin RL, Young AB, Penney JB (1989) The functional anatomy of basal ganglia disorders. Trends Neurosci 12: 366-375.

Aldridge JW, Berridge KC (1998) Coding of serial order by neostriatal neurons: a "natural action" approach to movement sequence. J Neurosci 18: 2777-2787.

Alexander GE, Crutcher MD (1990) Functional architecture of basal ganglia circuits: neural substrates of parallel processing. Trends Neurosci 13: 266-271.

Alonso J-M, Usrey WM, Reid RC (1996) Precisely correlated firing in cells of the lateral geniculate nucleus. Nature 383: 815-819.

Andrew C, Pfurtscheller G (1996) Event-related coherence as a tool for studying dynamic interaction of brain regions. Electroencephalogr Clin Neurophysiol 98: 144-148.

Apicella P, Scarnati E, Ljungberg T, Schultz W (1992) Neuronal activity in monkey striatum related to the expectation of predictable environmental events. J Neurophysiol 68: 945-60.

Apicella P (2002) Tonically active neurons in the primate striatum and their role in the processing of information about motivationally relevant events. Eur J Neurosci 16: 2017-26.

Astolfi L, Cincotti F, Mattia D, Salinari S, Babiloni C, Basilisco A, Rossini PM, Ding L, Ni Y, He B, Marciani MG, Babiloni F (2004) Estimation of the effective and functional human cortical connectivity with structural equation modeling and directed transfer function applied to high-resolution EEG. Magn Reson Imaging 22: 1457-70.

Averbeck BB, Lee D (2004) Coding and transmission of information by neural ensembles. Trends Neurosci 27: 225-30.

Aziz TZ, Peggs D, Sambrook MA, Crossman AR (1991) Lesion of the subthalamic nucleus for the alleviation of 1-methyl-4-phenyl-1,2,3,6-tetrahydropyridine (MPTP)-induced parkinsonism in the primate. Mov Disord 6: 288-92.

Azouz R, Gray CM (2003) Adaptive coincidence detection and dynamic gain control in visual cortical neurons in vivo. Neuron 37: 513-23.

Baker, SN, Olivier E, Lemon RN (1997) Coherent oscillations in monkey motor cortex and hand muscle EMG show task-dependent modulation. J Physiol 50: 225-241.

Baker MR, Baker SN (2003) The effect of diazepam on motor cortical oscillations and corticomuscular coherence studied in man. J Physiol 546: 931-42.

Bamford NS, Zhang H, Schmitz Y, Wu NP, Cepeda C, Levine MS, Schmauss C, Zakharenko SS, Zablow L, Sulzer D (2004) Heterosynaptic dopamine neurotransmission selects sets of corticostriatal terminals. Neuron 42: 653-63.

Bar-Gad I, Bergman H (2001) Stepping out of the box: information processing in the neural networks of the basal ganglia. Curr Opin Neurobiol 11: 689-95.

Bar-Gad I, Morris G, Bergman H (2003a) Information processing, dimensionality reduction and reinforcement learning in the basal ganglia. Prog Neurobiol 71: 439-473.

Bar-Gad I, Heimer G, Ritov Y, Bergman H (2003b) Functional correlations between neighboring neurons in the primate globus pallidus are weak or nonexistent. J Neurosci 23: 4012-6.

Bar-Gad I, Elias S, Vaadia E, Bergman H (2004) Complex locking rather than complete cessation of neuronal activity in the globus pallidus of a 1-methyl-4-phenyl-1,2,3,6-tetrahydropyridine-treated primate in response to pallidal microstimulation. J Neurosci 24: 7410-9.

Bedard C, Kroger H, Destexhe A (2004) Modeling extracellular field potentials and the frequency-filtering properties of extracellular space. Biophys J 86: 1829-42.

Belluscio MA, Kasanetz F, Riquelme LA, Murer MG (2003) Spreading of slow cortical rhythms to the basal ganglia output nuclei in rats with nigrostriatal lesions. Eur J Neurosci 17: 1046-52.

Benabid AL, Pollak P, Gross C, Hoffmann D, Benazzouz A, Gao DM, Laurent A, Gentil M, Perret J (1994) Acute and long-term effects of subthalamic nucleus stimulation in Parkinson's disease. Stereotact Funct Neurosurg 62: 76-84.

Benazzouz A, Gross C, Feger J, Boraud T, Bioulac B (1993) Reversal of rigidity and improvement in motor performance by subthalamic high-frequency stimulation in MPTP-treated monkeys. Eur J Neurosci 5: 382-9.

Berardelli A, Rothwell JC, Hallett M, Thompson PD, Manfredi M, Marsden CD (1998) The pathophysiology of primary dystonia. Brain 121: 1195-212.

Bergman H, Wichmann T, DeLong MR (1990) Reversal of experimental parkinsonism by lesions of the subthalamic nucleus. Science 249(4975): 1436-8.

Bergman H, Wichmann T, Karmon B, DeLong MR (1994) The primate subthalamic nucleus. II. Neuronal activity in the MPTP model of parkinsonism. J Neurophysiol 72: 507-20.

Bergman H, Feingold A, Nini A, Raz A, Slovin H, Abeles M, Vaadia E (1998) Physiological aspects of information processing in the basal ganglia of normal and parkinsonian primates. Trends Neurosci 21: 32-38.

Berke JD, Okatan M, Skurski J, Eichenbaum HB (2004) Oscillatory entrainment of striatal neurons in freely moving rats. Neuron 43: 883-896.

Berke JD, Paletzki RF, Aronson GJ, Hyman SE, Gerfen CR (1998) A complex program of striatal gene expression induced by dopaminergic stimulation. J Neurosci 18: 5301-10.

Berns GS, Sejnowski TJ (1998) A computational model of how the basal ganglia produce sequences. J Cogn Neurosci 10:108-21.

Beurrier C, Bioulac B, Hammond C (2000) Slowly inactivating sodium current (I(NaP)) underlies single-spike activity in rat subthalamic neurons. J Neurophysiol 83: 1951-7.

Bevan MD. Magill PJ, Terman D, Bolam JP, Wilson CJ (2002a) Move to the rhythm: oscillations in the subthalamic nucleus-external globus pallidus network. Trends Neurosci 25: 525-531.

Bevan MD, Magill PJ, Hallworth NE, Bolam JP, Wilson CJ (2002b) Regulation of the timing and pattern of action potential generation in rat subthalamic neurons in vitro by GABA-A IPSPs. J Neurophysiol 87: 1348-62.

Bevan MD, Booth PAC, Eaton SA, Bolam JP (1998) Selective innervation of neostriatal interneurons by a subclass of neuron in the globus pallidus of the rat. J Neurosci 19: 9438-9452.

Blazquez PM, Fujii N, Kojima J, Graybiel AM (2002) A network representation of response probability in the striatum. Neuron 33: 973-82.

Bolam JP (Ed) (1992) Experimental neuroanatomy. Oxford University Press, Oxford, UK.

Bolam JP, Smith Y, Ingham CA, von Krosigk M, Smith AD (1993) Convergence of synaptic terminals from the striatum and the globus pallidus onto single neurones in the substantia nigra and the entopeduncular nucleus. Prog Brain Res 99: 73-88.

Bolam JP, Hanley JJ, Booth PA, Bevan MD (2000) Synaptic organisation of the basal ganglia. J Anat 196: 527-542.

Boraud T, Bezard E, Guehl D, Bioulac B, Gross C (1998) Effects of L-DOPA on neuronal activity of the globus pallidus externalis (GPe) and globus pallidus internalis (GPi) in the MPTP-treated monkey. Brain Res 787: 157-60.

Boraud T, Bezard E, Bioulac B, Gross CE (2000) Ratio of inhibited-to-activated pallidal neurons decreases dramatically during passive limb movement in the MPTP-treated monkey. J Neurophysiol 83: 1760-3.

Boraud T, Bezard E, Bioulac B, Gross CE (2001) Dopamine agonist-induced dyskinesias are correlated to both firing pattern and frequency alterations of pallidal neurones in the MPTP-treated monkey. Brain 124: 546-57.

Boraud T, Bezard E, Bioulac B, Gross CE (2002) From single extracellular unit recording in experimental and human Parkinsonism to the development of a functional concept of the role played by the basal ganglia in motor control. Prog Neurobiol 66: 265-283.

Breit S, Schulz JB, Benabid AL (2004) Deep brain stimulation. Cell Tissue Res 318: 275-88.

Brillinger DR (1981) Time series - data analysis and theory (2nd edn). Holden Day. San Francisco, USA.

Brooks DJ (2004) Neuroimaging in Parkinson's disease. NeuroRx 1: 243-54.

Brown P, Marsden CD (1998) What do the basal ganglia do? Lancet 351: 1801-1804.

Brown P (2000) Cortical drives to human muscle: the Piper and related rhythms. Prog Neurobiol 60: 97-108.

Brown P, Oliviero A, Mazzone P, Insola A, Tonali P, Di Lazzaro V (2001) Dopamine dependency of oscillations between subthalamic nucleus and pallidum in Parkinson's disease. J Neurosci 21: 1033-1038.

Brown P, Kupsch A, Magill PJ, Sharott A, Harnack D, Meissner W (2002) Oscillatory local field potentials recorded from the subthalamic nucleus of the alert rat. Exp Neurol 177: 581-585.

Brown P (2003) Oscillatory nature of human basal ganglia activity: relationship to the pathophysiology of Parkinson's disease. Mov Disord 18: 357-363.

Brown EN, Kass RE, Mitra PP (2004a) Multiple neural spike train data analysis: state-of-the-art and future challenges. Nat Neurosci 7: 456-61.

Brown P, Mazzone P, Oliviero A, Altibrandi MG, Pilato F, Tonali PA, Di Lazzaro V (2004b) Effects of stimulation of the subthalamic area on oscillatory pallidal activity in Parkinson's disease. Exp Neurol 188: 480-90.

Brovelli A, Ding M, Ledberg A, Chen Y, Nakamura R, Bressler SL (2004) Beta oscillations in a large-scale sensorimotor cortical network: directional influences revealed by Granger causality. Proc Natl Acad Sci USA 101: 9849-54.

Bullock TH (1997) Signals and signs in the nervous system: the dynamic anatomy of electrical activity is probably information-rich. Proc Natl Acad Sci USA 94: 1-6.

Burgess N, O'Keefe J (2003) Neural representations in human spatial memory. Trends Cogn Sci 7: 517-9.

Buzsáki G (2002) Theta oscillations in the hippocampus. Neuron 33: 325-340.

Buzsáki G, Draguhn A (2004) Neuronal oscillations in cortical networks. Science 304: 1926-1929.

Buzsaki G (2004) Large-scale recording of neuronal ensembles. Nat Neurosci 7: 446-51.

Calabresi P, Centonze D, Gubellini P, Pisani A, Bernardi G (2000) Acetylcholine-mediated modulation of striatal function. Trends Neurosci 23: 120-6.

Cavelier P, Hamann M, Rossi D, Mobbs P, Attwell D (2005) Tonic excitation and inhibition of neurons: ambient transmitter sources and computational consequences. Prog Biophys Mol Biol 87: 3-16.

Cassidy M, Mazzone P, Oliviero A, Insola A, Tonali P, Di Lazzaro V, Brown P (2002a) Movement-related changes in synchronisation in the human basal ganglia. Brain 125: 1235-1246.

Cassidy MJ, Brown P (2002b) Hidden Markov based autoregressive analysis of stationary and non-stationary electrophysiological signals for functional coupling studies. J Neurosci Methods 116: 35-53.

Cassidy MJ, Brown P (2003) Spectral phase estimates in the setting of multidirectional coupling. J Neurosci Methods 127: 95-103.

Castro-Alamancos MA, Calcagnotto ME (2001) High-pass filtering of corticothalamic activity by neuromodulators released in the thalamus during arousal: in vitro and in vivo. J. Neurophysiol 85: 1489-1497.

Cavelier P, Hamann M, Rossi D, Mobbs P, Attwell D (2005) Tonic excitation and inhibition of neurons: ambient transmitter sources and computational consequences. Prog Biophys Mol Biol 87: 3-16.

Centonze D, Picconi B, Gubellini P, Bernardi G, Calabresi P (2001) Dopaminergic control of synaptic plasticity in the dorsal striatum. Eur J Neurosci 13: 1071-7.

Challis RE, Kitney RI (1990) Biomedical signal processing (in four parts). Part 1: time-domain methods. Med Biol Eng Comput 28: 509-524.

Christensen TA, Lei H, Hildebrand JG (2003) Coordination of central odor representations through transient, non-oscillatory synchronization of glomerular output neurons. Proc Natl Acad Sci USA 100: 11076-81.

Christakos CN (1997) On the detection and measurement of synchrony in neural populations by coherence analysis. J Neurophysiol 78: 3453-3459.

Chrobak JJ and Buzsaki G (1996) High-frequency oscillations in the output networks of the hippocampal-entorhinal axis of the freely behaving rat. J Neurosci 16: 3056-66.

Chudasama Y, Baunez C, Robbins TW (2003) Functional disconnection of the medial prefrontal cortex and subthalamic nucleus in attentional performance: evidence for corticosubthalamic interaction. J Neurosci 23: 5477-85.

Chudler EH, Sugiyama K, Dong WK (1993) Nociceptive responses in the neostriatum and globus pallidus of the anesthetized rat. J Neurophysiol 69: 1890-1903.

Connors BW, Amitai Y (1997) Making waves in the neocortex. Neuron 18: 347-9.

Contreras D, Steriade M (1995) Cellular basis of EEG slow rhythms: a study of dynamic corticothalamic relationships. J Neurosci 15: 604-22.

Contreras D, Steriade M (1996) Spindle oscillation in cats: the role of corticothalamic feedback in a thalamically generated rhythm. J Physiol 490: 159-79.

Contreras D, Destexhe A, Sejnowski TJ, Steriade M (1997) Spatiotemporal patterns of spindle oscillations in cortex and thalamus. J Neurosci 17: 1179-1196.

Conway BA, Halliday DM, Farmer SF, Shahani U, Maas P, Weir AI, Rosenberg JR (1995) Synchronization between motor cortex and spinal motoneuronal pool during the performance of a maintained motor task in man. J Physiol 489: 917-24.

Courtemanche R, Fujii N, Graybiel AM (2003) Synchronous, focally modulated beta-band oscillations characterize local field potential activity in the striatum of awake behaving monkeys. J Neurosci 23: 11741-11752.

Cragg SJ, Baufreton J, Xue Y, Bolam JP, Bevan, MD (2004) Synaptic release of dopamine in the subthalamic nucleus. Eur J Neurosci 20: 1788-1802.

Creutzfeld OD, Watanabe S, Lux HD (1966) Relations between ECOG phenomena and potentials of single cortical cells. I. Evoked responses after thalamic and epicortical stimulation. Electroencephalogr Clin Neurophysiol 20: 1-18.

Csicsvari J, Jamieson B, Wise KD, Buzsaki G (2003a) Mechanisms of gamma oscillations in the hippocampus of the behaving rat. Neuron 37: 311-22.

Csicsvari J, Henze DA, Jamieson B, Harris KD, Sirota A, Bartho P, Wise KD, Buzsaki G (2003b) Massively parallel recording of unit and local field potentials with silicon-based electrodes. J Neurophysiol 90: 1314-23.

deCharms RC (1998) Information coding in the cortex by independent or coordinated populations. Proc Natl Acad Sci USA 95: 15166-8.

deCharms RC, Zador A (2000) Neural representation and the cortical code. Annu Rev Neurosci 23:613-47.

DeLong MR, Crutcher MD, Georgopoulos AP (1985) Primate globus pallidus and subthalamic nucleus: functional organization. J Neurophysiol 53: 530-43.

DeLong MR (1990) Primate models of movement disorders of basal ganglia origin. Trends Neurosci 13: 281-285.

Donoghue JP, Wise SP (1982) The motor cortex of the rat: cytoarchitecture and microstimulation mapping. J Comp Neurol 212: 76-88.

Donoghue JP, Sanes JN, Hastopoulos, NG, Gaál G (1998) Neural discharge and local field potential oscillations in primate motor cortex during voluntary movements. J Neurophysiol 79: 159-173.

Ehringer H, Hornykiewicz O (1960) Distribution of noradrenaline and dopamine (3-hydroxytyramine) in the human brain and their behavior in diseases of the extrapyramidal system. Klin Wochenschr. 38: 1236-9.

Engel AK, Fries P, Singer W (2001) Dynamic Predictions: oscillations and synchrony in top-down processing. Nat Rev Neurosci 2: 704-716.

Engel AK, Moll CK, Fried I, Ojemann GA (2005) Invasive recordings from the human brain: clinical insights and beyond. Nat Rev Neurosci 6: 35-47.

Escola L, Michelet T, Macia F, Guehl D, Bioulac B, Burbaud P (2003) Disruption of information processing in the supplementary motor area of the MPTP-treated monkey: a clue to the pathophysiology of akinesia? Brain 126: 95-114.

Fahn S, Sulzer D (2004) Neurodegeneration and neuroprotection in Parkinson disease. NeuroRx 1:139-54.

Farmer SF (1998) Rhythmicity, synchronization and binding in human and primate motor systems. J Physiol 509: 3-14.

Farmer SF (2002) Neural rhythms in Parkinson's disease. Brain 125: 1175-1176.

Fell J, Fernandez G, Klaver P, Elger CE, Fries P (2003) Is synchronized neuronal gamma activity relevant for selective attention? Brain Res Brain Res Rev 42: 265-72.

Fein G, Raz J, Brown FF, Merrin EL (1988) Common reference coherence data are confounded by power and phase effects. Electroencephalogr Clin Neurophysiol 69: 581-584.

Filion M, Tremblay L (1991) Abnormal spontaneous activity of globus pallidus neurons in monkeys with MPTP-induced parkinsonism. Brain Res 547: 142-51.

Florian G, Andrew C, Pfurtscheller G (1998) Do changes in coherence always reflect changes in functional coupling. Electroencephalog Clin Neurophysiol 106: 87-91.

Fogelson N, Williams D, Tijssen M, van Bruggen G, Speelman H, Brown P (2005) Different Functional Loops between Cerebral Cortex and the Subthalmic Area in Parkinson's Disease. Cereb Cortex *In Press* doi:10.1093/cercor/bhi084.

Fries P, Roelfsema PR, Engel AK, Konig P, Singer W (1997) Synchronization of oscillatory responses in visual cortex correlates with perception in interocular rivalry. Proc Natl Acad Sci USA 94: 12699-704.

Fries P, Neuenschwander S, Engel AK, Goebel R, Singer W (2001a) Rapid feature selective neuronal synchronization through correlated latency shifting. Nat Neurosci 4: 194-200.

Fries P, Schroder JH, Singer W, Engel AK (2001b) Conditions of perceptual selection and suppression during interocular rivalry in strabismic and normal cats. Vision Res 41: 771-83.

Frost JD (1968) ECOG-intracellular potential relationships in isolated cerebral cortex. Electroencephalogr Clin Neurophysiol 24: 434-443.

Fujii N, Graybiel AM (2005) Time-varying covariance of neural activities recorded in striatum and frontal cortex as monkeys perform sequential-saccade tasks. Proc Natl Acad Sci USA 102: 9032-7.

Fujimoto K, Kita H (1992) Responses of substantia nigra pars reticulata units to cortical stimulation. Neurosci Lett 142: 105-109.

Fujimoto K, Kita H (1993) Response characteristics of subthalamic neurons to the stimulation of the sensorimotor cortex in the rat. Brain Res 609: 185-192.

Galarreta M, Hestrin S (1999) A network of fast-spiking cells in the neocortex connected by electrical synapses. Nature 402: 72-5.

Garcia L, D'Alessandro G, Bioulac B, Hammond C (2005) High-frequency stimulation in Parkinson's disease: more or less? Trends Neurosci 28: 209-16.

Gdowski MJ, Miller LE, Parrish T, Nenonene EK, Houk JC (2001) Context dependency in the globus pallidus internal segment during targeted arm movements. J Neurophysiol 85: 1998-1004.

Georgopoulos AP, DeLong MR, Crutcher MD (1983) Relations between parameters of step-tracking movements and single cell discharge in the globus pallidus and subthalamic nucleus of the behaving monkey. J Neurosci 3: 1586-98.

Gerfen CR, Wilson CJ (1996) The basal ganglia. In: Handbook of Chemical Neuroanatomy 12: Integrated Systems of the CNS III, edited by Swanson LW, Björklund A, and Hökfelt, T. London: Elsevier: 371-468.

German DC, Nelson EL, Liang CL, Speciale SG, Sinton CM, Sonsalla PK (1996) The neurotoxin MPTP causes degeneration of specific nucleus A8, A9, and A10 dopaminergic neurons in the mouse. Neurodegeneration 5: 299-312.

Gervasoni D, Lin SC, Ribeiro S, Soares ES, Pantoja J, Nicolelis MA (2004) Global forebrain dynamics predict rat behavioral states and their transitions. J Neurosci 24: 11137-47.

Glaser EM, Ruchkin DS (1976) Principles of neurobiological signal analysis. New York, NY: Academic Press.

Goldberg JA, Boraud T, Maraton S, Haber SN, Vaadia E, Bergman H (2002) Enhanced synchrony among primary motor cortex neurons in the 1-methyl-4-phenyl-1,2,3,6-tetrahydropyridine primate model of Parkinson's disease. J Neurosci 22: 4639-53.

Goldberg JA, Rokni U, Boraud T, Vaadia E, Bergman H (2004) Spike synchronization in the cortex-basal ganglia networks of parkinsonian primates reflects global dynamics of the local field potentials. J Neurosci 24: 6003-6010.

Gotman J (1990) The use of computers in analysis and display of EEG and evoked potentials. In. Current practice of clinical electroencephalography. 4th ed. (Daly AA and Pedley A, eds.), Raven Press, New York, USA: 51-83.

Goto Y, O'Donnell P (2001) Network synchrony in the nucleus accumbens in vivo. J Neurosci 21: 4498-4504.

Gray CM, McCormick DA (1996) Chattering cells: superficial pyramidal neurons contributing to the generation of synchronous oscillations in the visual cortex. Science 274: 109-13.

Graybiel AM, Aosaki T, Flaherty AW, Kimura M (1994) The basal ganglia and adaptive motor control. Science 265: 1826-31.

Graybiel AM (1995) Building action repertoires: memory and learning functions of the basal ganglia. Curr Opin Neurobiol 5: 733-741.

Greengard P, Allen PB, Nairn AC (1999) Beyond the dopamine receptor: the DARPP-32/protein phasphatase-1 cascade. Neuron 23: 435-447.

Grosse P, Cassidy MJ, Brown P (2002) EEG-EMG, MEG-EMG and EMG-EMG frequency analysis: physiological principles and clinical applications. Clin Neurophysiol 113: 1523-1531.

Gulley JM, Kuwajima M, Mayhill E, Rebec GV (1999) Behavior-related changes in the activity of substantia nigra pars reticulata neurons in freely moving rats. Brain Res 845: 68-76.

Gurney K, Prescott TJ, Redgrave P (2002) A computational model of action selection in the basal ganglia. II. Analysis and simulation of behaviour. Biol Cybern 84: 411-23.

Gundersen HJ, Bagger P, Bendtsen TF, Evans SM. Korbo L, Marcussen N, Moller A, Nielsen K, Nyengaard JR, Pakkenberg B, Sorensen FB, Vesterby A, West MJ (1988) The new stereological tools: disector, fractionator, nucleator and point sampled intercepts and their use in pathological research and diagnosis. Apmis 96: 857-881.

Haber SN (2003) The primate basal ganglia: parallel and integrative networks. J Chem Neuroanat 26: 317-330.

Halliday DM, Rosenberg JR, Amjad AM, Breeze P, Conway BA, Farmer SF. (1995) A framework for the analysis of mixed time series/point process data - theory and application to the study of physiological tremor, single motor unit discharges and electromyograms. Prog Biophys Mol Biol 64: 237-278.

Halliday, DM & Rosenberg, JR (1999) Time and frequency domain analysis of spike train and time series data. In: Modern Techniques in Neuroscience Research, (Eds. U. Windhorst & H. Johansson), Springer-Verlag, Ch 18: 503-543.

Halliday DM, Conway BA, Farmer SF, Rosenberg JR (1999) Load-independent contributions from motor-unit synchronisation to human physiological tremor. J Neurophysiol 82: 664-675.

Handel A, Glimcher PW (1999) Quantitative analysis of substantia nigra pars reticulata activity during a visually guided saccade task. J Neurophysiol 82: 3458-75.

Hamani C, Saint-Cyr JA, Fraser J, Kaplitt M, Lozano AM (2004) The subthalamic nucleus in the context of movement disorders. Brain 127: 4-20.

Hanson JE, Jaeger D (2002) Short-term plasticity shapes the response to simulated normal and parkinsonian input patterns in globus pallidus. J Neurosci 22: 5164-5172.

Hanson JE, Smith Y, Jaeger D (2004) Sodium channels and dendritic spike initiation at excitatory synapses in globus pallidus neurons. J Neurosci 24: 329-340.

Hassani OK, Mouroux M, Feger J (1996) Increased subthalamic neuronal activity after nigral dopaminergic lesion independent of disinhibition via the globus pallidus. Neuroscience 72: 105-15.

Hauber W (1998) Involvement of basal ganglia transmitter systems in movement initiation. Prog Neurobiol 56: 507-540.

Heimer G, Bar-Gad I, Goldberg JA, Bergman H (2002) Dopamine replacement therapy reverses abnormal synchronization of pallidal neurons in the 1-methyl-4-phenyl-1,2,3,6-tetrahydropyridine primate model of parkinsonism. J Neurosci 22: 7850-7855.

Hemsley KM, Crocker AD (2001) Changes in muscle tone are regulated by D1 and D2 dopamine receptors in the ventral striatum and D1 receptors in the substantia nigra. Neuropsychopharmacology 25: 514-26.

Hoover JE, Strick PL (1993) Multiple output channels in the basal ganglia. Science 259(5096): 819-21.

Horikawa K, Armstrong WE (1991) A biocytin-containing compound N-(2-aminoethyl)biotinimide for intracellular labeling and neuronal tracing studies: comparison with biocytin. J Neurosci Methods 37: 141-150.

Hu D, Itoga CA, Tierny PL, Soucy AL, Ghiglieri V, Bergstrom DA, Walters JR (2002) Slow oscillations in globus pallidus (GP) local field potential (LFP) in anesthetized rats and mice exhibit coherence with striatal and hippocampal (HP) LFP. Soc Neurosci Abstr 28: 765.2.

Hubbard JI, Llinás R, Quastel DMJ (1969) Extracellular field potentials in the central nervous system. In: Electrophysiological analysis of synaptic transmission. Edward Arnold Ltd, London, UK: 265-293.

Hudson JL, van Horne CG, Strömberg I, Brock S, Clayton J, Masserano J, Hoffer BJ, Gerhardt GA (1993) Correlation of apomorphine- and amphetamine-induced turning with nigrostriatal dopamine content in unilateral 6-hydroxydopamine lesioned rats. Brain Res 626: 167-174.

Hutcheon B, Yarom Y (2000) Resonance, oscillation and the intrinsic frequency preferences of neurons. Trends Neurosci 23: 216-22.

Jackson A, Gee VJ, Baker SN, Lemon RN (2003) Synchrony between neurons with similar muscle fields in monkey motor cortex. Neuron 38: 115-25.

Jaeger D, Gilman S, Aldridge JW (1993) Primate basal ganglia activity in a precued reaching task: preparation for movement. Exp Brain Res 95: 51-64.

Jaeger D, Gilman S, Aldridge JW (1995) Neuronal activity in the striatum and pallidum of primates related to the execution of externally cued reaching movements. Brain Res 694: 111-27.

Jenner P (2003) The MPTP-treated primate as a model of motor complications in PD: primate model of motor complications. Neurology 61: S4-11.

Joel D, Weiner I (1994) The organization of the basal ganglia-thalamocortical circuits: open interconnected rather than closed segregated. Neuroscience 163: 363-79.

Jog MS, Kubota Y, Connolly CI, Hillegaart V, Graybiel AM (1999) Building neural representations of habits. Science 286: 1745-9.

Johansson RS, Birznieks I (2004) First spikes in ensembles of human tactile afferents code complex spatial fingertip events. Nat Neurosci 7: 170-7.

Johnson DH (1996) Point process models of single-neuron discharges. J Comput Neurosci 3: 275-299.

Kaminski MJ, Blinowska KJ (1991) A new method of the description of the information flow in the brain structures. Biol Cybern 65: 203-210.

Kandel, ER, Schwartz JH, and Jessell TM (2000) Principles of neural science. 4th ed. McGraw-Hill, USA.

Kasanetz F, Riquelme LA, Murer MG (2002) Disruption of the two-state membrane potential of striatal neurones during cortical desynchronisation in anaesthetised rats. J Physiol 543: 577-589.

Kemp JM, Powell TP (1971a) The structure of the caudate nucleus of the cat: light and electron microscopy. Philos Trans R Soc Lond B Biol Sci 262: 383-401.

Kemp JM, Powell TP (1971b) The synaptic organization of the caudate nucleus Philos Trans R Soc Lond B Biol Sci 262: 403-12.

Kemp JM, Powell TP (1971c) The termination of fibres from the cerebral cortex and thalamus upon dendritic spines in the caudate nucleus: a study with the Golgi method. Philos Trans R Soc Lond B Biol Sci 262: 429-39.

Kelly RM, Strick PL (2004) Macro-architecture of basal ganglia loops with the cerebral cortex: use of rabies virus to reveal multisynaptic circuits. Prog Brain Res 143: 449-459.

Kilner JM, Baker SN, Salenius S, Jousmaki V, Hari R, Lemon RN (1999) Task-dependent modulation of 15-30 Hz coherence between rectified EMGs from human hand and forearm muscles. J Physiol 516: 559-70.

Kimura M (1990) Behaviorally contingent property of movement-related activity of the primate putamen. J Neurophysiol 63: 1277-96.

Kimura M, Kato M, Shimazaki H, Watanabe K, Matsumoto N (1996) Neural information transferred from the putamen to the globus pallidus during learned movement in the monkey. J Neurophysiol 76: 3771-86.

Kita H, Kita T (2001) Number, origins, and chemical types of rat pallidostriatal projection neurons. J Comp Neurol 437: 438-448.

Kita H, Kitai ST (1994) The morphology of globus pallidus projection neurons in the rat: an intracellular staining study. Brain Res 636: 308-319.

Klausberger T, Magill PJ, Marton LF, Roberts JD, Cobden PM, Buzsaki G, Somogyi P (2003) Brain-state- and cell-type-specific firing of hippocampal interneurons in vivo. Nature 421: 844-8.

Klein C, Ozelius LJ (2002) Dystonia: clinical features, genetics, and treatment. Curr Opin Neurol 15: 491-7.

Kocsis B, Bragin A, Buzsáki G (1999) Interdependence of multiple theta generators in the hippocampus: a partial coherence analysis. J Neurosci 19: 6200-6212.

Kolomiets BP, Deniau JM, Glowinski J, Thierry AM (2003) Basal ganglia and processing of cortical information: functional interactions between trans-striatal and trans-subthalamic circuits in the substantia nigra pars reticulata. Neuroscience 117: 931-938.

Konig P, Engel AK, Singer W (1996) Integrator or coincidence detector? The role of the cortical neuron revisited. Trends Neurosci 19: 130-7.

Koos T, Tepper JM (1999) Inhibitory control of neostriatal projection neurons by GABAergic interneurons. Nat Neurosci 2: 467-72.

Korzeniewska A, Manczak M, Kaminski M, Blinowska KJ, Kasicki S (2003) Determination of information flow direction among brain structures by a modified directed transfer function (dDTF) method. J Neurosci Methods 125: 195-207.

Kreiss DS, Mastropietro CW, Rawji SS, Walters JR (1997) The response of subthalamic nucleus neurons to dopamine receptor stimulation in a rodent model of Parkinson's disease. J Neurosci 17: 6807-6819.

Kühn AA, Williams D, Kupsch A, Limousin P, Hariz M, Schneider GH. Yarrow K, Brown P (2004) Event-related beta desynchronization in human subthalamic nucleus correlates with motor performance. Brain 127: 735-746.

Kuhn AA, Trottenberg T, Kivi A, Kupsch A, Schneider GH, Brown P (2005) The relationship between local field potential and neuronal discharge in the subthalamic nucleus of patients with Parkinson's disease. Exp Neuro 194: 212-20.

Lampl I, Yarom Y (1993) Subthreshold oscillations of the membrane potential: a functional synchronizing and timing device. J Neurophysiol 70: 2181-6.

Laurent G (2002) Olfactory network dynamics and the coding of multidimensional signals. Nat Rev Neurosci 3: 884-895.

Lee IH, Assad JA (2003) Putaminal activity for simple reactions or self-timed movements. J Neurophysiol 89: 2528-37.

Levy R, Hutchison WD, Lozano AM, Dostrovsky JO (2000) High-frequency Synchronization of Neuronal Activity in the Subthalamic Nucleus of Parkinsonian Patients with Limb Tremor. J Neurosci 20: 7766-7775.

Levy R, Dostrovsky JO, Lang AE, Sime E, Hutchison WD, Lozano AM (2001) Effects of apomorphine on subthalamic nucleus and globus pallidus internus in patients with Parkinson's disease. J Neurophysiol 86: 2249-2460.

Levy R, Ashby P, William DH, Lang AE, Lozano AM, Dostrovsky JO (2002a) Dependence of subthalamic nucleus oscillations on movement and dopamine in Parkinson's disease. Brain 125: 1196-1209.

Levy R, Hutchison WD, Lozano AM, Dostrovsky JO (2002b) Synchronized neuronal discharge in the basal ganglia of parkinsonian patients is limited to oscillatory activity. J Neurosci 22: 2855-2861.

Linazasoro G (2004) Recent failures of new potential symptomatic treatments for Parkinson's disease: causes and solutions. Mov Disord 19:743-54.

Liu X, Ford-Dunn HL, Hayward GN, Nandi D, Miall RC, Aziz TZ, Stein J (2002) The oscillatory activity in the Parkinsonian subthalamic nucleus investigated using the macro-electrodes for deep brain stimulation. Clin Neurophysiol 113: 1667-1672.

Leblois A, Boraud T, Meissner W, Bergman H, Hansel D (2006) Competition between feedback loops underlies normal and pathological dynamics in the basal ganglia. J Neurosci 26: 3567-83.

Logothetis NK, Wandeall BA (2004) Interpreting the BOLD signal. Annu Rev Physiol 66: 735-69.

Lopes da Silva FH, Vos JE, Mooibroek JN, Van Rotterdam A (1980) A partial coherence analysis of thalamic and cortical alpha rhythms in dog – a contribution towards a general model of cortical organisation of rhythmic activity. In: Event Related Changes in Cortical Rhythmic Activities - Behavioural Correlates, edited by Pfurtscheller G. Amsterdam: Elsevier/North-Holland Biomedical Press: 33-59.

Lopez da Silva F, Pijn JP, Boeijinga P (1989) Interdependence of EEG signals: linear vs. nonlinear associations and the significance of time delays and phase shifts. Brain Topogr 2: 9-18.

Lozano AM, Abosch A (2004) Pallidal stimulation for dystonia. Adv Neurol 94: 301-8.

Lytton WW, Sejnowski TJ (1991) Simulations of cortical pyramidal neurons synchronized by inhibitory interneurons. J Neurophysiol 66: 1059-79.

MacLeod K, Backer A, Laurent G (1998) Who reads temporal information contained across synchronized and oscillatory spike trains? Nature 395: 693-698.

MacKay WA (1997) Synchronised neuronal oscillations and their role in motor processes. Trends Cog Sci 1: 176-183.

Magee JC, Cook EP (2000) Somatic EPSP amplitude is independent of synapse location in hippocampal pyramidal neurons. Nat Neurosci 3: 895-903.

Magill PJ, Bolam JP, Bevan MD (2000) Relationship of activity in the subthalamic nucleus-globus pallidus network to cortical electroencephalogram. J Neurosci 20: 820-833.

Magill PJ, Bolam JP, Bevan MD (2001) Dopamine regulates the impact of the cerebral cortex on the subthalamic nucleus-globus pallidus network. Neuroscience 106: 313-330.

Magill PJ, Sharott A, Bevan MD, Brown P, Bolam JP (2004) Synchronous unit activity and local field potentials evoked in the subthalamic nucleus by cortical stimulation. J Neurophysiol 92: 700-714.

Mahon S, Deniau JM, Charpier S (2001) Relationship between EEG potentials and intracellular activity of striatal and cortico-striatal neurons: an in vivo study under different anesthetics. Cereb Cortex 11: 360-373.

Maloney KJ, Cape EG, Gotman J, Jones BE (1997) High-frequency gamma electroencephalogram activity in association with sleep-wake states and spontaneous behaviors in the rat. Neuroscience 76: 541-55.

Marsden JF, Limousin-Dowsey P, Ashby P, Pollak P, Brown P (2001a) Subthalamic nucleus, sensorimotor cortex and muscle interrelationships on Parkinson's disease. Brain 124: 378-388.

Marsden J, Limousin-Dowsey P, Fraix V, Pollak P, Odin P, Brown P (2001b) Intermuscular coherence in Parkinson's disease: effects of subthalamic nucleus stimulation. Neuroreport 12: 1113-7.

Matsumura M, Kojima J, Gardiner TW, Hikosaka O (1992) Visual and oculomotor functions of monkey subthalamic nucleus. J Neurophysiol 67: 1615-32.

Matsumura M, Chen D, Sawaguchi T, Kubota K, Fetz EE (1996) Synaptic interactions between primate precentral cortex neurons revealed by spike-triggered averaging of intracellular membrane potentials in vivo. J Neurosci 16: 7757-67.

Maurice N, Deniau JM, Glowinski J, Thierry AM (1999) Relationships between the prefrontal cortex and the basal ganglia in the rat: physiology of the cortico-nigral circuits. J Neurosci 19: 4674-4681.

Maurice N, Thierry AM, Glowinski J, Deniau JM (2003) Spontaneous and evoked activity of substantia nigra pars reticulata neurons during high-frequency stimulation of the subthalamic nucleus. J Neurosci 23:9929-36.

Mazurek ME, Shadlen MN (2002) Limits to the temporal fidelity of cortical spike rate signals. Nat Neurosci 5: 463-71.

Meissner W, Dovero S, Bioulac B, Gross C, Bezard E (2003a) Compensatory regulation of striatal neuropeptide gene expression occurs before changes in metabolic activity of basal ganglia nuclei. Neurobiol Dis 13: 46-54.

Meissner W, Prunier C, Guilloteau D, Chalon S, Gross CE, Bezard E (2003b) Time-course of nigrostriatal degeneration in a progressive MPTP-lesioned macaque model of Parkinson's disease. Mol Neurobiol 28: 209-18.

Meissner W, Leblois A, Hansel D, Bioulac B, Gross CE, Benazzouz A, Boraud T (2005) Subthalamic high frequency stimulation resets subthalamic firing and reduces abnormal oscillations. Brain 128: 2372-82.

Mena-Segovia J, Bolam JP, Magill PJ (2004) Pedunculopontine nucleus and basal ganglia: Distant relatives or part of the same family? Trends Neurosci 27: 585-588.

Moore CI, Nelson SB, Sur M (1999) Dynamics of neuronal processing in rat somatosensory cortex. Trends Neurosci 22: 513-20.

Morris G, Arkadir D, Nevet A, Vaadia E, Bergman H (2004) Coincident but distinct messages of midbrain dopamine and striatal tonically active neurons. Neuron 43: 133-43.

Mima T, Matsuoka T, Hallett M (2001) Information flow from the sensorimotor cortex to muscle in humans. Clin Neurophysiol 112: 122-126.

Mink JW (1996) The basal ganglia: focused selection and inhibition of competing motor programs. Prog Neurobiol 50: 381-425.

Mizumori SJ, Barnes CA, McNaughton BL (1990) Behavioral correlates of theta-on and theta-off cells recorded from hippocampal formation of mature young and aged rats. Exp Brain Res 80: 365-73.

Mitzdorf U (1985) Current-source density method and application in cat cerebral cortex: investigation of evoked potentials and EEG phenomena. Physiol Rev 65: 37-100.

Munk MH Roelfsema PR König P Engel AK, Singer W (1996) Role of reticular activation in the modulation of intracortical synchronization. Science 272: 271-274.

Murthy VN, Fetz EE (1992) Coherent 25- and 35- Hz oscillations in the sensorimotor cortex of awake behaving monkeys. Proc Natl Acad Sci USA 89: 5670-5674.

Murthy VN, Fetz EE (1996a) Synchronization of neurons during local field potential oscillations in sensorimotor cortex of awake monkeys. J Neurophysiol 76: 3968-3982.

Murthy VN, Fetz EE (1996b) Oscillatory activity in sensorimotor cortex of awake monkeys: synchronization of local field potentials and relation to behavior. J Neurophysiol 76: 3949-67.

Murer MG, Tseng KY, Kasanetz F, Belluscio M, Riquelme LA (2002) Brain oscillations, medium spiny neurons, and dopamine. Cell Mol Neurobiol 22: 11-32.

Nambu A, Tokuno H, Hamada I, Kita H, Imanishi M, Akazawa T, Ikeuchi Y, Hasegawa N (2000) Excitatory cortical inputs to pallidal neurons via the subthalamic nucleus in the monkey. J Neurophysiol 84: 289-300.

Nambu A, Tokuno H, Takada M (2002) Functional significance of the cortico-subthalamo-pallidal 'hyperdirect' pathway. Neurosci Res 43: 111-117.

Neuper C, Pfurtscheller G (2001) Event-related dynamics of cortical rhythms: frequency-specific features and functional correlates. Int J Psychophysiol 43: 41-58.

Nicola SM, Surmeier DJ, Malenka RC (2000) Dopaminergic modulation of neuronal excitability in the striatum and nucleus accumbens. Ann Rev Neurosci 23: 185-215.

Niedermeyer E, Lopes da Silva F (2005) Electroencephalography: Basic Principles, Clinical Applications and Related Fields (Fifth Edition). Lippincott, Williams and Wilkins, Philadelphia, USA.

Nini A, Feingold A, Slovin H, Bergman H (1995) Neurons in the globus pallidus do not show correlated activity in the normal monkey, but phase-

locked oscillations appear in the MPTP model of parkinsonism. J Neurophysiol 74: 1800-1805.

Nowak LG, Bullier J (2000) Cross-correlograms for neuronal spike trains. Different types of temporal correlation in the neocortex, their origin and significance. Time in the Brain. Harwood Academic Publishers. Netherlands: 53-96.

Nunez PL, Srinivasan R, Westdorp AF, Wijesinghe RS, Tucker DM, Silberstein RB, Cadusch PJ (1997) EEG coherency. I. Statistics, reference electrode, volume conduction, Laplacians, cortical imaging, and interpretation at multiple scales. Electroencephalogr Clin Neurophysiol 103: 499-515.

Obeso JA, Rodriguez-Oroz MC, Rodriguez M, Lanciego JL, Artieda J, Gonzalo N, Olanow CW (2000) Pathophysiology of the basal ganglia in Parkinson's disease. Trends Neurosci 23(10 Suppl): S8-19.

Onn SP, West AR, Grace AA (2000) Dopamine-mediated regulation of striatal neuronal and network interactions. Trends Neurosci 23(10 Suppl): S48-56.

O'Keefe J (1993) Hippocampus, theta, and spatial memory. Curr Opin Neurobiol 3: 917-24.

O'Keefe J, Recce ML (1993) Phase relationship between hippocampal place units and the EEG theta rhythm. Hippocampus 3: 317-30.

O'Keefe J, Burgess N (1999) Theta activity, virtual navigation and the human hippocampus. Trends Cogn Sci 3: 403-406.

Okun MS, Vitek JL (2004) Lesion therapy for Parkinson's disease and other movement disorders: update and controversies. Mov Disord 19: 375-89.

Oorschot DE (1996) Total number of neurons in the neostriatal, pallidal, subthalamic, and substantia nigral nuclei of the rat basal ganglia: a stereological study using the cavalieri and optical disector methods. J Comp Neurol 366: 580-99.

Orth M, Tabrizi SJ (2003) Models of Parkinson's disease. Mov Disord 18: 729-37.

Pan HS, Walters JR (1988) Unilateral lesion of the nigrostriatal pathway decreases the firing rate and alters the firing pattern of globus pallidus neurons in the rat. Synapse 12: 650-6.

Papa SM, Desimone R, Fiorani M, Oldfield EH (1999) Internal globus pallidus discharge is nearly suppressed during levodopa-induced dyskinesias. Ann Neurol 46: 732-8.

Parent A, Hazrati LN (1995a) Functional anatomy of the basal ganglia. I. The cortico-basal ganglia-thalamo-cortical loop. Brain Res Brain Res Rev 20: 91-127.

Parent A, Hazrati LN (1995b) Functional anatomy of the basal ganglia. II. The place of subthalamic nucleus and external pallidum in basal ganglia circuitry. Brain Res Brain Res Rev 20: 128-54.

Paxinos G, Watson C (1986) The rat brain in stereotaxic coordinates (2nd Edn). Academic Press, Sydney, AUS

Penttonen M and Buzsáki G (2003) Natural logarithmic relationship between brain oscillators. Thal Rel Sys 2: 145-152.

Perkel DH, Gerstein GL, Moore GP (1967) Neuronal spike trains and stochastic point processes II. simultaneous spike trains. Biophys J 7: 419-440.

Pesaran B, Pezaris JS, Sahani M, Mitra PP, Andersen RA (2002) Temporal structure in neuronal activity during working memory in macaque parietal cortex. Nat Neurosci 5: 805-811.

Pfurtscheller G, Stancak A Jr, Neuper C (1996) Event-related synchronization (ERS) in the alpha band--an electrophysiological correlate of cortical idling: a review. Int J Psychophysiol 24: 39-46.

Perez-Orive J, Mazor O, Turner GC, Cassenaer S, Wilson RI, Laurent G (2002) Oscillations and sparsening of odor representations in the mushroom body. Science 297: 359-65.

Pikovsky A, Rosenblum M, Kurths J (2001) Synchronisation: A universal concept in non-linear sciences. Cambridge University Press. Cambrige. UK.

Plenz D, Kital ST (1999) A basal ganglia pacemaker formed by the subthalamic nucleus and external globus pallidus. Nature 400(6745): 677-82.

Plenz D (2003) When inhibition goes incognito: feedback interaction between spiny projection neurons in striatal function. Trends Neurosci 26: 436-43.

Priori A, Foffani G, Pesenti A. Bianchi A, Chiesa V, Baselli G, Caputo E, Tamma F, Rampini P, Egidi M, Locatelli M, Barbieri S, Scarlato G (2002) Movement-related modulation of neural activity in human basal ganglia and its L-DOPA dependency: recordings from deep brain stimulation electrodes in patients with Parkinson's disease. Neurol Sci 23: S101-S102.

Ramanathan S, Hanley JJ, Deniau JM, Bolam JP (2002) Synaptic convergence of motor and somatosensory cortical afferents onto GABAergic interneurons in the rat striatum. J Neurosci 22: 8158-69.

Rappelsberger P, Petsche H (1988) Probability mapping: power and coherence analyses of cognitive processes. Brain Topogr 1: 46-54.

Raz A, Feingold A, Zelanskaya V, Vaadia E, Bergman H (1996) Neuronal synchronization of tonically active neurons in the striatum of normal and parkinsonian primates. J Neurophysiol 76: 2083-2088.

Raz A, Vaadia E, Bergman H (2000) Firing Patterns and Correlations of Spontaneous Discharge of Pallidal Neurons in the Normal and the Tremulous 1-Methyl-4-Phenyl-1,2,3,6-Tetrahydropyridine Vervet Model of Parkinsonism. J Neurosci 20: 8559-8571.

Raz A. Frechter-Mazar V, Feingold A, Abeles M, Vaadia E, Bergman H (2001) Activity of pallidal and striatal tonically active neurons is correlated in MPTP-treated monkeys but not in normal monkeys. J Neurosci 21: RC128 (1-5).

Reiner A, Albin RL, Anderson KD, D'Amato CJ, Penney JB, Young AB (1988) Differential loss of striatal projection neurons in Huntington disease. Proc Natl Acad Sci USA 85: 5733-7.

Reyes AD, Fetz EE (1993) Two modes of interspike interval shortening by brief transient depolarizations in cat neocortical neurons. J Neurophysiol 69: 1661-72.

Reyes AD, Rubel EW Spain WJ (1996) In vitro analysis of optimal stimuli for phase-locking and time-delayed modulation of firing in avian nucleus laminaris neurons. J Neurosci 16: 993-1007.

Rodriguez R, Kallenbach U, Singer W, Munk MH (2004) Short- and long-term effects of cholinergic modulation on gamma oscillations and response synchronization in the visual cortex. J Neurosci 24:10369-78.

Roelfsema PR, Engel AK, König P, Singer W (1997) Visuomotor integration is associated with zero time-lag synchronization among cortical areas. Nature 385: 157-161.

Rosenberg JR, Amjad AM, Breeze P, Brillinger DR, Halliday DM (1989) The Fourier approach to the identification of functional coupling between neuronal spike trains. Prog Biophys Mol Biol 53: 1-31.

Rosenberg JR, Halliday DM, Breeze P, Conway BA (1998) Identification of patterns of neuronal activity; partial spectra, partial coherence, and neuronal interactions. J Neurosci Methods 83: 57-72.

Rosenblum M, Pikovsky A (2004) Delayed feedback control of collective synchrony: an approach to suppression of pathological brain rhythms. Phys Rev E Stat Nonlin Soft Matter Phys 70: 041904.

Ruskin DN, Bergstrom DA, Walters JR (2002) Nigrostriatal lesion and dopamine agonists affect firing patterns of rodent entopeduncular nucleus neurons. J Neurophysiol 88: 487-96.

Ryan LJ, Sanders DJ, Clark KB (1992) Auto- and cross-correlation analysis of subthalamic nucleus neuronal activity in neostriatal- and globus pallidal-lesioned rats. Brain Res 583: 253-261.

Salenius S, Portin K, Kajola M, Salmelin R, Hari R (1997) Cortical control of human motoneuron firing during isometric contraction. J Neurophysiol 77: 3401-5.

Salinas E, Sejnowski TJ (2001) Correlated neuronal activity and the flow of neural information. Nat Rev Neurosci 2: 539-50.

Samii A, Nutt JG, Ransom BR (2004) Parkinson's disease. Lancet 363:1783-93.

Sanes JN, Donoghue JP (1993) Oscillations in local field potentials of the primate motor cortex during voluntary movement. Proc Natl Acad Sci USA 90: 4470-4.

Sato F, Lavallee P, Levesque M, Parent A (2000) Single-axon tracing study of neurons of the external segment of the globus pallidus in primate. J Comp Neurol 417: 17-31.

Sato M, Hikosaka O (2002) Role of primate substantia nigra pars reticulata in reward-oriented saccadic eye movement. J Neurosci 22: 2363-73.

Schneider JS, Rothblat DS (1996) Alterations in intralaminar and motor thalamic physiology following nigrostriatal dopamine depletion. Brain Res 742: 25-33.

Schultz W, Romo R (1987) Responses of nigrostriatal dopamine neurons to high-intensity somatosensory stimulation in the anesthetized monkey. J Neurophysiol 57: 201-17.

Schultz W, Romo R (1990) Dopamine neurons of the monkey midbrain: contingencies of responses to stimuli eliciting immediate behavioral reactions. J Neurophysiol 63: 607-24.

Schultz W (2002) Getting formal with dopamine and reward. Neuron 36: 241-63.

Schultz W, Tremblay L, Hollerman JR (2003) Changes in behavior-related neuronal activity in the striatum during learning. Trends Neurosci 26: 321-8.

Schwarting RKW, Huston JP (1996a) Unilateral 6-hydroxydopamine lesions of meso-striatal dopamine neurons and their physiological sequelae. Prog Neurobiol 49: 215-266.

Schwarting RKW, Huston JP (1996b) The unilateral 6-hydroxydopamine lesion model in behavioral brain research. Analysis of functional deficits, recovery and treatments. Prog Neurobiol 50: 275-331.

Serrien DJ, Cassidy MJ, Brown P (2003) The importance of the dominant hemisphere in the organization of bimanual movements. Hum Brain Mapp 18: 296-305.

Serrien DJ, Pogosyan AH, Cassidy MJ, Brown P (2004) Anticipatory cortico-cortical interactions: switching the task configuration between effectors. Exp Brain Res 154: 359-67.

Shadlen MN, Newsome WT (1994) Noise, neural codes and cortical organization. Curr Opin Neurobiol 4: 569-79.

Shadlen MN, Movshon JA (1999) Synchrony unbound: critical evaluation of the temporal binding hypothesis. Neuron 24: 67-77.

Shen B, Nadkarni M, Zappulla RA (1999) Spectral modulation of cortical connections measured by EEG coherence in humans. Clin Neurophysiol 110: 115-125.

Shink E, Bevan MD, Bolam JP, Smith Y (1996) The subthalamic nucleus and the external pallidum: two tightly interconnected structures that control the output of the basal ganglia in the monkey. Neuroscience 73: 335-357.

Silberstein P, Kuhn AA, Kupsch A, Trottenberg T, Krauss JK, Wohrle JC, Mazzone P, Insola A, Di Lazzaro V, Oliviero A, Aziz T, Brown P (2003) Patterning of globus pallidus local field potentials differs between Parkinson's disease and dystonia. Brain 126: 2597-608.

Silberstein P, Pogosyan A, Kuhn AA, Hotton G, Tisch S, Kupsch A, Dowsey-Limousin P, Hariz MI, Brown P (2005) Cortico-cortical coupling in Parkinson's disease and its modulation by therapy. Brain 128: 1277-91.

Singer W (1994) Time as coding space? Curr Opin Neurobiol 9: 189-94.

Singer W (1999) Neuronal synchrony: a versatile code for the definition of relations? Neuron 24: 49-65.

Smeets WJ, Marin O & Gonzalez A (2000) Evolution of the basal ganglia: new perspectives through a comparative approach. J Anat 196: 501-17.

Smith Y, Bolam JP (1990) The output neurones and the dopaminergic neurones of the substantia nigra receive a GABA-containing input from the globus pallidus in the rat. J Comp Neurol 296: 47-64.

Smith Y, Bevan MD, Shink E, Bolam JP (1998) MIcrocircuitry of the direct and indirect pathways of the basal ganglia. Neuroscience 86: 353-387.
Smith, Y, Kieval, JZ (2000) Anatomy of the dopamine system in the basal ganglia. Trends Neurosci 23 (suppl 10): S28-S33.

Smith Y, Raju DV, Pare JF, Sidibe M (2004) The thalamostriatal system: a highly specific network of the basal ganglia circuitry. Trends Neurosci 27: 520-527.

Soares J, Kliem MA, Betarbet R, Greenamyre JT, Yamamoto B, Wichmann T (2004) Role of external pallidal segment in primate parkinsonism: comparison of the effects of 1-methyl-4-phenyl-1,2,3,6-tetrahydropyridine-induced parkinsonism and lesions of the external pallidal segment. J Neurosci 24: 6417-26.

Song WJ, Baba Y, Otsuka T, Murakami F (2000) Characterization of Ca(2+) channels in rat subthalamic nucleus neurons. J Neurophysiol 84: 2630-7.

Spauschus A, Marsden J, Halliday DM, Rosenberg JR, Brown P (1999) The origin of ocular microtremor in man. Exp Brain Res 126: 556-562.

Sporns O, Tononi G, Edelman GM (2000a) Connectivity and complexity: the relationship between neuroanatomy and brain dynamics. Neural Netw 13: 909-22.

Sporns O, Tononi G, Edelman GM (2000b) Theoretical neuroanatomy: relating anatomical and functional connectivity in graphs and cortical connection matrices. Cereb Cortex 10: 127-41.

Stanford IM (2003) Independent neuronal oscillators of the rat globus pallidus. J Neurophysiol 89: 1713-7.

Steriade M (1997) Synchronized activities of coupled oscillators in the cerebral cortex and thalamus at different levels of vigilance. Cereb Cortex 7:583-604.

Steriade M (2000) Corticothalamic resonance, states of vigilance and mentation. Neuroscience 101: 243-276.

Steriade M (2001) The intact and sliced brain. MIT Press. USA

Stern EA, Kincaid AE, Wilson CJ (1997) Spontaneous subthreshold membrane potential fluctuations and action potential variability of rat corticostriatal and striatal neurons in vivo. J Neurophysiol 77: 1697-1715.

Stern EA, Jaeger D, Wilson CJ (1998) Membrane potential synchrony of simultaneously recorded striatal spiny neurons in vivo. Nature 394: 475-478.

Stevens CF, Zador AM (1998) Input synchrony and the irregular firing of cortical neurons. Nat Neurosci 1: 210-7.

Stopfer M, Bhagavan S, Smith BH, Laurent G (1997) Impaired odour discrimination on desynchronization of odour-encoding neural assemblies. Nature 390: 70-74.

Tallon-Baudry C, Bertrand O (1999) Oscillatory gamma activity in humans and its role in object representation. Trends Cogn Sci 3: 151-162.

Terman D, Rubin JE, Yew AC, Wilson CJ (2002) Activity patterns in a model for the subthalamopallidal network of the basal ganglia. J Neurosci 22: 2963-76.

Thatcher RW, Krause PJ, Hrybyk M (1986) Cortico-cortical associations and EEG coherence: a two compartmental model. Electroenceph Clin Neurophysiol 64: 123-143.

Thatcher RW, Walker RA, Giudice S (1987) Human cerebral hemispheres develop at different rates and ages. Science 236: 1110-1113.

Theoret H, Boire D, Herbin M, Ptito M (1999) Stereological evaluation of substantia nigra cell number in normal and hemispherectomized monkeys. Brain Res 835: 354-359.

Tononi G, Edelman GM (1998) Consciousness and complexity. Science 282: 1846-51.

Traub RD, Whittington MA, Colling SB, Buzsaki G, Jefferys JG (1996) Analysis of gamma rhythms in the rat hippocampus in vitro and in vivo. J Physiol 493: 471-84.

Tseng KY, Kasanetz F, Kargieman L, Riquelme LA, Murer MG (2001) Cortical slow oscillatory activity is reflected in the membrane potential and spike trains of striatal neurons in rats with chronic nigrostriatal lesions. J Neurosci 21: 6430-6439.

Turner RS, Anderson ME (1997) Pallidal discharge related to the kinematics of reaching movements in two dimensions. J Neurophysiol 77: 1051-74.

Ungless MA, Magill PJ, Bolam JP (2004) Uniform inhibition of dopamine neurons in the ventral tegmental area by aversive stimuli. Science 303(5666): 2040-2.

Urbain N, Gervasoni D, Soulière F, Lobo L, Rentéro N, Windels F Astier B, Savasta M, Fort P, Renaud B, Luppi PH, Chouvet G (2000) Unrelated course of subthalamic nucleus and globus pallidus neuronal activities across vigilance states in the rat. Eur J Neurosci 12: 3361-3374.

Usrey WM (2002) The role of spike timing for thalamocortical processing. Curr Opin Neurobiol 12: 411-7.

VanRullen R, Guyonneau R, Thorpe SJ (2005) Spike times make sense. Trends Neurosci 28: 1-4.

van Lier H, Drinkenburg WH, van Eeten YJ, Coenen AM (2004) Effects of diazepam and zolpidem on EEG beta frequencies are behavior-specific in rats. Neuropharmacology 47: 163-74.

Varela F, Lachaux JP, Rodriguez E, Martinerie J (2001) The brainweb: phase synchronization and large-scale integration. Nat Rev Neurosci 2: 229-39.

Vergara R, Rick C, Hernandez-Lopez S, Laville JA, Guzman JN, Galarraga E, Surmeier DJ, Bargas J (2003) Spontaneous voltage oscillations in striatal projection neurons in a rat corticostriatal slice. J Physiol 553: 169-82.

Villa AEP (2000) Evidence about temporal structure in multi-unit recordings. 1-52. Time in the Brain. Harwood Academic Publishers. Netherlands.

Von Stein A, Chiang C, Konig P (2000) Top-down processing mediated by interareal synchronization. Proc Natl Acad Sci USA 97: 14748-53.

Walter BL, Vitek JL (2004) Surgical treatment for Parkinson's disease. Lancet Neurol 3: 719-28.

Wennberg RA, Lozano AM (2003) Intracranial volume conduction of cortical spikes and sleep potentials recorded with deep brain stimulating electrodes. Clinical Neurophysiology 114: 1403-1418.

West MO (1998) Anesthetics eliminate somatosensory-evoked discharges of neurons in the somatotopically organized sensorimotor striatum of the rat. J Neurosci 18: 9055-9068.

West MJ (1999) Stereological methods for estimating the total number of neurons and synapses: issues of precision and bias. Trends Neurosci 22: 51-61.

West MJ, Gundersen HJ (1990) Unbiased stereological estimation of the number of neurons in the human hippocampus. J. Comp Neurol 296: 1-22.

Whittington MA, Faulkner JH, Doheny HC, Traub RD (2000) Neuronal fast oscillations as a target site for psychoactive drugs. Pharmacol Ther 86: 171-190.

Whittington MA, Traub RD (2003) Interneuron diversity series: inhibitory interneurons and network oscillations in vitro. Trends Neurosci 26: 676-682.

Wichmann T, Bergman H, DeLong MR (1994) The primate subthalamic nucleus. I. Functional properties in intact animals. J Neurophysiol 72: 494-506.

Wichmann T, DeLong MR (1996) Functional and pathophysiological models of the basal ganglia. Curr Opin Neurobiol 6: 751-758.

Wichmann T, Bergman H, Starr PA, Subramanian T, Watts RL, DeLong MR (1999) Comparison of MPTP-induced changes in spontaneous neuronal discharge in the internal pallidal segment and in the substantia nigra pars reticulata in primates. Exp Brain Res 125: 397-409.

Wichmann T, Kliem MA (2004) Neuronal activity in the primate substantia nigra pars reticulata during the performance of simple and memory-guided elbow movements. J Neurophysiol 91: 815-27.

Widnell K (2005) Pathophysiology of motor fluctuations in Parkinson's disease. Mov Disord 20 Suppl 11: S17-22.

Williams D, Tijssen M, van Bruggen, G, Bosch A, Insola A, Di Lazzaro V, Mazzone P, Oliviero, A, Quartarone A, Speelman H, Brown P (2002) Dopamine dependent changes in the functional connectivity between basal ganglia and cerebral cortex in the human. Brain 125: 1558-1569.

Williams D, Kuhn A, Kupsch A, Tijssen M, van Bruggen G, Speelman H, Hotton G, Yarrow K, Brown P (2003) Behavioural cues are associated with modulations of synchronous oscillations in the human subthalamic nucleus. Brain 126: 1975-85.

Zheng T, Wilson CJ (2002) Corticostriatal combinatorics: the implications of corticostriatal axonal arborizations. J Neurophysiol 87: 1007-17.